Newtonian and Non-Newtonian Flows through Mini-channels and Micro-scale Orifices for SAGD Applications

by

Shadi Ansari

A thesis submitted in partial fulfillment of the requirements for the degree of

Master of Science

Department of Mechanical Engineering
University of Alberta

Abstract

This experimental investigation examined the inflow to a producer well geometry found in a typical steam assisted gravity drainage (SAGD) process. The flow of Newtonian and non-Newtonian fluid through mini-channels ($D_h = 0.837$ μm) and micro-scale orifices (keystone slots, $D_h = 0.858$ μm) were considered. The major goal was to describe the velocity distribution and this was undertaken using particle image velocimetry (PIV).

The velocity profile determined for the flow through the long channel was used to find the rheological parameters of the fluid. Theory of the rheology of non-Newtonian fluids along with PIV measurements were used to find the flow index, n, and flow consistency index, k. These where validated against commercial rheometer. It was shown that measuring the velocity distribution of a non-Newtonian fluid can be used to identify rheological property of the fluid.

The second set of experiments considered the flow of Newtonian (water), and non-Newtonian (polyacrylamide) fluids to study the respective velocity profiles using PIV. The results showed that an increase in slot angle, θ, increased the gradient at which the velocity reduced along the channel. At low flow rates, the increase in slot angle ($\theta \geq 6°$) caused a flow separation phenomenon which was only present for the Newtonian fluid. Comparison with theory showed that the Newtonian flow profiles found from experiment matched well while for the non-Newtonian fluid the profiles deviated from expected. This was a result of the contraction-expansion geometry which increased the shear rate giving the fluid a pseudo-Newtonian-like behavior.

Preface

This thesis is original work by Shadi Ansari. Part of Chapters 4 and 5 of this thesis have been published as Ansari, S., Rashid, M. A. I., Chatterjee, O., Waghmare, P. R., Ma, Y., & Nobes, D. (2015) "*Visualization of the viscous effects of non-Newtonian fluids flowing in mini-channels*", and as Ansari, S., Rashid, M. A. I., Waghmare, P. R., Ma, Y., & Nobes, D. (2015) "*Newtonian and non-Newtonian flows through micro scale orifices*" in proceeding of the 10th, Pacific Symposium on Flow Visualization and Image Processing.

Acknowledgements

I would like to express my sincere gratitude to my supervisor Dr. David S. Nobes for his continuous support during the whole of my study. I greatly appreciate his patience in motivating me and sharing his knowledge for all challenges I had. Conversations with him always kept me at higher level of thinking and were true inspirations. I could not imagine having an advisor who is better than him.

I am also grateful for Dr. Prashant Waghmare for his kindness in letting me use his laboratory and research facilities. Thanks to my friends and lab mates for their support, friendship and help. Especially I thank my friends Yishak Yusuf and Rouholluh Shokri for their help and useful comments for my thesis.

Special thanks go to my loving husband, Ali Baladi, who has not only been a husband but also the greatest colleague, friend, and one to truly rely on for anything anytime. Finally, a greatest thank you to my parents and my brother for providing me support during my whole life and believing me all along. I owe it to you all!

Funding support for this project was made available by RGL Reservoir Management Inc. and the Natural Sciences and Research Council (NSERC) of Canada.

Shadi Ansari

January, 2016

Table of Contents

List of Tables

List of Figures

List of Symbols and Acronyms

Symbol/Acronyms	Description	Unit
CR	Controlled rate	-
CS	Controlled stress	-
D_h	Hydraulic diameter	µm
D_{L1}	Diameter of lamp collector	mm
D_{L2}	Diameter of condenser	mm
D_{Lamp}	Diameter of Lamp	mm
D_p	Diameter of particle	µm
$\frac{dp}{dx}$	Pressure drop	Pa/m
FL_1	Focal length of lamp collector	mm
FL_2	Focal length of condenser	mm
g	Gravitational constant	m/s^2
k	Flow consistency index	$Pa.s^n$
K	velocity decay coefficient	-
l	Length of slot	µm
L	Effective measuring gap	mm
LSV	Laser speckle velocimetry	-
n	Flow index	-
N	Sample Size	-
PIV	Particle image velocimetry	-
PTV	Particle tracking velocimetry	-
Q	Flow rate	ml/hr or ml/min
R_1	Internal radius of the measuring cup	mm
R_2	Internal radius of the measuring bob	mm
R_3	External radius of the measuring bob	mm
R_4	External radius of the measuring cup	mm
Re	Newtonian Reynolds number	-
Re^*	Non-Newtonian Reynolds number	-
SAGD	Steam assistant gravity drainage	-

SD	Standard deviation	-
$SE_{\bar{x}}$	Standard error	-
t	Time	s
u	Velocity in x direction	m/s
U_{max}	Maximum velocity	m/s
U_x	Centerline mean velocity	m/s
U_o	Outlet velocity of the orifice	m/s
v	Velocity in y direction	m/s
v_s	Settling velocity	m/s
w	Width of the slot entrance	μm
$\bar{x}$	Mean value of samples	-
x_p	Virtual origin	μm
$\{x_1, x_2, \dots, x_N\}$	Observed values in viscosity measurement	-
	Greek letters	
τ	Shear stress	Pa
τ_{xx}	Stress in *x* direction	Pa
τ_{xy}	Stress in *y* direction	Pa
τ_{xz}	Stress in *z* direction	Pa
μ	Viscosity	Pa.s
γ	Shear rate	1/s
θ	Slot angle	°
ρ	Fluid density	kg/m^3
ρ_p	Particle density	kg/m^3

Chapter 1. Literature Review

1.1 Introduction

In Alberta, the main resources of oilsand are not accessible using mining and only 20-50% of the oil can be recovered using the primary and the secondary recovery techniques [1]. One of the ways to recover these resources at deeper depths is to use *in-situ* extraction processes such as the steam assistant gravity drainage (SAGD) process. SAGD is a thermal *in-situ* enhanced oil recovery method in which two parallel horizontal wells are drilled into the reservoir as shown in Figure 1-1. In this process, steam is produced on the surface and is then injected to the reservoir using the upper (injection) well to mobilize the bitumen by lowering its viscosity. After a decrease in viscosity, gravity acts on the bitumen for it to flow into the lower (production) well. A mixture of bitumen, water and produced sand is pumped to the surface for further separation and processing. Bitumen is the final product from this process which requires the prevention if possible or decreasing the rate of sand production. Therefore, a suitable sand control method should be used to hold sand in the reservoir, depending on the *in-situ* properties of the reservoir [1- 4].

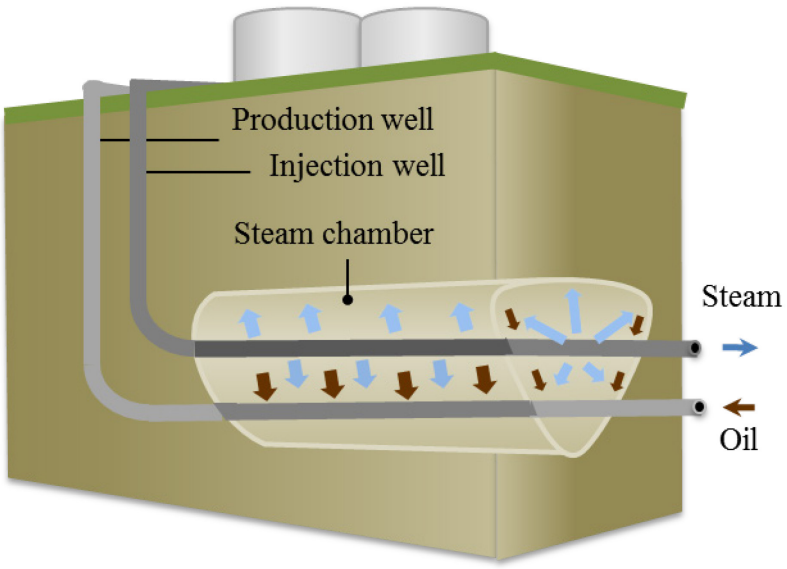

Figure 1-1.Schematic of Steam assistant gravity drainage process

For SAGD process different mechanical sand control methods can be used such as slotted liners, screens and gravel packs (or combinations). Slotted liners are presently being widely preferred because of their low cost of production, and lower pressure drop of the flow through the open slot [5]. Slotted liners are commonly used for reservoirs with high viscosity oil (>10^4cP at 25℃ [6]) and consolidated sand with high permeability. The lifetime of slotted liners can decrease if the sand contains a significant amount of clay with large grain size. To increase the performance of the slotted liners, factors which can affect the wells such as plugging, fouling and corrosion should be investigated and recognized [5].

The SAGD process relies on the performance of the wells and there are many factors which affect the stability of wells. These factors can be categorized into two groups of controllable and uncontrollable (natural) factors [7-11]. Controllable factors are well inclination and azimuth [7], bottom-hole pressure

[8], physical/chemical interaction between the formation and the fluid [7], transient pore pressure, temperature and erosion [7]. Uncontrollable factors are natural failures such as unconsolidated formations and naturally over-pressured [9] or induced over-pressured shale collapse, high *in-situ* stresses, tectonic stresses and transportable formations [7-11].

Plugging and scaling of slotted liners are the most important issues which should be resolved to improve well performance. Plugging of slots may occur due to sand particle that could not pass through and/or the accumulation of scale from compounds such as calcium carbonate and asphaltene [13]. According to studies [14- 15], there are different parameters which cause these phenomena. Scaling can be caused due to either the nature of the produced sands in the reservoir or the geometry of the slotted liners.

The composition of the oil sand is one of the factors which can affect bitumen extraction and the scaling of the slotted liners. Oil sand deposits consist of 4-18 wt. % of bitumen, 2-15 wt. % water and 55-80 wt. % inorganic materials [16]. Both fine and coarse sands are produced from the reservoir. Generally, the coarse sand will not cause any problem for the extraction process while the fines are unfavorable. The fine particles may interact with bitumen, water or solvent as a result of their small particle size, high specific surface area, swelling capacity, cation exchange capacity and layer charge. The rheology of the bitumen mixture will be affected by the concentration of sand and its size distribution [16]. Bitumen behaves as a Newtonian fluid at high temperature while adding mineral particles to the bitumen will change its rheology to non-Newtonian fluid [17].

Figure 1-2 shows three different shapes of slots which are commonly used [18] for SAGD process: straight, keystone and rolled. A straight slot has a uniform cross section all over the slot but in the case of a keystone and rolled slots, the cross sectional area increases toward the inner surface of the pipe. This increment of the cross section area is believed to help to decrease scaling and plugging of the slot [19] and the fine or sand can move toward the pipe without sticking in the slot. The rolled slot (sometimes referred to as seamed [18]) is the modification of the keystone slotted liner with an arc at the inlet of the slot. This slot performs better [19] as anti-plugging but is harder to manufacture making it less common than keystone slots [16, 19].

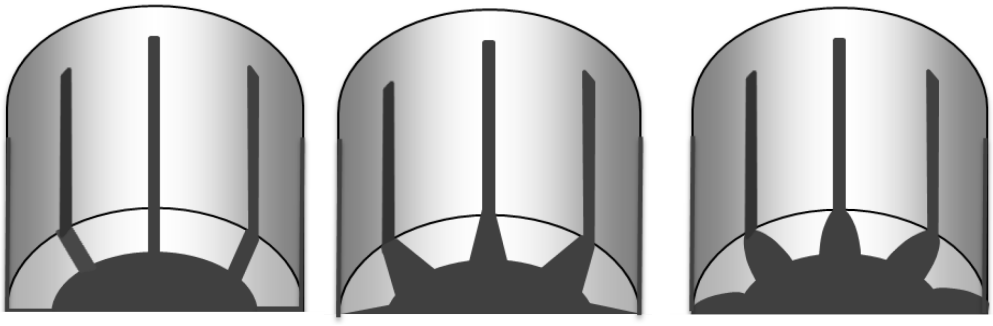

(a) (b) (c)

Figure 1-2. Schematics of slots shapes in SAGD process
(a)straight (b)keystone ,and (c) rolled

In this study, the flow through slots is investigated. Experimental techniques were applied to identify the distribution of major flow parameters (i.e. velocity distribution) as the flow behavior of the fluid and slot geometry varied. The research was primarily based on observations that employed optical measurement techniques. Relevant literature and the major objectives set are discussed in the remaining parts of this chapter. Chapters that follow will discuss the details of

approaches used in the methodology, after which results are presented with description of their analysis. Conclusions based on these results along with recommendations for future research works are forwarded in the final chapter of this thesis.

1.2 Rheology of bitumen and the mixture of bitumen and sands

A fluid's viscosity depends on its physical and chemical nature, temperature, pressure, shear rate, time and electrical field [20]. Fluids can behave either Newtonian or non-Newtonian. As shown in Figure 1-3, Newtonian fluids have a constant slope in the graph of shear rate (γ) versus shear stress (τ), which represents a constant viscosity of the fluid with respect to shear rate. For non-Newtonian fluids however, the viscosity varies nonlinearly with changing shear rate. Non-Newtonian fluids can be divided to the three sub groups of shear thinning, shear thickening and Bingham plastics [21].

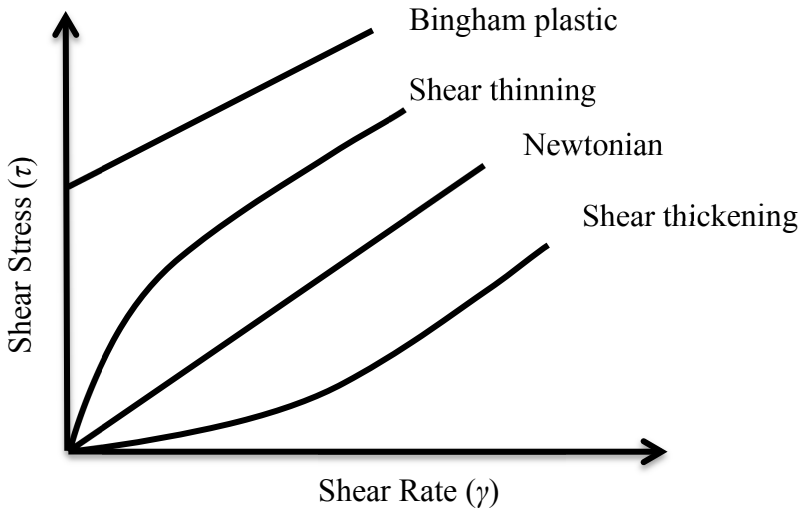

Figure 1-3. Definition of Newtonian and non-Newtonian fluids

In-situ oil sands are a mixture of bitumen (4 -16 wt. %) and mineral solids (55-80 wt. %) balanced with water. The bitumen is a viscous hydrocarbon with high molecular mass. The percentage of each component in the ore defines the overall efficiency of the recovery process [22]. High bitumen content leads to high processing efficiency, whereas a low content makes the recovery process much harder due to the undesirable production of sand [23].

The solid components of oil sands are mostly clay particles and quartz sand. The content and size of the minerals in oil sands depend on the reservoir's nature. The recovery of the bitumen faces difficulties when high concentrations of the solid particles that are smaller than 12 μm (ultra-fines) are present due to their strong bond [22]. The amount of sand particles and their size distribution affect the rheology of the bitumen mixture. Bitumen behaves as Newtonian fluid at low shear rate (~10 (1/s)). However, the presence of mineral particles changes the rheology to non-Newtonian [17]. Effects of the particles properties on the fluid behavior were studied [22, 24] and the mixture of the particles and bitumen have a shear thinning behavior [24]. The non-Newtonian effect is more dominant at the lower shear rates (~10 (1/s)) and it decreases as shear rate increases. The higher viscosity of the mixture at lower shear rate is due to the presence of a networked structure in the solid suspensions. The structures of the solid bonds will be disintegrated by increasing the shear rate which result in decreasing of the mixture viscosity [17, 22].

Study of oilsand mixtures revealed that by increasing the concentration of the particles, non-Newtonian behavior of the solution intensified [17]. At low

solid concentrations there were no strong inter-particle forces observed as a result of long distance between particles. In low concentration suspensions, the effect of particles on the behavior of the suspension is not severe. However, at higher concentrations of the mineral solids, the distance between particles becomes smaller which results in strong inter-particle forces. These forces will change the behavior of the solution in general [17].

The bitumen in oil sand reserves could therefore be considered as a non-Newtonian fluid. This behavior is consistent as long as particles are present in the mixture where the fluid's shear thinning behavior intensifies as the concentration of particles is increased. The size distribution of particles was also given as a factor which affected the behavior of the suspension. At a given concentration of the particles, the viscosity of the solution could be increased by decreasing the size of particles. This increment of the viscosity is due to stronger and more stable structure of smaller particles compared to bigger particles [17].

1.3 Study of flow through mini-channels

Channels with dimensions greater than 200 μm and less than 3 mm are commonly called mini-channels [27]. Interest to improve mini-channels and micro-channels performance has grown in recent years because of their increased application in many areas. These channels have small volumes and high surface-to-volume ratio which makes these devices suitable for different applications such as inkjet printer heads [28] and heat exchangers [29]. These devices also gained popularity in biological [30] and chemical analysis [31] since their scale matches the present biological structures. They can also be a good choice for the transportation of biological materials [31] or chemical samples [32].

Different flow behaviors can be seen in micro- and mini-scale channels [33, 38]. The molecular effects in mini-channels are more significant provided that certain effects of the continuum are intensified [32]. Comparisons of these flows have been done in a number of studies based on respective pressure drop [34] and transient Reynolds number [37] of the flows. It was shown that hydraulic diameter [38], Reynolds number [37, 38], and surface roughness [35] have effect on the characteristics of the Newtonian flow.

Experimental study of the velocity profile of water showed that in micro-tubes with diameters >80 μm the incompressible laminar flow had the same characteristics as it would found in macro-tubes [35]. Results showed that the velocity profile of water through narrow channels as small as 25.9 μm followed the Naiver-Stokes equations and they behave as macro-scale flows [39].

The transition of laminar flow to turbulence could change in micro-channels depending on the width and the surface roughness of channels. Study of water flow through circular channels detected that early transition happened in the micro-channel and the critical Reynolds number for transition would be different depending on the size of the micro-channel [37]. Depending on the hydraulic diameter of the flow the critical Reynolds number can be in range of 1500 to 2000 [35, 36].

Most of the studies on flow through rectangular micro-channels have used Newtonian fluids [34, 38]. In comparison there has been little attention given to the study of non-Newtonian fluids in micro-channels. Kozicki et al. (1966) developed a Reynolds number for this type of non-Newtonian flow [40]. The modified theoretical Reynolds number for a power law fluid, Re^*, considers non-Newtonian parameters of the fluid and it is defined as:

$$Re^* = \frac{\rho D_h^n u^{2-n}}{k}\left(\frac{n}{a+bn}\right)^n 8^{1-n} \qquad (1\text{-}1)$$

where ρ is the fluid density, D_h is the hydraulic diameter; u is the average velocity, μ is the fluid viscosity; n is the flow index; k is the flow consistency; and a and b are constants which depend on the shape of cross section. For circular pipes $a = 0.25$ and $b = 0.75$ and for square channels $a = 0.2121$ and $b = 0.6766$. This relationship is the general case and by substituting $k = \mu$ and $n = 1$ the equation will be same as the *Re* number for a Newtonian fluid case as [40]:

$$Re = \frac{\rho D_h u}{\mu} \tag{1-2}$$

In most the industrial applications, transport of a fluid is involved. In order to transport liquid in micro-channels, the viscosity of the fluid is a critical factor [41] that needs to be characterized. In order to measure the viscosity of the fluid only ex situ viscosity measurements have typically been undertaken [42]. For this measurement a rheometer is typically used to measure the rheology of the fluid based on the variation of the shear rate and shear stress. However, in some applications [43] *in-situ* viscosity measurement was required to find the rheological behavior of the liquid.

The theoretical equations for Newtonian and non-Newtonian flows through channels with different geometries have been described by different researchers [44, 45]. However, there are limited works that studied the effect of non-Newtonian behavior on the velocity profile at different flow rates in rectangular cross section and determination of different parameters of the fluid characteristics such as viscosity based on the velocity profile.

1.4 Flow of Newtonian and non-Newtonian fluids through orifices

Scaling and plugging of the slotted liners in producer wells decreases the productivity of SAGD. Replacing and cleaning of slotted liners is an expensive operation and consumes much time. Therefore, the behavior of bitumen flow into the producer well needs to be fully understood to find a solution to minimize the possibility of scaling and plugging [15].

Slots of the keystone geometry have performed better in terms of minimizing plugging than straight slots. The design of these slots is based on the particle size distribution of the formation sand [46]. The slot width on the outer diameter of the liner is made to be small enough to control sand while the inner diameter width is large enough to allow passage for grains which passed through the outside width [18].

Slots having rectangular cross section area with the widths ranging from 0.355 to 6.35 mm with corresponding depth (pipe thickness) ~ 16 mm are commonly reported to have good sand control and stability [18]. The large width to depth ratio of slots give made similar flow characteristics to long micro-orifices with rectangular cross-section. In order to have a fundamental understanding of the fluid flow through slotted liners studying the flow field through long micro-orifices could be very helpful.

The area of flow through micro-orifices has become popular because of their wide application in different fields [47- 53]. Numerical studies mostly

showed a good agreement with the experimental results [47]. The flow through orifices can be influenced by a number of parameters. Study of the velocity field through an expansion or contraction requires the geometry of the cross section of orifice, aspect ratio of the orifice to the channel, sharpness of the edges of the orifice, Reynolds number and the rheology of the fluid to be considered [47- 53].

Different cross sections such as rectangular and circular [52] have been used for various industrial applications. The velocity field, pressure drop and shape of flow structures within the fluid flow such as vortices for flow across orifices vary with slot shape [53]. Correction factors were used in order to account for the change in orifice geometry on the effect on pressure drop and velocity profiles [53].

The effects of Reynolds number and the aspect ratio (orifice width to channel width) on the velocity profiles were also studied and vortices were found in the corners behind sudden expansions at $\mathrm{Re} \leq 43.7$ [54]. The length of these corner vortices was influenced by the Reynolds number and the aspect ratio considered [54, 55]. Here, vortices expanded as Reynolds number and the aspect ratio both increased. Observations also showed that the possibility for lip vortices to be present downstream the orifice was higher at the higher flow rates [56]. Asymmetric flow was also caused after the expansion of the orifice as Reynolds number increased.

Experimental studies showed that the sharpness of edges in expansion and contraction of orifices also caused the generation of vortices. For the same flow regime, a lip vortex was only present for the case of sharp edges but not for round

corners. The corner vortices that were observed for the round corners were with lower intensity as compared to the sharp edges [59, 61].

The rheology of the fluid also affected the velocity profiles for flow through micro-orifices. According to Ternik et al. (2010), shear thickening fluids reached the fully developed state closer to the expansion plane than shear thinning fluids [62]. For shear thinning fluids, the flow redeveloped farther downstream the channel and reattachment was close to the expansion plane than for shear thickening fluids. Studies showed that the reattachment of the flow shifted away from the expansion plane with an increase in the power law flow index [62].

Review of the relevant literature shows that most present research activities in both numerical and experimental studies put more focus on turbulent flow which left much about creeping fluid flows to still remain unclear. Less attention was given to non-Newtonian while, in in many applications, the operating liquids behave as non-Newtonian fluids [63]. In previous studies the main focus was on the circular cross section orifices to simplify the geometry. The flow development in rectangular orifices with varying cross section area has received little attention in the literature.

1.5 Flow velocity measurement techniques

Common methods that can be used to measure velocity fall in the three categories [64] of pressure measurement [65], anemometry measurement [66] and optical measurement [68]. The respective advantages and disadvantages of these measurement techniques come from their interference in flow field and/or the coverage of measured area they offer [67].

A pressure measurement technique to find the velocity field is limited to stationary flows because of the pressure time delay of the measurement gets interrupted when gas or liquid oscillation occurs. This method can only be used with frequencies up to several Hz. An anemometry method can alternatively be used for both stationary and non-stationary flows at frequencies in the order of kHz. The disadvantage of this measuring system is that it is a point measurement and requires small dimensions of the probes (D =1.5 mm) [67].

Among flow measurement techniques used in fluid mechanics research, optical measurements [67] are now mostly commonly used since they are non-intrusive methods and enable identification of the vectors and scalar quantities of the flow. They also allow a spatial distribution of the parameter of interested to be measured. Particle tracking velocimetry (PTV) [69], particle image velocimetry (PIV) [70] and laser speckle velocimetry (LSV) [71] are as some of the more popular techniques which are used in studies that include optical measurement. In these techniques the fluid flow field velocity is measured indirectly by measuring the displacement of tracer particles in the flow [67, 72].

Figure 1-4 shows images that correspond to the different optical measurement techniques to study a given flow. Figure 1-4 (a) represents PTV (low density of tracer particle) which enables tracking the motion of individual particles. For the case of medium seeding density, Figure 1-4(b), a group of particles can be tracked to measure the flow filed for which standard statistical PIV is suitable. Figure 1-4 (c) corresponds to LSV where it is not possible to track individual particles since they overlap in most cases and following the speckle is needed. In these measurement techniques, areas within the images are called interrogation regions (windows) and are used to determine the movement of particle in an elapsed time [68] within that region.

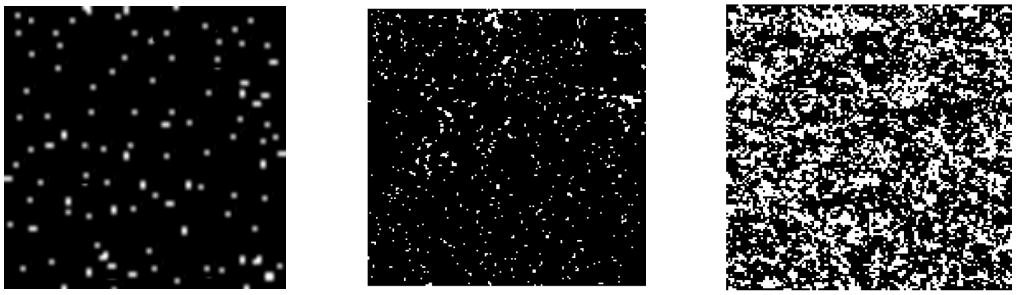

(a) (b) (c)

Figure 1-4. Picture of three cases of particle density: (a) low (PTV), (b) medium (PIV), and (c) high image density (LSV) [68]

For the type of flow that this study is concerned with, PIV was selected as the suitable method. It was required to have particle density that was enough to measure the flow field near the channel walls but not too dense that following a group of particles becomes impossible.

1.6 Particle image velocimetry

Particle image velocimetry (PIV) method is now a common fluid mechanics measurements approach because of its advantages over other optical methods [70]. The PIV method has ability to record image in large field in the flow field while other methods can only measure the velocity at the single point. These features make the method appropriate to study the velocity field for various applications such as high speed flows and the boundary layers of the fluid [68].

Figure 1-5 shows the typical setup of PIV measurement. In the setup, a laser is utilized as a light source to illuminate the tracer particles in the flow field at least twice in a short time. The light scattered off of the particles is recorded either on a single frame or on a sequence of frames in pulse of time, t, to $t + \Delta t$. Data processing is aimed at finding the average displacement of tracer particles over small interrogation in the image. After the displacement of tracer particles is determined the velocity of the fluid can be identified using the time interval of the laser pulse [68].

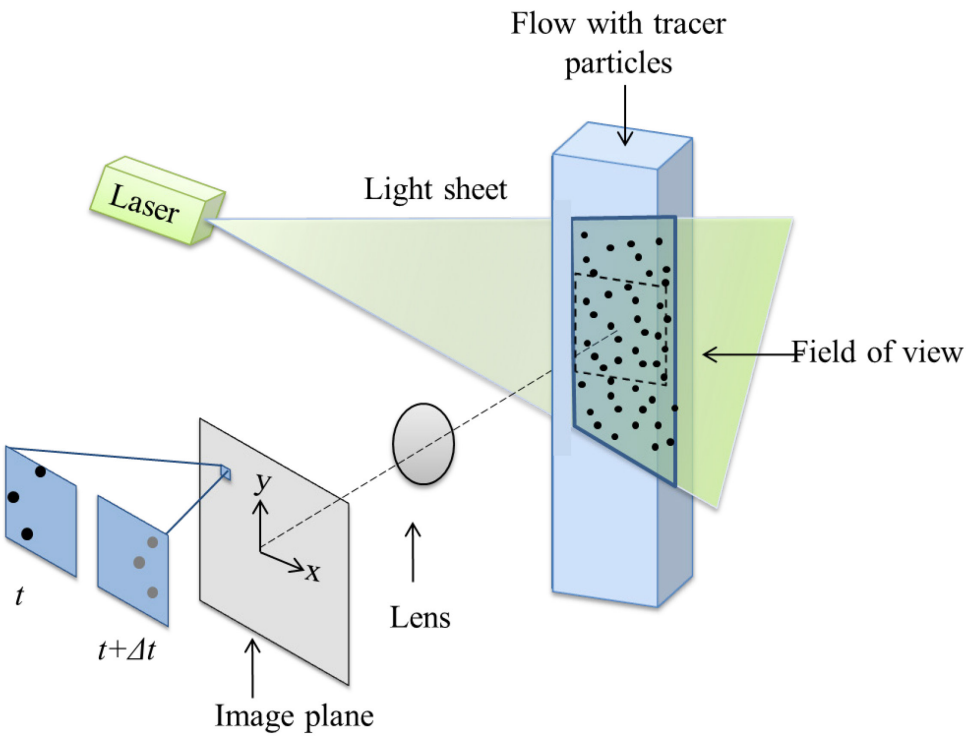

Figure 1-5. Schematic showing experimental setup for particle image velocimetry

Micro-PIV (μPIV) is a method used to study the velocity field of flow through micro and mini scale channels. The measurement principles are the same as PIV and the velocity of the fluid is determined using the displacement of the tracing particles. In this setup, microscope objective is used to focus on the region of interest. Using the objective lens the region of investigation can be as small as $50 \times 50\ \mu m^2$. The tracer particles used in this setup have diameter of 200 nm to 2 μm. in order to find the displacement of the particles all tracer particles will be illuminated in volume of the fluid and only the particles which are in focus will be collected by objective lens [73].

1.7 Objectives

Based on works that were so far reported in the literature, some gaps have been identified in the study of velocity profile for flows of Newtonian and non-Newtonian fluids through rectangular microchannels and orifices. The aim of this research was to identify the effect of important parameters such as geometry, and rheology of the fluid, on the velocity distribution and determining rheological parameters from the velocity profile. The current work included two different experimental studies for: (1) flow through micro-channels; and (2) flow through keystone slots.

The velocity profiles of Newtonian and non-Newtonian flows through micro-channel were used to identify the effect of flowrate and rheology on the velocity field. The fluid's rheological parameters such as flow index were also determined by using its velocity profile and the results were compared with those from rheological measurement.

The flow of Newtonian and non-Newtonian fluids through slots used in SAGD slotted liners was studied to investigate the effect of slot geometry, rheology, and flow rate on the velocity profile. The results of this experiment were used to identify the optimum geometry that could minimize scaling in slotted liners used for SAGD process. The pressure field for the flow through slots was also determined by making used of the velocity distribution results.

1.8 Thesis Outline

The thesis includes 5 chapters and 3 appendices. Brief descriptions for the chapters that follow are highlighted below.

Chapter 2- Experimental setup

This chapter provides the details of experimental setup and flow cell design to study the velocity field of flow through mini-channel and slots. The processing procedure of the experimental results is described in sections contained in the chapter.

Chapter 3- Rheology of polyacrylamide solution

In this chapter a standard procedure of the preparation of a polyacrylamide solution used for the test non-Newtonian solution is described. The polyacrylamide rheology and effect of different parameters such as concentration, mixing time and shelf time are discussed in detail in respective sub-sections.

Chapter 4- Results of micro-channel experiment

The effect of rheology of the fluid and the flow rate on the velocity profile flow through micro channel is presented. Determination of the rheology of the fluid based on the velocity profiles and validation of measured results is outlined.

Chapter 5- Results of Newtonian and non-Newtonian flows through keystone slots.

In this chapter PIV measurement of the velocity field of Newtonian and non-Newtonian flows is explained. The effect of geometry of the slots on the

velocity profile which was studied using seven flow cells starting from straight slot to 12° keystone slot is described.

Chapter 6- Conclusion and future work

The conclusions drawn from analyses of the experimental results are given in the last chapter of the thesis. Suggestions for the direction of future research works is also included based on the findings and concluding remarks.

Appendix A: MATLAB code for straight channel experiment

Appendix B: MATLAB code for keystone slots experiment

Appendix C: Graphs of velocity profile for straight mini-channels

Appendix D: Graphs of Flow of Newtonian and non-Newtonian flow through keystone slots

Chapter 2. Experimental Setup

2.1 Introduction

Two sets of experiment were conducted to investigate the velocity field of the flow through slotted liners in SAGD process. The aim of the first set of experiments was to investigate the effects of viscosity of the working fluid by measuring the distribution of the velocity field through a straight mini-channel. The goal of the second one was to identify the effect of slot geometry on fluid transport by mapping the velocity profile. Since the field of view of each experiment was different, two arrangements of setup were employed to study the fluid flow. Each setup of experiments was divided into two groups: the optical setup and the flow loop setup.

This chapter describes the experimentation in five sections. The first section describes the optical setup which was employed to investigate the velocity profile of the fluid flow through the mini-channel. The optical setup which was used to study the velocity field for slots is explained in the second section. In the third section the flow cell design and manufacturing method used for different cases is illustrated. Finally, description of the criteria used to select tracer particles for each case follows in the fourth section before the final section on details of the image processing procedure.

2.2 Optical setup to study the velocity field of flow through a mini-channel

Study of velocity profile of Newtonian and non-Newtonian flows through mini-channels helps to understand the flow phenomena of micro-flows. The velocity profile of fluid flow through a mini-channel can also be used to determine the rheology of a fluid. In this study, shadowgraph particle image velocimetry was adopted to find the velocity field within the channel.

A schematic of experimental setup is shown in Figure 2-1. The setup can be seen to have two parts: the optical setup and flow cell loop. The optical setup consists of a camera, LED light source and a function generator. For the measurement of the velocity field a microscopic objective lens was used on camera to capture sequence of images for the flow along the channel. A green, high current LED light source was employed in pulsed mode to freeze the motion of tracer particles. To ensure that the light intensity over the image was distributed evenly, the position of the LED, lamp collector, condenser lens, and chip were calculated to enable the use of a Köhler illumination configuration [75, 76]. The LED and camera were triggered using the function generator which was set for continuous square waves with frequencies of 90 Hz, offset of 2.5 V and amplitude of 5 Vpp.

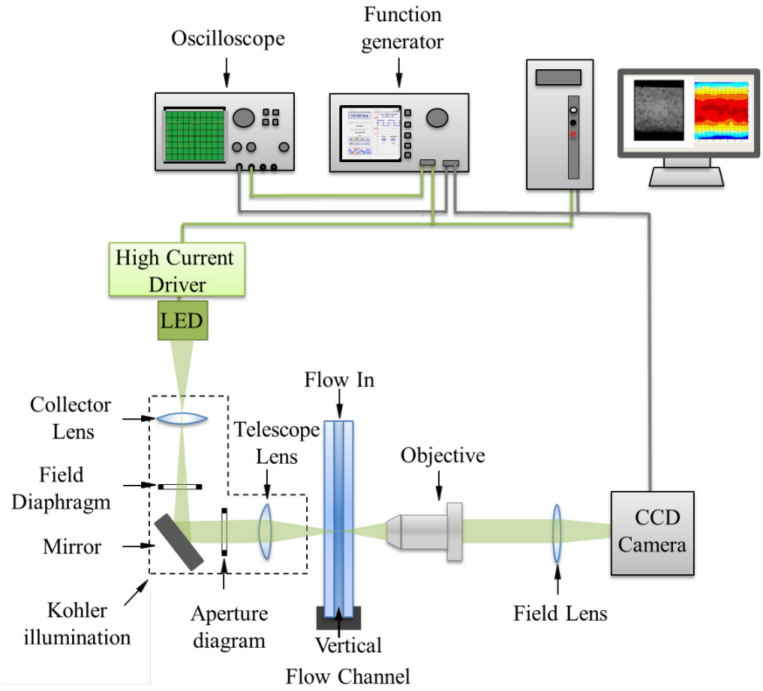

(a)

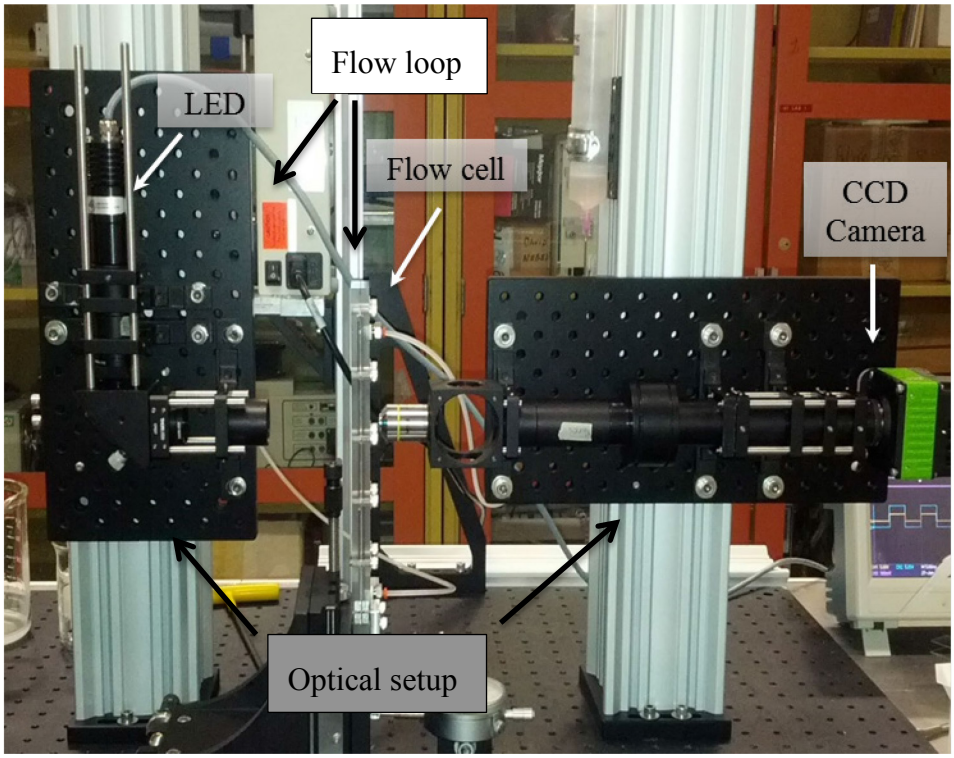

(b)

Figure 2-1. Experimental setup to study the velocity profile of flow through straight mini-channel: (a)schematic of the setup, and (b) picture of the setup

2.2.1 Camera

In order to capture the motion of the particles in the sample fluid, a CMOS camera (SP-5000M-PMCL-CX; JAI Inc.) with a maximum frame rate of 134 fps was used. In this experiment the camera was set at a frequency of the 90 fps with a resolution of 2560 × 2048 pixels to capture a time series of images. In these set of images the field of view was 26.8 × 21.4 mm and the particles have the average diameter of around 4-5 pixels.

A microscopic objective lens with magnification of ten times (10 × MPLN; Olympus, Japan) was used to focus on the region of interest. This objective lens has a 10.5 mm working distance, depth of field of 8.5 μm, and numerical aperture of 0.25. In order to make sure that the middle plane of the channel is in focus, a dial indicator was used to determine the bisector of the far and near positions of the channel window. The settings used for the camera is shown in Table 2-1.

Table 2-1.Experimental setting and specifications for camera

Resolution	2560 × 2048
Total pixels	5,242,880
Sensor type	CMOS
Maximum flow rate	134 fps
Shutter speed	10-8,000,000 μs
Frame rate used in this experiment	90 fps
Exposure mode	Timed
Exposure time	10 μs
Frame start trigger mode	on
Gain	120 units

2.2.2 LED

LED light sources have some advantages that make them more applicable than lasers for some PIV experiments. The LED light source has longer life time and it provides incoherent light. In pulsed mode systems, the LED light is more stable in time and has a constant spatial intensity distribution [78]. In this experiment the LED was coupled to a Köhler illumination configuration with the aim to provide an even distributed light across the image. The LED was used in the pulse mode with frequency of 90 Hz. The particles in each images moves around 3-4 times of their diameter so the LED flash time interval between images was short enough to freeze the motion of particle.

2.2.3 Köhler Illumination

The Köhler illumination configuration that was first described in 1893 [77] offers bright, efficient and even illumination in specimen fields. It also minimizes the internal stray light and helps to control the contrast as well as the depth of field. A schematic of a typical Köhler illumination configuration is shown in Figure 2-2 coupled to a microscope. In this arrangement, a lamp collector is in a position which focuses the light emitted from different points of the lamp to a focal point at the position of the field diaphragm. This point source of light expands in a controlled manner that fills the aperture diaphragm completely which is located in front of the condenser. The condenser was positioned to bring the illumination light into focus such that the focal plane overlaps with the focal plane of the imaging system which is positioned exactly along the optical axis of the camera [75, 77]. This results in an even distribution of light across the field of view. Specifications of the lamp collector, condenser and the specimen which were used in this experiment are summarized in Table 2-2.

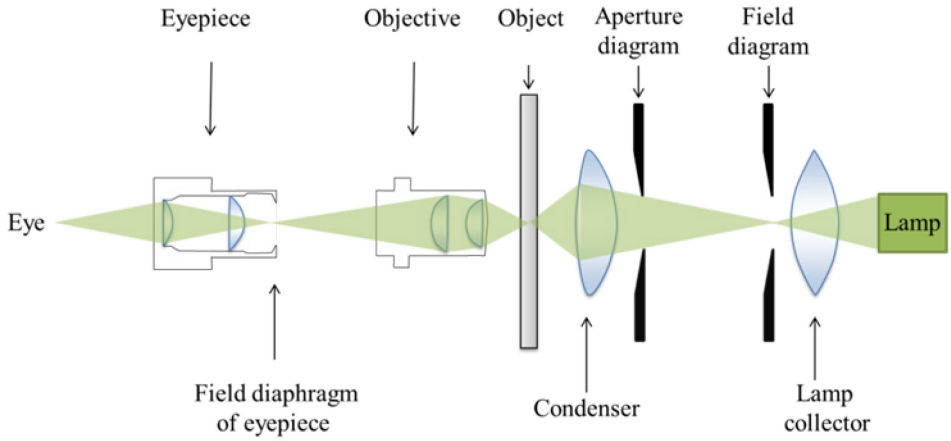

Figure 2-2. A schematic of the Köhler illumination configuration

Table 2-2.Specification of instruments in the optical setup (all units are in mm)

Diameter of lamp collector (D_{L1})	25.4
Diameter of condenser (D_{L2})	25.4
Focal length of lamp collector (FL_1)	40
Focal length of condenser(FL_2)	45
Diameter of Lamp (D_{Lamp})	17

To calculate the position of and distances between the instruments in the optical setup the following equations were used [77]:

Distance between lamp and lamp collector:

$$d_1 = FL_1\left(\frac{D_{Lamp} + D_{L2}}{D_{L2}}\right) \tag{2-1}$$

Distance between lamp collector and condenser:

$$d_2 = \frac{d_1 \times FL_1}{d_1 - FL_1} \tag{2-2}$$

Distance between condenser and spot diameter:

$$d_3 = \frac{d_2 \times FL_2}{d_2 - FL_2} \tag{2-3}$$

and, system length = $d_1 + d_2 + d_3$

Using the above equations d_1, d_2, d_3 and system length for the experiments were found to be 66.8 mm, 99.8 mm, 82 mm, and 248.5 mm, respectively.

2.3 Optical setup to study the velocity field of flow through slots

To capture the flow velocity profile through slots on the slots, an imaging system was setup as shown in Figure 2-3(a). To study the realistic SAGD process, where bitumen flows as a result of pressure drop and gravity, the flow cell was oriented to have a vertical down flow direction. The camera used all the settings for the experiment setup described in the previous section remained the same. A 50 mm lens (AF NIKKOR 50 mm 1:1.4D; Nikon) with an *f*-number of 4 and extension tube were used to capture the complete slot in the field of view. This setup had field of view of 11.25 × 9 mm. To freeze the motion of particles suspended in the flow, a green 4" × 4" side-fired LED (BX0404-520 nm; Advanced Illumination) was used in pulsed mode with frequency of 90 Hz. The LED and camera were controlled using the same settings for function generator as in the previous experiment as it is mentioned in Table 2-1. The picture of the setup is shown in Figure 2-3 (b), which shows the vertical flow cell, LED, and the camera to capture the flow through keystone slot.

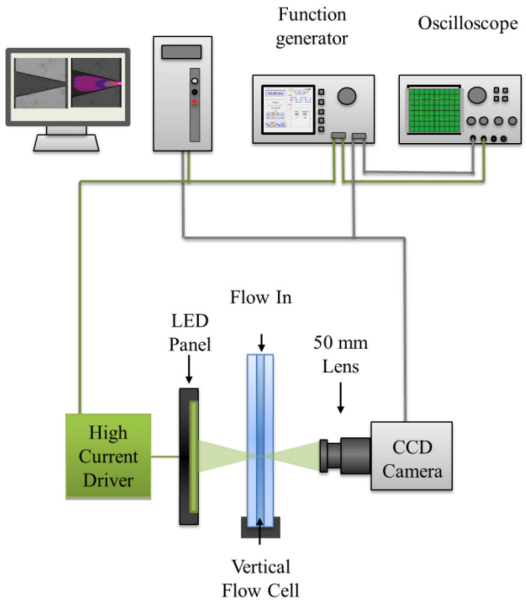

(a)

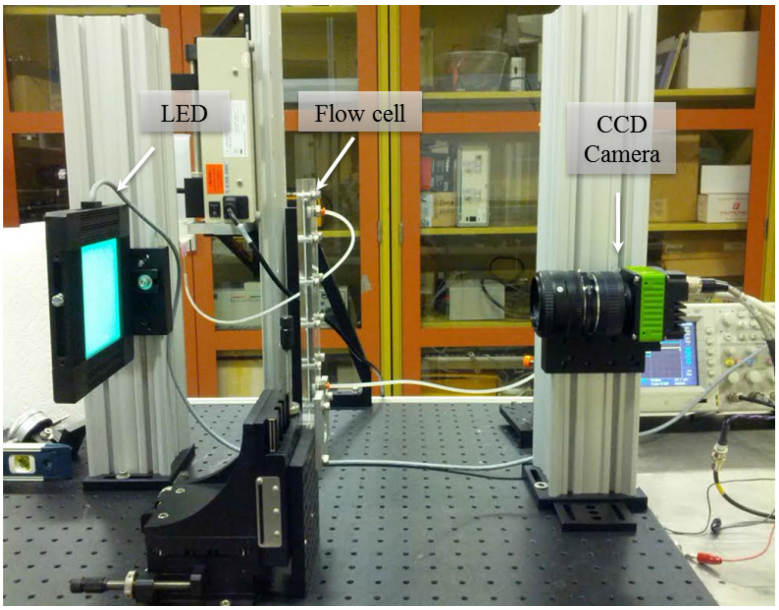

(b)

Figure 2-3. Experimental setup to study the flow velocity profile through slot, (a) schematic of the setup and (b) picture of the setup

2.4 Flow loop

The flow loop for the experiment consisted of a flow chip, connection tubes, and a pump. As shown in Figure 2-1 and Figure 2-3, the flow cells were oriented for a vertical flow direction to include the effect of gravity in the experiment. To provide consistent flow through the channel, flow was injected using a syringe pump. The flow cell was filled with the sample fluid from the bottom of the cell to ensure that it entirely filled and avoid the presence of bubbles in the system.

2.4.1 Flow cell design

The size of the slots for slots depends on the size of sand in the reservoir and the desired open area for the flow. The common ranges for width and length of slots is 0.254 - 6.35 mm (0.01″ – 0.250″) and 38.1 - 76.2 mm (1.5″ – 3″) respectively [18, 19]. As shown in Figure 1-2, two different cross-sectional shape of slots: straight and keystone where investigated.

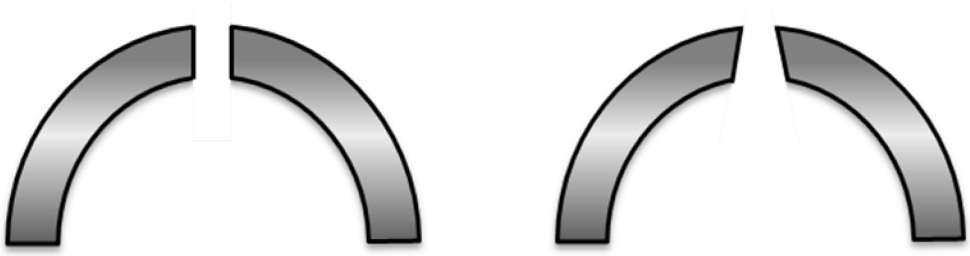

(a) (b)

Figure 2-4. Shapes of slots used in slotted liners for SAGD process
(a)straight, and (b) keystone

To reproduce the in-situ profile for use in experiments and allow excellent optical access flow cells for straight and keystone slots were designed based on the dimensions provided from the slotted liners manufacturing company (RGL Reservoir Management Inc., Nisku, Canada). Seven flow cells were solid modeled using commercial software (SolidWorks, Dassault Systèmes SolidWorks Corp.) to study the effect of slot angle of the slot on the flow velocity profile. Each flow cell consisted of 3 layers: two outer surfaces as a holder/window and an inner one as a flow channel. Figure 2-5 shows the design of the long mini-channel, straight and keystone slots. Design of a long straight mini-channel that was used to study the Newtonian and non-Newtonian velocity profile is shown in Figure 2-5 (a). Figure 2-5 (b) and (c) show the details of straight and keystone slots where θ represents slot angle. Seven flow cells with slot angles of $\theta = 0°$ (straight), 2°, 4°, 6°, 8°, 10°, and 12°, with a width of 0.5842 mm and length of 8.992 mm were designed.

In order to cut the flow cells in desired dimensions a laser cutter (VersaLaser; Universal Laser Systems) was used The laser cutter had a 50 W carbon dioxide laser with 10.6 μm angle and 0.14417 mm offset. Therefore, the offset of the laser cutter had to be considered when designing the models for the slots. The flow cells were made from transparent PMMA (1.5 mm, Optix acrylic; Plaskolit Inc.) with the thickness of 1.5 mm.

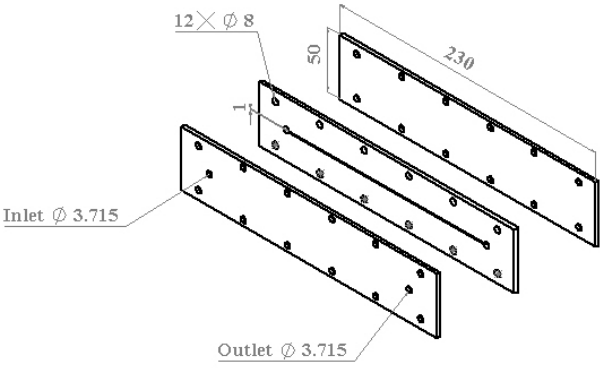

(a)

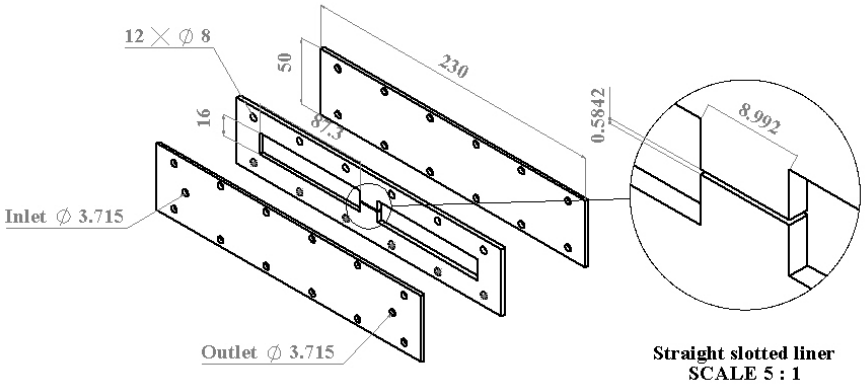

(b)

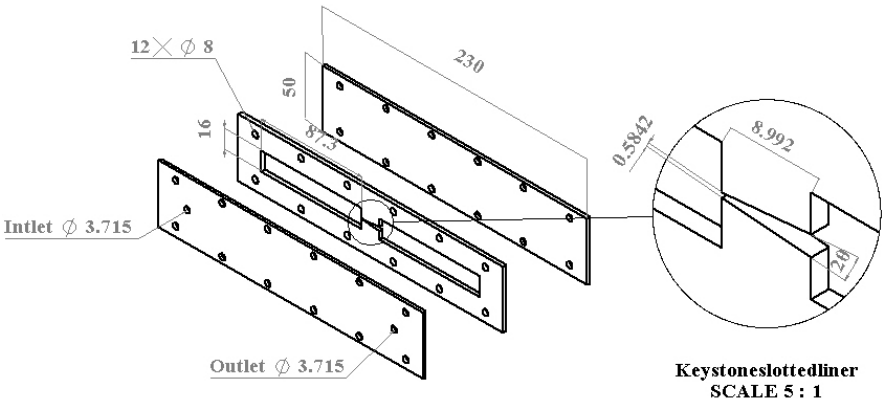

(c)

Figure 2-5. Design of the flow cells for (a) straight mini-channel (b) straight slot, and (c) keystone slot

To ensure that the laser cutter cut properly and according to desired orders, the characteristics of the drawing had to be changed from line to vector. The thickness of the lines was set at exactly 0.05 mm with 0.14417 mm offset toward the outside of sketch and the scale of the drawing was set at 1:1. The laser cutter cut the lines in order of their colors. The laser cutter was set properly to ensure that the slots were cut smoothly and it creates the sharp angles of the entrance accurately. The optimum setting for laser cutter to cut 1.5 mm PMMA sheet was 7 % of power with 60 % of full speed.

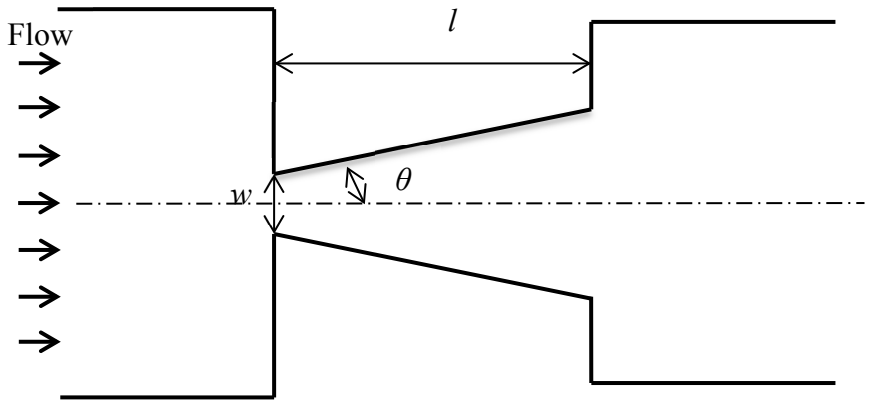

Figure 2-6. Schematic of keystone slot

The dimensions of the long mini-channel and the slots were measured after manufacturing using the imaging system. The width of straight mini-channel after calibration of the camera was found to be 0.6903 mm. However, for the case of the keystone slots as it is shown in Figure 2-6, several parameters such as the length to width ratio (l/w), the slot angle (θ) and the sharpness of the entrance of channels were considered to ensure that the geometries of prepared slots are acceptable. The picture of all flow cells for different slot angles are shown in Figure 2-7. The width to length ratio and the slot angles of slots for seven

different cases were measured using camera. The measurements are given in Table 2-3. In all cases, the entrance sharpness and alignment of the slots were captured by the imaging system. Figure 2-8 shows the entrance of θ = 6° slots as an example, in which the entrance was sharp and the entrance edges were aligned. Length to width ratio (l/w) of all flow cells were ~ 18. Due to the offset applied in the laser cutter, the lengths of channels may have a slight deviation from their desired value.

Table 2-3.Dimensions of slots after manufacturing

Slot	slot angle (θ)
Straight slot	0.03°
2 ° slot	1.82°
4 ° slot	3.79°
6 ° slot	6.06°
8 ° slot	8.21°
10 ° slot	9.78°
12 ° slot	11.98°

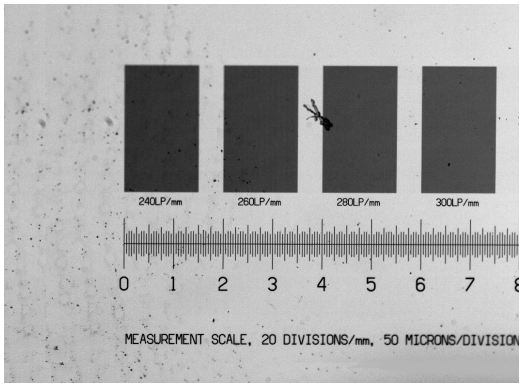

(a)

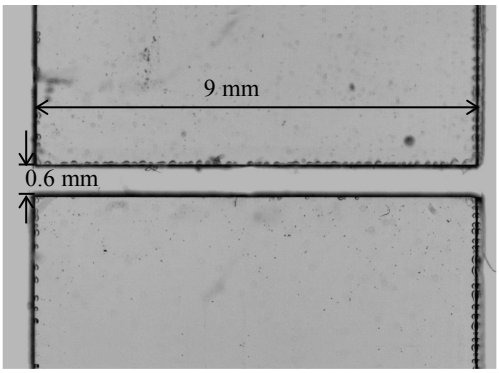

(b)

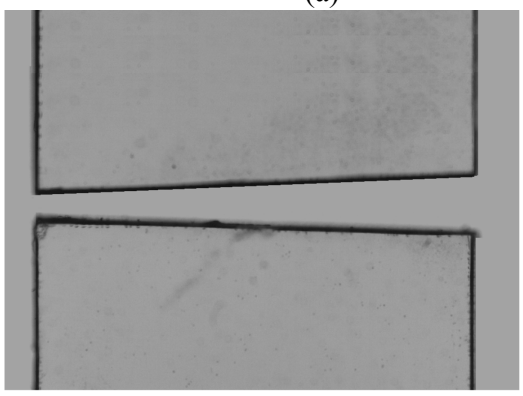

(c)

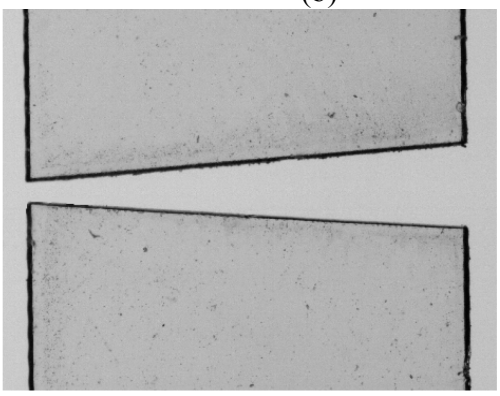

(d)

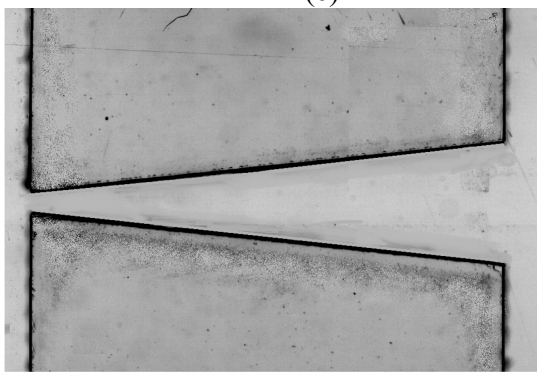

(e)

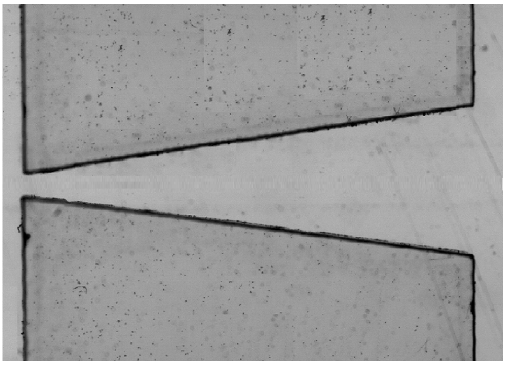

(f)

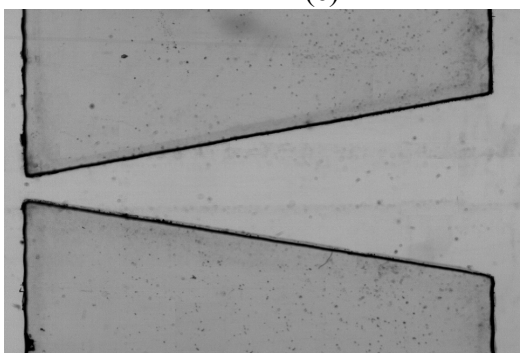

(g)

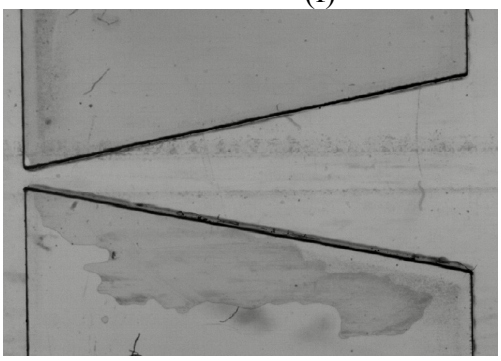

(h)

Figure 2-7. Pictures of keystone slots with different slot angles (a) Target, (b) θ = 0° (straight), (c) θ = 2°, (d) θ = 4°, (e) θ = 6°, (f) θ = 8°, (g) θ = 10°, and (g) θ = 12° keystone slot

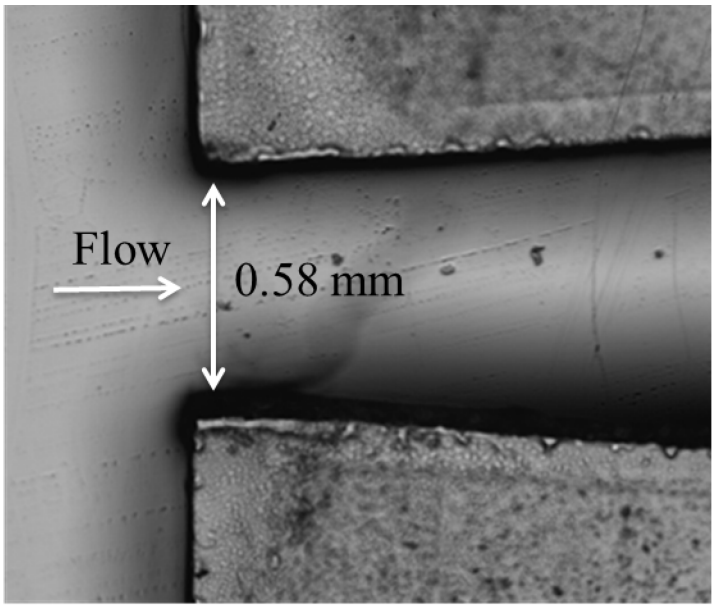

Figure 2-8. Picture of the entrance for $\theta = 6°$ keystone slot

Figure 2-9 (a) shows images of the final flow cell used to study the fluid flow through a micro-channel and Figure 2-9 (b) shows $\theta = 12°$ keystone slot flow cell. The layers of the flow cells were fixed together using twelve #10-24 hex socket cap head screws where two O-rings were placed between them to prevent leaking of the system. Push-to-connect straight adapters (Push-to-Connect Tube Fitting for Air and Water, Straight Adapter for 1/8" Tube OD X 10-32 UNF Male) were also used for the connection of inlet and outlet of the flow cell.

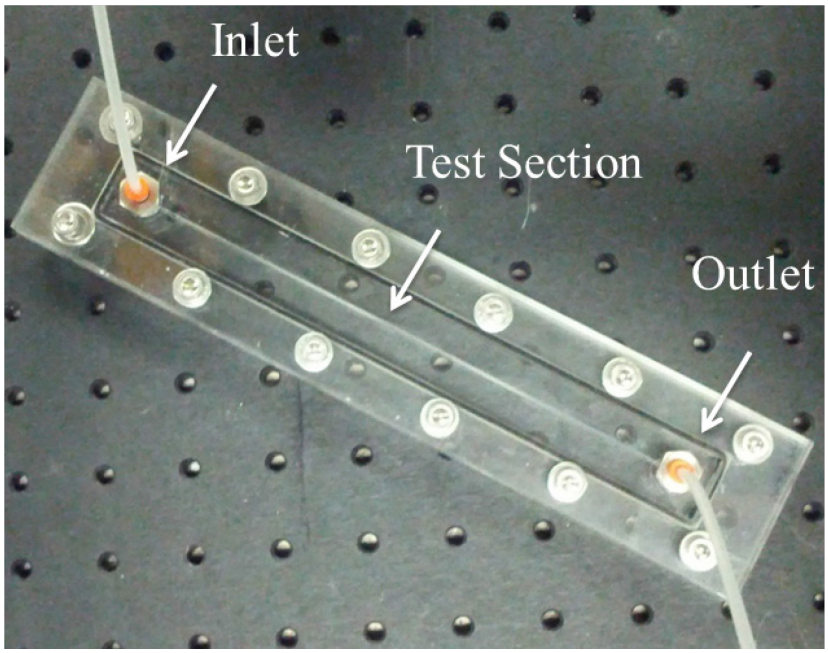

(a)

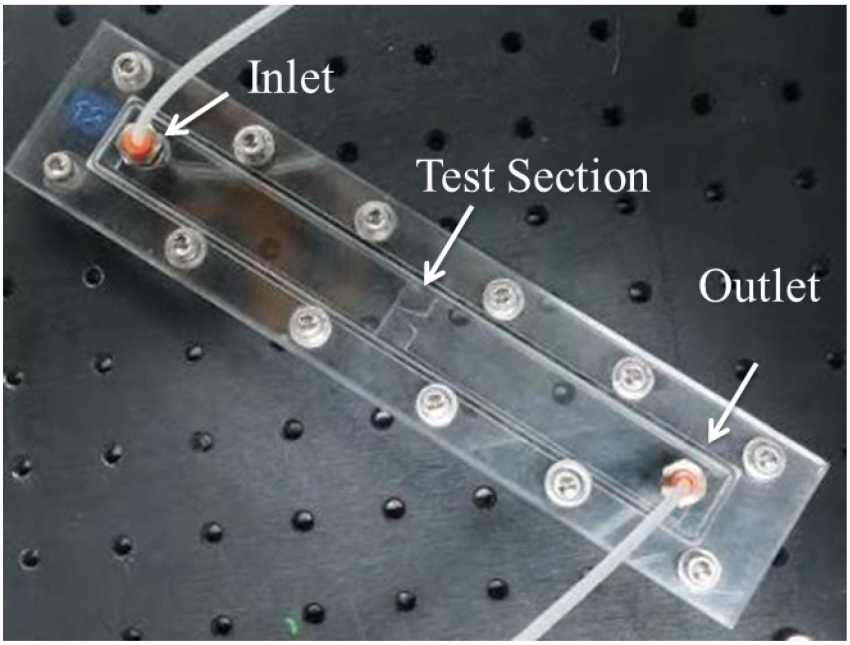

(b)

Figure 2-9. Flow cell showing the flow channel and flow inlet and outlet (a) straight mini-channel, and (b) θ =12° keystone slot

2.4.2 Control fluid and flow rate

Distilled water and different concentrations of polyacrylamide solution were used as the Newtonian and non-Newtonian fluid, respectively, to study the effect of rheology on the velocity profile. The preparation procedure of polyacrylamide solutions are described in Chapter 4. Different flow rates of fluid were studied in the experiment and the required flow rate was set on the syringe pump (PHD 2000, Harvard Apparatus) and a 1ml plastic syringe was used to inject the fluid to the flow channel.

In the case of studying the flow through mini-channels, four flow rates of Q = 0.025, 0.05, 0.075 and 0.01 ml/min were used. For the flow through slots, however, the flow rates for the experiment where calculated using operational values for real cases in SAGD process (provided by RGL Reservoir Management Inc., Nisku, Canada). It is expected that in the field the flow rate of produced bitumen varies from 20 to 160 ml/ (hr.slot). Figure 2-10 represents a straight slot used in industrial applications. A decrement of slot cross section area can be seen from the result of the manufacturing process. An average slot cross sectional area of 15.85 mm^2 was used to estimate the appropriate flow rate for the experiments. According to the measurements of slot's entrance width, the average area of the inlet was 0.9 mm^2. The minimum and maximum flow rates calculated accordingly were 1.14 ml/hr and 9.09 ml/hr, respectively. Therefore, three flow rates of Q = 1, 5.5 and 10 ml/hr were used for the experiments.

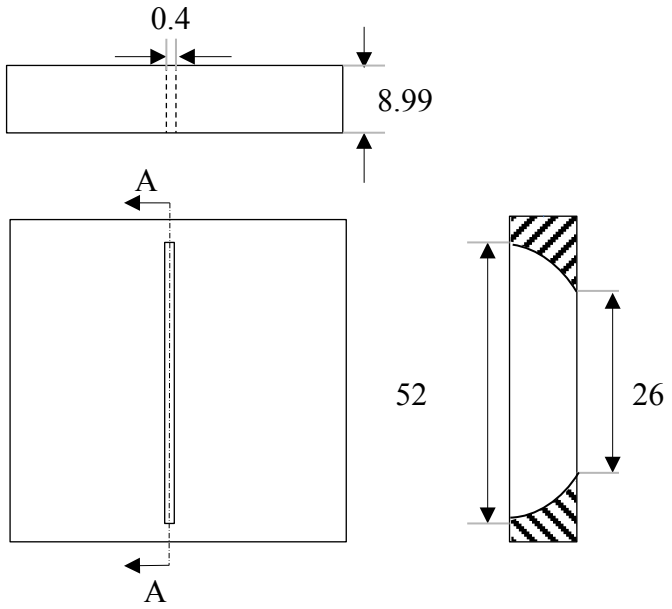

Figure 2-10. Design of straight slot in the industry (dimensions in mm)

2.5 Tracer particles

Particle image velocimetry is a non-interfering method in which the velocity field of tracer particles is measured instead of fluid velocity. It is so important to use the appropriate tracer particles to avoid any disagreements between the particles and fluid motion. Finding the suitable seeding particles depends on the nature of the fluid flow. The size of tracer particles added to the flow must have adequate image contrast. There are some criteria to select the tracer particles such as size, density of particles and camera's field of view. It is important to choose the particles which follow the motion of the fluid elements.

Seeding particles should be small enough to follow the flow and at the same time large enough to have adequate light scattering. In general, tracer particles used for gases should be much smaller than the ones for liquid flow. To obtain

optimal assessment the particles should be homogeneously distributed in the fluid. Therefore, seeding of the liquid solution can be expected to be much easier than gas solutions since it can be done only by adding and mixing sufficient amount of solid seeding particles [79]. For this work, the flow was in the liquid phase and solid sphere particles were used as tracing particles.

Density of the seeding particles used affects the velocity lag. Therefore, particles with the same density of the fluid should be used to make sure that the particles are suspended in the fluid. Velocity lag in gas flows will be higher than liquid flows due to the difference between the density of the bulk flow and the tracing particles [79, 81].

In this study flow in the liquid phase was studied in both sets of experiments required solid tracer particles. In order to achieve suitable tracing, different seeding particles were used in each experiment depending on the field of view. To study fluid flow through mini-channels with a small field of view, 1 μm fluorescent particles were used to have 1-2 pixels size in the images for individual particles. For large field of view images, 18 μm particles were used.

2.5.1 1μm fluorescent particles

Dyed red aqueous fluorescent particles (R0100, Thermoscientific Company) with mean diameter of 1μm were used as tracer particles in the study of flow through mini-channels. Specifications of these fluorescent beads are summarized in Table 2-4. An image of the water/tracer particle solution in the mini-channels is

shown in Figure 2-11. This highlights the uniformity and homogeneity of the suspended tracer particles in the solution.

Table 2-4. Properties of fluorescent particles

Colour	Red
Composition	Polystyrene
Diameter (Metric) Mean	1.0 μm
Dye Type	Fire fli Fluorescent Red (542/612 nm)
Density	1.05 g/cc
Refractive Index at 25°C	1.59 at 589 nm

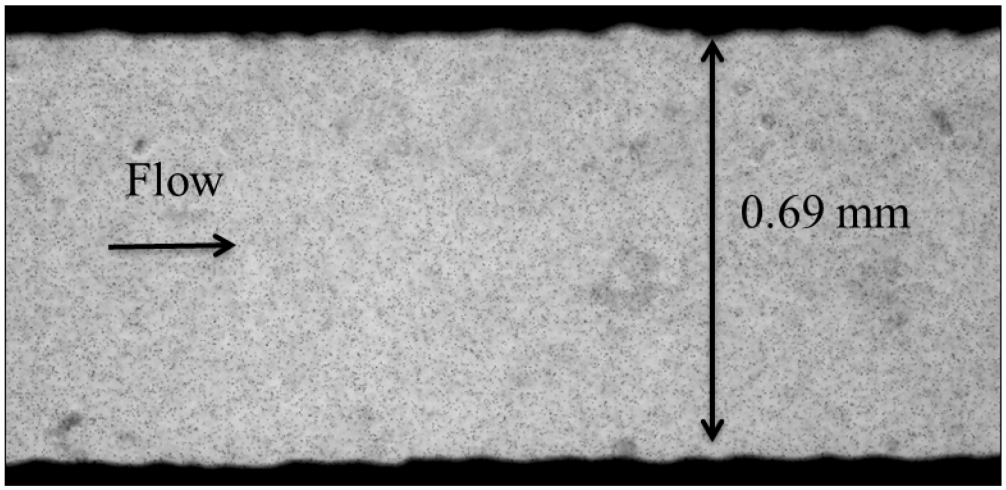

Figure 2-11. Picture of tracer particle suspended in the fluid flowing through mini-channel

In order to make sure that the particles are suspended in the fluid the settling velocity of the particles was calculated using the equation below

$$v_s = \frac{g(\rho_p - \rho_f)D_p^2}{18\mu_f} \quad (2\text{-}4)$$

where v_s is the settling velocity, g is gravitational constant, ρ_p and ρ_f are the density of the particle and fluid, respectively, D_p is the diameter of the particle, and μ_f is the viscosity of fluid.

The settling velocity of the 1 μm particles suspended in water was calculated to be 3.055×10^{-8} m/s according to the properties listed in Table 2-4, and taking density and viscosity of water at 25 ℃ ($\rho_f = 1000$ kg/m^3 and $\mu_f = 0.000891$ kg/m.s). With the frame rate of the camera at 90 fps, the movement of the particles in the fluid as a result of particle settling was 3.39×10^{-4} μm /frame. This is significantly much smaller than the movement of the particle in one frame due to the fluid motion (~4 μm/frame). It was therefore concluded that the particles will follow the flow.

2.5.2 Hollow glass sphere particles with mean diameter of 18 μm

To study the flow through different cases of slots, hollow non-porous microspheres were used (110P18, Potters Industries LLC, USA). The particles specifications are summarized in Table 2-5. To make the tracer particles evenly distributed in the fluid, particles were first mixed with the fluid and then left to stand/sediment for 1 hour. During this time light particle separated to the top of

the container and heavy particles to the bottom. The fluid in the middle was then sampled as the particles used as an experimental fluid. Figure 2-12 shows an image of tracer particles and the fluid through $\theta = 6°$ slot as a sample. As it is shown in the figure, the particles were evenly distributed.

Table 2-5. Properties of 18μm particles

Color	White
Composition	Fused Borosilicate Glass (ASTM C169)
Diameter (Metric) Mean	18.0 μm
Density	1.10 ± 0.05 g/cc
Maximum working Pressure	10000 psi

The settling velocity of the particles in the water solution was calculated using (2-4) and the properties of the particle given in Table 2-5. The settling velocity for the 18 μm particles was 1.97×10^{-5} m/s, representing 0.218 μm movements in each frame. Movement as a result of flow rate of the fluid was ~ 4 times the diameter of the particle (~72 μm). The movement of the particle due to settling was therefore much smaller than the motion due to the fluid flow. This confirmed that the particles followed the flow and were unaffected by gravity.

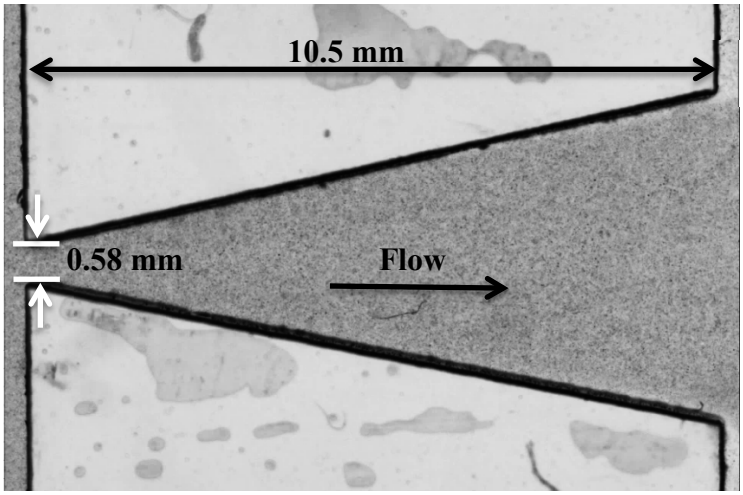

Figure 2-12. Picture of tracer particle suspended in the fluid flowing through keystone slot

2.5.3 Image preprocessing:

Intensity variation in the image has an effect on the correlation signals. The brightness of the particles, the uniformity of the illumination, irregular particle shape and out-of-plane motion affect the prominence of the correlation peak. Therefore, image improvement before its processing is necessary. The aim of preprocessing of images is to improve the image contrast and make the intensity of the particles to the same level.

The first step in preprocessing in shadowgraph PIV is to invert the raw image shown in Figure 2-13 (a) to make the background dark and the particles bright as shown in Figure 2-13 (b). A geometric mask was then applied to decrease the noise of background. A non-linear filter with a sliding minimum algorithm was applied with 4×4 pixels window size to subtract the minimum intensity from each window. The resultant image as shown in Figure 2-13 (b) was then ready for PIV processing.

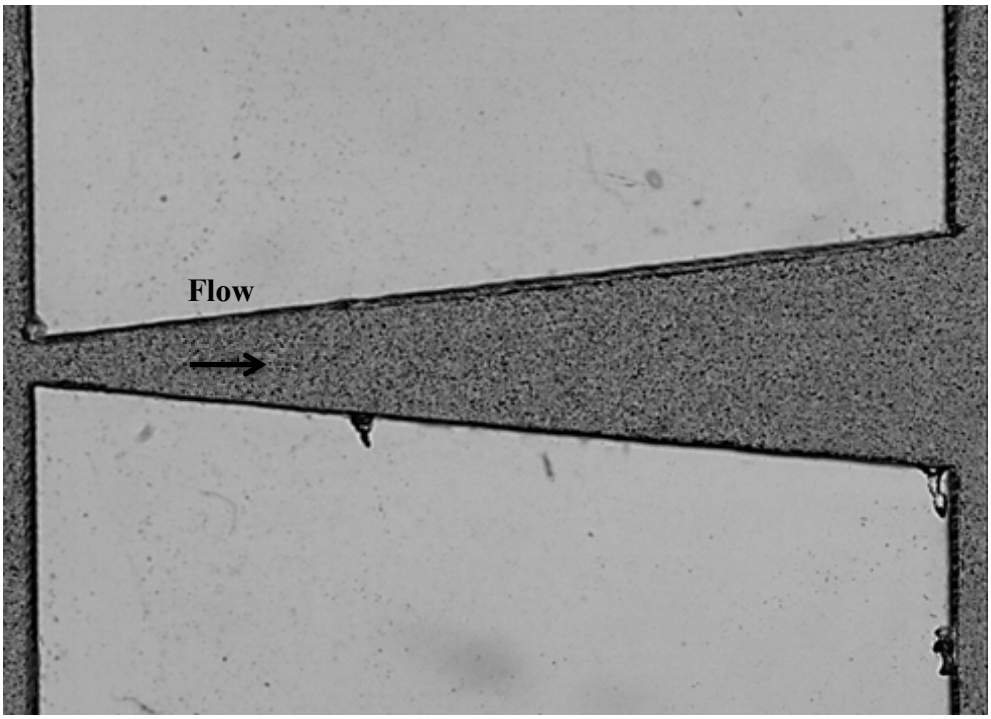

(a)

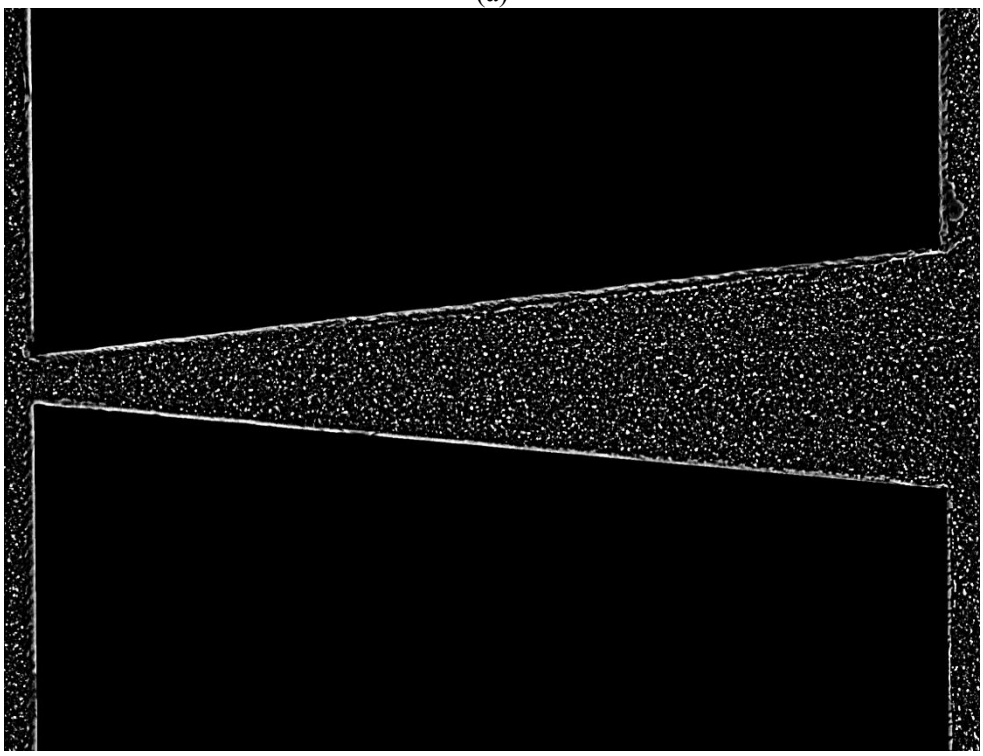

(b)

Figure 2-13. Images of keystone slot used for PIV analyses

(a) raw image, and (b) inverted PIV image with geometric mask

2.5.4 Processing

After applying proper preprocessing procedure a multi-pass sequential cross-correlation algorithm (DaVis 8.2, LaVision GmbH) was used to determine the velocity vectors from the images with decreasing window size. For the first interrogation window, 64 × 64 pixels with 87% overlap was used, while the second pass had window size of 32 × 32 pixels with 87% overlap. Two different cases of a window weighting function with shape of square 1:1 and elliptical 4:1 were studied to see the effect of window shape on the resolution of the flow field on the wall of the slot. The results were the same between the elliptical and square shapes in this experiment as it is shown in Figure 2-14. Therefore, square window shape was selected to process the images since the processing time was much shorter than elliptical one.

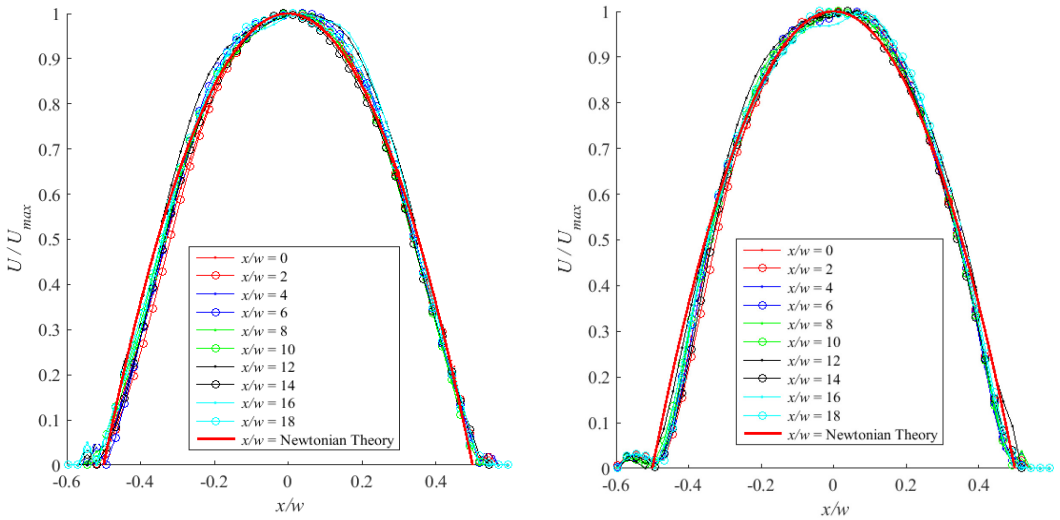

(a) (b)

Figure 2-14.Velocity profile of water through straight slot using (a) square 1:1 and (b) elliptical 4:1 interrogation window shape

2.5.5 Post processing:

In the post processing of the images, the data was smoothed and out-lier vectors remove to provide smooth vector plots. The average of the processed vector fields was obtained using the statistics tool in the software. In case of straight mini-channel the results used the average of 500 images, and in case of keystone slots the final velocity profiles were obtained by averaging 200 images.

To apply a further post processing operation, four different processing codes were developed to do the post processing of the data using commercial software (MATLAB The Mathworks Inc.). The first code (Appendix A-1 and B-3) plotted the average velocity vector map of the straight mini-channel in a normalized scale. In this plot the velocity was normalized based on the maximum velocity in the channel and the length of the channel was normalized according to the entrance width. An example of processed velocity vector maps for the flow of water through straight mini-channel, and $\theta = 10°$ keystone slot are shown in Figure 2-15 (a) and (b). All the vectors of the flow in the *y* direction and 1 out of 7 vectors in the *x* direction are shown in Figure 2-15 (a). In case of keystone slots half of the vectors in *y* direction and 1 out of 35 of vectors in *x* direction are represented.

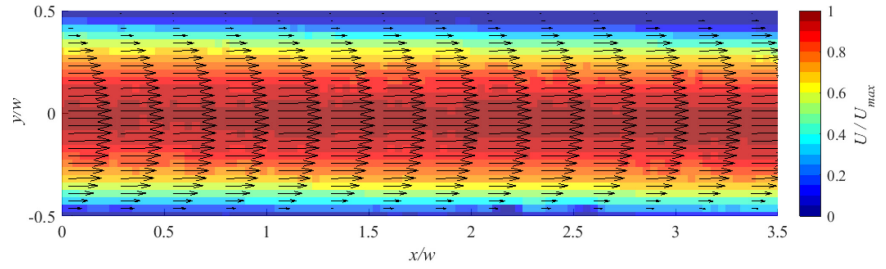

(a)

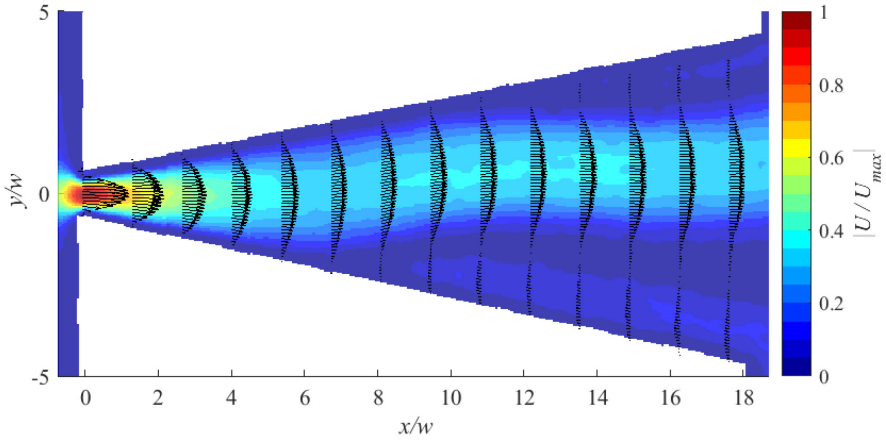

(b)

Figure 2-15. Velocity vector map for water flow through (a) straight mini-channel and (b) θ =10° keystone slot

The second code (Appendix A-1) plotted the normalized velocity profiles of the Newtonian and non-Newtonian fluids through mini-channel to compare them with corresponding theory. Figure 2-16 (a) shows an example of the normalized velocity profile of water through mini-channel in compare with the Newtonian theory, and Figure 2-16 (b) shows the velocity profile of 0.1 wt. % polyacrylamide solution at the middle of channel and the non-Newtonian theory.

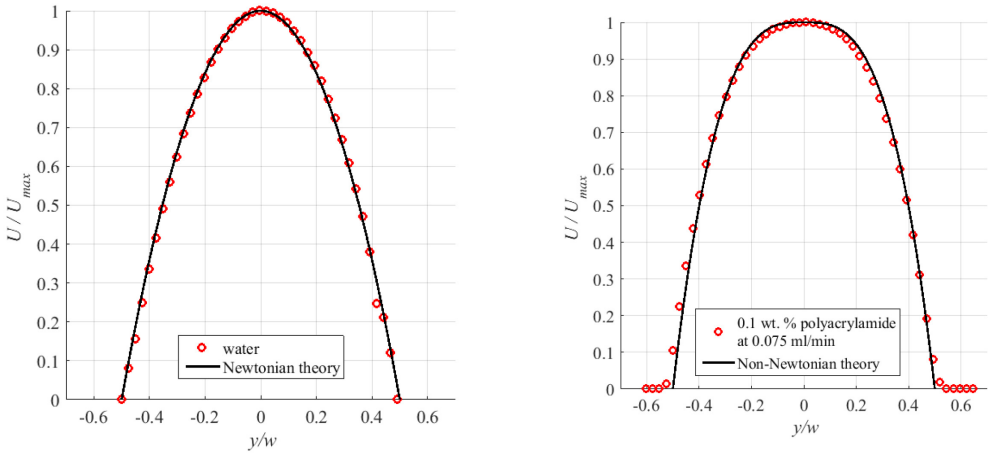

(a) (b)

Figure 2-16. Plots for comparison of average velocity profile of (a)water with Newtonian theory, (b)0.1 wt. % polyacrylamide solution with non-Newtonian theory at Q =0.075 ml/min

The third one (Appendix B-1 and B-2) plotted the velocity profiles of Newtonian and non-Newtonian fluids at ten locations beginning from the inlet of the channel as it is shown in Figure 2-16. In these plots the velocity was obtained from the velocity and length of the slot which was normalized based on the maximum velocity, and width of the channel at the specific position, respectively Details of the procedure followed in the plotting are given in Section 5.2.

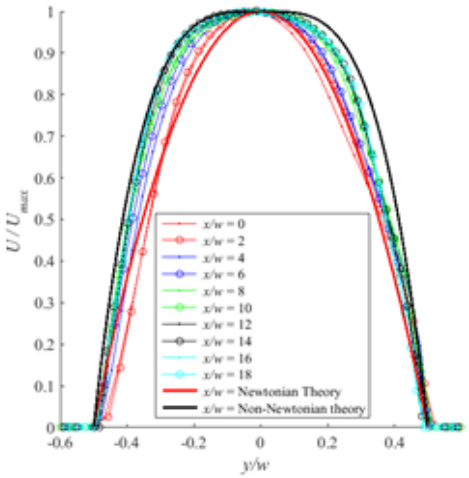

Figure 2-17. velcoity profile of 0.2 wt. %polyacrylamide flow through θ =2° slot at flow rate of 10 ml/hr in compare to Newtonian and non-Newtonian theory

2.6 Uncertainty analysis

There are some factors that should be considered to increase the uncertainty of results from PIV measurement including illumination and the distribution and concentration of particles. In PIV measurement, in order to freeze the motion of tracer particles in the flow field, the duration of the illumination light should be significantly short. The time delay between the pulses should be long to have an adequate particle displacement between the images. However, this delay should be appropriately set to prevent the particles moving out-of-plane leaving the focal plane of the camera. The focus on the camera should also be set to the middle of the flow channel.

One of the more important factors and assumptions in PIV is that the particles follow the flow. In order to confirm this, the settling velocities of the particles used for both experiments were calculated. The displacements of tracer particles in the flow as a result of the settling velocity were 3.39×10^{-4} μm and 0.218 μm in a single frame for 1 μm and 18 μm particles, respectively. The comparison of the movement due to settling and the fluid movement which are ~4 μm and ~72 μm for 1 μm and 18 μm particles, respectively, showed that the movement of the particles due to the settling velocity is significantly small.

The processing interrogation window size is another factor that should be considered as one of the sources for uncertainty. In order to have acceptable results different processing procedures and different window sizes were utilized to find the velocity profile of the flow. The details of the velocity processing procedure are described in the corresponding sections of Chapters 3 and 5.

For suitable averaging of the velocity field the number of the images collected should be enough so that the average has converged. Figure 2-18 shows the average velocities of random sample of images plotted against the number of images. The total average velocity line was used to examine the convergence of the average. Based on the plot it was seen that the average velocity of the flow converged after 50 images. However, further confirmation using standard deviation and the standard error was also done.

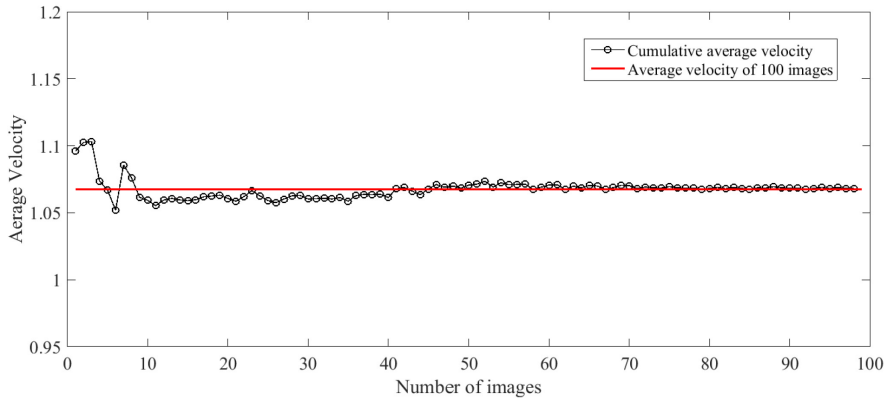

Figure 2-18. Plot of cumulative average velocity of sample images compared to the average velocity of 100 images

A random sample set of images was chosen to find the standard deviation and the standard error of the last 20% of the collected data (20 images). In order to find the standard deviation and error, the cumulative average of the flow was determined and the standard deviation was calculated using:

$$SD = \sqrt{\frac{1}{N-1}\sum_{i=1}^{N}(x_i - \overline{x})^2} \tag{2-5}$$

$$SE_{\bar{x}} = \frac{SD}{\sqrt{N}} \tag{2-6}$$

where SD is the standard deviation, $SE_{\bar{x}}$ is standard error, $\{x_1, x_2, \ldots, x_N\}$ are the observed values, N is the sample size, and $\bar{x}$ is the mean value of samples. [97].

The standard deviation for the average velocity of flow through straight channel, and keystone slots were calculated to be 0.06 %, and 0.3052 %, respectively. The standard error values were further found to be 0.0134 %, and 0.0682 % for the straight channel and keystone slots, respectively So it was concluded that the variation of the average velocity was insignificant and the size of captured images could be said to be enough.

Chapter 3. Rheology of Polyacrylamide Solution

Polyacrylamide in solution form has been used for different applications in various industries such as oil production, acid stimulation treatments and wastewater treatment as a drag reducing agent and velocity profile modification [82, 83]. This solution has been shown to have shear thinning, non-Newtonian behavior [85] making it a potential candidate as a working fluid for the current research. It is a transparent fluid which has a viscosity higher than water. The transparency of polyacrylamide solution makes it an appropriate fluid for application in PIV measurements. To use a polyacrylamide solution its rheology needs to be well known as it is a function of polymer concentration.

The most essential parameter to illustrate the behavior of polyacrylamide solution is its viscosity. There are several factors that can affect the viscosity of polyacrylamide solution such as temperature, pressure, concentration, and time [82- 92]. Effects of different parameters on viscosity of polyacrylamide solution have been studied over different ranges and conditions. Temperature has the most profound effect on viscosity of polyacrylamide solution while the effects from pressure and time are important but less significant [82- 92].

The effect of temperature on the viscosity of polyacrylamide solution was studied [83- 86] and it was found that the polyacrylamide solution behaved as a non-Newtonian fluid. Experiments revealed that at low shear rates, temperature

had more effect on viscosity of the polyacrylamide solution while at higher shear rates the effect was negligible [84]. The effect of pressure on viscosity showed that, at constant concentration and shear rate, the viscosity curve increased exponentially by increasing pressure [83].

The viscosity of polyacrylamide solution is not stable at room temperature [13]. Since there was not enough evidence to support the effect of shelf time on the viscosity of polyacrylamide solution, the effects of shear stress, concentration and shelf time on the viscosity of polyacrylamide solution were included in this study. The following sections of this chapter present details. The results investigated the rheology of a polyacrylamide solution to be used in further work.

3.1 Chemical properties of polyacrylamide

Polyacrylamide is a polymer of high molecular weight made up of acrylamide subunits which is essentially non-ionic and needs to be copolymerized with other monomers to produce the ionic polyacrylamide [89]. Partial hydrolysis of polyacrylamide or copolymerization of acrylamide and acrylic acid produce anionic (negative charge) polyacrylamide. The cationic (positive charge) polyacrylamide is produced as a result of copolymerization of quaternary ammonium derivatives of acrylamide with acrylamide. The chemical structure of the polyacrylamide, anionic polyacrylamide and cationic polyacrylamide are shown in Figure 3-1, where A_1 is ─O─ or ─NH─, R_3 is an alkylene having 1 to 3 carbon atoms and R_4, R_5, and R_6 represent either ethyl or methyl group [88, 93].

The difference of the structure of the polyacrylamide solution will change the possibility of having a chemical reaction with other elements such as water leading to potential decrease in its shelf time.

The cationic solutions are less stable than the anionic emulsions [89]. The reason for the insatiability of the solutions is the hydrolysis of the cationic solutions with time. During hydrolysis the cationic groups get converted into anionic acrylate groups by giving an amphoteric polymer which results in reducing the cationicity of the solution. The hydrolysis of the cationic solutions makes the shelf time of the solution very short which in some cases can go to less than 10 minutes. The experiments for this study used ionic polyacrylamide solution since it was more stable than the cationic one [89].

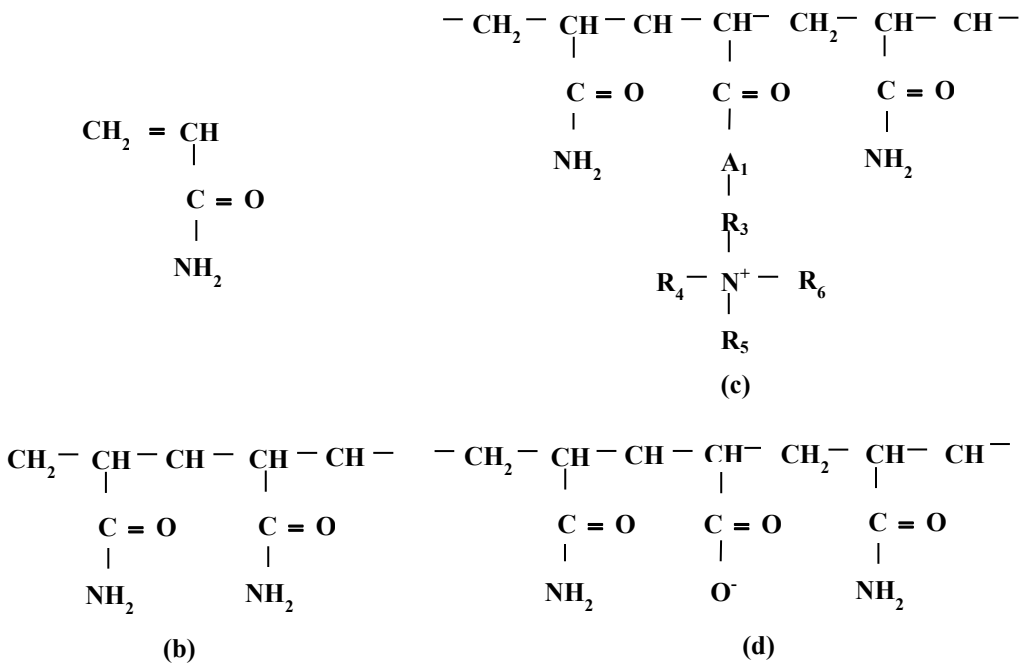

Figure 3-1. Chemical structure of (a) acrylamide, (b) polyacrylamide, (c) cationic polyacrylamide, and (d) anionic polyacrylamide[93]

3.2 Preparation of polyacrylamide solution

In order to study the effect of concentration on the rheology of hydrolyzed polyacrylamide, solutions with concentrations of 0.1 wt. % to 0.5 wt. %. with 0.1 wt. % interval were prepared. Consistency and repeatability of the sample's preparation was considered to have reliable results.

The solutions were prepared using a commercial sample of high molecular weight anionic polyacrylamide powder (BASF SE, Germany). The properties of the polyacrylamide powder are summarized in Table 3-1. The mixing procedure followed by slowly adding 0.5 g of polyacrylamide to 500ml of deionized water in order to make a solution with concentration of 0.1 wt. % (1000 ppm). The solution was then mixed for 3 hours with a magnetic stirrer at the speed of 100 rpm.

To have a satisfactory measurement and avoid the presence of bubbles in the system, a vacuum pump was used for degasification of the solution after mixing. The degasification time depended on the bubbles in the solution and the solution was degasified until all bubbles completely disappeared. After degasification the viscosity of the polymer was studied using double-gap cylinder rheometer.

Table 3-1. Properties of polyacrylamide powder used for preparation of the solution

Physical form	Off-white granular powder
Particle size	98 % <1000 μm
Bulk density	0.7 g/cm^3
pH of 1 % solution at 25 °C	7.2

3.3 Specification of the rheometer

Different types of rheometer are available for varying applications such as dynamic shear rheometer, pipe or capillary, rotational, cone, and plate and liner shear. The rotational cylinder is more applicable in the oil industry since it is suitable to find the rheology of Bingham plastics and Herschel-Bulkley solutions. In this experiment, the rheometer (Rotational Rheometer: RheolabQC, Anton Paar USA Inc.) with a double gap cylinder measuring system (DG42) was used to measure the viscosity of polyacrylamide solution [95].

A schematic of the measuring bob and cup is shown in Figure 3-2and the dimensions of the measuring cell are summarized in Table 3-2. In the double gap system, the end faces of the rings were so thin that the effect of the end could be neglected. The outer cylinder, called the cup, remained stationary and temperature control was connected to it. The inner cylinder, called the bob or rotor, was driven by a motor with defined torque value [9]. The range of shear rate and viscosity for this measuring system were 4×10^{-2} to 9×10^{3} 1/s and 10^{-4} to 7×10^{3} Pa.s, respectively.

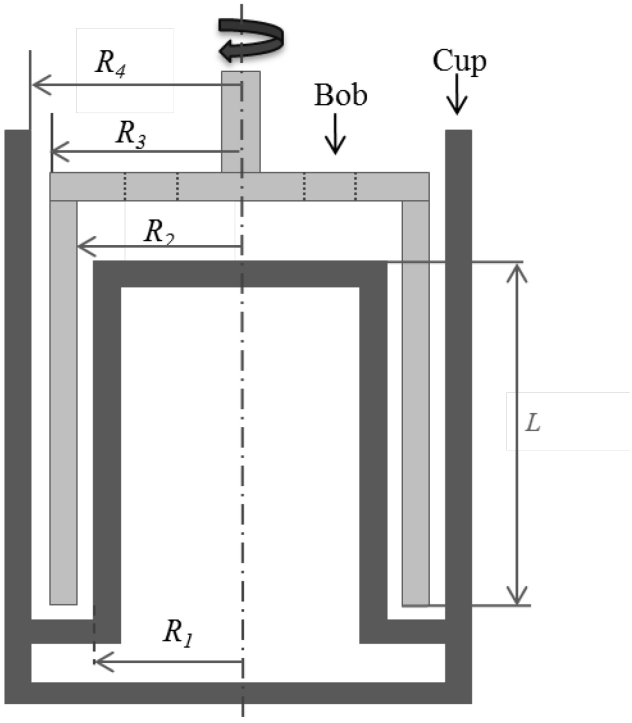

Figure 3-2. Schematic of rotational rheometer used to measure viscosity

Table 3-2-Dimensions of the measuring cup and bob of the rheometer (mm)

Internal radius of the measuring cup (R_1)	19.75
Internal radius of the measuring bob (R_2)	20.25
External radius of the measuring bob (R_3)	21.00
External radius of the measuring cup (R_4)	21.50
Effective measuring gap (L)	78.70

To study the viscosity measurement at constant temperature, a water bath was connected to the rheometer and circulated water at a set temperature in the system. The maximum variation of temperature from the set temperature during the experiment was ±0.02 °C. To avoid temperature difference between the polyacrylamide solution and the measuring cell, the solution was retained in the measuring system 10 minutes before the measurements began.

Commercial software (Rheoplus/32 V3.62, Anton Paar USA Inc.) was used to control and monitor the rheometer. This rheometer could carry out measurements with two test modes: controlled stress (CS) which could provide controlled stress input to determine shear rate and controlled rate rheometer (CR) which could control shear rate to determine shear stress. In this experiment, the yield shear stress was measured by setting the shear rate [95].

To have reliable result from the rheometer and account for its limits, the higher viscosity was measured at lower shear rate and for low viscous fluids the operating shear rate had to be set at higher level. For the polyacrylamide solution, the best range to measure the effect of shear rate on viscosity was controlled shear rate within the range of 10 to 1000 1/s.

3.4 Non-Newtonian effects of a polyacrylamide solution under shear

There are several models which illustrated the relation between shear rate, shear stress and viscosity for shear thinning and shear thickening fluids. The most common model is Ostwald-de Waele power law model [15]. According to this model, the relation between shear rate, shear stress and viscosity can be characterized by:

$$\tau = k * \gamma^n \tag{3-1}$$

$$\mu = k * \gamma^{n-1} \tag{3-2}$$

where τ is shear stress [Pa], γ is shear rate [s^{-1}], μ is viscosity [Pa.s], k is the flow consistency [$Pa.s^n$] and n is the flow index. Factors k and n can be found by curve fitting of the shear rate and shear stress data. The flow index (n) is a factor which characterizes the behavior of the fluid. For a flow of $n < 1$, the fluid has a shear thinning behavior whereas for $n > 1$ the fluid has a shear thickening behavior. While for n equal to 1, the fluid has a viscosity response that is Newtonian in nature [15].

Taking the logarithm of equations (3-1) and (3-2) such that:

$$\log(\tau) = n \log(\gamma) + \log(k) \tag{3-3}$$

$$\log(\mu) = (n-1) \log(\gamma) + \log(k) \tag{3-4}$$

show a linear relationship between shear rate, τ, and viscosity, μ. Plot of $\log(\mu)$ vs. $\log(\gamma)$ using equation (3-4) will give the slope of the graph ($n-1$) and, y-intercept, $\log(k)$.

To find the rheology of the polyacrylamide solution, its viscosity was plotted for different shear rates (10-1000 1/s) as shown in Figure 3-3. The results showed that the viscosity of polyacrylamide solution was not linear with respect to shear rate and it decreased with increasing increment of a shear rate. Hence, the results reflect polyacrylamide's behavior as a shear thinning fluid for this range of shear rate. As it is shown in Figure 3-3 (a), the plot of $\log(\mu)$ and $\log(\gamma)$ has linear relation appropriate for a power law fluid. According to Figure 3-3 (b), the shear thinning behavior of the fluid was more significant at the lower shear rate and the dependency of viscosity to shear rate decreased with increasing shear rate. It also explained why temperature has more effect at lower shear rate on the viscosity [91].

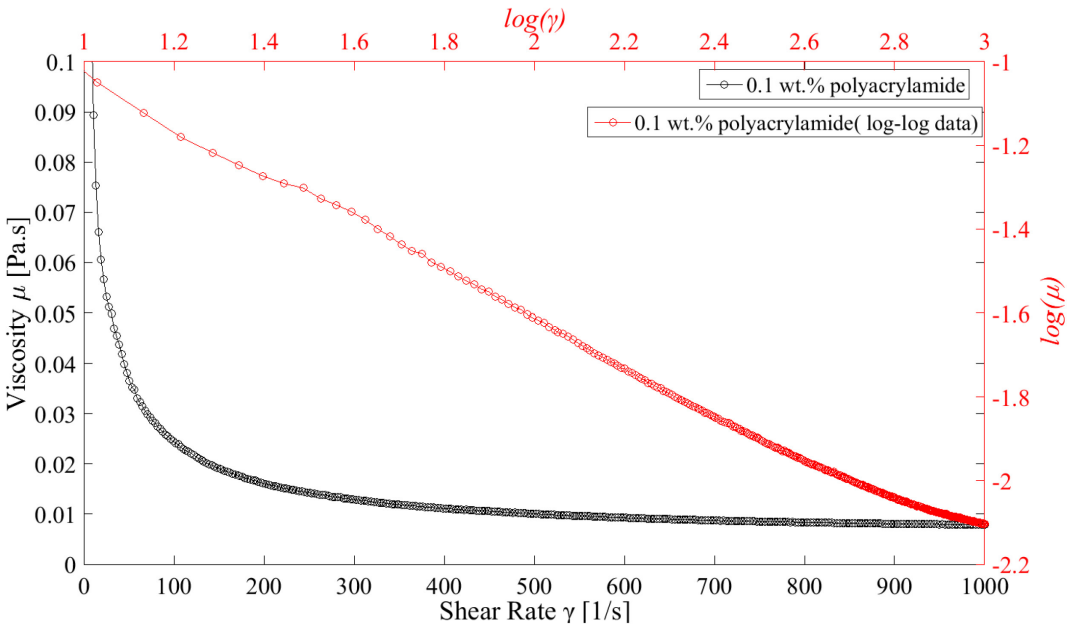

(a)

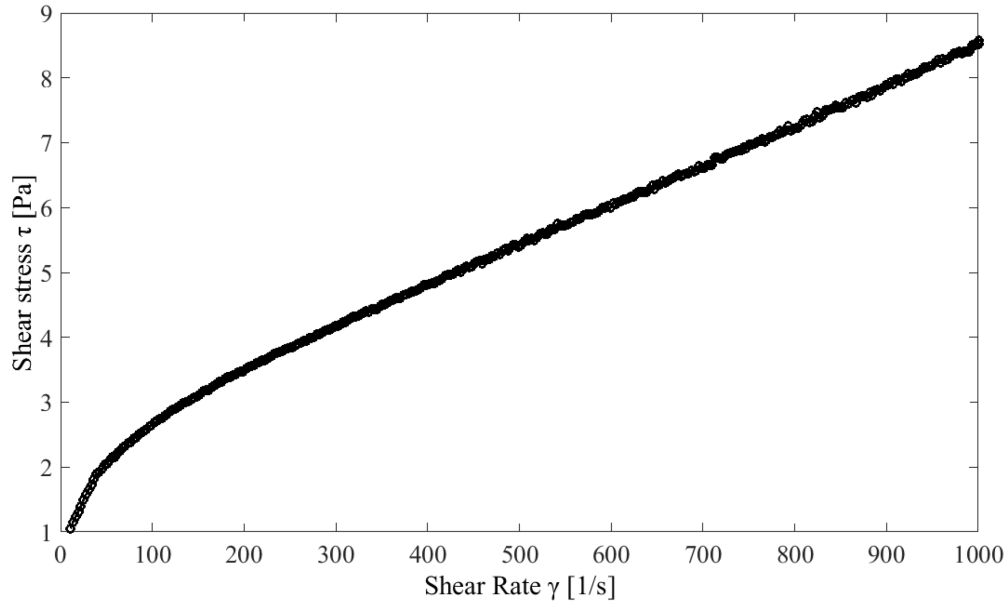

(b)

Figure 3-3. Rheological measurements for 0.1 wt. % polyacrylamide solution.(a) the variation in viscosity with the change in the shear rate, and (b) the variation in the stress with respect to the shear rate

3.5 Repeatability

The sample measurement and the preparation were studied for repeatability. In order to see the repeatability of the mixing procedure, the viscosity of two samples with the same concentration of 0.1 wt. % and preparation procedure was measured. The condition of both measurements was at constant temperature of 25°C and shear rate between 10 and 1000 1/s. Figure 3-4 (a) shows the viscosity measurement of two samples of polyacrylamide solution. In order to confirm the agreement between results, standard deviation and standard error of the results were calculated using equations (2-5) and (2-6).

The standard errors for the repeatability of the samples' preparation are shown in Figure 3-4 (b). It was concluded that the viscosity of the solution is same for both samples. The maximum error in the repeatability was 0.1 % and the standard deviation was 0.000121. These small values for the standard deviation and error showed that the value of the results for the two sample preparation were very close to the mean and these two results had good agreement. It was thus concluded that the procedure of mixing for polyacrylamide solution was repeatable.

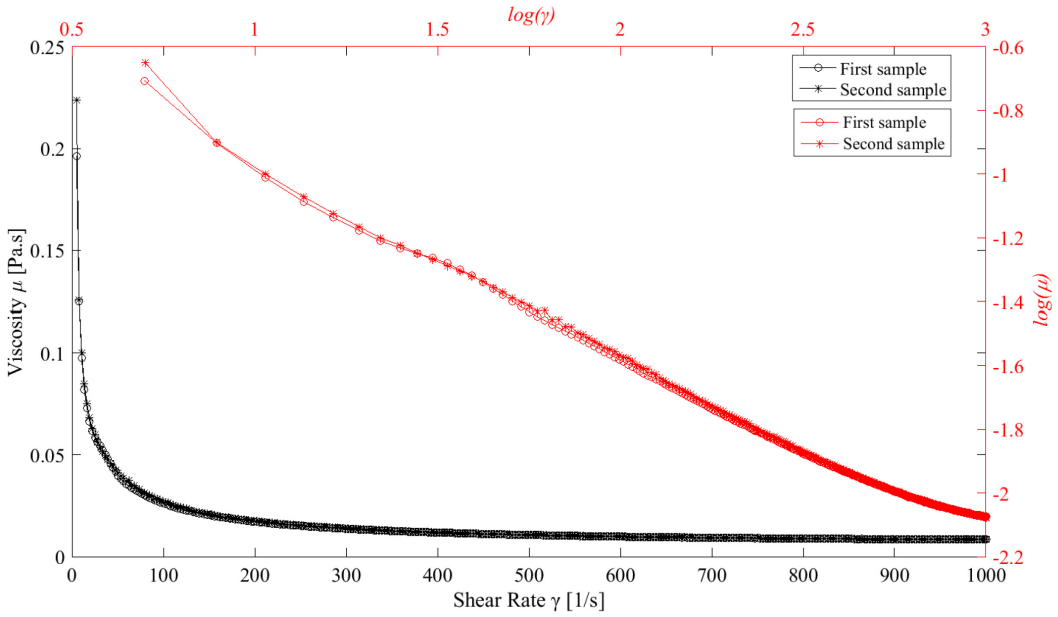

(a)

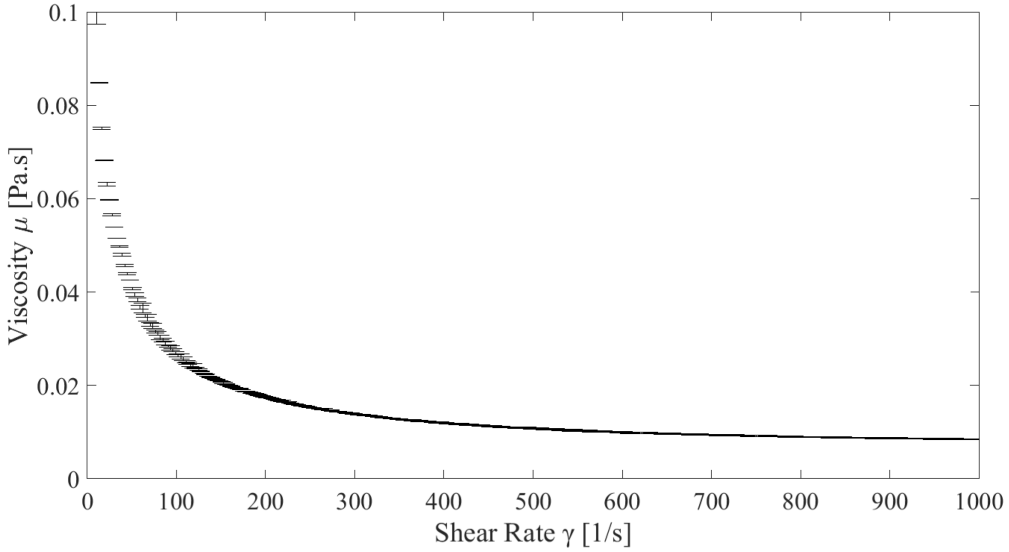

(b)

Figure 3-4. (a) Repeatability of polyacrylamide solution preparation procedure, and (b) Error of the repeatability for mixing procedure

Mixing time was another factor considered which could change the viscosity of the polymer solutions. In order to make sure the time of mixing was enough and the polymer particles mixed properly, polyacrylamide solution with the concentration of 0.1 wt. % prepared according to the same procedure was mixed for two sets of times - one for 3 hours and another one for 6 hours. For time of mixing, standard deviation and maximum error were found to be 0.001188 and is 0.084, respectively. According to Figure 3-5 which showed small variation in the value of the viscosity of the fluid for different mixing times, it was concluded that 3 hours was sufficient for mixing the polymer solution.

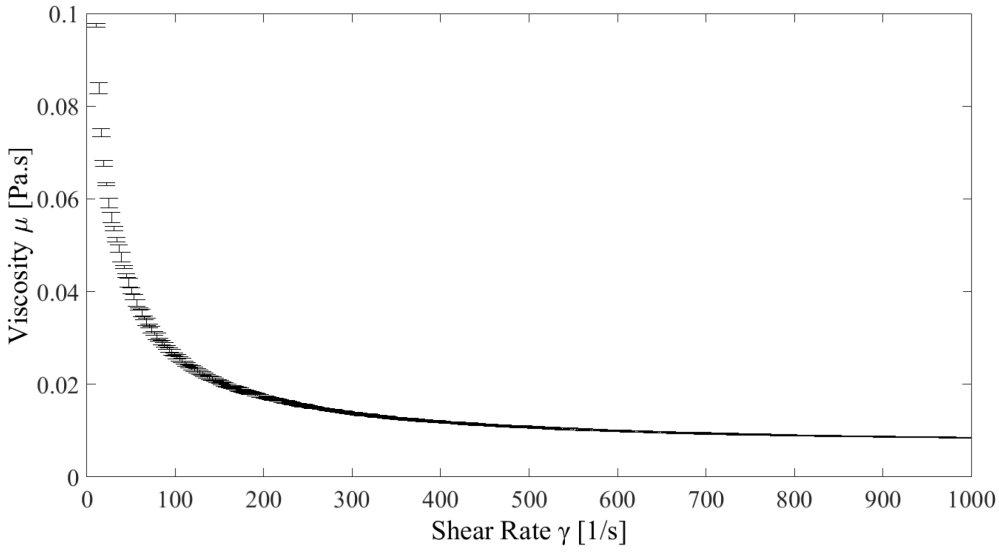

Figure 3-5 Error of the mixing time in polyacrylamide solution

3.6 Effect of concentration on the rheology of polyacrylamide solution

Concentration was also an important factor that could have an effect on the rheology and viscosity of the solution. To study the effect of polymer concentration on viscosity and the flow index (*n*) of fluid, five concentrations of polyacrylamide solutions were studied. The viscosities of sample with 0.1 wt. %, 0.2 wt. %, 0.3 wt. %, 0.4 wt. %, and 0.5 wt. % of polyacrylamide solution were measured at shear rate of 10 to 1000 1/s.

Figure 3-6 shows that all samples have shear thinning behavior. Also, the viscosity of the polyacrylamide solutions increased with increasing concentration. Figure 3-6 (b) shows the linear relation of $\log(\mu)$ and $\log(\gamma)$ for all concentration; however the slope of each concentration is different. The absolute value of slope is highest in case of 0.5 wt. % polyacrylamide and it decreases by decreasing the concentration which shows flow index (*n*) of the higher concentration is less than the one for lower concentration.

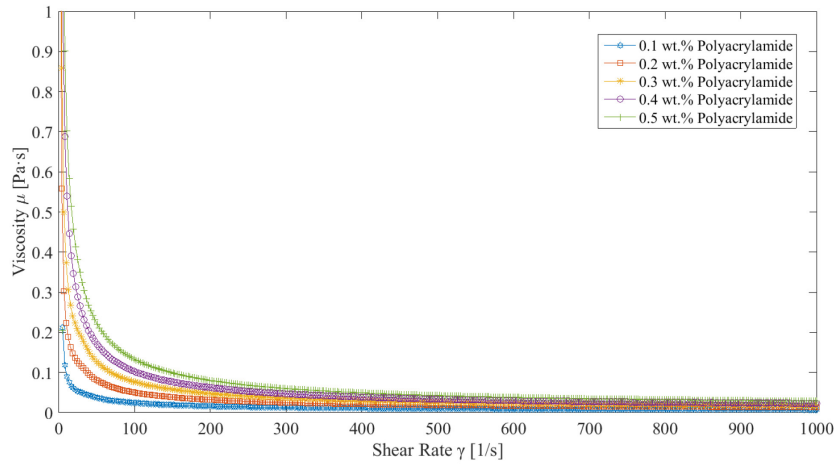

(a)

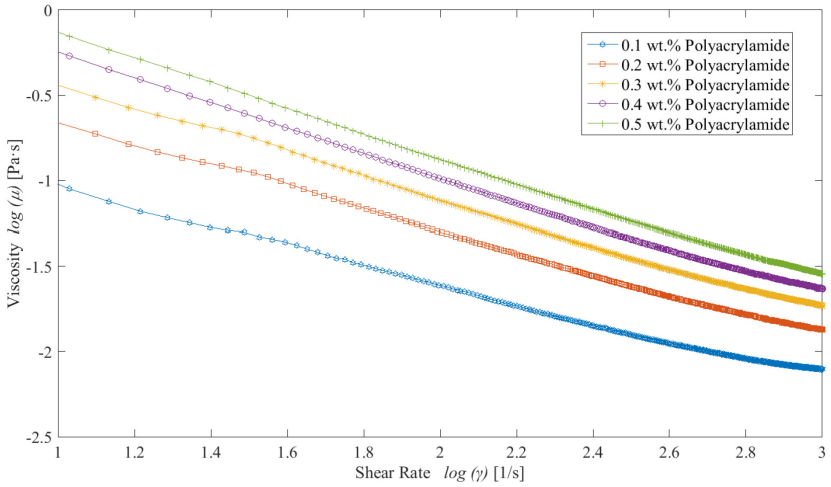

(b)

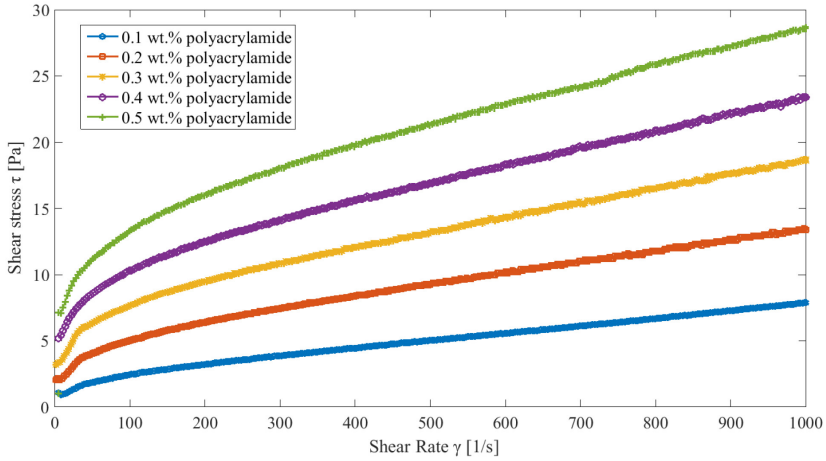

(c)

Figure 3-6. (a) variation in viscosity with the change in the shear rate for different polyacrylamide concentrations, (b) logarithm of viscosity vs. logarithm of shear rate for different polyacrylamide concentration, and (c) variation in shear stress with the change in the shear rate for different polyacrylamide concentrations

In order to compare the shear thinning behavior of different concentrations, the flow index (n) for each concentration were calculated using Ostwald-de Waele power law and the results are given in Table 3-3. As it is shown in Figure 3-7, the flow index (n) of the fluid decreased and flow consistency index increased as the concentration increased. The decrement in the flow index (n) showed that, in polyacrylamide solution, the shear thinning behavior was intensified when the concentration increased.

Table 3-3. Rheological parameters for different concentrations of polyacrylamide solution using Ostwald-de Waele power law model

Solution concentration	Flow index (n)	Flow Consistency (k)	R^2
0.1 wt.% Polyacrylamide	0.469	0.054	0.987
0.2 wt.% Polyacrylamide	0.377	0.813	0.989
0.3 wt.% Polyacrylamide	0.341	3.115	0.992
0.4 wt.% Polyacrylamide	0.323	7.112	0.992
0.5 wt.% Polyacrylamide	0.304	11.61	0.980

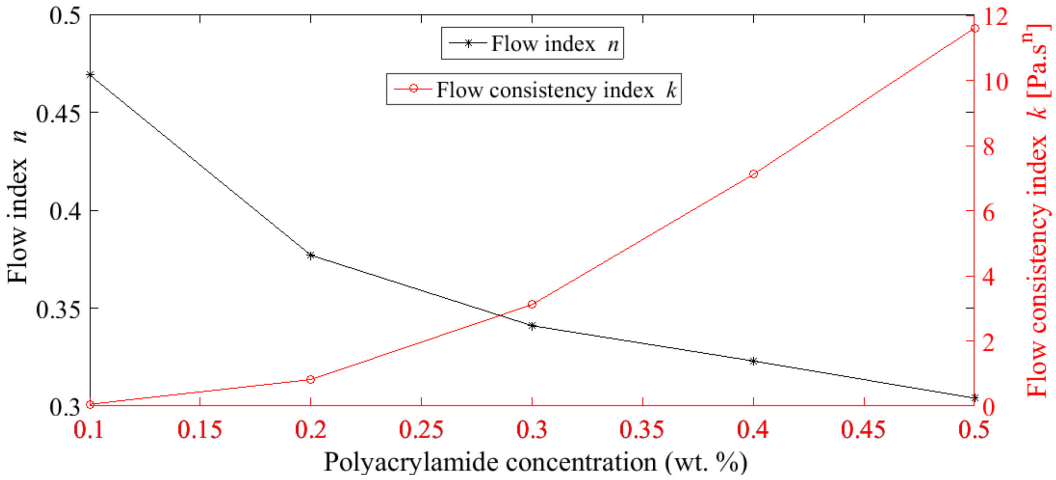

Figure 3-7. Variation in flow index (n) and flow consistency index (k) of the flow with the change in concentration of polyacrylamide solution

3.7 Effect of time on viscosity of polyacrylamide solution

The viscosity of 0.1 wt. % polyacrylamide solution was measured daily using the same rheometer for a total of 30 days. The measurement was done at shear rate between 10 and 1000 1/s at 25 °C for half an hour for each run. In order to study the viscosity, one liter of the sample was prepared at the beginning of the measurement from which 20 ml of the sample was taken for each experiment. The results of the viscosity measurement of anionic polyacrylamide solution with their error bar are shown in Figure 3-8. There was no trend which showed the increment or decrement of the viscosity at different days. Maximum calculated standard deviation and error were 0.003107 is 0.073242, respectively for this case It was concluded that the viscosity of the 0.1 wt. % anionic polyacrylamide solution did not change with time for up to 30 days.

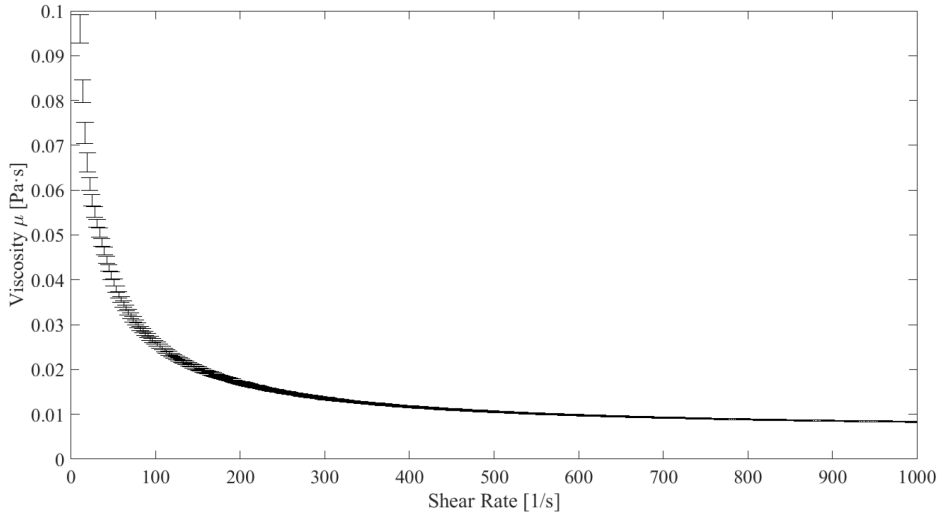

Figure 3-8. Error of variation in viscosity of 0.1 wt. % polyacrylamide solution for 30 days

3.8 Conclusion

In order to find an optimum mixing condition and solution with stable rheology for the time of this study, the rheological parameters for anionic polyacrylamide solution were measured using a commercial rheometer to investigate the effect of shear rate, mixing procedure, concentration, and shelf time.

The experimental results showed the viscosity of the polyacrylamide solution varies by shear rate. Viscosity of the fluid decreased as the shear rate increased which showed the fluid had a shear thinning behavior. This shear thinning behavior was much intense at lower flow rates and the fluid behaved as a Newtonian fluid at higher shear rates. The log-log plot of shear rate and viscosity showed a linear relation which demonstrated that polyacrylamide solutions followed a power low relationship. The flow index (n) and consistency (k) of the fluid were determined by fitting of the plot of shear rate and viscosity of the fluid in a linear model.

The repeatability of the sample was examined by measuring the viscosity of the two samples with same mixing procedure. Results confirmed the repeatability and consistency of the procedure used to prepare polyacrylamide solutions. The increment of mixing time did not have effect on the viscosity of the polyacrylamide solution and 3 hours of mixing was adequate for solution to mix.

The viscosity measurement of five concentrations of polyacrylamide solutions showed that the viscosity of the polymer increases as the concentration

increases. However, all concentrations maintained a shear thinning behavior. The flow index (n) of the fluid decreased as concentration increased which led to more intense shear thinning behavior of the fluid.

The viscosity of 0.1 wt. % polyacrylamide solution was studied for 30 days to study the effect of shelf time on the rheology of the fluid. The results showed that the viscosity and shear thinning behavior of the fluid remained the same throughout. Based on the results it was concluded that anionic polyacrylamide solution can be used as a non-Newtonian fluid in experiments with the mixing procedure confirmed to be repeatable; and the rheology of the fluid stable for 30 days.

Chapter 4. Velocity Profile of Newtonian and Non-Newtonian Fluids through a Mini-channel

4.1 Introduction

Results from study of a fluid's velocity profile could also be used in the investigation of its rheology. The aim of the experiments in this study was to find the fluid flow index, *n*, which represents the rheology of the fluid, based on the velocity profile generated in a long channel. Water (Newtonian) and three concentrations of polyacrylamide solution (non- Newtonian) were used as the sample fluids to study the rheology. Four flow rates were also studied to investigate the effect of flow rate on the flow index (*n*).

The first part of this chapter discusses the theoretical background on the velocity profile of the Newtonian and non-Newtonian fluids. In the following section, results from the effect of rheology and flow rate on the fluid velocity profile are presented. The flow indices for the fluid which were found from experimental velocity profile were compared to the measurements taken using a commercial rheometer and are described in the last section of this chapter.

4.2 Theory of Newtonian and non-Newtonian fluid through mini-channels

Different studies have developed equations, which showed the velocity profile of Newtonian and non-Newtonian fluids with respect to different positions along a flow channel [45, 100]. The equations for the velocity profiles of Newtonian and non-Newtonian fluids that also account for viscosity were developed based on the momentum conservation law.

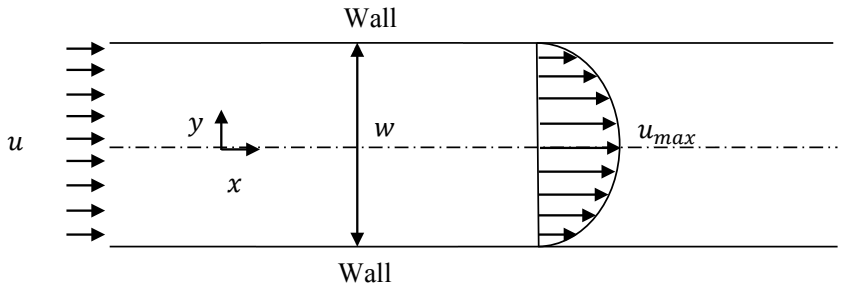

Figure 4-1. Schematic for fully developed velocity profile domain

Figure 4-1 shows a schematic for the domain commonly used to study the velocity fields of the non-Newtonian fluids. As the fluid with constant flow rate enters a channel of width, w, the velocity field requires a certain length to become fully developed depending on the Reynolds number of the flow [102]. In this region, where the flow is fully developed, the maximum velocity is attained at the centerline of the channel. A general equation for the law of momentum conservation along x axis can be defined as:

$$\rho\left(\frac{\partial u}{\partial t}+u\frac{\partial u}{\partial x}+v\frac{\partial u}{\partial y}+w\frac{\partial u}{\partial z}\right)=-\frac{dp}{dx}+\frac{\partial}{\partial x}(\tau_{xx})+\frac{\partial}{\partial y}(\tau_{xy})+\frac{\partial}{\partial z}(\tau_{xz})+g_c \quad (4\text{-}1)$$

This can be used to derive an equation for the velocity profile following the approach of [101]. Here, ρ is the density of the fluid; p is pressure; g_c is the gravitational constant; u, v and w are the velocities along x, y, and z, respectively; and τ_{xx}, τ_{xy} and τ_{xz} are the stresses in x, y and z directions, respectively.

The relation of the stress in different directions with the velocity gradient can be defined as:

$$\tau_{xx}=\mu_{eff}\left(\frac{\partial u}{\partial x}+\frac{\partial u}{\partial x}\right) \quad (4\text{-}2)$$

$$\tau_{xy}=\mu_{eff}\left(\frac{\partial u}{\partial y}+\frac{\partial v}{\partial x}\right) \quad (4\text{-}3)$$

$$\tau_{xz}=\mu_{eff}\left(\frac{\partial u}{\partial z}+\frac{\partial w}{\partial x}\right) \quad (4\text{-}4)$$

Assumptions are made here for the derivation were, the flow is incompressible flow; steady state flow $\left(\frac{\partial u}{\partial t}=0\right)$; unidirectional flow along the x direction $(v, w=0)$; fully developed profile $\left(\frac{\partial}{\partial x}=0\right)$; maximum velocity at the center $\left(y=0;\ \frac{du}{dy}=0\right)$; and no slip boundary condition.

After applying these assumptions a simplified equation for general conservation of momentum could be obtained. The velocity profiles as well as the maximum velocity for non-Newtonian fluid in fully developed regime were thus found to be:

$$u(y) = \frac{n}{n+1}\left(\frac{1}{k}\frac{dp}{dx}\right)^{\frac{1}{n}}\left(y^{\frac{n+1}{n}} - (\frac{w}{2})^{\frac{n+1}{n}}\right) \tag{4-5}$$

$$u_{max} = \frac{n}{n+1}\left(\frac{1}{k}\frac{dp}{dx}\right)^{\frac{1}{n}}(-\frac{w}{2})^{\frac{n+1}{n}} \tag{4-6}$$

where n is the flow index, and k is flow consistency of the fluid in the channel.

The velocity profile can be expressed in a normalized form as:

$$\frac{u}{u_{max}} = 1 - (\frac{2y}{w})^{\frac{n+1}{n}} \tag{4-7}$$

This equation was obtained by normalizing the velocity field showed in equation (4-5) using the maximum velocity from equation (4-6) and the position (y) using the width of channel (w).

Flow index (n) for Newtonian fluids where $n = 1$ results in equation (4-7) to represent a parabolic profile. If the pressure gradient is constant and the shear stress distribution is linear in the fully developed regime, the profile described can be considered as a plane Poiseuille flow [45].

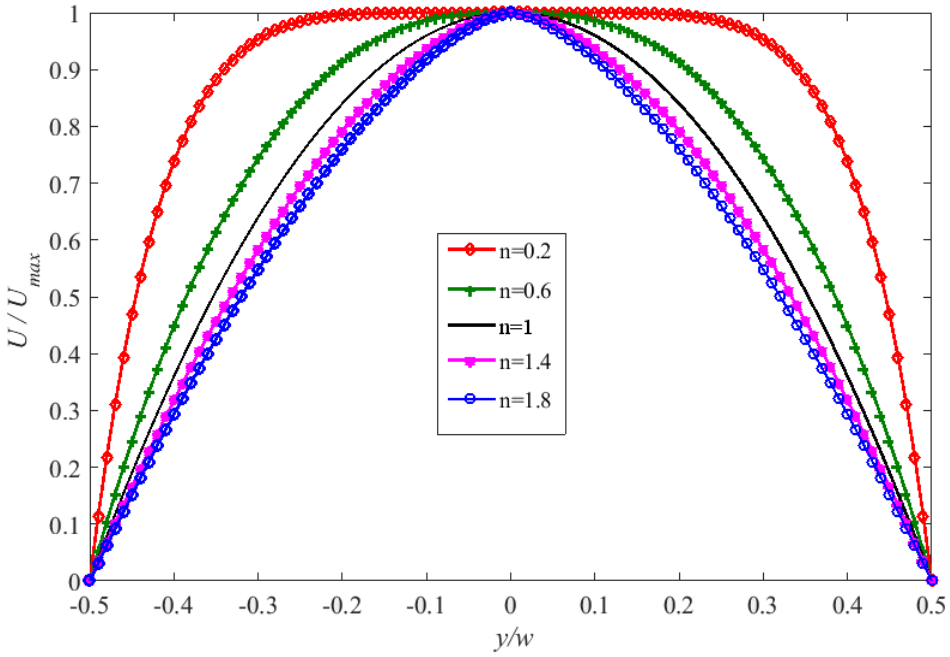

Figure 4-2. Plot of comparison for velocity profile of Newtonian and non-Newtonian fluids after [101]

Figure 4-2 shows a comparison of velocity profile for different groups of Newtonian and non-Newtonian fluids. When the fluid is Newtonian (n = 1), the velocity profile has a parabolic shape. While for non-Newtonian fluids two different cases arise depending on the shear thinning or shear thickening behavior of the fluid. In case of shear thinning fluid, $n < 1$, the profile has a plug flow at the center of the profile. For the case of shear thickening fluid, $n > 1$, the velocity profile is sharp in the center.

4.3 Study of the effect of fluid rheology and flow rate on velocity profile

The effect of rheology of fluid on the fully developed velocity profile through mini-channels was studied using the experimental setup shown in Figure 2-1. In this study, the velocity profiles of water as Newtonian with polyacrylamide solution by different concentrations (0.1 wt. %, 0.3 wt. %, and 0.5 wt. %) as non-Newtonian fluids were compared to find the effect of rheology on the velocity profile. Different flow rates of Q = 0.025, 0.05, 0.075 and 0.1 ml/min were set on the syringe pump to study the velocity profile in the laminar or creeping flow regime.

The Reynolds numbers of water flow were calculated using equation (1-2) in which the hydraulic diameter of the channel (D_h), density (ρ) and viscosity (μ) of water at 25 ℃ are 8.37×10^{-4} m, 999.97 kg/m^3 and 0.001 kg/m.s respectively. For flow rate of Q = 0.025, 0.05, 0.075 and 0.1 ml/min Reynolds numbers are 0.379, 0.757, 1.136, and 1.515 respectively. For the case of non-Newtonian flows, equation (1-1) was used to calculate the Reynolds number. Table 4-1 shows the summary of all parameters and Reynolds numbers for polyacrylamide solutions at different flow rates. According to the Reynolds number which are less than 1 it can be concluded that all flows are in creeping flow region.

Table 4-1. Table of parameters and Reynolds number for polyacrylamide solutions through mini-channel at different flow rates

Concentration (wt. %)	Flow index (n)	Flow consistency (k)	Hydraulic Diameter D_h [m]	Flowrate Q [ml/min]	Velocity [m/s]	Reynolds number Re
0.1	0.469	0.054	9.55×10^{-4}	0.025	3.97×10^{-4}	0.012
				0.05	7.94×10^{-4}	0.036
				0.075	1.19×10^{-4}	0.067
				0.1	1.59×10^{-4}	0.104
0.3	0.341	3.115	9.55×10^{-4}	0.025	3.97×10^{-4}	2.45×10^{-4}
				0.05	7.94×10^{-4}	7.94×10^{-4}
				0.075	1.19×10^{-4}	1.51×10^{-3}
				0.1	1.59×10^{-4}	2.44×10^{-3}
0.5	0.304	11.61	9.55×10^{-4}	0.025	3.97×10^{-4}	6.82×10^{-5}
				0.05	7.94×10^{-4}	2.21×10^{-4}
				0.075	1.19×10^{-4}	4.4×10^{-4}
				0.1	1.59×10^{-4}	7.16×10^{-4}

Figure 4-3 shows the velocity profile vector map for water and polyacrylamide solution at flow rate of Q = 0.025 ml/min. The vectors showed the local normalized velocity profile and all the vectors were shown in y direction and 1 out of 7 vectors in the x direction for all cases. All plots in this chapter had the velocity normalized based on the maximum velocity and the position based on the width of channel.

Shown in Figure 4-3 (a) to (d), the maximum velocity for all cases was at the center line and the velocity decreased as it approached the wall of the channel. The region for maximum velocity was small in the case of water and the size of this region increased by increasing the concentration of the polyacrylamide solution. This result showed the growth of the plug flow region as a result of intensification in shear thinning behavior of polyacrylamide solutions.

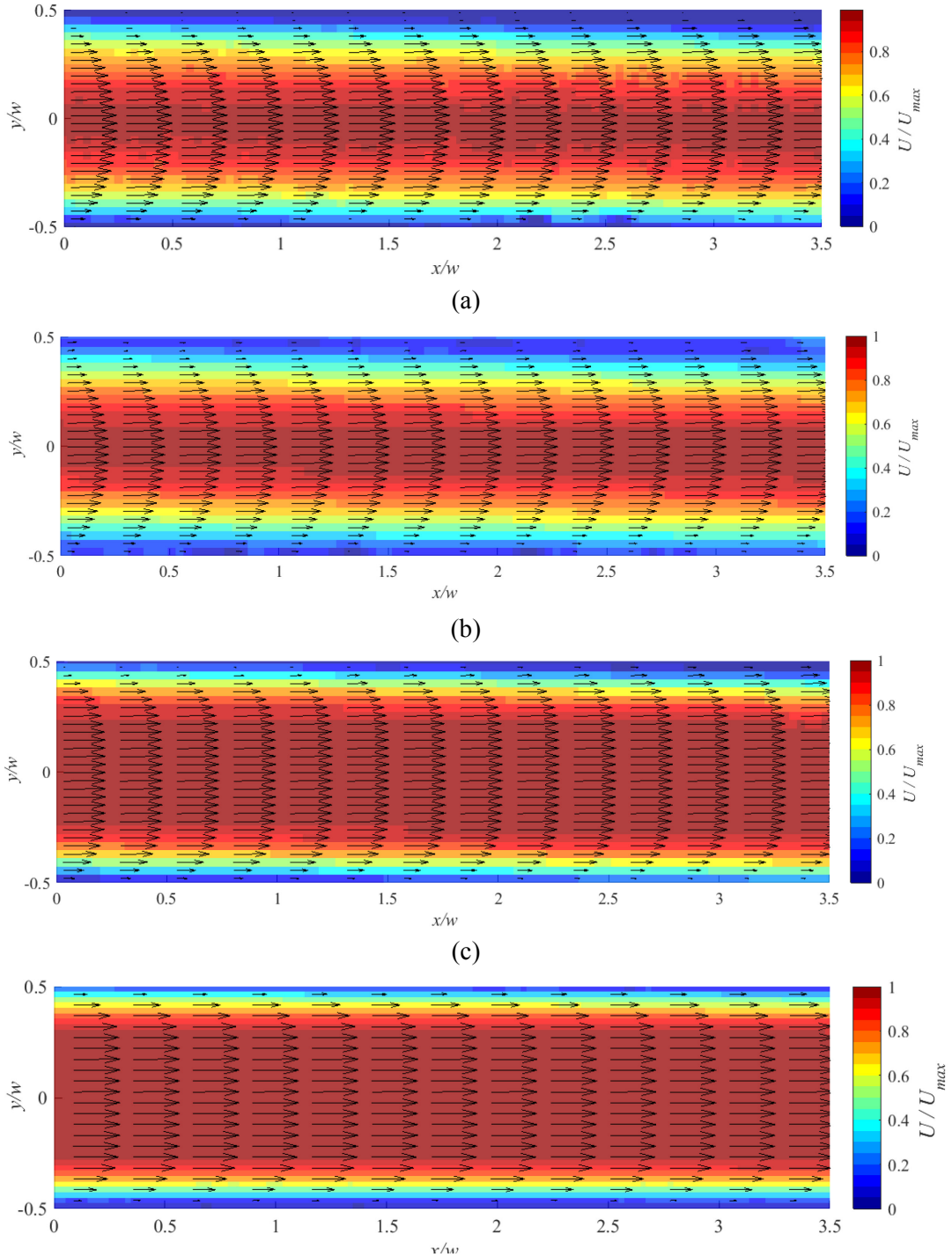

Figure 4-3. Average velocity profile vector map with a background color map of velocity magnitude for (a) water, (b) 0.1 wt. % polyacrylamide, (c) 0.3 wt. % polyacrylamide, and (d) 0.5 wt. % polyacrylamide through mini-channel at Q = 0.025 ml/min

In order to have a detail study of velocity profile for different fluids, normalized velocity profiles of water and different concentrations of polyacrylamide solutions were compared for the same flow rates. As shown in Figure 4-4, water had a parabolic profile and polyacrylamide solution had a top-hat velocity profile. The consistency in the profiles resulted from the flows being fully developed. The increment of the plug flow region between 0.1 wt. % and 0.3 wt. % polyacrylamide solutions was more profound than the case between 0.3 wt. % and 0.5 wt. % polyacrylamide solutions. It was concluded that the increment of shear thinning behavior of polyacrylamide as a result of increment of the concentration was much higher at lower concentrations.

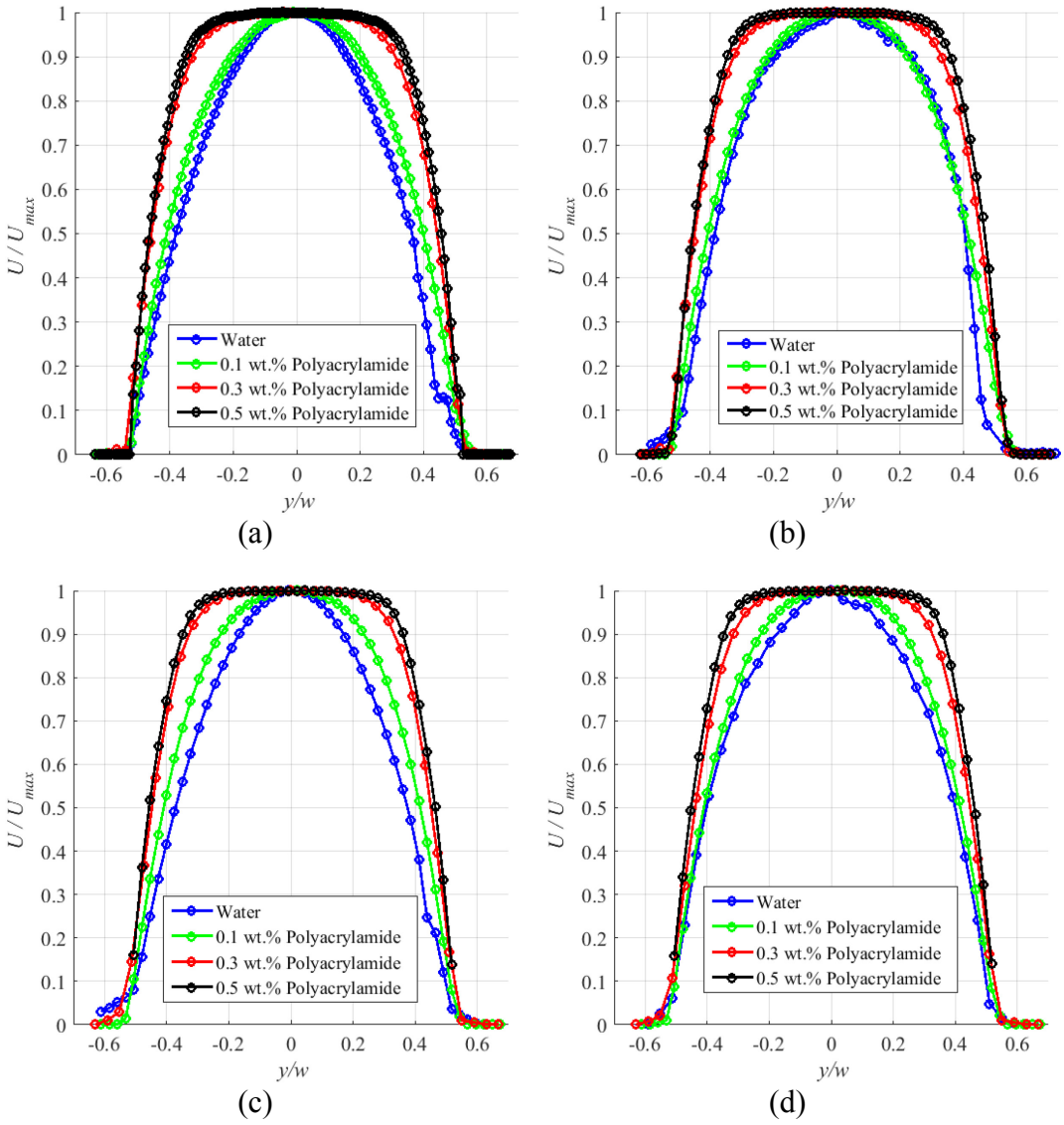

Figure 4-4. Velocity profile of water, 0.1 wt. % polyacrylamide, 0.3 wt. % polyacrylamide and 0.5 wt. % polyacrylamide at (a) Q = 0.025 ml/min, (b) Q = 0.05 ml/min, (c) Q = 0.075 ml/min and (d) Q = 0.1 ml/min

The effects of flow rate on the velocity profile of Newtonian and non-Newtonian fluid were studied for the flow rates of 0.025 ml/min, 0.05 ml/min, 0.075 ml/min, and 0.1 ml/min. Normalized velocity profile for each fluid sample was plotted for different flow rates and the results are given in Figure 4-5. It was concluded that the flow rate of water and polyacrylamide solution did not have any effect on velocity profile shape for the range used in this study.

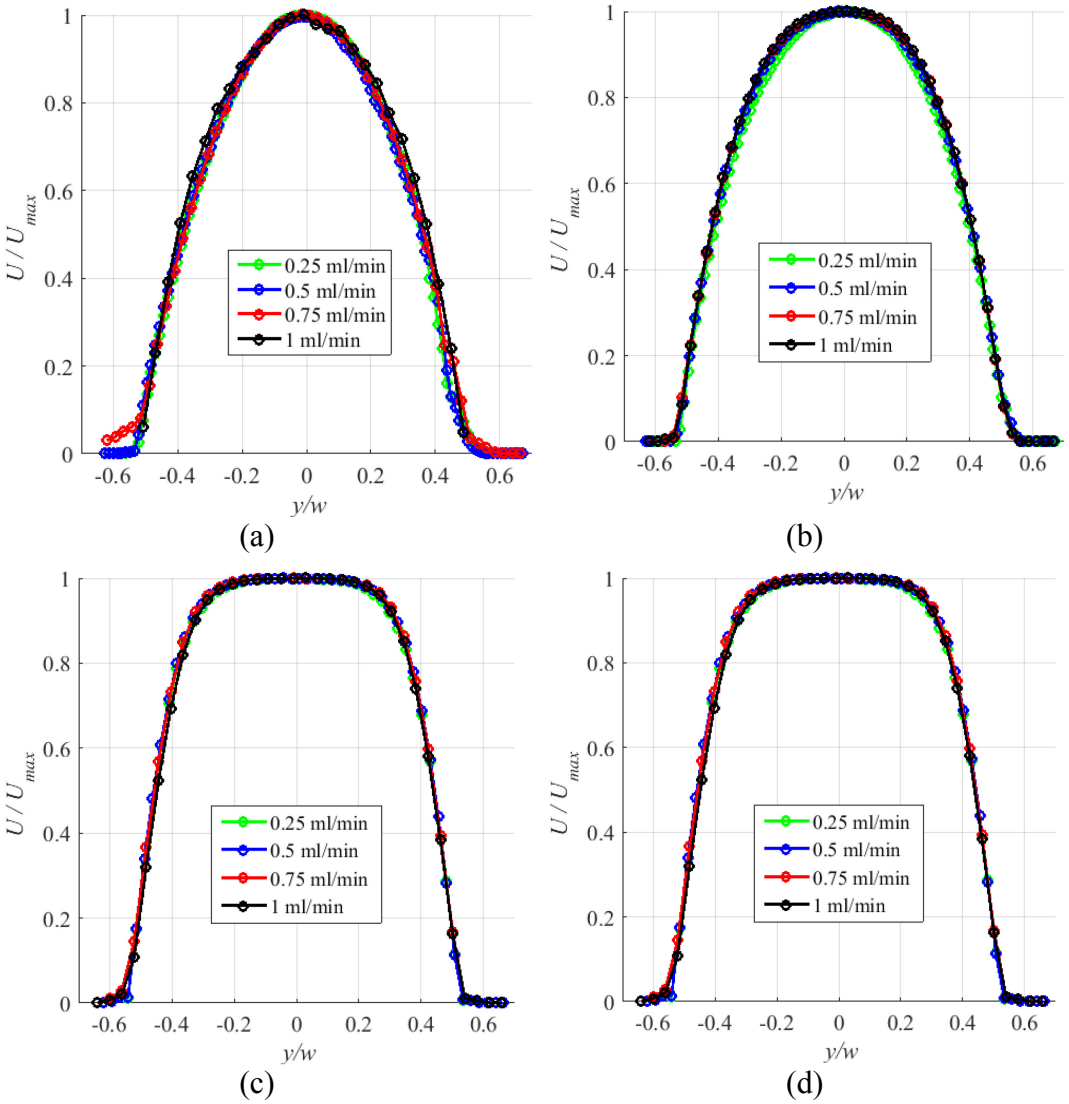

Figure 4-5. Comparison of effect of flow rate on the velocity profile (a) water, (b) 0.1 wt. % polyacrylamide, (c) 0.3 wt. % polyacrylamide, (d) 0.5 wt. % polyacrylamide.

4.4 Comparison of the velocity profile of Newtonian and non-Newtonian fluid with corresponding theory

In order to compare the experimental results with Newtonian and non-Newtonian theory, equation (4-7) was used. A fluid index of $n = 1$ was used for water and for polyacrylamide solution; the measured flow index (n) from the rheometer was used. According to the rheometer measurements, the flow indices for 0.1 wt. %, 0.3 wt. %, and 0.5 wt. % polyacrylamide solutions were 0.49, 0.31, and 0.26, respectively.

Figure 4-6 (a) shows the average of 200 images of velocity profile of water at $Q = 0.075$ ml/min in the middle of channel compared to the theory for flow of Newtonian fluids (see Appendix C for complete set of figures for all flow rates). Experimental results showed parabolic profile for all the different flow rates studied. The flow of Newtonian fluids having such a profile that was similar to that of a plane Poiseuille flow [45]. The comparison with theory also showed a good agreement of the experimental results for velocity profile given the conditions of constant pressure gradient.

Similar comparison of velocity profiles of 0.1 wt. %, 0.3 wt. %, and 0.5 wt. % polyacrylamide solutions with non-Newtonian theory are shown in, Figure 4-6 (b), (c) and (d), respectively (see Appendix C for complete set of figures for all conditions). The velocity of polyacrylamide solutions for all concentrations showed a profile developing toward a top-hat with decreasing flow index (n). There was a strong indication that the experimental results of velocity

profiles matched non-Newtonian flow theory for all cases and more investigations were required to validate this result.

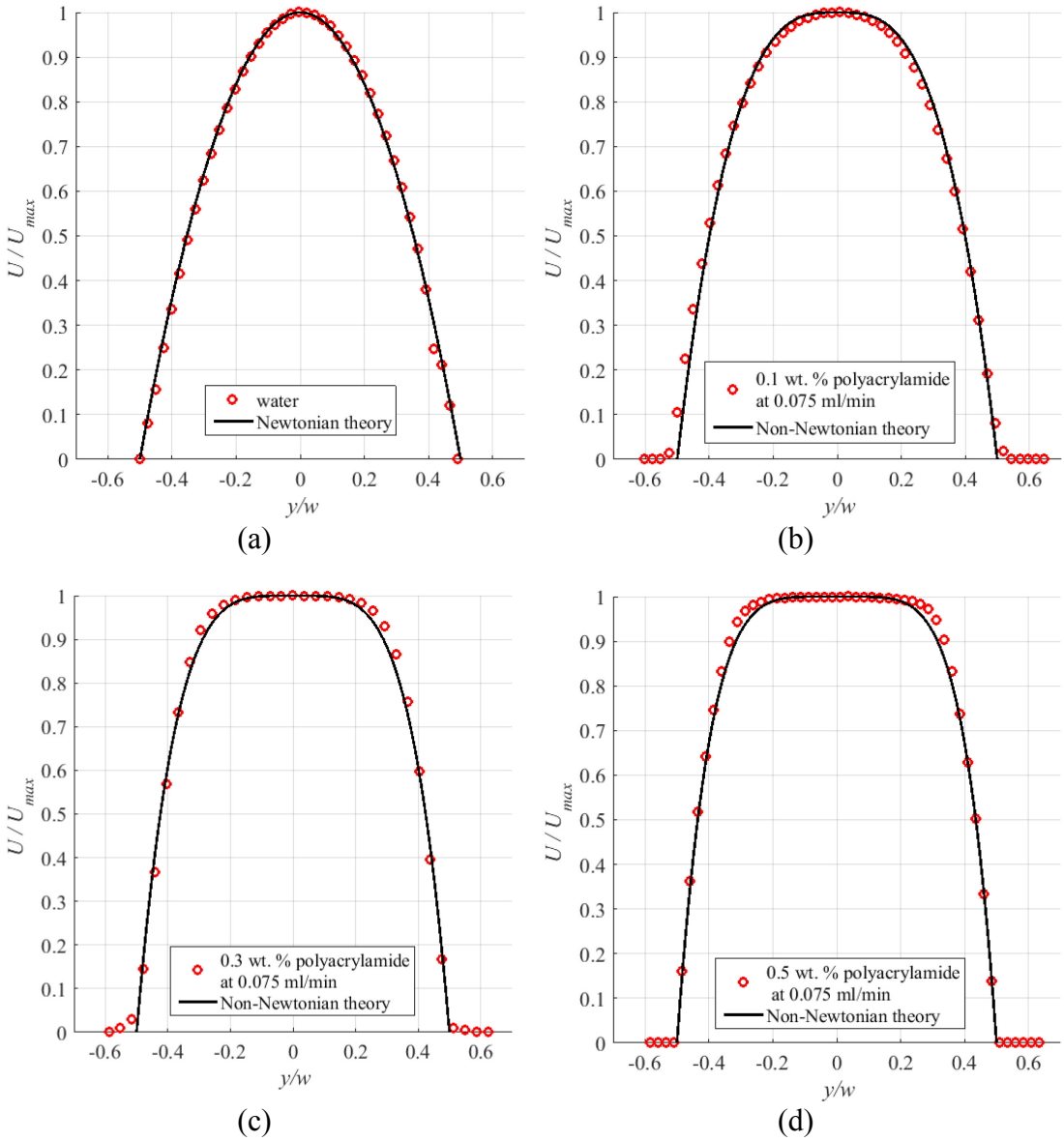

Figure 4-6. Plots for comparison of average velocity profile of (a)water with Newtonian theory, (b) 0.1 wt. % ,(c) 0.3 wt. % and (d)0.5 wt. % polyacrylamide solution with non-Newtonian theory at Q = 0.075 ml/min

Fluid flow index (n) for the experimental result was obtained from the velocity profile of the respective fluids and compared with the rheometer measurements. In order to find the flow index (n) from experimental results, the flow index (n) was estimated by curve fitting of the experimental results using the power law equation shown in (4-8) and compared with equation (4-7).

$$\frac{u}{u_{max}} = (a\frac{y}{w})^b + c \tag{4-8}$$

where a, b and c were defined as:

$$\frac{a}{c} = (-2)^{\frac{n+1}{n}} \tag{4-9}$$

$$b = \frac{n+1}{n} \tag{4-10}$$

The experimental results for velocity profiles were plotted and the power law curve was fitted as shown in Figure 4-7. The parameters of a, b and c were calculated using equation (4-8). (See Appendix C for complete set of figures for all conditions and calculated parameters)

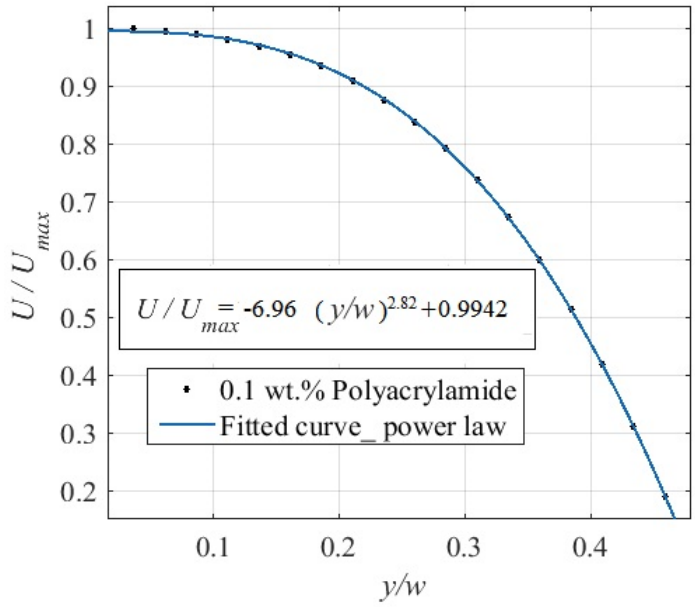

Figure 4-7. Curve-fitted plots of 0.1 weight % polyacrylamide solution at 0.025 ml/min

According to the results, the averaged equation to describe the velocity profile for 0.1 wt. %, 0.3 wt. %, and 0.5 wt. % polyacrylamide solutions are shown in equation (4-11), (4-12) and (4-13), respectively.

$$\frac{u}{u_{max}} = (-7.11\ \frac{y}{w})^{3.075} + 0.996 \quad (4\text{-}11)$$

$$\frac{u}{u_{max}} = (-17.50\ \frac{y}{w})^{4.156} + 1.008 \quad (4\text{-}12)$$

$$\frac{u}{u_{max}} = (-23.985\ \frac{y}{w})^{4.775} + 1.0155 \quad (4\text{-}13)$$

Table 4-2. Comparison of flow index calculated by curve fitting and rheometer measurement for different concentration of polyacrylamide

Solution	Flow rate *(Q)* (ml/min)	*a*	*b*	*c*	*n*	Average	Rheometer measurement
0.1 wt. % Polyacrylamide	0.025	-6.96	2.82	0.9942	0.55	0.482	0.49
	0.05	-6.43	3.94	0.9961	0.34		
	0.075	-7.62	2.69	0.9956	0.59		
	0.1	-7.43	2.85	0.9983	0.54		
0.3 wt. % Polyacrylamide	0.025	-16.49	4.08	1.005	0.325	0.317	0.31
	0.05	-17.78	4.17	1.008	0.315		
	0.075	-14	3.99	1.014	0.335		
	0.1	-21.75	4.37	1.005	0.296		
0.5 wt. % Polyacrylamide	0.025	-27.23	4.83	1.004	0.261	0.265	0.26
	0.05	-26.22	4.68	1.014	0.272		
	0.075	-21.8	4.88	1.028	0.258		
	0.1	-20.69	4.71	1.016	0.269		

The fluid flow index (*n*) was calculated based on equations shown in Table 4-2. By comparing the average of flow index (*n*) obtained after curve fitting of the experimental velocity profile and the flow index, *n*, which was measured using the rheometer, it was concluded that the experimental results matches the theory. The result of this study confirms that the flow behavior of non-Newtonian fluid can be obtained using the fluid velocity profile.

4.5 Conclusion

Flows of Newtonian and non-Newtonian fluids through micro channels were studied at different flow rates to find the effects of rheology and flow rate on the fully developed velocity profiles. The results were validated by comparing experimental results with corresponding equations in Newtonian and non-Newtonian flow theories derived based on the conservation of momentum. The flow indices which were important parameters in the study of the fluids' rheology were also compared with the experimental results.

The flow of Newtonian fluid showed a parabolic velocity profile for all the flow rates. The comparison of the experimental velocity profile of water with the Newtonian theory also showed a good agreement. The flow rates did not have any effect on the developed velocity profile of the Newtonian fluid.

Three concentrations of the polyacrylamide solution were used to study the flow of non-Newtonian fluid. The velocities for all these solutions had a top-hat profile, which was due to the shear thinning behavior of the polyacrylamide solution. The region of plug flow in the velocity profile of polyacrylamide solution increased as the concentration of the fluid increased since the shear thinning behavior of the fluid intensified. There wasn't any noticeable change in the shape of velocity profile for non-Newtonian fluid with increasing flow rate within the range used in this study. The comparison between the estimated fluid flow index (n) based on the curve fitting of the velocity profile and the results from viscosity measurement using a rheometer also matches.

It was concluded that the change in the rheology of the fluid led to a change in its velocity profile. Flow rate did not have any effect on the velocity profile of both water and polyacrylamide solution in the range of the flow rate experimented. According to comparison of the experimental and non-Newtonian theory, it was concluded that the fluid flow index (n) could be estimated using the fluid velocity profile in the fully developed region.

Chapter 5. Velocity Profile of Newtonian and Non-Newtonian Fluids Through Keystone Slots

5.1 Introduction

Plugging and scaling of slotted liners is one of the main issues in SAGD process that needs to be addressed. The study of fluid velocity profile through slots could be a powerful tool to find the optimum geometry to decrease the possibility of the scaling in slotted liners. There are different parameters that should be considered to determine the velocity through slots such as the geometry of slot, rheology of the fluid and flow rate.

Due to the varying Newtonian and non-Newtonian behavior of bitumen mixture, the fluids selected for experiments of this study included both. The primary reason behind this selection was to enable comparison between results for the flow of Newtonian and non-Newtonian fluids. Including non-Newtonian fluid also allowed investigating the effect of concentration on both the fluid rheology and the flow behavior. Accordingly, water was used as Newtonian fluid whereas two different concentrations of polyacrylamide solution (0.2 wt. % and 0.4 wt. %) were used as the non-Newtonian fluid for the experiments.

As shown Figure 2-6, seven cases of slot geometry with different slot angles starting from θ = 0° to 12°. These all have the same entrance width which were studied to find the effect of geometry on the velocity profile of fluid through the slot using the scaling outlined in Figure 5-1. An increase in the slot angle for the slots also increased the cross-sectional area which enabled the study of the effect of area on the velocity distribution. Results from experiments on these slot geometries were used to identify the slot angle that could be used for a better velocity profile with respect to minimizing plugging and scaling.

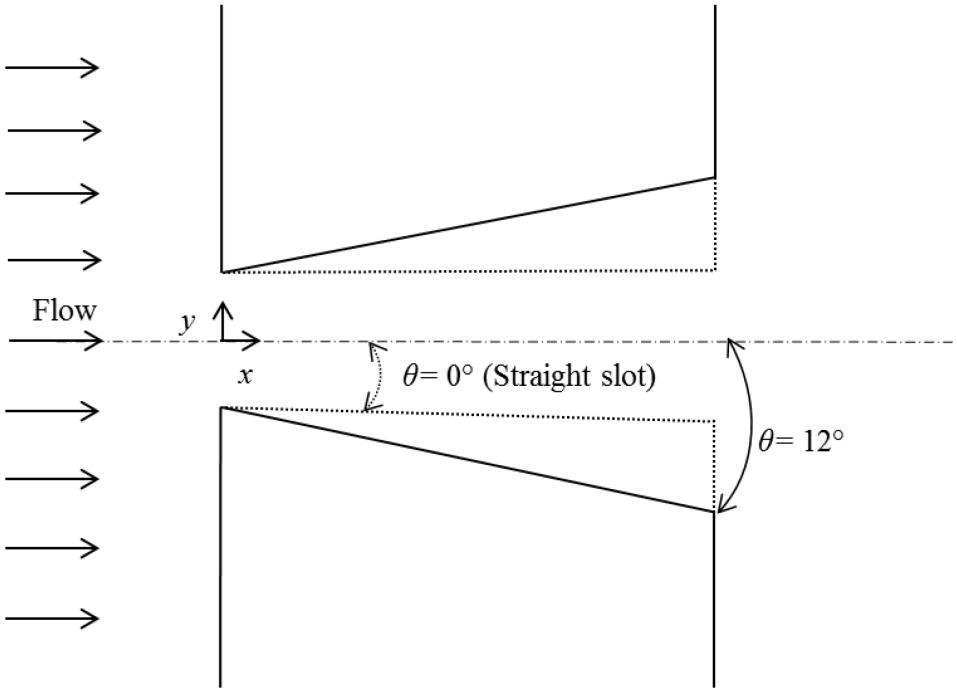

Figure 5-1. Schematic of keystone slot with different slot angles

The production rate of bitumen may vary based on different conditions which lead to decrease of flow rate through slotted liners such as performance on flow control devices, formation of condensed oil pool, and open area available for

inflow. Different flow rates of water and polyacrylamide solution were used for the experiments to study the effect of changing production rate on the velocity profile of fluid through slots.

The results obtained from experiments of this study are presented in this chapter which consists of four sections. The results of velocity profile of water through straight and keystone slots are given in the first section for different conditions. The second section presents the velocity profiles of 0.2 wt. % and 0.4 wt % polyacrylamide solutions through the different slot geometries. Results for the development of velocity profiles to compare Newtonian and non-Newtonian fluids through different slot geometries at different flowrates are given in the third section. The chapter ends with concluding remarks given in the last section.

.

5.2 Processing procedure of the velocity profile in keystone slots

To study the effect of slot angle of slots on the shape of velocity profile, the respective velocity distributions of fluids at ten different positions were studied. In order to show the processing procedure, velocity profile of 0.2 wt. % polyacrylamide solution through $\theta = 10°$ keystone slot at $Q = 1$ ml/ hr was used as the representative case. More fluctuation in the velocity profile as compares to other cases was observed at this combination of flow conditions.

Figure 5-2 shows the raw average velocity profile of 0.2 wt. % polyacrylamide solution through $\theta = 10°$ keystone slot at $Q = 1$ ml/hr. In this figure the ratio x/w was used to indicate the position in the channel along the direction of the flow. When the ratio is $x/w = 0$, for example, it refers to the position at the entrance of channel. Accordingly, increasing numbers for the value of this ratio show that the position is farther downstream the channel.

Figure 5-2 shows that the maximum velocity is at the inlet of channel and starts to decrease as the profile position moves toward the outlet of channel. This decrease in velocity can be attributed to the $\theta = 10°$ slot angle in the keystone slot which resulted in incremental change in the cross sectional area along the channel length.

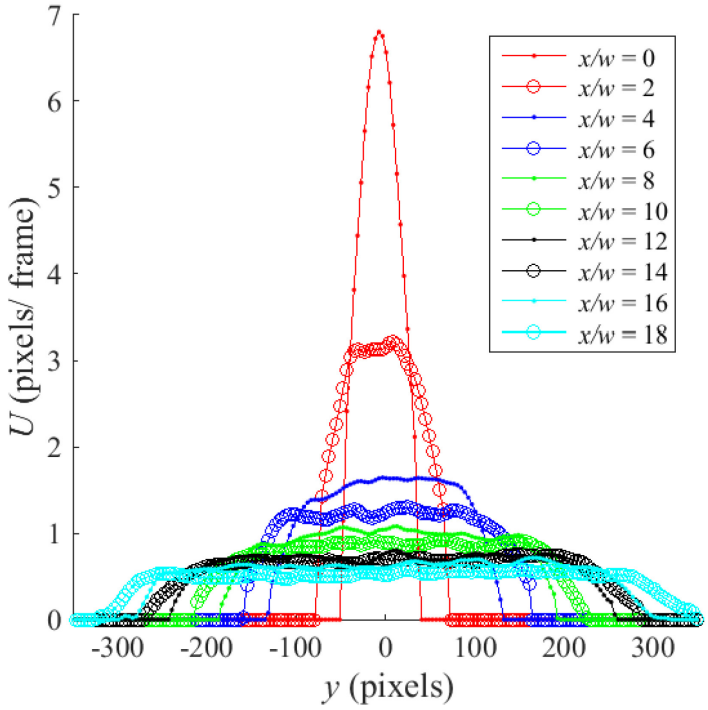

Figure 5-2. Average velocity profile of 0.2 wt. % polyaryclamide solution through $\theta = 10°$ keystone slot at $Q = 1$ ml/hr

The axes in Figure 5-2 show the velocity in pixels/frame and the width of channel in pixels. However, in order to compare the velocity profiles through slots of different shape and at different flow rates, the velocity and the width needed to be normalized. Therefore, at a given location within the channel along the direction of flow, the magnitude of the velocity and the width were normalized using the maximum velocity and the local width of the channel, respectively, both at that same location of the velocity profile. Figure 5-3 (a) shows the normalized velocity profile of 0.2 wt. % polyacrylamide solution through θ =10° slot at $Q = 1$ ml/hr which corresponds to Figure 5-2.

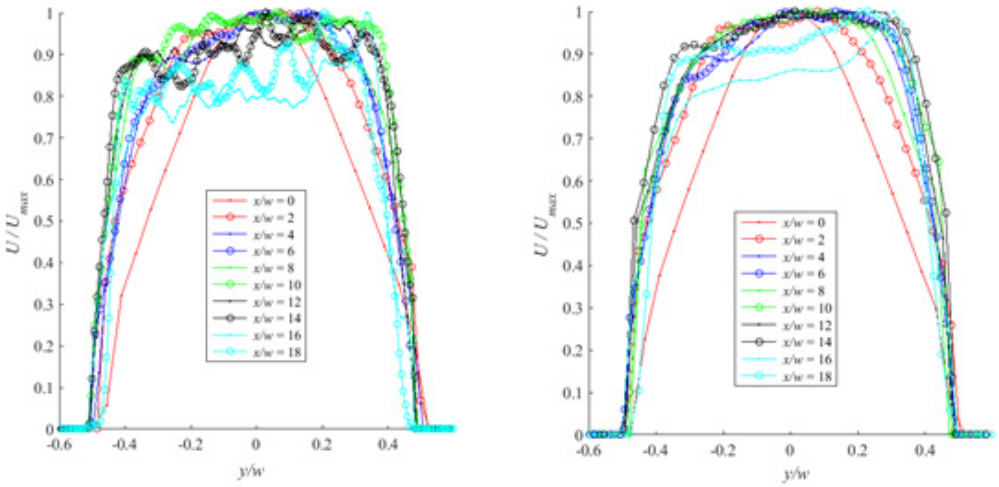

(a) (b)

Figure 5-3 -Normalized average velocity profile of 0.2 wt. % polyaryclamide solution through θ =10° keystone slot at Q = 1 ml/hr using (a)single processing procedure (b) the hybrid processing procedure

These profiles were obtained by processing the particle images using a multi-pass interrogation scheme with window sizes of 64 × 64 followed by 32 × 32 and 87% overlap. The plots show fluctuations in the velocity profile for positions at close proximity to the outlet of the channel. It was further observed that this condition was magnified as the flow profile approached the outlet. This instability was because the inlet width of the channel was 8 times smaller than the outlet for θ = 10° slot angle. As it is shown in Figure 5-2, the incremental increase in cross sectional area leads to a decrease in displacement of particles from ~7 pixels per frame at the inlet to ~1 pixel per frame at the outlet of the channel. This small displacement of the particles relative to the minimum resolution of measurable particle displacement (~1/10th pixel) promotes the fluctuations which appear in the velocity profiles. The window sizes that were suitable for processing of data therefore needed to be small (32 × 32 pixels) for the positions for which

the velocity profile was located $0 \leq x/w \leq 4$ and larger (64 × 64 pixels) for $6 \leq x/w \leq 18$.

Around the inlet of channel where the velocity is higher, the displacement of the particles closer to the walls of the channel would not be represented if a larger PIV correlation window was used. Larger window size was instead needed to achieve a smooth plot to represent the velocity distribution around the outlet of the channel. For the plots shown in Figure 5-3 (b), the multi pass hybrid scheme used for the processing had window sizes of 64 × 64 and 32 × 32 and 87% for $0 \leq x/w \leq 4$. For $6 \leq x/w \leq 18$, 128× 128 and 64× 64 with 75% overlap was used. It can be seen from the plots that representation of velocity profiles with less fluctuation was achieved by the adapted processing approach.

5.3 Velocity profile of water through keystone slots

The velocity profiles of water at different flow rates of Q = 1, 5.5 and 10 ml/hr through seven cases of slot geometry (θ = 0°, 2°, 4°, 6°, 8°, 10°, and 12° slot angles) were studied to find the effect of geometry and flow rate. The hydraulic diameter of the channel (D_h), density (ρ) and viscosity (μ) of water at 25 ℃ were 8.37×10^{-4}, 999.97 kg/m^3 and 1×10^{-3} kg/m.s, respectively. Using equation (1-2), respective values for the flows' Reynolds numbers (*Re*) were 0.27, 1.467and 1.67, for flowrates of 1 ml/hr, 5.5 ml/hr and 10 ml/hr. These Reynolds numbers put the flows in the category of creep flow for the case of low flow rate and laminar flow in case of higher flow rates. For a better representation of the velocity profile of water through these geometries, velocity vector maps for all

cases were used. In these plots the velocity was normalized based on the maximum velocity of the flow field and the positions were normalized by the inlet width of channel.

Figure 5-4 shows the vector map for flow of water through slots with different slot angles at Q = 1 ml/hr (see Appendix D for complete set of figures for all conditions). For the velocity of water through straight slots shown in Figure 5-4 (a) the maximum velocity occurred at the center of the channel and it remained as such along the channel length.

For the case of flow through keystone slots shown in Figure 5-4 (b) – (g), the maximum velocity was at the entrance of slot and a decrease is its magnitude was observed at is went downstream channel. This phenomenon was due to the incremental increase in cross-sectional area of the channel toward the channel exit. The plots also showed that the position at which the velocity started to decrease came closer to the channel inlet as the slot angle increased. This observation was common to all the flow rates used in the experiments (Q = 5.5 and 10 ml/hr).

The velocity profile of water at Q = 1 ml/hr was symmetric for the keystone slots that had slot angles smaller than $\theta < 6°$. An asymmetric flow was observed in slots slot angles that were greater or equal to $\theta \geq$] 6°. The velocity vector maps also indicated flow separation that occurred at different positions for different slot angles. Reverse flow phenomena were seen for the cases where the slot angle was greater than or equal to $\theta \geq 6°$ represented by plots given in

Figure 5-4 (e) – (g). The velocity vector maps also showed that increased slot angles resulted in flow separation at a position closer to the entrance of the slots.

When a flow rate of Q = 5.5ml/hr was used, the velocity profiles showed symmetry with no flow separation observed for all slot geometries (Appendix D). At higher slot angles ($\theta \geq 6°$) fluctuations in the profile where the location of maximum velocity deviated from the centerline of the channel was observed downstream the channel closer to the outlet. The velocity profile a flow rate of Q = 10ml/hr also showed that the flow was symmetric with no separation. No fluctuations in the profile were observed at this flow rate.

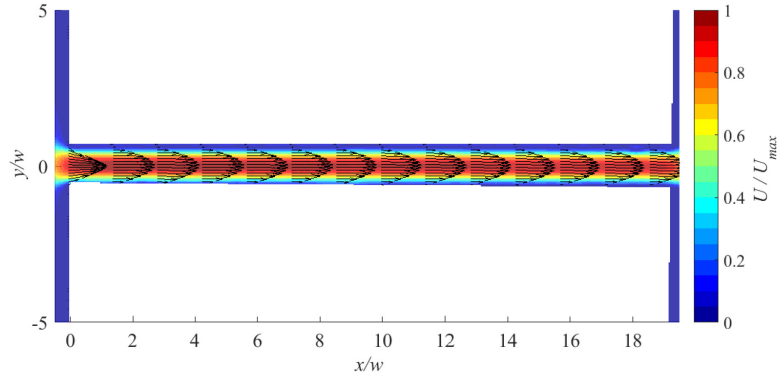

(a) Water flow through keystone slot with $\theta = 0°$(straight) at $Q = 1$ml/hr

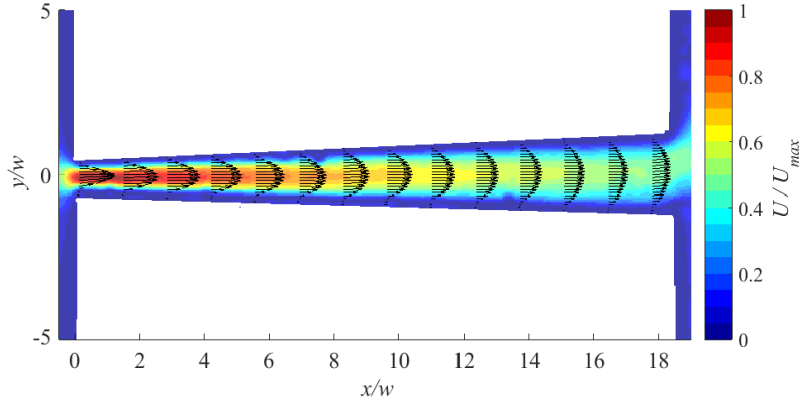

(b) Water flow through keystone slot with $\theta = 2°$at $Q = 1$ml/hr

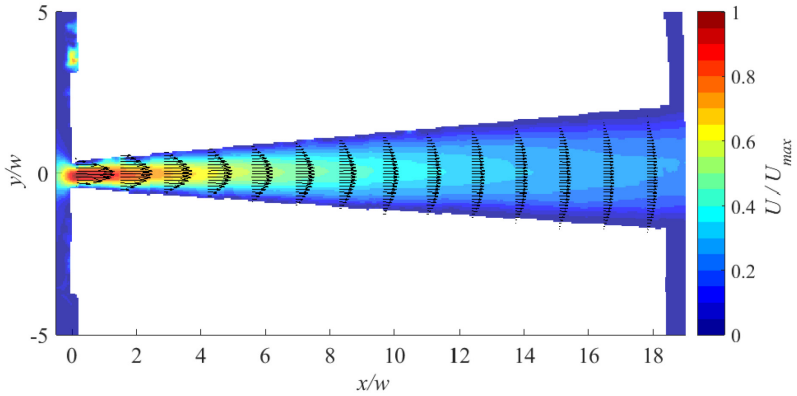

(c) Water flow through keystone slot with $\theta = 4°$ at $Q = 1$ml/hr

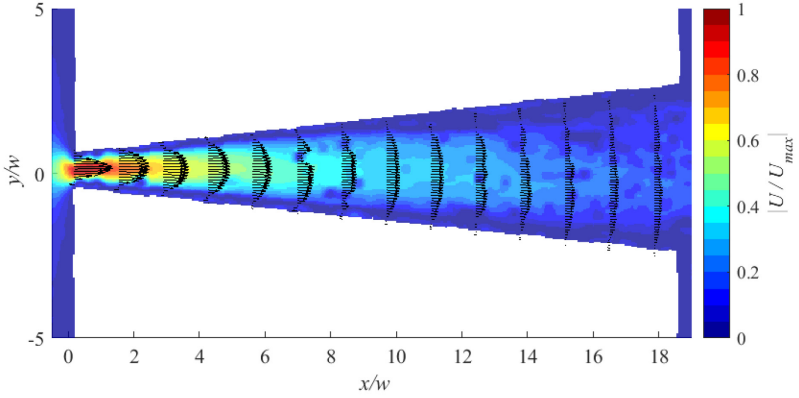

(d) Water flow through keystone slot with $\theta = 6°$ at $Q = 1$ml/hr

Figure 5-4. Vector map of water flow at $Q = 1$ ml/ hr through (a) $\theta = 0°$ (straight), (b) $\theta = 2°$, (c) $\theta = 4°$, (d) $\theta = 6°$, (e) $\theta = 8°$, (f) $\theta = 10°$, and (g) $\theta = 12°$ keystone slot

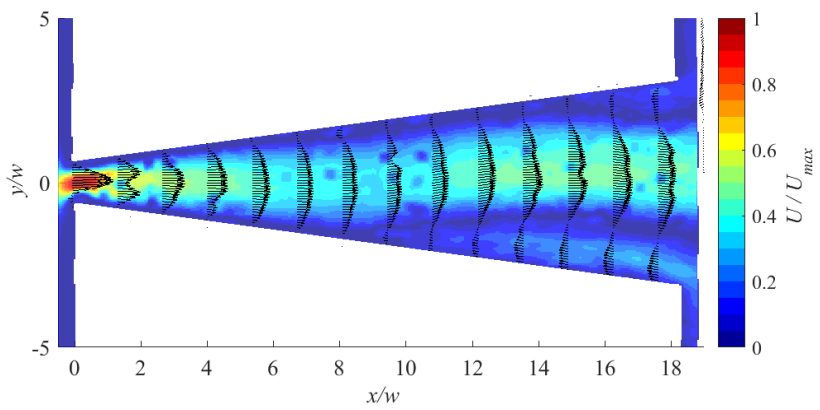

(e) Water flow through keystone slot with $\theta = 8°$ at Q = 1ml/hr

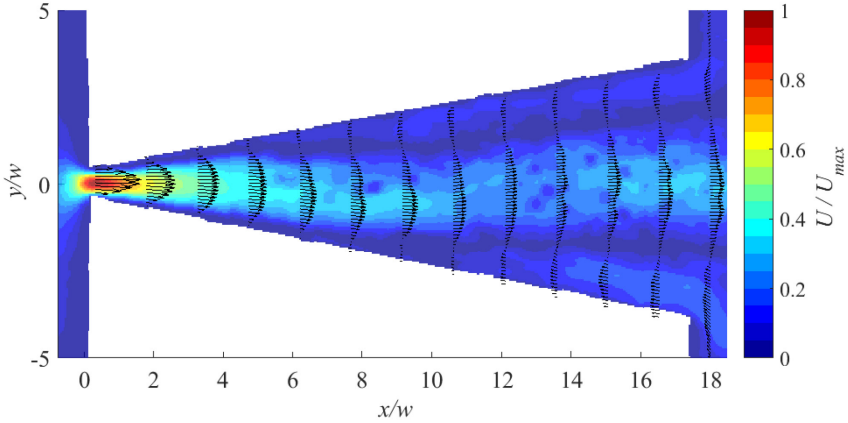

(f) Water flow through keystone slot with $\theta = 10°$ at Q = 1ml/hr

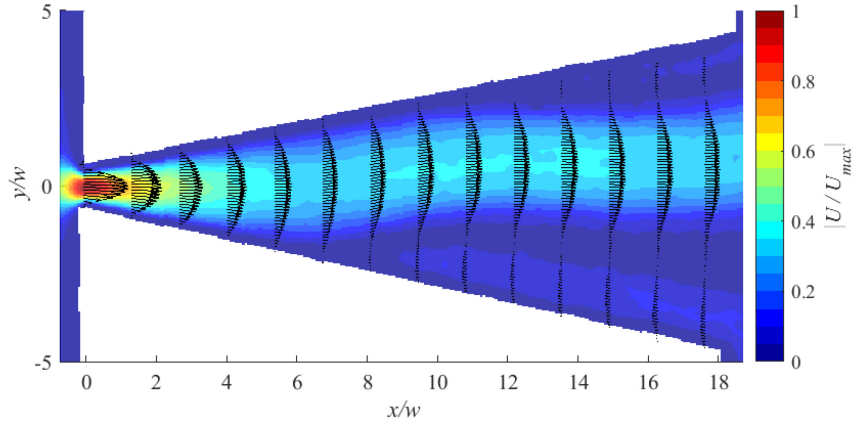

(g) Water flow through keystone slot with $\theta = 12°$ at Q = 1ml/hr

Figure 5-4 *(continued)*

In order to study the effect of slot angle on the shape of velocity profile, the velocity profiles of water through the slots of different geometries were plotted. Figure 5-5 shows the plots that were made using experimental results for ten different positions along the channel in the direction of the flow for the flow rate of Q = 1 ml/hr (see Appendix D for complete set of figures for all conditions).

The flow through the slots with keystone shapes does not become fully developed as a result of the incremental increase in cross sectional area of the slot. In order to see this effect on the shape of velocity profile a comparison of the unsteady flow (transient) experimental results was plotted with the fully developed case in a long straight channel described by the theoretical model given by equation (4-7). The PIV processing procedure presented in section 5.2 was used to generate these plots.

The positions along the channel that were considered to plot the different velocity profiles are given in Figure 5-5 (a) where $x/w = 0$ and $x/w = 18$ represent the inlet and outlet of the slot, respectively. The velocity profiles of water through straight, θ = 2°, and θ =4° keystone slots are given in Figure 5-5 (b), (c), and (d), respectively. The shape of the plots have a parabolic profile showing a similar shape that was expected from the theory for the flow of Newtonian fluids that are in a fully developed region. The shape of velocity profile for these slot angles did not change with position along the channel. The consistency in the shape of the velocity profile for flow through straight slot θ = 0° confirmed that the length of the channel was enough for the flow fully develop

near the entrance of slot at this flow rate. The same condition was true for all flow rates as seen from the plots given in Appendix D.

The Reynolds number for the flow can also be used to determine the channel length required for a flow to become fully developed. In case of laminar flow the length required for full development of a flow can be found from the relation given by [102]:

$$\frac{L}{D_h} \sim 0.06\, Re \tag{5-1}$$

where L is the length required for a flow to be fully developed; and D_h is hydraulic diameter defined as:

$$D_h = \frac{4 \times \text{cross section area}}{\text{wetted perimeter}} \tag{5-2}$$

Using equation (5-1) the calculated values for L corresponding to all the slots used in the experiments were less than 0.1mm. This further study confirms that for the case of flow passing through the straight slot, the velocity profiles from the experimental results are in agreement with Newtonian fluids' flow theory.

Figure 5-5 (e) – (h) show the plots for the flow through keystone slots with slot angle greater than or equal to $\theta \geq 6°$. The primary observation from these plots was the local and global minimum points which showed flow separation and reverse flow. Representation of the profiles in such a way showed the indications seen in velocity vector maps in Figure 5-4 more clearly. According to these profiles reverse flow was observed at both walls of the channel. Reverse flow occurred closer to the inlet of channel as slot angle increased up to $\theta = 10°$,

however, for the case of $\theta = 12°$ the extent of the reverse flow observed was significantly less than that for $\theta = 10°$. The extent of flow separation was maximum for slot with $\theta = 10°$ and in this case the reverse flow had the maximum value which was equal to 70 % of the maximum velocity of water for the given cross section.

The velocity profiles for water at Q = 5.5 and 10 ml/hr are given in Appendix D. The results showed no flow separation or reverse flow for these flow rates. It was also seen that the velocity profiles had symmetry that shows the similar shape as expected from the theoretical profile for the cases of slot angle that were less than $\theta < 6°$. For $\theta \geq 6°$ the velocity profiles lacked symmetry relative to the ones at lower angles for these flow rates which led to inclination of the flow to one side of the wall.

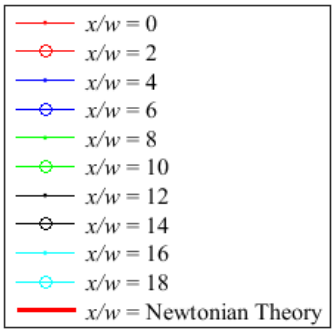

(a)

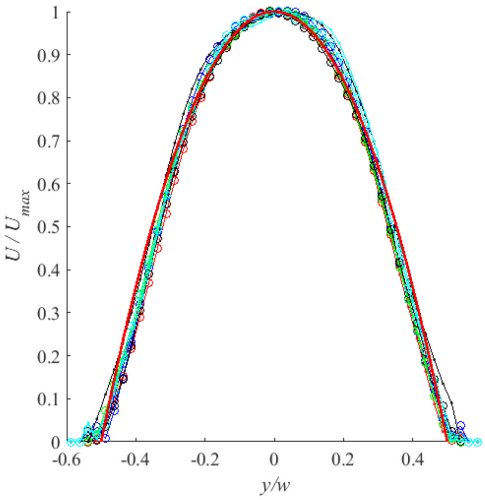

(b) Water flow through keystone slot with $\theta = 0°$ (straight) at Q = 1ml/hr

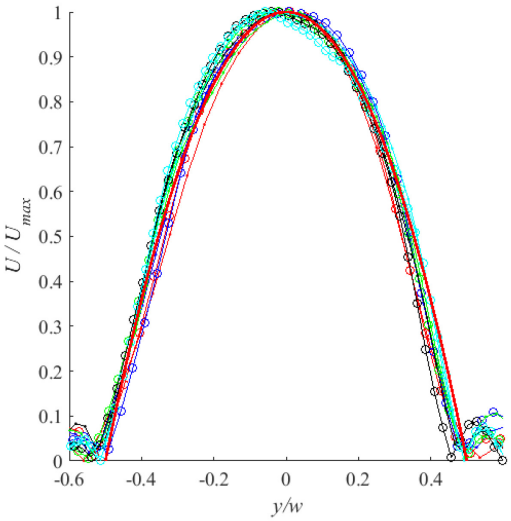

(c) Water flow through keystone slot with $\theta = 2°$ at Q = 1ml/hr

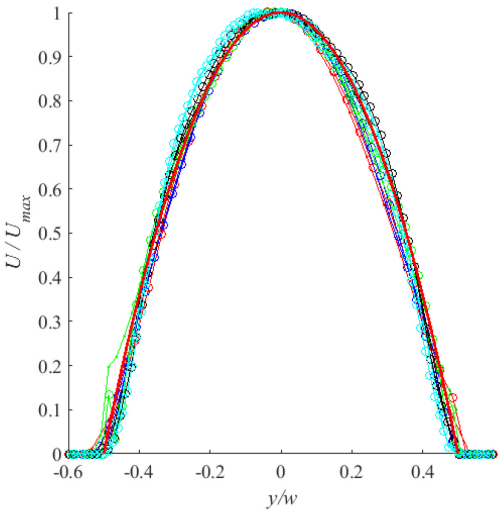

(d) Water flow through keystone slot with $\theta = 4°$ at Q = 1ml/hr

Figure 5-5. The velocity profile of water at ten positions starting from the entrance of the channel at Q = 1 ml/hr at different (b) $\theta = 0°$ (straight), (c) $\theta = 2°$, (d) $\theta = 4°$, (e) $\theta = 6°$, (f) $\theta = 8°$, (g) $\theta = 10°$, (h) $\theta = 12°$ keystone slots in compare to Newtonian theoretical profile

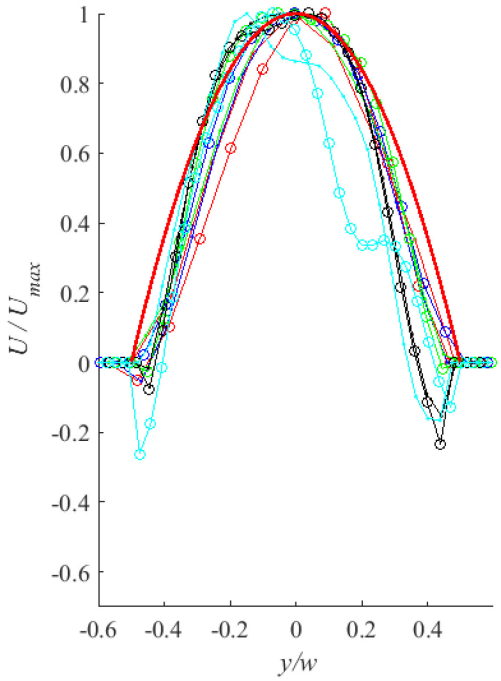

(e) Water flow through keystone slot with $\theta = 6°$ at Q = 1ml/hr

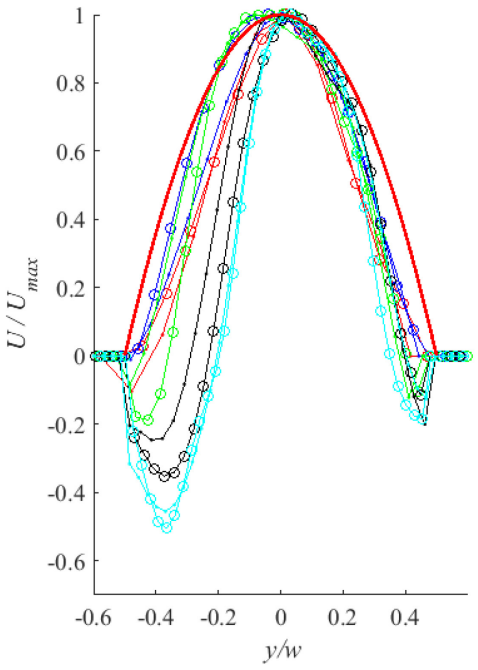

(f) Water flow through keystone slot with $\theta = 8°$ at Q = 1ml/hr

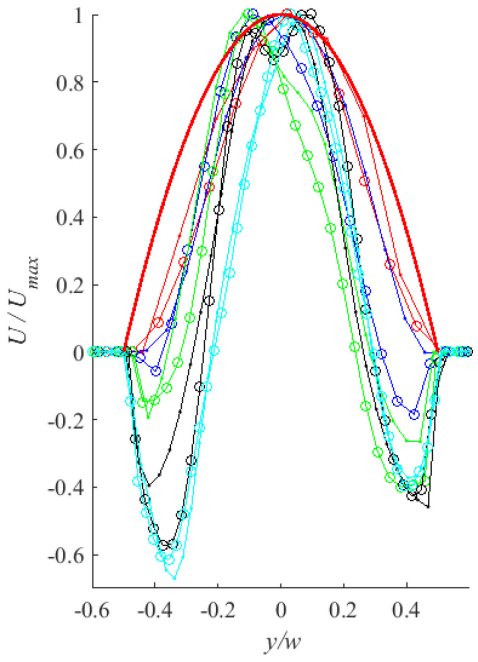

(g) Water flow through keystone slot with $\theta = 10°$ at Q = 1ml/hr

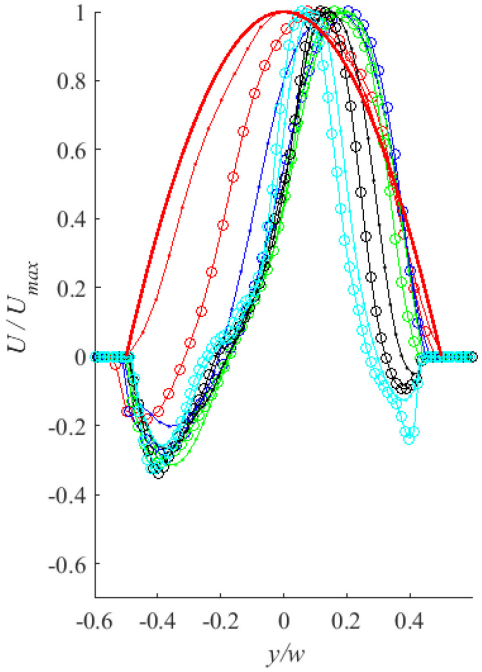

(h) Water flow through keystone slot with $\theta = 12°$ at Q = 1ml/hr

Figure 5-5 (continued)

5.4 Velocity profile of non-Newtonian solutions through keystone slots

The velocity profiles for the flow of non-Newtonian fluid (0.2 wt. %, and 0.4 wt. % polyacrylamide solutions) through the different geometries of keystone slots were studied. The levels of slot angles used for the slots and the values for the flow rates remained the same as those used in the case of water. The main objective was to study the effect of polyacrylamide's shear thinning behavior described in Chapter 3 on its velocity profile. The respective Reynolds numbers of the two concentrations of polyacrylamide solutions were determined according to equation (1-1). In this equation hydraulic diameter of the channel (D_h), density (ρ) of 0.2 wt. %, and 0.4 wt. % polyacrylamide solutions at 25 ℃ are 8.37×10^{-4} m, 999.1 kg/m^3, and 998.3 kg/m^3, respectively. The calculated values of Reynolds numbers for different flow rate are given in Table 5-1**.** The numbers showed that the flow required even smaller distance from the entrance to become fully developed as compared to the case of water.

Table 5-1. Reynolds number of polyacrylamide solutions at different concentrations and flow rates

Concentration (wt. %)	Flow index (n)	Flow consistency (k)	Flow rate Q (ml/hr)	Re
0.2	0.377	0.813	1	6.06×10^{-4}
			5.5	9.75×10^{-3}
			10	2.58×10^{-2}
0.4	0.323	7.112	1	1.23×10^{-2}
			5.5	1.78×10^{-2}
			10	2.41×10^{-2}

The vector plots given in Figure 5-6 and Figure 5-7 show the results obtained for a flow rate of Q = 1 ml/hr for 0.2 wt. %, and 0.4 wt. % polyacrylamide solutions, respectively. The complete set of figures for the other flow rates are given in Appendix D. From Figure 5-6 and Figure 5-7 it was seen that the flow profile had its maximum velocity at the inlet of the channel and the velocity magnitude generally decreased towards the outlet. This observation was similar to the case of water; however, the change in velocity was attributed to the non-Newtonian nature of the polyacrylamide solution. The flow of both concentrations of polyacrylamide solution showed similar trend in its decrease in velocity for all slot geometries.

At both concentrations of polyacrylamide solution and all flow rates, no flow separation was observed. This was attributed to the shear thinning behavior of the fluid which prevented occurrence of any reverse flow. This non-Newtonian nature of polyacrylamide solution also resulted in significantly lower levels of fluctuation that were observed in the case of water. The flow fluctuation seen downstream was also much smaller at higher flow rates (Q = 5.5 and 10ml/hr) than for 1.1 ml/hr.

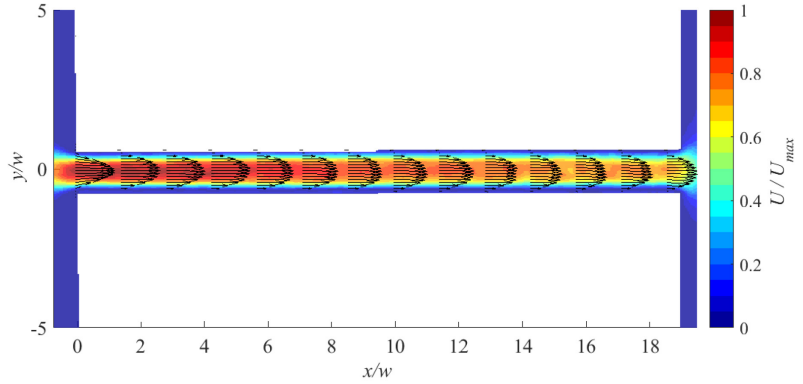

(a) 0.2 wt. % polyacrylamide solution flow through keystone slot with θ =0° (straight) at Q = 1ml/hr

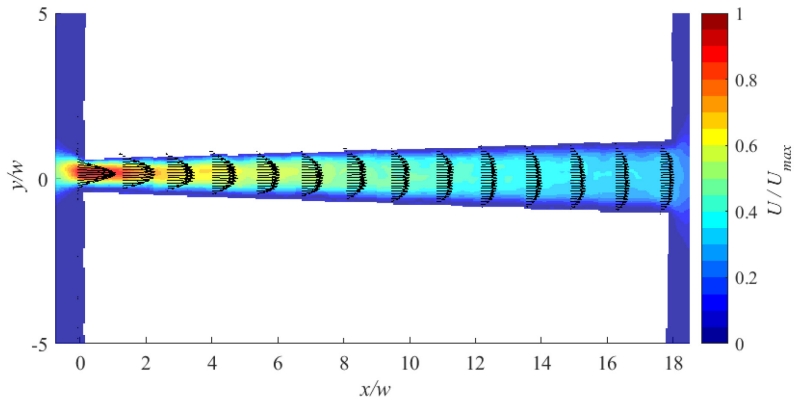

(b) 0.2 wt. % polyacrylamide solution flow through keystone slot with θ = 2° at Q = 1ml/hr

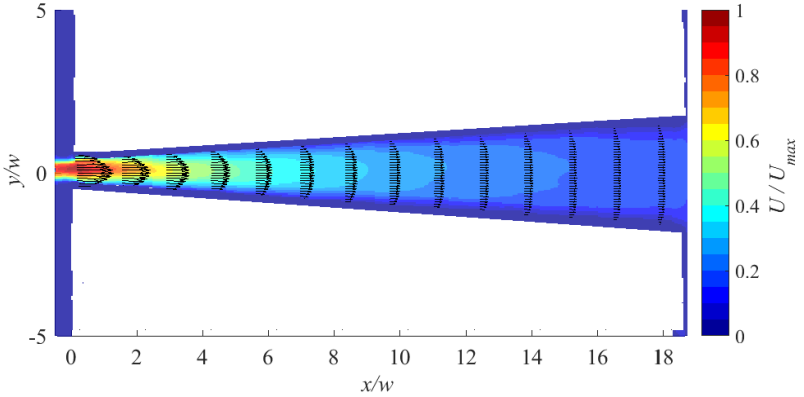

(c) 0.2 wt. % polyacrylamide solution flow through keystone slot with θ = 4° at Q = 1ml/hr

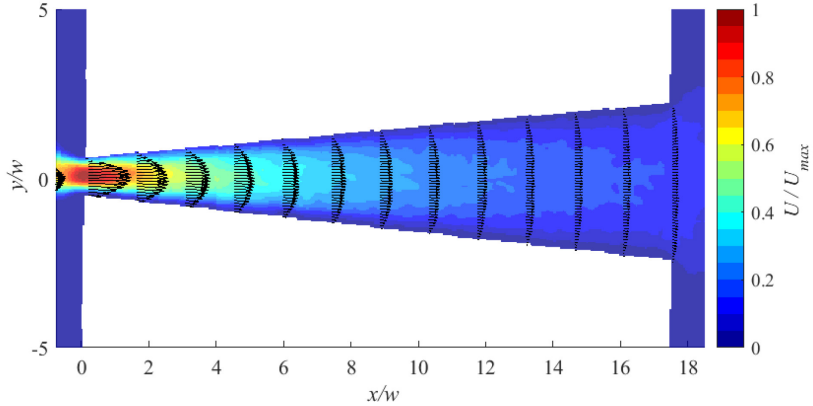

(d) 0.2 wt. % polyacrylamide solution flow through keystone slot with θ = 6° at Q = 1ml/hr

Figure 5-6. Vector map of 0.2 wt. % polyacrylamide solution flow at Q = 1 ml/ hr through (a) θ = 0° (straight), (b) θ = 2°, (c) θ = 4°, (d) θ = 6°, (e) θ = 8°, (f) θ = 10°, and (g) θ = 12° keystone slot

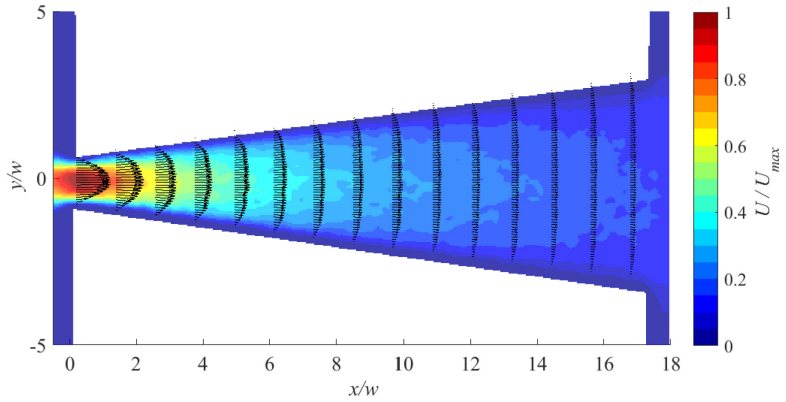

(e) 0.2 wt. % polyacrylamide solution flow through keystone slot with $\theta = 8°$ at Q = 1ml/hr

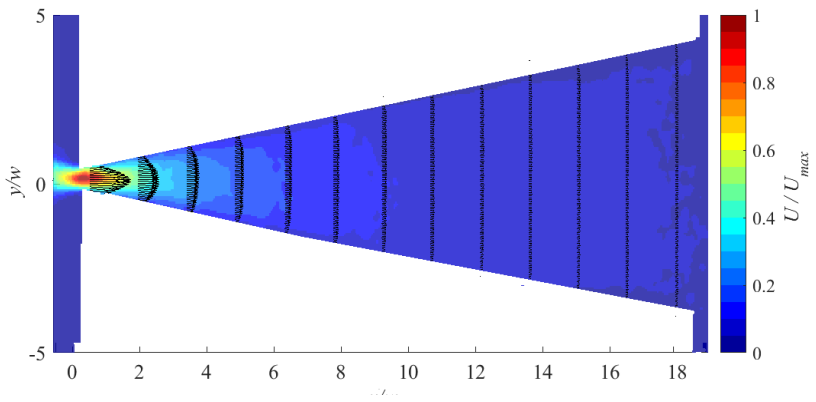

(f) 0.2 wt. % polyacrylamide solution flow through keystone slot with $\theta = 10°$ at Q = 1ml/hr

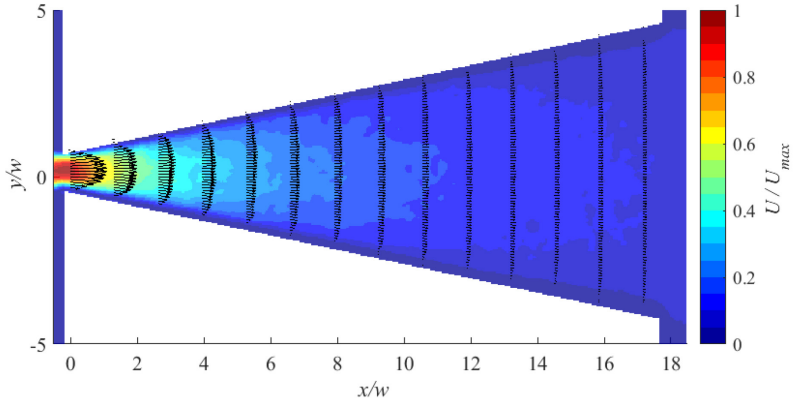

(g) 0.2 wt. % polyacrylamide solution flow through keystone slot with
$\theta = 12°$ at Q = 1ml/hr

Figure 5-6*(continued)*

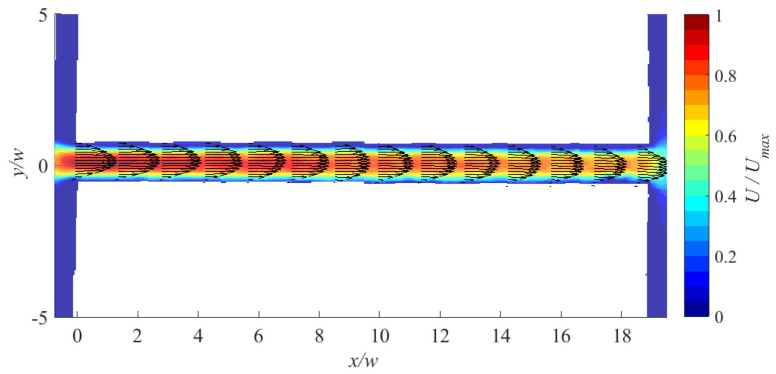

(a) 0.4 wt. % polyacrylamide solution flow through keystone slot with θ =0° (straight) at Q = 1ml/hr

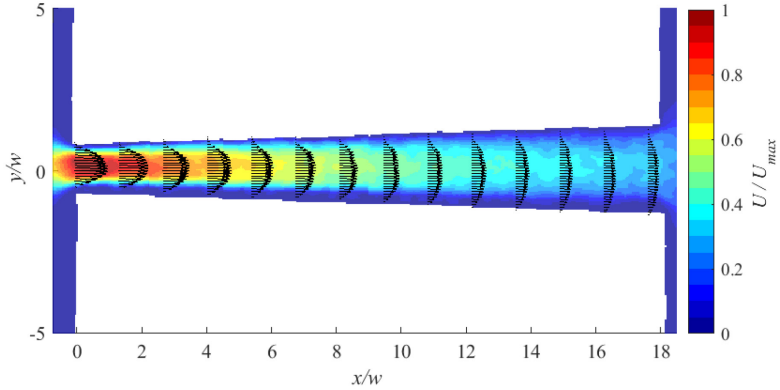

(b) 0.4 wt. % polyacrylamide solution flow through keystone slot with θ = 2° at Q = 1ml/hr

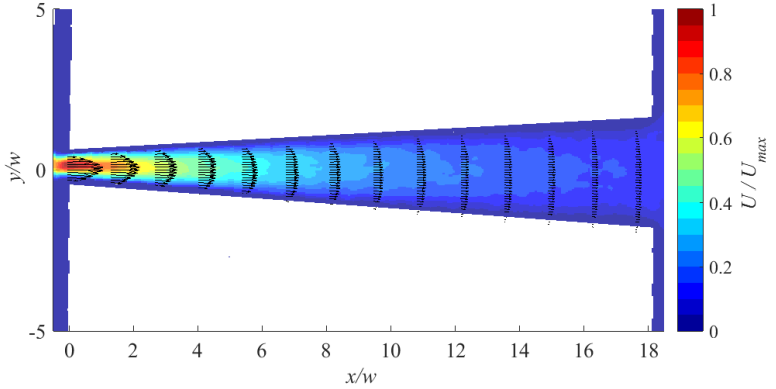

(c) 0.4 wt. % polyacrylamide solution flow through keystone slot with θ = 4° at Q = 1ml/hr

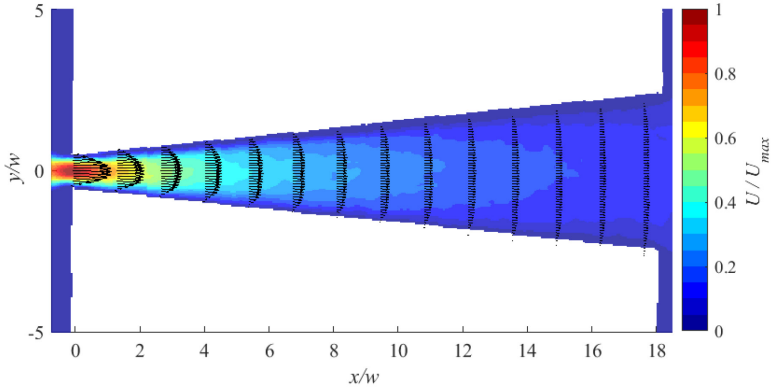

(d) 0.4 wt. % polyacrylamide solution flow through keystone slot with θ = 6° at Q = 1ml/hr

Figure 5-7. Vector map of 0.4 wt. % polyacrylamide solution flow at Q = 1 ml/ hr through (a) θ = 0° (straight), (b) θ = 2°, (c) θ = 4°, (d) θ = 6°, (e) θ = 8°, (f) θ = 10°, and (g) θ = 12° keystone slot

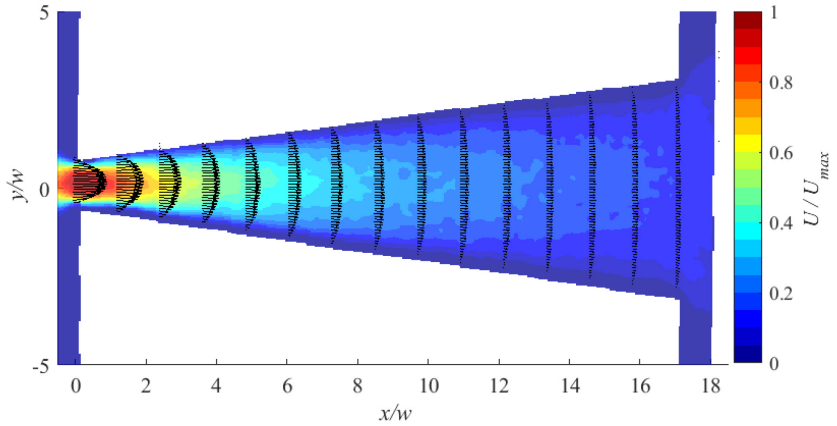

(e) 0.4 wt. % polyacrylamide solution flow through keystone slot with $\theta = 8°$ at Q = 1ml/hr

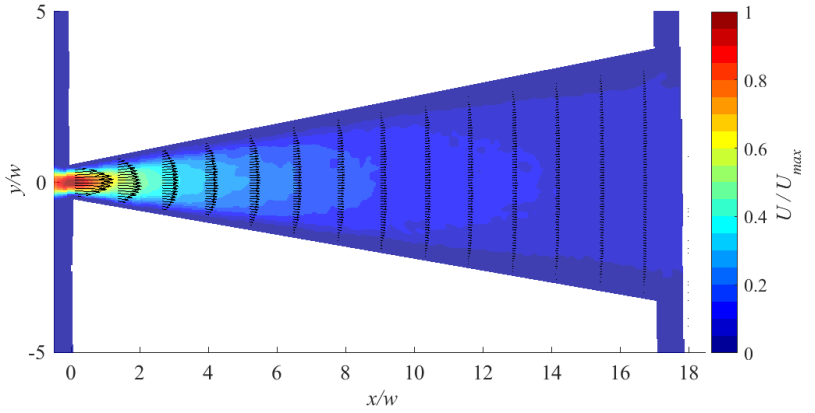

(f) 0.4 wt. % polyacrylamide solution flow through keystone slot with $\theta = 10°$ at Q = 1ml/hr

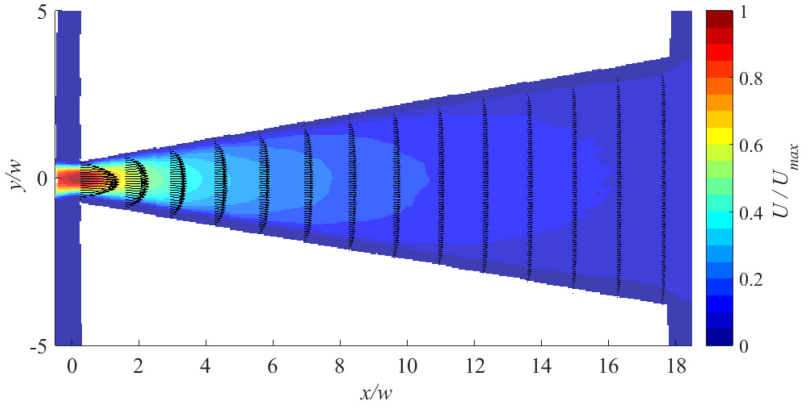

(g) 0.4 wt. % polyacrylamide solution flow through keystone slot with $\theta = 12°$ at Q = 1ml/hr

Figure 5-7 *(continued)*

The normalization of the velocity profile plots for 0.2 wt. %, and 0.4 wt. % polyacrylamide solutions followed the same procedure as for water. The results for the flow of both solutions through the different geometries of slots at 1ml/hr are shown in Figure 5-8 and Figure 5-9. In the figures the theoretical velocity profiles for both Newtonian and the non-Newtonian fluids are also included to compare the shape of the velocity profile in unsteady case with the theory of a fully developed velocity profile in a long straight channel. The flow indices of 0.37 and 0.27 were used for 0.2 wt. % and 0.4 wt. % polyacrylamide solutions, respectively to plot the non-Newtonian flow profile. These values for the flow indices were obtained from rheometer measurements. Normalized plots for 5.5 and 10 ml/hr are given in Appendix D.

From Figure 5-8 and Figure 5-9, the absence of flow separation seen in the corresponding vector plots for the case of polyacrylamide solution was confirmed. All the plots showed a plug flow type profile for the case of straight channel. In general, the profiles approached the shear thinning profiles as the flow went farther downstream the channel ($x/w \sim 10$) for all slot angles. The top hat flow becomes more significant for the flow through slots with higher slot angle as a result of a decrease in shear rate which intensifies the shear thinning behavior of the flow.. The effect of increasing the slot angle showed a more significant top hat profile for 0.4 wt. % polyacrylamide solution in comparison to 0.2 wt. %.

Due to increasing shear rate as the channel converged at the entrance, the non-Newtonian behavior of polyacrylamide solution reduced which resulted in its behavior as a Newtonian fluid as it is shown in Figure 3-6 (a). This phenomenon

can be seen from the plots given in Figure 5-8 which show parabolic profile rather than top hat profile at the entrance of the channel. At higher slot angles ($\theta \geq 6°$), however, increasing cross-sectional area led to lower shear rate which intensified the non-Newtonian behavior. This could be seen from the plots for higher slot angles which show a top hat profile as a result of intensification of the shear thinning behavior of the flow.

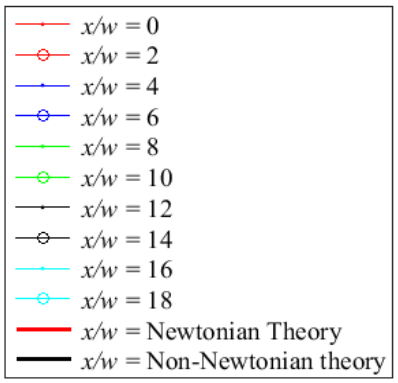

(a)

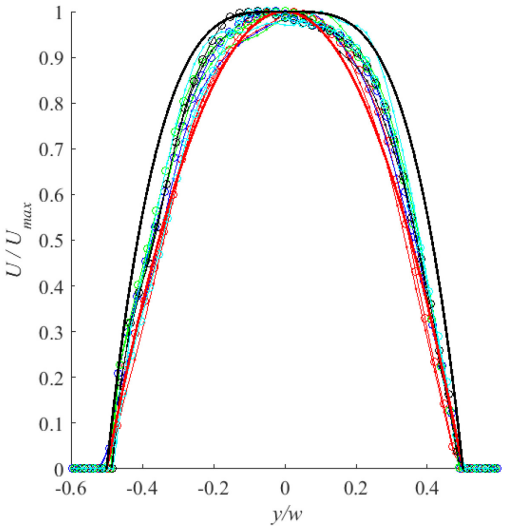

(b) 0.2 wt. % polyacrylamide flow through keystone slot with θ =0° (straight) at Q = 1ml/hr

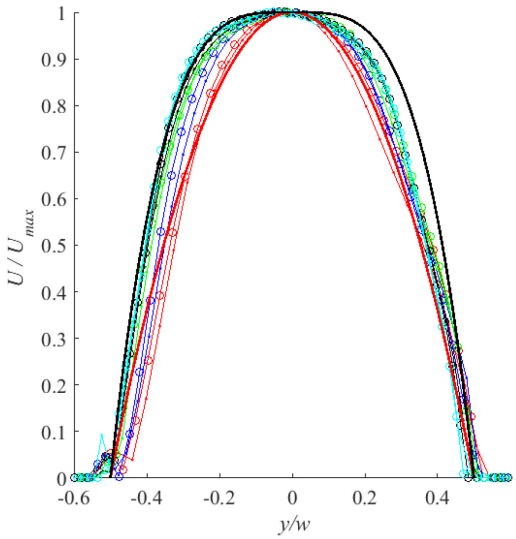

(c) 0.2 wt. % polyacrylamide flow through keystone slot with θ = 2° at Q = 1ml/hr

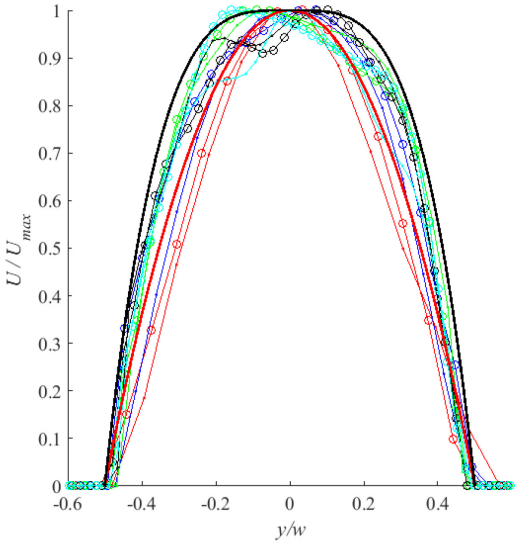

(d) 0.2 wt. % flow through keystone slot with θ = 4° at Q = 1ml/hr

Figure 5-8. The velocity profile of 0.2 wt. % polyacrylamide at ten positions starting from the entrance of the channel at Q = 1 ml/hr at (b) θ = 0° (straight), (c) θ = 2°, (d) θ = 4°, (e) θ = 6°, (f) θ = 8°, (g) θ = 10°, and (h) θ = 12° keystone slot keystone slots in compare to Newtonian and non-Newtonian theoretical profile

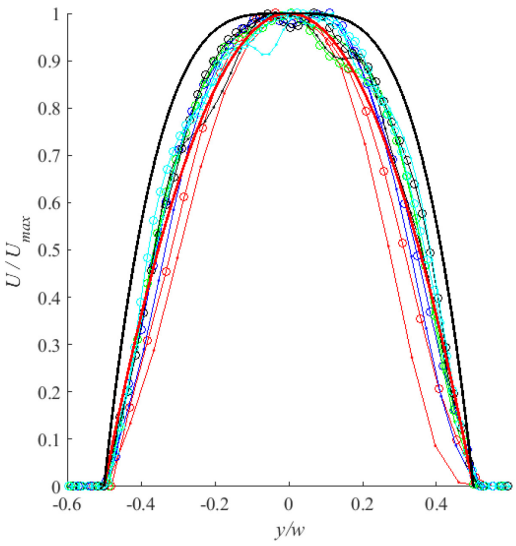

(e) 0.2 wt. % polyacrylamide flow through keystone slot with $\theta = 6°$ at Q = 1ml/hr

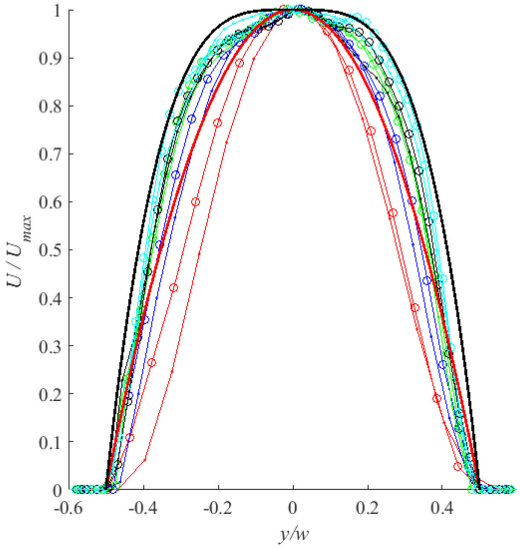

(f) 0.2 wt. % polyacrylamide flow through keystone slot with $\theta = 8°$ at Q = 1ml/hr

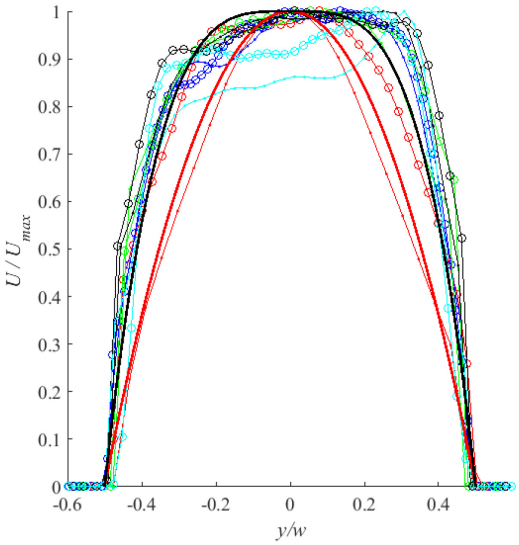

(g) 0.2 wt. % polyacrylamide flow through keystone slot with $\theta = 10°$ at Q = 1ml/hr

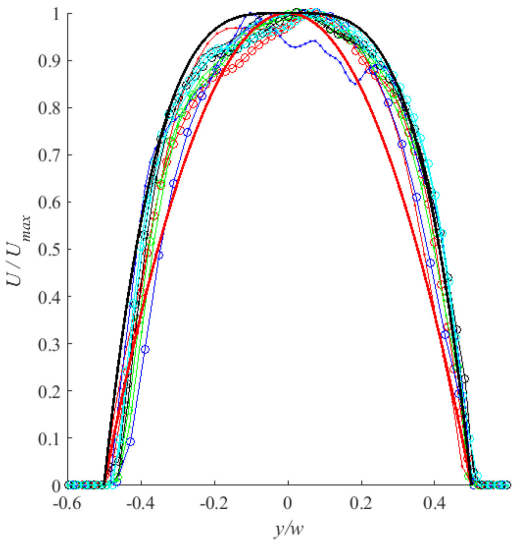

(h) 0.2 wt. % polyacrylamide flow through keystone slot with $\theta = 12°$ at Q = 1ml/hr

Figure 5-8 (continued)

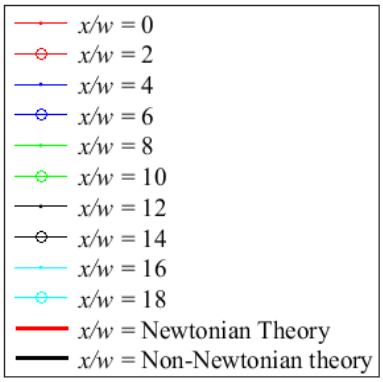

(a)

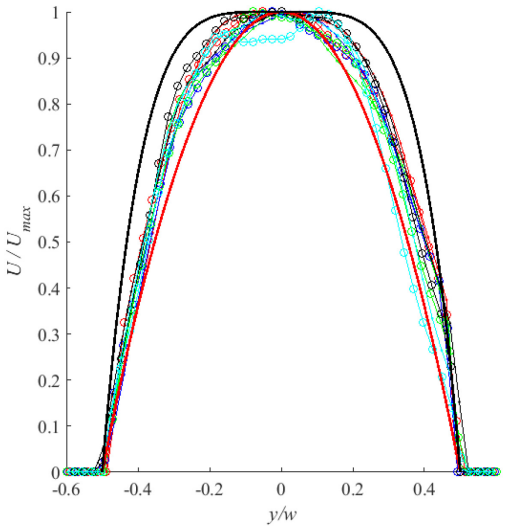

(b) 0.4 wt. % polyacrylamide flow through keystone slot with $\theta = 0°$ (straight) at Q = 1ml/hr

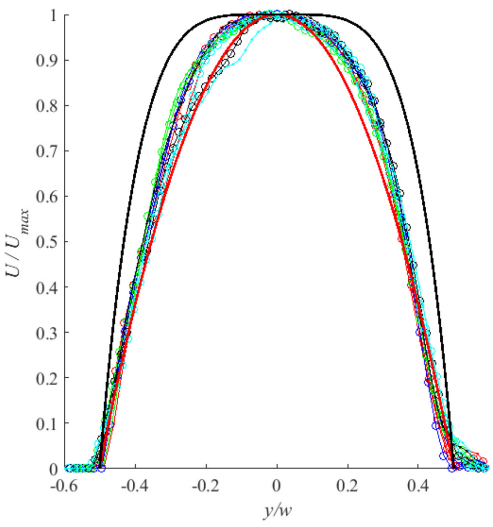

(c) 0.4 wt. % polyacrylamide flow through keystone slot with $\theta = 2°$ at Q = 1ml/hr

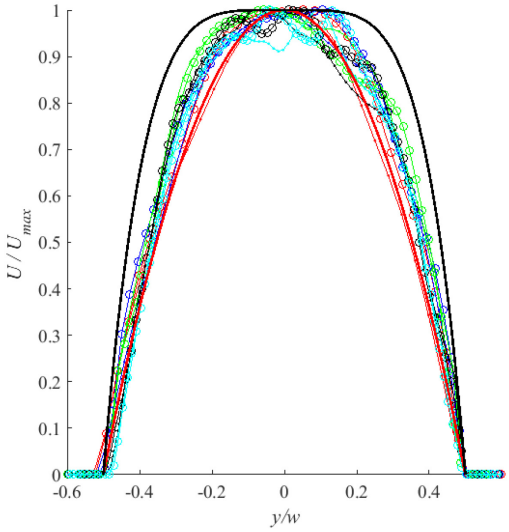

(d) 0.4 wt. % polyacrylamide flow through keystone slot with $\theta = 4°$ at Q = 1ml/hr

Figure 5-9. The velocity profile of 0.4 wt. % polyacrylamide at ten positions starting from the entrance of the channel at Q = 1 ml/hr at different (b) $\theta = 0°$ (straight), (c) $\theta = 2°$, (d) $\theta = 4°$, (e) $\theta = 6°$, (f) $\theta = 8°$, (g) $\theta = 10°$, and (h) $\theta = 12°$ keystone slots in compare to Newtonian and non-Newtonian theoretical profile

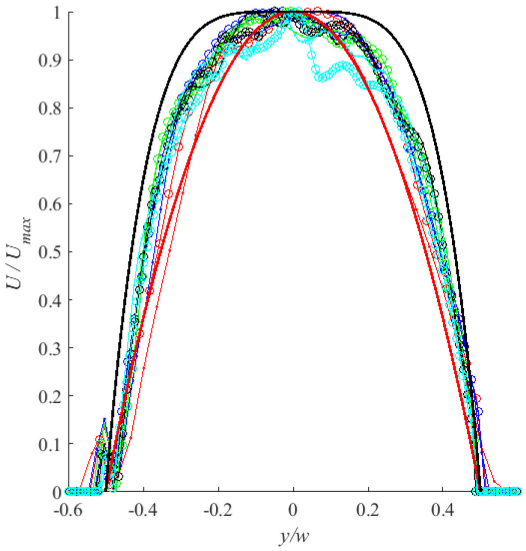

(e) 0.2 wt. % polyacrylamide flow through keystone slot with $\theta = 6°$ at Q = 1ml/hr

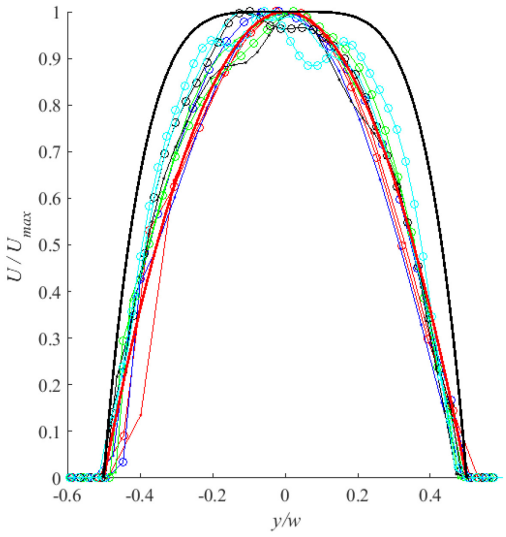

(f) 0.2 wt. % polyacrylamide flow through keystone slot with $\theta = 8°$ at Q = 1ml/hr

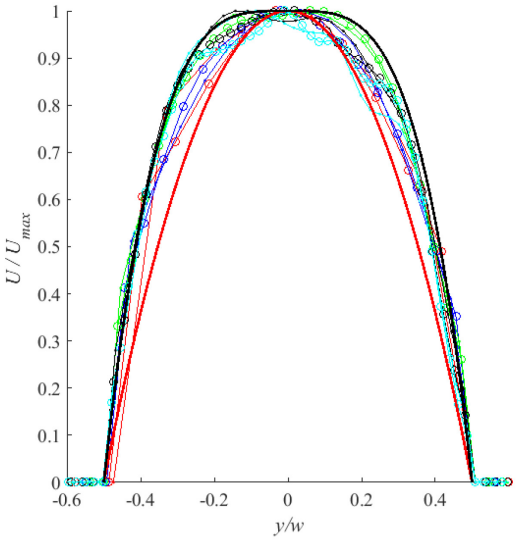

(g) 0.2 wt. % polyacrylamide flow through keystone slot with $\theta = 10°$ at Q = 1ml/hr

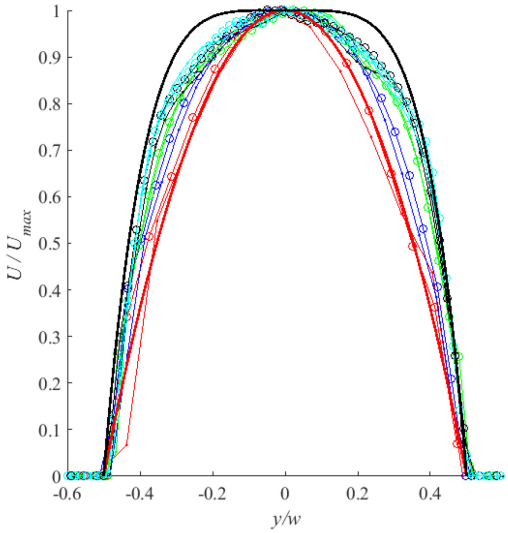

(h) 0.2 wt. % polyacrylamide flow through keystone slot with $\theta = 12°$ at Q = 1ml/hr

Figure 5-9 (continued)

5.5 Comparison of the velocity decay profiles through keystone slots

The effects of geometry and flow rate on the velocity profiles of Newtonian and non-Newtonian fluids through keystone slots were compared. Figure 5-10 shows the respective plots for the velocity profile of the flow in the maximum velocity in the field of the channel ($U_{max}(x)$). In these plots, the velocity was normalized based on the maximum velocity at entrance of channel ($U_{max}(0)$) and the position, *x,* was normalized based on the width of channel entrance.

An overall look at the profiles showed similar trends for all cases tested. The velocities at all flow rates had an increase to reach to the maximum value near the inlet of channel and it then decreased as the flow progressed towards the outlet of the channel. The decrease in velocity ranged from 5 to 90% of the maximum value depending on flow rate, rheology of the fluid and the slot angles of keystone slots. The velocity of water decreases less than the velocity of polyacrylamide solutions and by increasing the concentration of the polyacrylamide solution the velocity decreased faster as results of stronger shear thinning behavior of the fluid.

The velocity decrease was clearly seen in all cases and it was higher for higher slot angles as a result of increment of the downstream cross section area of the channel. The decrement in the velocity profile through straight slot may have been due to frictional effects which were more significant on polyacrylamide solutions than on water especially at lower slot angles. The fluctuations observed

during the flow of water were also seen here for lower flowrate (1 ml/ hr). This fluctuation was seen more in higher slot angles ($\theta \geq 6°$) and intensified as the angle became larger. In Figure 5-10 (e)–(h) the plot for water at low flow rate could be noticed as outliers which are due to the flow separation phenomenon shown in the corresponding vector plots discussed in previous section.

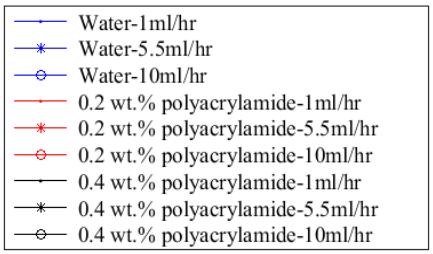

(a)

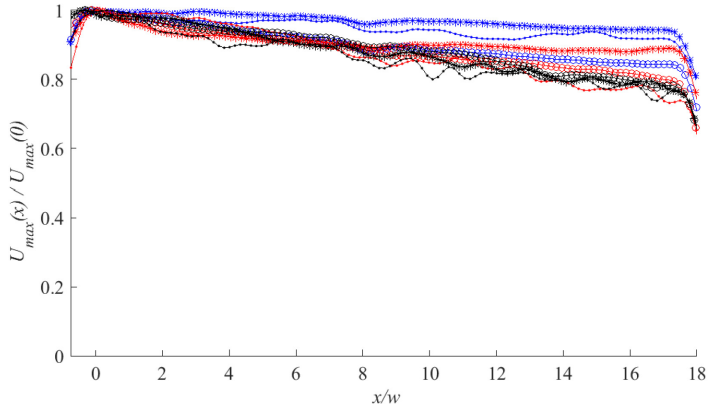

(b) Newtonian and non-Newtonian flow through keystone slot with $\theta = 0°$ (straight) at different flow rates

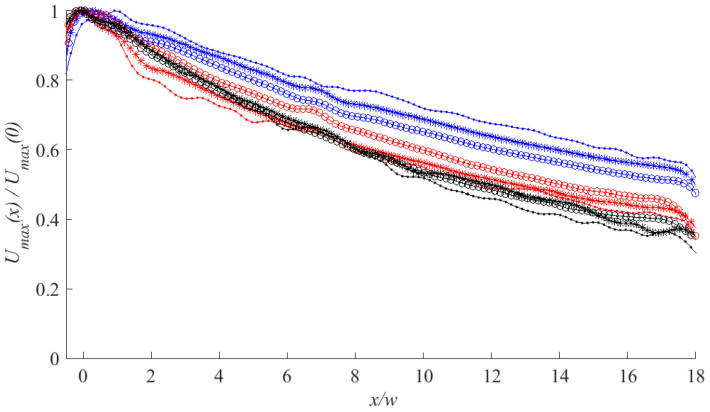

(c) Newtonian and non-Newtonian flow through keystone slot with $\theta = 2°$ at different flow rates

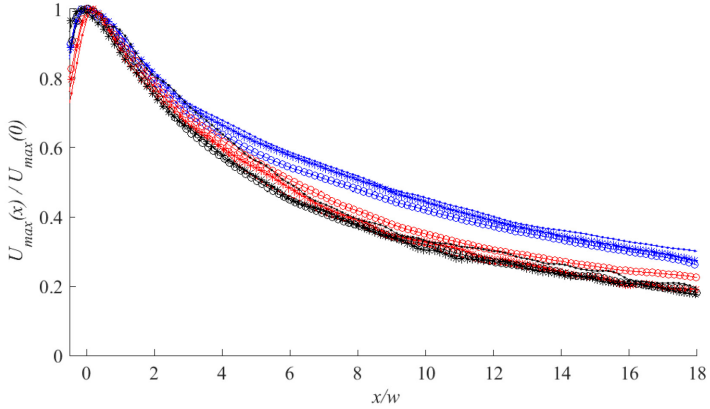

(d) Newtonian and non-Newtonian flow through keystone slot with $\theta = 4°$ at different flow rates

Figure 5-10. Comparison of the velocity profiles of Newtonian and non-Newtonian through (b) $\theta = 0°$ (straight), (c) $\theta = 2°$, (d) $\theta = 4°$, (e) $\theta = 6°$, (f) $\theta = 8°$, (g) $\theta = 10°$, (h) $\theta = 12°$ keystone slot

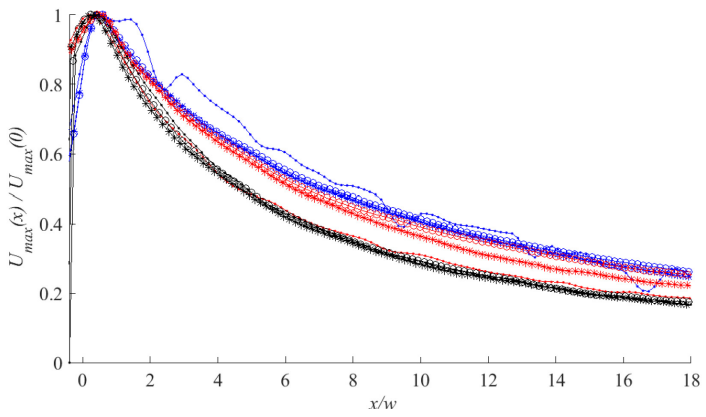

(e) Newtonian and non-Newtonian flow through keystone slot with $\theta = 6°$ at different flow rates

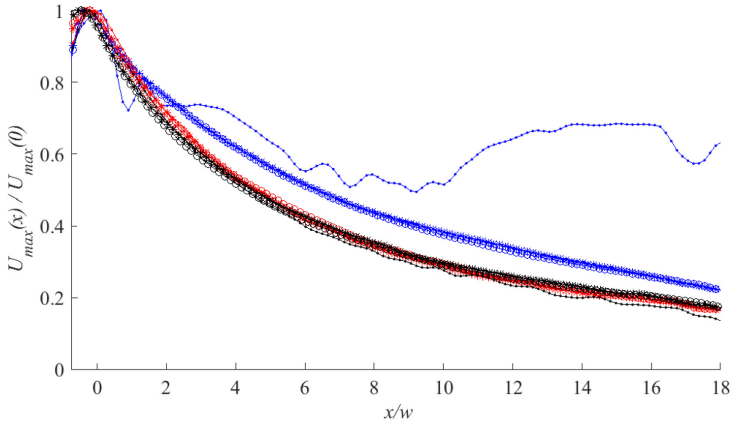

(f) Newtonian and non-Newtonian flow through keystone slot with $\theta = 8°$ at different flow rates

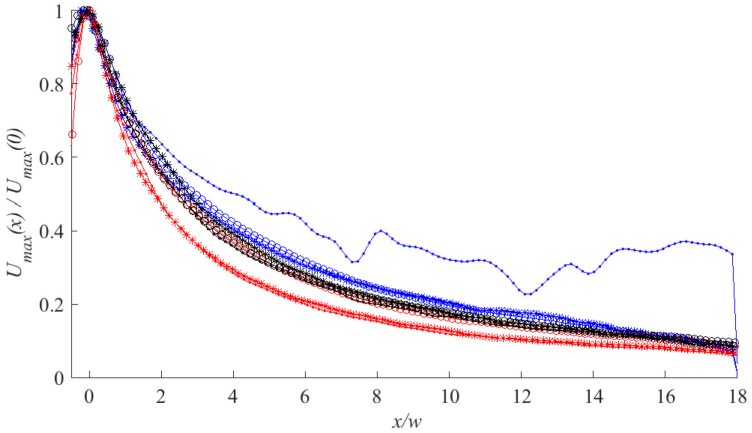

(g) Newtonian and non-Newtonian flow through keystone slot with $\theta = 10°$ at different flow rates

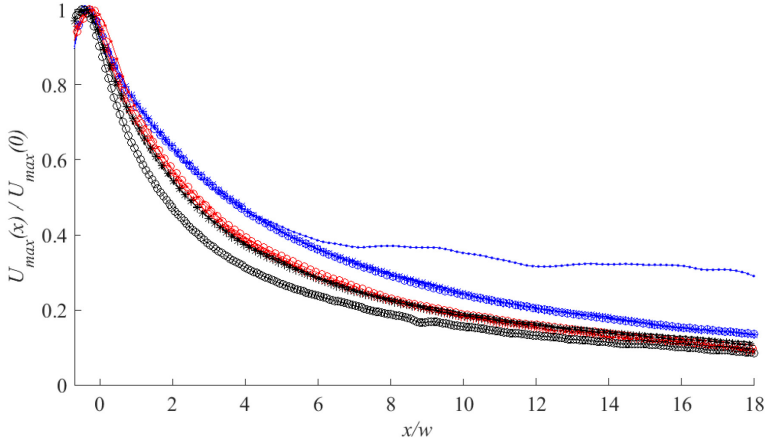

(h) Newtonian and non-Newtonian flow through keystone slot with $\theta = 12°$at different flow rates

Figure 5-10 *(continued)*

The expansion of the flow into a diverging channel has similarities to the decay of a jet. The axial velocity profile of the jet on the centerline of the flow can be modeled as [103]:

$$\frac{U_x}{U_o} = K\,\frac{w}{x - x_p} \tag{5-3}$$

where U_x is the centerline mean velocity, U_o the outlet velocity of the orifice and x is the position along the jet, x_p is the position of the virtual origin of the jet from the entrance of the orifice and K is the velocity decay coefficient. The reciprocal of the equation shows a linear relationship between normalized velocity and normalized position along the jet with a slope of $1/K$ [103].

According to Figure 5-11, Figure 5-12, and Figure 5-13, the reverse of normalized velocity profile and normalized position show in general a linear relationship. In these graphs $U_x = U_{max}(x)$ which is the maximum velocity at position x, and $U_o = U_{max}(0)$ which is the maximum velocity of the inlet of the slot. The plots for water through slots with $\theta \geq 6°$ at Q = 1ml/hr showed a different non-linear trend as a result of flow separation described in section 5.3. With increasing slot angle the slopes of the plots, $1/K$, increased which showed that the decay number, K decreases as in the flow cross sectional area increases. Fluctuation was observed downstream of the flow through slots with higher angles as a result of increase in cross sectional area. As the concentration of polyacrylamide solution increased, an increase in fluctuations could also be seen in the profiles.

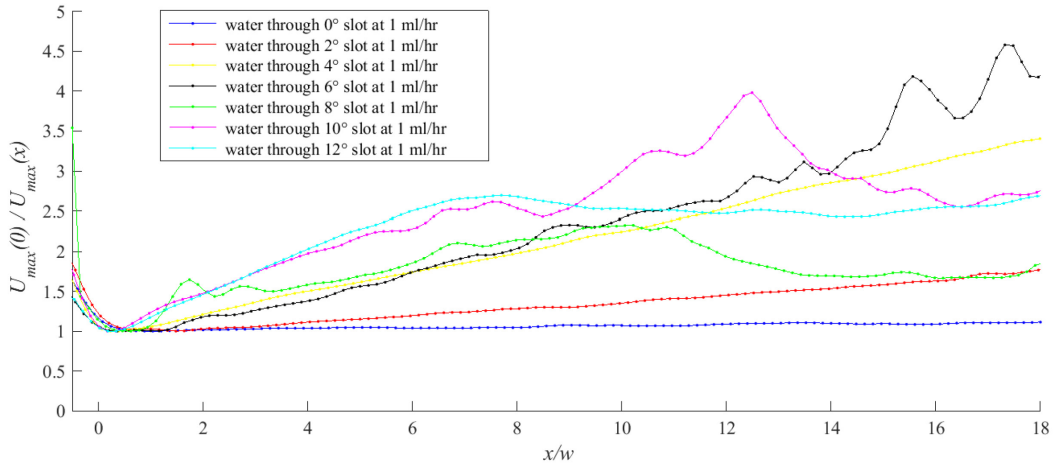

(a)

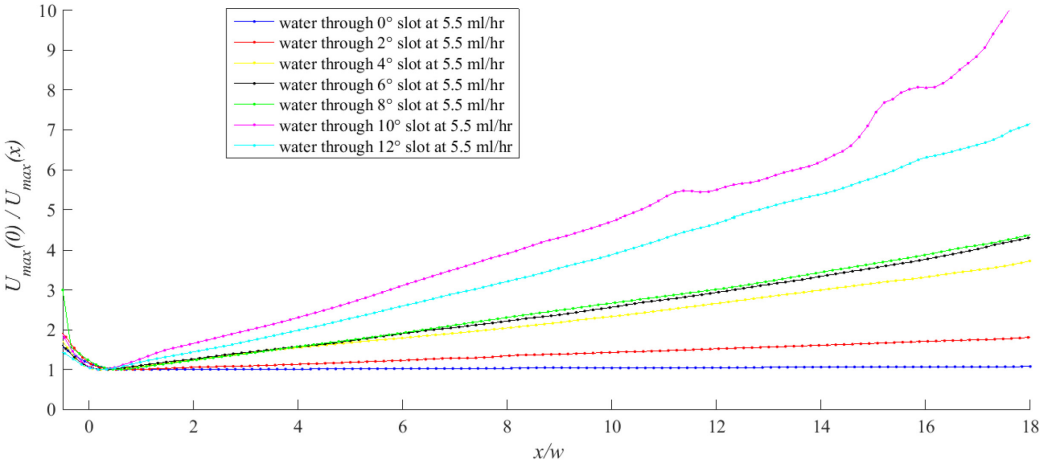

(b)

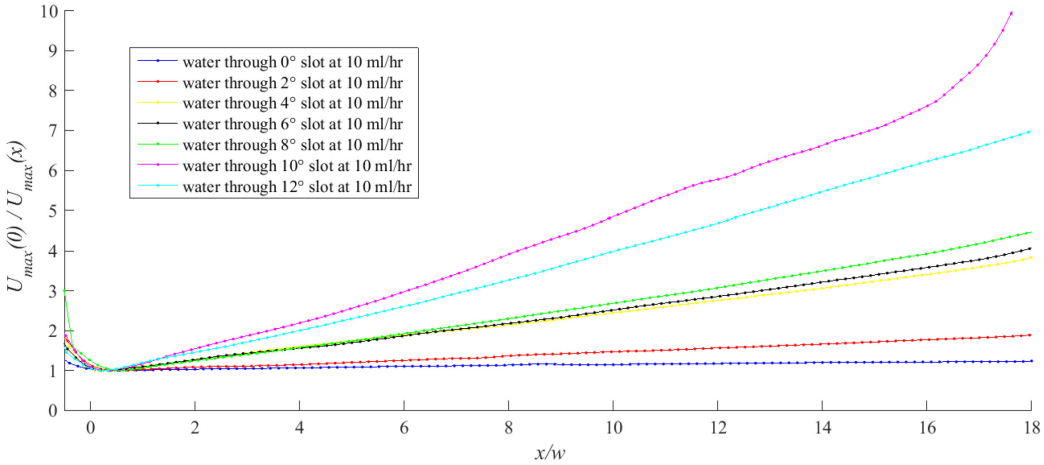

(c)

Figure 5-11. Comparison of the velocity profiles of Newtonian flow through different slot angles at (a) Q =1 ml/hr , (b) Q =5.5 ml/hr and (c) Q =10 ml/hr

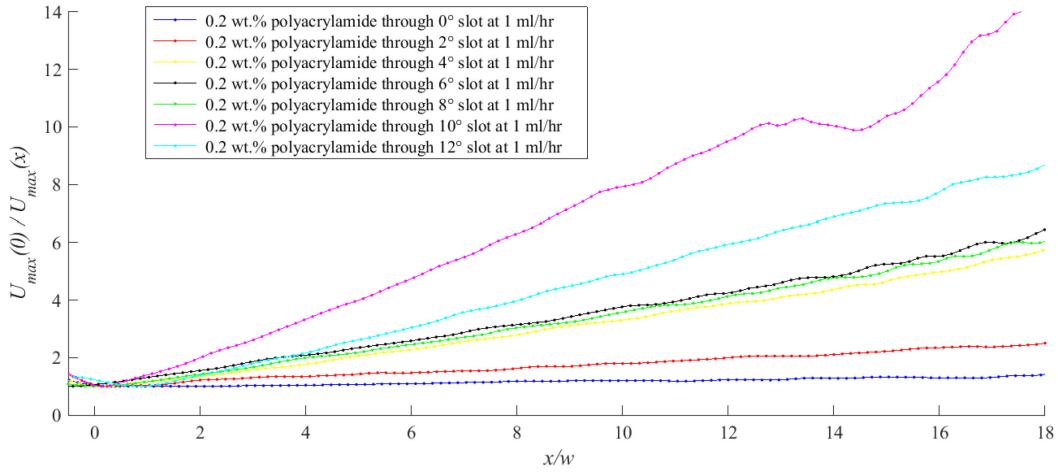

(a)

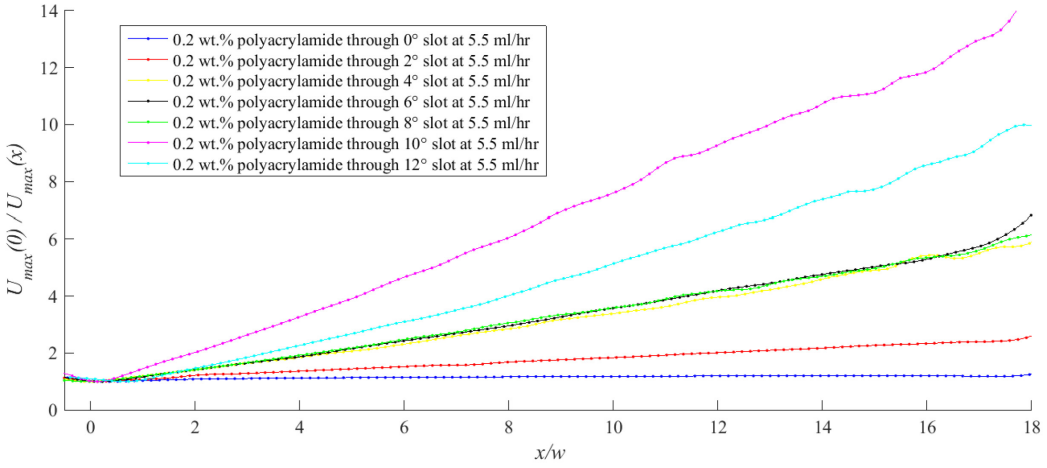

(b)

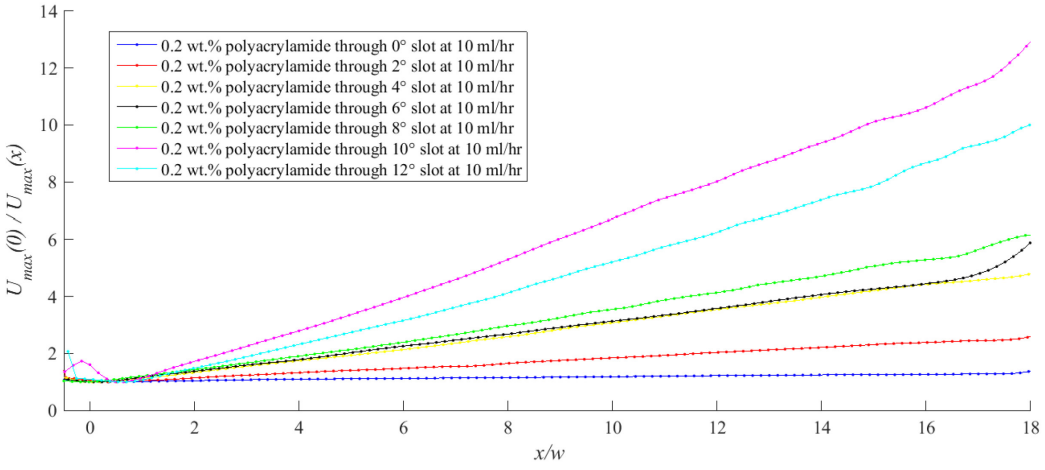

(c)

Figure 5-12. Comparison of the velocity profiles of non-Newtonian (0.2 wt.% polyacrylamdie solution)flow through different slot angles at (a) Q =1 ml/hr , (b) Q =5.5 ml/hr and (c) Q =10 ml/hr

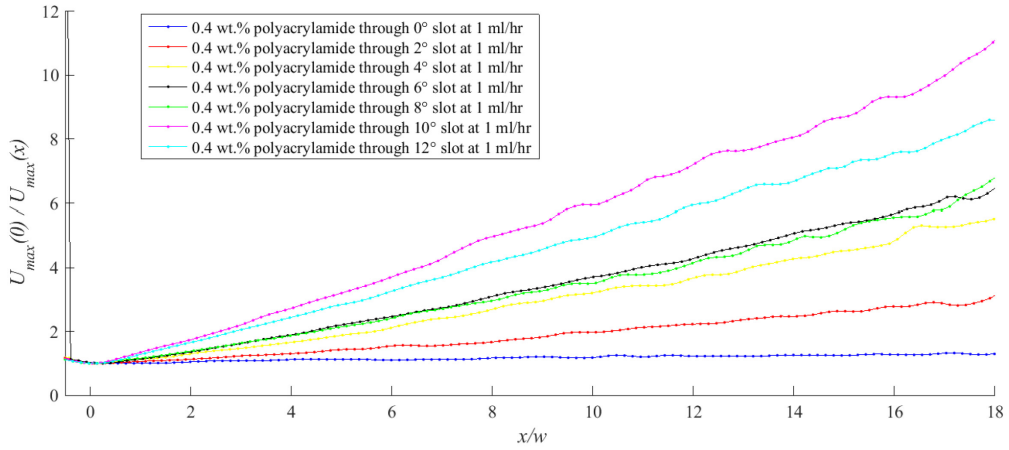

(a)

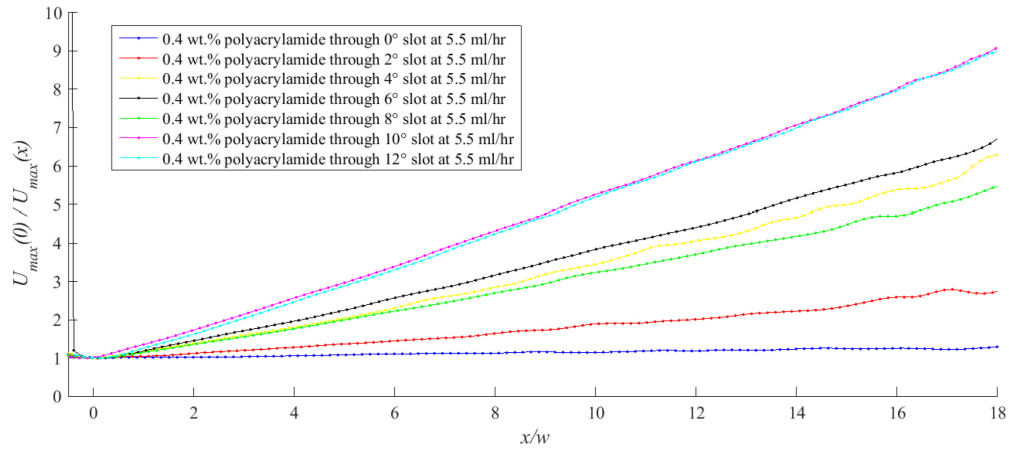

(b)

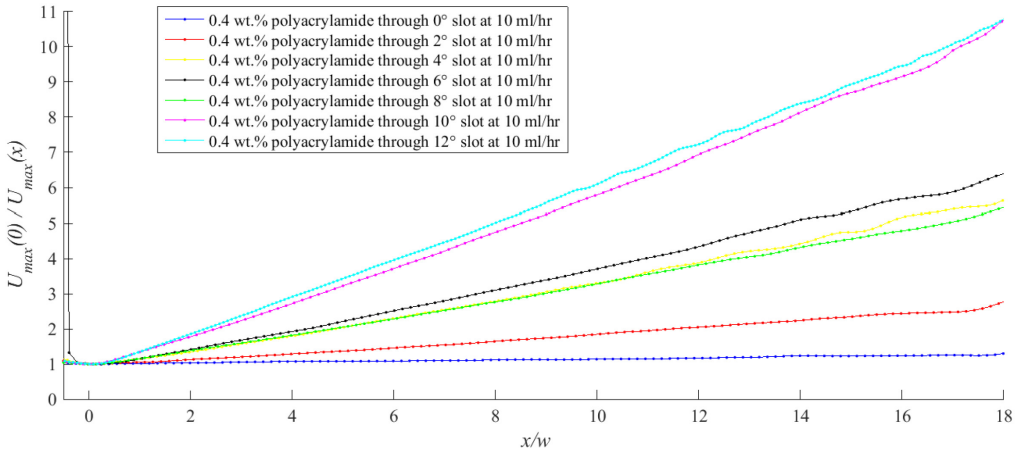

(c)

Figure 5-13. Comparison of the velocity profiles of non-Newtonian (0.2 wt.% polyacrylamdie solution)flow through different slot angles at (a) Q =1 ml/hr , (b) Q =5.5 ml/hr and (c) Q =10 ml/hr

The reversed normalized velocity data were fitted to a linear model (see Appendix D-4). The slopes of respective curves were plotted against slot angle, θ, as shown in Figure 5-14. Overall, an increase in slot angle resulted in a corresponding increase in slope. The slope also increased as the concentration of the polyacrylamide solution increased. The minimum slope in velocity was observed for water, and 0.4 wt. % polyacrylamide solution had the maximum slope. There is a difference in trend between the slope of water at the minimum flow rate of Q = 1 ml/hr, which was due to the flow separation described in Section 5.3 (for $\theta \geq 6°$). It should be noted that the slope for the flows for the conditions where separation was observed was determined use the region form the inlet of the channel to where separation occurred. These results, therefore, showed that the reduction in velocity increased as the slot angle and/or shear thinning behaviour of the fluid increased.

For the flow through slots with $\theta = 10°$, plots showed a clear deviation from the trend in the remanding data. This may be a result of variation in the slot's geometry due to manufacturing. Specifically, inlet conditions may be a strong contributing factor. However, the possibilities for an actual fluid mechanic phenomenon being the cause this observation shall not be disregarded and further investigations may aim at confirming this.

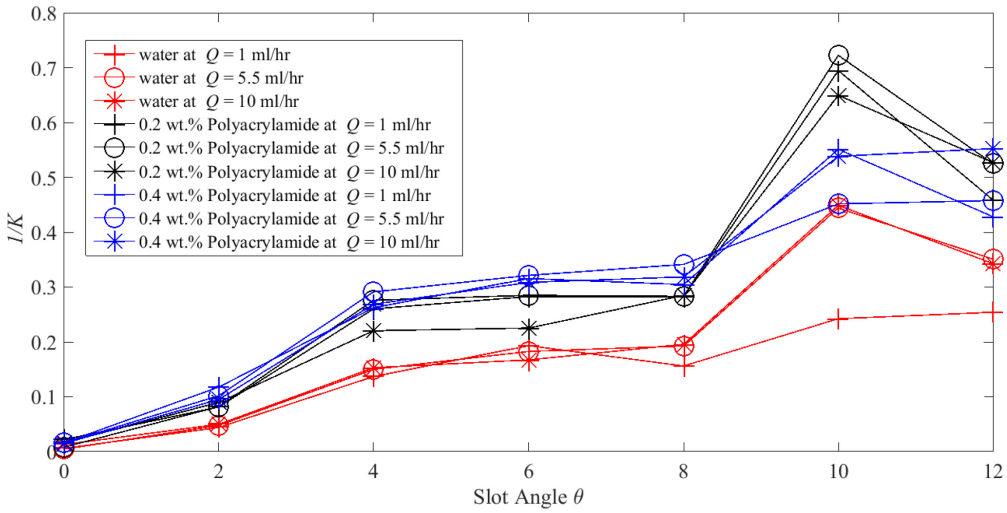

Figure 5-14. Plot of variation in slope of inverese normalized velocity number with slot angle

5.6 Conclusion

Experimental results showed that the velocity profile through different keystone slots geometries varied with the rheology of the fluid, flow rate and slot angle. The following paragraphs summarize the major conclusion arrived at from observations.

Velocity profile of water had a parabolic profile through slots with lower slot angles ($\theta < 6°$). For slots with $\theta \geq 6°$, flow separation and reverse flow phenomena were observed at flow rate of Q = 1 ml/hr and no flow separation were observed in higher flow rates. The intensity of flow separation condition was at maximum for a slot angle of θ =10°. As the slot angle increases, the position where flow separated occurred closer to the channel inlet.

The velocity distributions for 0.2 wt. % and 0.4 wt. % polyacrylamide were plotted and the results were compared with theoretical profiles for Newtonian and

non-Newtonian fluids to study the effect of the unsteady condition originated from the increase in cross section area on the shape of the velocity profile. At the entrance of the channel the flow behave as Newtonian flow while, at higher slot angles of ($\theta \geq 6°$) higher cross-sectional areas along the channel length led to a reduced shear rate and a Newtonian-like behavior of the fluid. This condition resulted in the profile to have similarities to the Newtonian theory than the non-Newtonian theory. No flow separation was observed for the flow of 0.2 wt. % and 0.4 wt. % polyacrylamide solutions through all channels and at all flow rates. However, fluctuations in the velocities around the channel outlet were observed. Such fluctuations were much higher in the case of water.

Comparison of the profiles for Newtonian and non-Newtonian fluids showed a similar trend of velocity reduction as the flow progressed downstream in the channel. At all flow rates, it was common to both fluids to have an increase in velocity to the maximum at the inlet of the channel followed by a steady reduction. The reduction in velocity was lower in water and higher for polyacrylamide solutions which further increased with increasing concentration. Small region of fluctuation was observed at the flow through slots with larger slot angles.

Chapter 6. Conclusions and Future Work

The effects of geometry of channel, fluid rheology, and flow rate on the velocity distribution of flow through mini-channel and orifices were studied. The orifices tested had the keystone geometry used for SAGD slotted liners. To study the effect of rheological properties of the fluid water (Newtonian) and polyacrylamide solution (non-Newtonian) were used. Polyacrylamide solution was chosen following study of its rheological properties which showed that it had consistent non-Newtonian (shear thinning) behavior over a long period of time. The velocity distributions were identified using particle image velocimetry which enabled a non-intrusive measurement of the flow field. A unique hybrid processing scheme was developed to process image data and plot the velocity profile.

6.1 Flow of Newtonian and non-Newtonian fluids through mini-channel

Experiments for the flow through long channel were conducted for different flowrates, Q, (0.025, 0.05, 0.075, and 0.1 ml/min), and concentrations of polyacrylamide solution (0.1, 0.3, and 0.5 wt. %). The velocity profile of Newtonian fluid had a parabolic shape which matched the corresponding theory and remained the same for all flowrates. Non-Newtonian fluids also showed profile of the top-hat shape that matched the theory. The top-hat region of the velocity profiles flattened more as the shear thinning behavior of the fluid intensified.

The rheological parameters for non-Newtonian fluid (flow index, n, and flow consistency index, k) were determined from the velocity profile using the power law model and non-Newtonian theory. These results were validated with measurement using a commercial rheometer. It was hence concluded that the velocity distribution results from PIV measurements can be coupled with non-Newtonian theories to determine the rheological properties of a fluid without the need to use a measurement device.

6.2 Flow of Newtonian and non-Newtonian fluids through keystone slots

The flows of Newtonian and non-Newtonian fluids through keystone slots of different slot angle, θ, (0°, 2°, 4°, 6°, 8°, 10°, and 12°) were investigated using results from PIV measurements. The experiments carried out studied flows at flow rates, Q, of 1, 5.5, and 10 ml/hr for which the Reynolds number, Re, was in the creeping to laminar flow regions ($6.06\times10^{-4} \leq Re \leq 1.67$). All the considered parameters showed significant effects on the velocity profile of Newtonian fluid. The flow of non-Newtonian fluid, however, was only affected by slot angle.

The flow of Newtonian fluid through all slot geometries maintained a parabolic profile for the velocity distribution. The change in flow rate did not have any effect on the shape of the velocity profile. The flow velocity had a decrease along the channel in all slot angles. As the slot angle, θ, increased there was an increase in the velocity gradient. Increase in cross sectional area due to the keystone profile was the reason for this condition.

Comparison of the velocity profile for non-Newtonian fluid with the theoretical plots showed that the flow behaves as a Newtonian fluid at the inlet of the channel. Since the channel inlet involved a contraction-expansion configuration, the shear rate of fluid is highly affected. This caused the rheology of the shear thinning fluid to change so that it showed a Newtonian-like behavior at the inlet of the channel. This effect of the channel inlet geometry was more profound for lower slot angles ($\theta < 6°$). The velocity of the flow decreased along the channel. Due to the shear thinning behavior and increase in the cross-sectional area, this gradient increased as the shear thinning behavior became more intense and for slot angles increased.

Flow rate, Q, and slot angle, θ, also had interacting effects on the flow of Newtonian fluid that resulted in flow separation at lower flow rates (1 ml/hr) and higher slot angles ($\theta \geq 6°$). This condition which was more apparent as the slot angle increased was not seen for the other flow rates tested. This phenomenon did not occur for the flow of non-Newtonian fluids.

6.3 Future work

The conclusions that were made from the results of this study are believed to have good contribution in selecting the geometry for minimal scaling of slots and optimum velocity distribution for maximum production. However, there remain areas on which future works shall be focused to for a clearer picture of the entire flow phenomenon. The following points are recommended as subjects for

future researches that are to aim at developing a more comprehensive description of the flow.

- The pressure drop for a flow field can be described by using the velocity distribution. The results from the PIV measurement of the velocity profile can be used to determine the pressure distribution.
- The use of circular saw blades for the manufacturing of slots results in different (lateral) lengths of slots on the outer and inner diameters of the liner. This condition makes determining the third component of velocity important. Photonic measurement of this out-of-plane velocity requires the use of stereo-PIV. The study of the flow through keystone slots can therefore improve by using this method.
- Geometries and arrangements of slots that are similar to those commonly used in the industry can be included to make further description of the flow. Rolled slots and/or multiple slot arrangements may be considered.
- The material used to make the flow chip can be made similar to that of the slotted liner to make investigation about other features related to the surface.
- In SAGD operation inflow of bitumen from the formation to the slots involves multiphase flow through porous media. The experiments on the flow regime can therefore include porous media and multiple phases to study flow conditions that are closer to real application scenarios.

References

[1] Purre, H. (1964).*U.S. Patent No. 3,116,792*. Washington, DC: U.S. Patent and Trademark Office.

[2] Burger, J., Sourieau, P., & Combarnous, M. (1986). Thermal methods of oil recovery. Gulf Publishing Co.,Houston, TX

[3] Lightbown, V. (2015). New SAGD technologies Show promise in reducing environmental impact of oil SAND production *Journal of Environmental Solutions for Oil, Gas, and Mining*, *1*(1), 47-58.

[4] Donaldson, E. C., Chilingarian, G. V., & Yen, T. F. (Eds.). (1989). *Enhanced oil recovery, II: Processes and operations*. Elsevier.

[5] Matanovic, D., Cikes, M., & Moslavac, B. (2012). *Sand Control in Well Construction and Operation*. Springer Science & Business Media.

[6] Mochinaga, H., Onozuka, S., Kono, F., Ogawa, T., Takahashi, A., & Torigoe, T. (2006). Properties of Oil sands and Bitumen in Athabasca. In *The Canadian Society of Exploration Geologists CSPG–CSEG–CWLS Convention* (pp. 14-17).

[7] McLellan, P. J. (1996). Assessing the risk of wellbore instability in horizontal and inclined wells. *Journal of Canadian Petroleum Technology*, *35*(05).

[8] Hawkes, C.D., McLellan, P.J. (1997): A New Model for Predicting Time-Dependent Failure of Shales: Theory and Application, paper 97-131presented at the 48th Annual Technical Meeting of The PetroleumSociety, 8-11 June, Calgary, Canada.

[9] Bowes, C., Procter, R. (1997): Drillers Stuck Pipe Handbook, 1997 Guidelines & Drillers Handbook Credits, Schlumberger, Ballater, Scotland.

[10] Pasic, B., Gaurina-Međimurec, N., & Matanovic, D. (2007). Wellbore Instability: Causes And Consequences/Nestabilnost Kanala Busotine: Uzroci I Posljedice. Rudarsko-geolosko-naftni zbornik, 19(1), 87.

[11] Warren, B. K., McLellan, P. J., & Pratt, C. A. (1995, January). Wellbore stability, drilling fluids design, and the drilling performance of horizontal wells in unconsolidated oil sands at Peace River, Alberta. In SPE/IADC Drilling Conference. Society of Petroleum Engineers.

[12] Al-Bahlani, A. M., & Babadagli, T. (2009). SAGD laboratory experimental and numerical simulation studies: A review of current status and future issues.*Journal of Petroleum Science and Engineering*, *68*(3), 135-150.

[13] Brand, S. (2010, January). Results from Acid Stimulation in Lloydminster SAGD Applications. In *SPE International Symposium and Exhibiton on Formation Damage Control*. Society of Petroleum Engineers.

[14] Goodman, W. H., Godfrey, M. R., Miller, T. M., & Comany, N. (2010, October). Scale and deposit formation in steam assisted gravity drainage (SAGD) facilities. In *The International Water Conference* (pp. 24-28).

[15] Lalchan, C. A., Wiggins, C. B., & Moriyama, C. (2011, January). Formulation of an Emulsified Thermal Acid Blend for SAGD Applications in Eastern Alberta. In *Canadian Unconventional Resources Conference*. Society of Petroleum Engineers.

[16] Osacky, M., Geramian, M., Ivey, D. G., Liu, Q., & Etsell, T. H. (2013). Mineralogical and chemical composition of petrologic end members of Alberta oil sands. *Fuel*, *113*, 148-157

[17] Samiei, S. (2007). Role of ultra-fine solid fractions on rheology of oil sands suspensions. In *Masters Abstracts International* (Vol. 46, No. 03).

[18] Bennion, D. B., Gupta, S., Gittins, S., & Hollies, D. (2009). Protocols for slotted liner design for optimum SAGD operation. *Journal of Canadian Petroleum Technology*, *48*(11), 21-26.

[19] Kumar, A., Srivastava, A. K., & Kumar, R. (2010, January). Design optimization of slotted liner completions in horizontal wells of mumbai high field. In *SPE Asia Pacific Oil and Gas Conference and Exhibition*. Society of Petroleum Engineers.

[20] Mezger, T. G. (2006). *The rheology handbook: for users of rotational and oscillatory rheometers*. Vincentz Network GmbH & Co KG.

[21] Yang, M. H. (2001). The rheological behavior of polyacrylamide solution II. Yield stress. *Polymer testing*, *20*(6), 635-642

[22] Liu, J., Xu, Z., & Masliyah, J. (2004). Role of fine clays in bitumen extraction from oil sands. *AIChE journal*, *50*(8), 1917-1927.

[23] Zhou, Z. A., Xu, Z., Masliyah, J. H., & Czarnecki, J. (1999). Coagulation of bitumen with fine silica in model systems *Colloids and Surfaces A: Physicochemical and Engineering Aspects*, *148*(3), 199-211

[24] Zhao, Y., & Machel, H. G. (2012). Viscosity and other rheological properties of bitumen from the Upper Devonian Grosmont reservoir, Alberta, Canada. *AAPG bulletin*, *96*(1), 133-153.

[25] Dealy, J. M. (1979). Rheological properties of oil sand bitumens. *The Canadian Journal of Chemical Engineering*, *57*(6), 677-683.

[26] Kett, I. (2012). *Asphalt materials and mix design manual*. William Andrew.

[27] Kandlikar, S. G., & Grande, W. J. (2003). Evolution of Microchannel Flow Passages--Thermohydraulic Performance and Fabrication Technology. *Heat transfer engineering*, *24*(1), 3-17.

[28] Wijshoff, H. (2008). *Structure-and fluid-dynamics in piezo inkjet printheads*. University of Twente.

[29] Han, Y., Liu, Y., Li, M., & Huang, J. (2012). A review of development of micro-channel heat exchanger applied in air-conditioning system. *Energy Procedia*,*14*, 148-153.

[30] Beebe, D. J., Mensing, G. A., & Walker, G. M. (2002). Physics and applications of microfluidics in biology. *Annual review of biomedical engineering*, *4*(1), 261-286.

[31] Lima, R., Fernandes, C. S., Dias, R., Ishikawa, T., Imai, Y., & Yamaguchi, T. (2011). Microscale flow dynamics of red blood cells in microchannels: an experimental and numerical analysis. In *Computational Vision and Medical Image Processing* (pp. 297-309). Springer Netherlands.

[32] Sharp, K. V., Adrian, R. J., Santiago, J. G., & Molho, J. I. (2002). Liquid flows in microchannels. *The MEMS Handbook, Mohamed Gad-El-Hak, editor. CRC Press, Boca Raton*.

[33] Hetsroni, G., Mosyak, A., Pogrebnyak, E., & Yarin, L. P. (2005). Fluid flow in micro-channels. *International Journal of Heat and Mass Transfer*, *48*(10), 1982-1998.

[34] Pfund, D., Rector, D., Shekarriz, A., Popescu, A., & Welty, J. (2000). Pressure drop measurements in a microchannel. *AIChE Journal*, *46*(8), 1496-1507.

[35] Li, Z. X. (2003). Experimental study on flow characteristics of liquid in circular microtubes. *Microscale Thermophysical Engineering*, *7*(3), 253-265.

[36] Yang, C. Y. (2003). Friction characteristics of water, R-134a, and air in small tubes. *Microscale Thermophysical Engineering 7*(4), 335-348.

[37] Wu, H. Y., & Cheng, P. (2003). Friction factors in smooth trapezoidal silicon microchannels with different aspect ratios *International Journal of Heat and Mass Transfer*, *46*(14), 2519-2525.

[38] Xu, B., Ooti, K. T., Wong, N. T., & Choi, W. K. (2000). Experimental investigation of flow friction for liquid flow in microchannels. *International Communications in Heat and Mass Transfer*, *27*(8), 1165-1176.

[39] Papautsky, I., Ameel, T., & Frazier, A. B. (2001, November). A review of laminar single-phase flow in microchannels. In *ASME, Proceedings of Int. Mech. Eng Congress Expos Proc (IMECE)* (Vol. 2, pp. 3067-3075).

[40] Kozicki, W., Chou, C. H., & Tiu, C. (1966). Non-Newtonian flow in ducts of arbitrary cross-sectional shape. *Chemical Engineering Science*, *21*(8), 665-679.

[41] Bourne, M. (2002). *Food texture and viscosity: concept and measurement*. N.Y. Academic press.

[42] Chakroborty, P., & Das, A. (2003). *Principles of transportation engineering*. PHI Learning Pvt. Ltd..

[43] Ponjavic, A., Dench, J., Morgan, N., & Wong, J. S. S. (2015). *In-situ* viscosity measurement of confined liquids. *RSC Advances*, *5*(121), 99585-99593.

[44] Tropea, C., Yarin, A. L., & Foss, J. F. (2007). *Springer Handbook of Experimental Fluid Mechanics.* Berlin: Springer Berlin Heidelberg.

[45] Kundu, P. K., & Cohen, L. M. (1990). Fluid Mechanics, 638 pp. *Academic, Calif*.

[46] Xie, J., Jones, S. W., Matthews, C. M., Wagg, B. T., Parker, P., & Ducharme, R. (2007). Slotted liner design for SAGD wells. *World oil*, *228*(6), 67-75.

[47] Rothstein, J. P., & McKinley, G. H. (1999). Extensional flow of a polystyrene Boger fluid through a 4: 1: 4 axisymmetric contraction/expansion. *Journal of non-Newtonian fluid mechanics*, *86*(1), 61-88.

[48] Sousa, P. C., Coelho, P. M., Oliveira, M. S. N., & Alves, M. a. (2009). Three-dimensional flow of Newtonian and Boger fluids in square–square contractions. Journal of Non-Newtonian Fluid Mechanics, 160(2-3), 122–139.

[49] Sousa, P. C., Coelho, P. M., Oliveira, M. S. N., & Alves, M. a. (2011a). Effect of the contraction ratio upon viscoelastic fluid flow in three-dimensional square–square contractions. Chemical Engineering Science, 66(5), 998–1009.

[50] Tsukahara, T., Motozawa, M., Tsurumi, D., & Kawaguchi, Y. (2013). PIV and DNS analyses of viscoelastic turbulent flows behind a rectangular orifice. International Journal of Heat and Fluid Flow, 41, 66–79

[51] Afonso, a. M., Oliveira, P. J., Pinho, F. T., & Alves, M. a. (2011). Dynamics of high-Deborah-number entry flows: a numerical study. Journal of Fluid Mechanics, 677, 272–304

[52] Kurosawa, O., Oana, H., Matsuoka, S., Noma, A., Kotera, H., & Washizu, M. (2006). Electroporation through a micro-fabricated orifice and its application to the measurement of cell response to external stimuli. *Measurement Science and Technology*, *17*(12), 3127.

[53] Zivkovic, V., Zerna, P., Alwahabi, Z. T. & Biggs, M. J. A pressure drop correlation for low Reynolds number Newtonian flows through a rectangular orifice in a similarly shaped micro-channel. Chem. Eng. Res. Des. 91, 1–6 (2013).

[54] Oliveira, M. S. N., Rodd, L. E., McKinley, G. H., & Alves, M. a. (2008). Simulations of extensional flow in microrheometric devices. Microfluidics and Nanofluidics, 5(6), 809–826.

[55] Tsai, C.-H., Chen, H.-T., Wang, Y.-N., Lin, C.-H., & Fu, L.-M. (2006). Capabilities and limitations of 2-dimensional and 3-dimensional numerical methods in modeling the fluid flow in sudden expansion microchannels. Microfluidics and Nano fluidics, 3(1), 13–18.

[56] Rodd, L. E., Cooper-White, J. J., Boger, D. V., & McKinley, G. H. (2007). Role of the elasticity number in the entry flow of dilute polymer solutions in micro-fabricated contraction geometries. *Journal of Non-Newtonian Fluid Mechanics*,*143* (2), 170-191.

[57] Walters, K., Webster, M. F., & Tamaddon- Jahromi, H. R. (2009). The numerical simulation of some contraction flows of highly elastic liquids and their impact on the relevance of the Couette correction in extensional rheology. Chemical Engineering Science, 64(22), 4632–4639.

[58] Chowdhury, M. R., & Fester, V. G. (2012). Modeling pressure losses for Newtonian and non-Newtonian laminar and turbulent flow in long square edged orifices. Chemical Engineering Research and Design, 90(7), 863–869.

[59] Mishra, C., & Peles, Y. (2005). Flow visualization of cavitating flows through a rectangular slot micro-orifice ingrained in a microchannel. Physics of Fluids, 17(11), 113602.

[60] Matallah, H., Townsend, P., & Webster, M. F. (1998). Recovery and stress-splitting schemes for viscoelastic flows. *Journal of Non-Newtonian Fluid Mechanics*,*75*(2), 139-166.

[61] Evans, R. E., & Walters, K. (1989). Further remarks on the lip-vortex mechanism of vortex enhancement in planar-contraction flows. *Journal of non-newtonian fluid mechanics*,*32*(1), 95-105.

[62] Ternik, P. (2010). New contributions on laminar flow of inelastic non-Newtonian fluid in the two-dimensional symmetric expansion: Creeping and slowly moving flow conditions. *Journal of Non-Newtonian Fluid Mechanics*, *165*(19), 1400-1411.

[63] Muzychka, Y. S., & Edge, J. (2008). Laminar Non-Newtonian Fluid Flow in Noncircular Ducts and Microchannels. Journal of Fluids Engineering, 130(11), 111201

[64] Jensen, K. D. (2004). Flow measurements. *Journal of the Brazilian Society of Mechanical Sciences and Engineering*,*26*(4), 400-419.

[65] Klopfenstein Jr, R. (1998). Air velocity and flow measurement using a Pitot tube. *ISA transactions*,*37*(4), 257-263.

[66] Bruun, H. H. (1996). Hot-wire anemometry: principles and signal analysis.*Measurement Science and Technology*, *7*(10), null.

[67] Ristić, S., Isaković, J., Ilić, B., & Ocokoljić, G. Review of methods for flow velocity measurement in wind tunnels.

[68] Raffel, M., Willert, C. E., & Kompenhans, J. (2013). *Particle image velocimetry: a practical guide*. Springer.

[69] Malik, N. A., Dracos, T., & Papantoniou, D. A. (1993). Particle tracking velocimetry in three-dimensional flows. *Experiments in Fluids*, *15*(4-5), 279-294.

[70] Adrian, R. J. (2005). Twenty years of particle image velocimetry, *Experiments in fluids*, *39*(2), 159-169.

[71] Dudderar, T. D., Meynart, R., & Simpkins, P. G. (1987). Laser speckle velocimetry. In *10th US National Congress of Applied Mechanics*(Vol. 1, pp. 187-200).

[72] Adrian, R. J. (1991). Particle-imaging techniques for experimental fluid mechanics. *Annual review of fluid mechanics*, *23*(1), 261-304.

[73] Lindken, R., Rossi, M., Große, S., & Westerweel, J. (2009). Micro-particle image velocimetry (μPIV): recent developments, applications, and guidelines. Lab on a Chip, 9(17), 2551-2567.

[74] Bastiaans, R. J. (2000). *Cross-correlation PIV; theory, implementation and accuracy*. Eindhoven University of Technology, Faculty of Mechanical Engineering.

[75] Murphy, D. B. (2002). Fundamentals of light microscopy and electronic imaging. John Wiley & Sons.

[76] Benner, G., & Probst, W. (1994). Köhler Illumination in the TEM: fundamentals and advantages. Journal of Microscopy, 174(3), 133-142.

[77] E. Keller & R. D. Goldman (2011). Light Microscopy. In R.Yuste (Ed.) *Imaging: a laboratory manual*. New York, NY: Cold Spring Harbor Laboratory Press.

[78] Willert, C., Stasicki, B., Klinner, J., & Moessner, S. (2010). Pulsed operation of high-power light emitting diodes for imaging flow velocimetry. Measurement Science and Technology, 21(7), 075402.

[79] Raffel, M., Willert, C. E., & Kompenhans, J. (2013). Particle image velocimetry: a practical guide. Springer.

[80] Melling, A. (1997). Tracer particles and seeding for particle image velocimetry. Measurement Science and Technology, 8(12), 1406.

[81] Novotný, J., & Manoch, L. (2012). The Criterion of Choosing the Proper Seeding Particles. Engineering Mechanics, 201.

[82] Taylor, K. C. (2003). Rheology of Hydrophobically Associating Polymers for Oilfield Applications. *Annual Transactions-Nordic Rheology Society*, *11*, 13-20.

[83] Ali, S., Mcatee, J. L., & Claesson, S. (1985). Thermodynamic properties of aqueous polyacrylamide solutions as a function of pressure and temperature. *European polymer journal*, *21*(1), 75-80.

[84] Shin, S., & Cho, Y. I. (1993). Temperature effect on the non-Newtonian viscosity of an aqueous polyacrylamide solution. *International communications in heat and mass transfer*, *20*(6), 831-844.

[85] Fang, L., & Brown, W. (1990). Dynamic properties of polyacrylamide gels and solutions.*Polymer*,*31*(10), 1960-1967

[86] Flew, S., & Sellin, R. H. J. (1993). Non-Newtonian flow in porous media-a laboratory study of polyacrylamide solutions. *Journal of non-Newtonian fluid mechanics*, *47*, 169-210.

[87] Maurer, H. R., & Allen, R. C. (1972). Useful buffer and gel systems for polyacrylamide gel electrophoresis. *Clinical Chemistry and Laboratory Medicine*, *10*(5), 220-225.

[88] Moss, N., & Dymond, B. (1978). Flocculation: theory and application. *Mine and Quarry Journal*, *5*, 1-8.

[89] Milne, A., Lian, E. G. W., Padilla, S. J. M., Ulloa, M., Martin, F. V., & Samuel, M. M. (2013). *U.S. Patent No. 8,413,719*. Washington, DC: U.S. Patent and Trademark Office.

[90] Yang, M. H. (2001). The rheological behavior of polyacrylamide solution II. Yield stress. *Polymer testing*, *20*(6), 635-642.

[91] Shin, Sehyun, and Young I. Cho. Laminar heat transfer in a rectangular duct with a non-Newtonian fluid with temperature-dependent viscosity. *International journal of heat and mass transfer* 37 (1994): 19-30.

[92] Schramm, G. (1994).*A practical approach to rheology and rheometry* (p. 121). Karlsruhe: Haake.

[93] Caulfield, M. J., Qiao, G. G., & Solomon, D. H. (2002). Some aspects of the properties and degradation of polyacrylamides. *Chemical reviews*, *102*(9), 3067-3084.

[94] Kulicke, W. M., Kniewske, R., & Klein, J. (1982). Preparation, characterization, solution properties and rheological behaviour of polyacrylamide. *Progress in polymer science*, *8*(4), 373-468.

[95] Schramm, G. (1994). *A practical approach to rheology and rheometry* (p. 121). Karlsruhe: Haake.

[96] Mezger, T. G. (2006). *The rheology handbook: for users of rotational and oscillatory rheometers*. Vincentz Network GmbH & Co KG.

[97] Kenney, J. F., & Keeping, E. S. (1954). Mathematics of statistics-part one. pp.77-80,

[98] Kundu, P. K., & Cohen, L. M. (1990). Fluid Mechanics, 638 pp. Academic, Calif.

[99] Tropea, C., Yarin, A. L., & Foss, J. F. (Eds.). (2007).Springer handbook of experimental fluid mechanics (Vol. 1). Springer Science & Business Media.

[100] Dodge, D. W., & Metzner, A. B. (1959). Turbulent flow of non-Newtonian systems. AIChE Journal, 5(2), 189-204.

[101] Rashid, M.A. (2016), *An Investigation of The Pressure Loss Characteristics for Highly Viscous Fluid Flow Through Narrow Slots*, MSc Thesis, Department of Mechanical Engineering, University of Alberta

[102] Janna, W. S. (2009).*Introduction to fluid mechanics*. CRC press

[103] Rajaratnam, N. (1976). Turbulent jets. New York, NY: Elsevier.

Appendix

Appendix A. **MATLAB code for straight channel experiment**

A-1. Code 1

```
%%%%%%%%%%%%%%%%%%%%%%%%%%%%%%%%%%%%%%%%%%%%%%%%%%%%%%%%%%%%
%%%
% Who   : Shadi Ansari
% When  : 2015
% Aim   : Load and plot a vector field using PIVMAT
%       : 1-Plot velocity of the flow is normalized based on
the maximum velocity in field
% 2-the velocity profile through narrow channel and compare
with %theory
%3- velocity vector map
% Data Set: Polyacrylamide & water in a straight channel
%%%%%%%%%%%%%%%%%%%%%%%%%%%%%%%%%%%%%%%%%%%%%%%%%%%%%%%%%%%%
%%%%%
 close all
clc % Clear command line
close all % Close figures
clear % Clear variables

% Open figures at particular positions
figure(1); figure(2); figure(3);
fX = 55; fY = 200;

set(1,'Pos',[fX fY 1350 600]);
set(2,'Pos',[fX+1*(600+15), fY 600 600]);
set(3,'Pos',[fX+2*(600+15), fY 600 600]);

%...........................................................
....%%..........................%...........................
....................................%

F = loadvec('vavg_pt1wtPA_pt025mlmin_90fps.vc7'); % Load
.vc7 file in the current directory (Non-Newtonian Fluids
only); this is the average velocity at all the positions
(one final average velocity image)
```

```
LOAD DATA.....................
%.....................................................
....%
%.........................SCALEDATA.....................
%.....................................................
....%

CW = 120; % Width of channel in pixels (CHECK EVERY TIME
FROM DAVIS)

Xoff = 0;  % horizontal flow (CHANGE EVERY TIME ACCORDINGLY)
Yoff = 20; % horizontal flow (CHANGE EVERY TIME ACCORDINGLY)

%.....................................................
....%
%....................VECTOR PROFILE -
F.....................
%.....................................................
....%

figure(1);
F.x =F.x/CW;       % normalizing the width of the channel
F.y =F.y/CW;       % normalizing the width of the channel

F.x  = F.x - Xoff;     % scaling
F.y  = F.y - Yoff;     % scaling

% F.vx = F.vx(find(F.vx));
max=max((F.vx(1,:)));

F.vx = abs(F.vx)/max;      % normalizing velocity profile in
x direction  based on the maximum velocity in the field

F.vy = abs(F.vy)/max; % normalizing velocity profile in y
direction  based on the maximum velocity in the field

showf(F,'norm','spacing',[4,2],'scalearrow',5); % Plot
vector profile and display in figure(1) - horizontal flow

xlabel('x ' (','FontName','Times New Roman','FontSize',16);
ylabel('y ','FontName','Times New Roman','FontSize',16);

% axis image
% axis tight
% axis equal

colorbar('hide')
c=colorbar('FontSize',16,'FontName','Times New Roman');
set(c, 'Position', [.92 .16 .02 .7]);
title(c,'{\itU / U_{max}} ','FontName','Times New
Roman','HorizontalAlignment','left');
```

```
%.....
....%
%.......VELOCITY - FITTED WITH NEWTONIAN THEORY
PROFILE..........
%.....
...%
figure(2);
[first, last] = size(F.vx);

MAX=zeros(first,1);
F.vx_out_scaled=zeros(size(F.vx));
 hold on;

for i = 1:first
    MAX(i) = max(F.vx(i,:));       % Find maximum velocity
of each row
    F.vx_scaled(i,:) = F.vx(i,:)/MAX(i);
% scaled velocities at all positions within one averaged
image

    plot(F.y/CW,F.vx_scaled(i,:),'.b');
end

YYY = -0.5:0.01:0.5;
  % since channel width is normalized
T_MAX = 1;
   % since I have already normalized velocity

Lam_YYY = T_MAX*(1-(YYY.^2)/(1/2)^2);

 % Newtonian Theory Profile, using formula, Lam = MAX*(1-
(F.y/(C_W/2)).^2)

hold on;
plot(F.y/CW,F.vx_scaled(round(first/2),:),'ro','LineWidth',2
);                        % Plot the normalized velocity at
middle of channel (averaged over 1000 images)

plot(YYY,Lam_YYY,'k','LineWidth',2); % Plot the Newtonian
theoretical profile

hold off;
 xlabel('{\it x/w}','FontName','Times New
Roman','FontSize',16);
ylabel('{\itU / U_{max}} ','FontName','Times New
Roman','FontSize',16);

leg1 = legend('0.25 weight % polyacrylamide','Newtonian
theory');     % change legend everytime as you change
concentration of polyacrylamide
set(leg1,'Location','south');
axis([-0.7,0.7,0,1]);
```

```
%..........................................................
%... VELOCITY - FITTED WITH NON_NEWTONIAN THEORY PROFILE...
%..........................................................

figure(3);

CH = 0.0015;    % Channel Height in m

A = CW*CH;   % m^2 channel cross section area
C = 2*(CW+CH);  % m circumference of cross section

D_hyd = 4*A/C;  % m Hydraulic diameter of channel

a = CW/2;
b = CH/2;
E = a/b;

rho = 700;      % kg/m^3 density of PA
n = 0.25;   % flow index % Get from curve-fitting parameter

a1 = 0.70731;
b1 = 0.11276;
% Re =
((D_hyd^n)*(F.vx_scaled(round(first/2),round(last/2))^(2-
n))*rho)/(k*(8^(n-1))*(((b1*n)+a1)/(n))^n);
% Reynolds Number = [Dhyd^n.vavg^(2-n).rho]/[k.2^(n-
3).{(b1*n+a1)/n}^n]
%..........................................................
%Theoretical Profile for 0.1 weight percent polyacrylamide.
%..........................................................

YYY1 = 0:0.01:0.5;

% Lam_YYY1 = (n/((2*n)+1))*(1-
((YYY1.^((n+1)/n))/((1/2)^((n+1)/n))))*(del_P.*(1/k))^(1/n);
  % non- Newtonian theory Profile, using formula,
 u = [n/(n+1)].[R^(n+1)/n -
r^(n+1)/n].[(dP/dz).(1/(2.k)]^(1/n)

Lam_YYY1 = (1-((YYY1.^((n+1)/n))/((1/2)^((n+1)/n))));

% Lam_YYY2 = real(Lam_YYY1);

YYY3 = -0.5:0.01:0;
% since channel width is 0.6903 mm

% Lam_YYY1 = (n/((2*n)+1))*(1-
%((YYY1.^((n+1)/n))/((1/2)^((n+1)/n))))*(del_P.*(1/k))^(1/n)
;
% Theory Profile, using formula,
%u = [n/(n+1)].[R^(n+1)/n -
r^(n+1)/n].[(dP/dz).(1/(2.k)]^(1/n)
```

```
Lam_YYY3 = (1-(((-YYY3).^((n+1)/n))/((1/2)^((n+1)/n))));

% Lam_YYY2 = real(Lam_YYY1);
u= F.vx_scaled(round(first/2),:).';
m=(F.y/0.00073).';

hold on;


plot(F.y/0.00073,F.vx_scaled(round(first/2),:),'ro','LineWid
th',2);            % Plot the average normalized velocity

  plot(YYY1,Lam_YYY1,'k','LineWidth',2);
 % Plot the theoretical profile
   plot(YYY3,Lam_YYY3,'k','LineWidth',2);
% Plot the theoretical profile


hold off;


xlabel('{\it x/w}','FontName','Times New
Roman','FontSize',16);
ylabel('{\itU / U_{max}} ','FontName','Times New
Roman','FontSize',16);


leg1 = legend('0.5 wt. % polyacrylamide at 0.025
ml/min','Non-Newtonian theory');     % change legend
everytime as you change concentration of polyacrylamide
set(leg1,'Location','south');
```

Appendix B. **MATLAB code for keystone slots experiment**

B-1. Code 3

```
%%%%%%%%%%%%%%%%%%%%%%%%%%%%%%%%%%%%%%%%%%%%%%%%%%%%%%%%%%%%
%%%
% Who   : Shadi Ansari
% When  : 2015
% Aim   : Load and plot a vector field using PIVMAT
%       : 1-Plot velocity of the flow and the position were
normalized based on the maximum velocity and width in the
position
% Data Set: Polyacrylamide & water in a keystone channel
%%%%%%%%%%%%%%%%%%%%%%%%%%%%%%%%%%%%%%%%%%%%%%%%%%%%%%%%%%%%
%%%%
clear
close all

% Set Parameters
input=160; %pixels of the inlet
output=160;%pixels of the outlet
length=1849;%pixels of the slot length
Originx=100;% set origin in x direction
Originy=800;% set origin in y direction

ratiolength=length/input %maximum ratio in x direction for
the inlet

tann =((output-input)/length)/2; %Tangent of the angle of
slot

angle= atand(tann)% angle of the slot

Ratiopixtopic=4.16 % ratio of the pixel to column (based on
the window size and overlap in processing)
AOx = 2000-round(Originx) %Origin in array(since the flow of
our experiment is right to left)


% Load data set
v_File= 'straight_water_max10.vc7';   % Specify the file
VEC = loadvec(v_File);  % Load the data into a variable

% Size and position figures
figure(1), set(gcf,'color','w');
sz_x = 600; sz_y = 600; % size of the figure

y_pos = 200; x_pos =75;  % position on the screen
set(1,'pos', [x_pos, y_pos, sz_x, sz_y]);

axes('position',[.1  .1  .85  .85]) % size of the plot in
the figure
VEC=rotatef(VEC,0.005); % rotate the vectors to  make sure
the channel is horizontal
```

```
% Set the Origin
VEC.x = (VEC.x) - Originx;
VEC.y = (VEC.y) - Originy;
VEC.vx = abs(VEC.vx);
VEC.vy = abs(VEC.vy);

step=round((length)/(10*Ratiopixtopic)) % step of between
velocity profiles

C0=round(AOx/Ratiopixtopic); %entrance of channel
 ratio1=0;

C1=round((AOx/Ratiopixtopic)-step);
ratio2=round(length/(10*input));

C2=round((AOx/Ratiopixtopic)-(2*step));
 ratio3=2*round(length/(10*input));

C3=round((AOx/Ratiopixtopic)-(3*step));
ratio4=3*round(length/(10*input));
C4=round((AOx/Ratiopixtopic)-(4*step));
ratio5=4*round(length/(10*input));

C5=round((AOx/Ratiopixtopic)-(5*step));
ratio6=5*round(length/(10*input));

C6=round((AOx/Ratiopixtopic)-(6*step));
ratio7=6*round(length/(10*input));

C7=round((AOx/Ratiopixtopic)-(7*step));
ratio8=7*round(length/(10*input));

C8=round((AOx/Ratiopixtopic)-(8*step));
ratio9=8*round(length/(10*input));

C9=round((AOx/Ratiopixtopic)-(9*step));
ratio10=9*round(length/(10*input));

width =input*1.2; %width of the inlet in pixel I don't know
why 1.2 is needed in this case!!

Vxmax= max((VEC.vx(C0,:))); % maximum velocity in the
position

VEC.vx = (VEC.vx/Vxmax); % normalizing the velocity in x
direction using maximum velocity in the position

VEC.vy = (VEC.vy/Vxmax); % normalizing the velocity in y
 direction using maximum velocity in the position
hold on

Vx = VEC.vx(C0,:);  plot(VEC.y/width,Vx,'r.-'); % plotting
the normalized velocity profile in the position of the
channel versus the normalized position
```

```
lp1  = (tann)*(step)*Ratiopixtopic; %finding the ½
difference between the width of channel and the width
entrance of channel based on the slot angle of the channel.

width1 =(width + 2*lp1); % width of channel in position

Vxmax1 = max((VEC.vx(C1,:)));
VEC.vx1 = (VEC.vx/Vxmax1);
VEC.vy1 = (VEC.vy/Vxmax1);
hold on
Vx1 = VEC.vx1(C1,:);  plot(VEC.y/width1,Vx1,'ro-');



lp2  = tann*(2*step)*Ratiopixtopic;
width2 =(width + 2*lp2);
Vxmax2 = max((VEC.vx(C2,:)));
VEC.vx2 = (VEC.vx/Vxmax2);
VEC.vy2 = (VEC.vy/Vxmax2);
hold on
Vx2 = VEC.vx2(C2,:);  plot(VEC.y/width2,Vx2,'b.-');

lp3  = tann*(3*step)*Ratiopixtopic;
width3 =(width + 2*lp3);
Vxmax3 = max((VEC.vx(C3,:)));
VEC.vx3 = (VEC.vx/Vxmax3);
VEC.vy3 = (VEC.vy/Vxmax3);
hold on
Vx3 = VEC.vx3(C3,:);  plot(VEC.y/width3,Vx3,'bo-');

lp4= tann*(4*step)*Ratiopixtopic;
width4 =(width + 2*lp4);
Vxmax4 = max((VEC.vx(C4,:)));
VEC.vx4 = (VEC.vx/Vxmax4);
VEC.vy4 = (VEC.vy/Vxmax4);
hold on
Vx4 = VEC.vx4(C4,:);  plot(VEC.y/width4,Vx4,'g.-');

lp5= (tann)*(5*step)*Ratiopixtopic;
width5 =(width + 2*lp5);
Vxmax5 = max((VEC.vx(C5,:)));
VEC.vx5 = (VEC.vx/Vxmax5);
VEC.vy5 = (VEC.vy/Vxmax5);
hold on
Vx5 = VEC.vx5(C5,:);  plot(VEC.y/width5,Vx5,'go-');

lp6= (tann)*(6*step)*Ratiopixtopic;
width6 =(width + 2*lp6);
Vxmax6 = max((VEC.vx(C6,:)));
VEC.vx6 = (VEC.vx/Vxmax6);
VEC.vy6 = (VEC.vy/Vxmax6);
hold on
Vx6 = VEC.vx6(C6,:);  plot(VEC.y/width6,Vx6,'k.-');
```

```
lp7= (tann)*(7*step)*Ratiopixtopic;
width7 =(width + 2*lp7);
Vxmax7 = max((VEC.vx(C7,:)));
VEC.vx7 = (VEC.vx/Vxmax7);
VEC.vy7 = (VEC.vy/Vxmax7);
hold on
Vx7 = VEC.vx7(C7,:);  plot(VEC.y/width7,Vx7,'ko-');

lp8= (tann)*(8*step)*Ratiopixtopic;
width8=(width + 2*lp8);
Vxmax8 = max((VEC.vx(C8,:)));
VEC.vx8 = (VEC.vx/Vxmax8);
VEC.vy8 = (VEC.vy/Vxmax8);
hold on
Vx8 = VEC.vx8(C8,:);  plot(VEC.y/width8,Vx8,'c.-');

lp9= (tann)*(9*step)*Ratiopixtopic;
width9 =(width + 2*lp9);
Vxmax9 = max((VEC.vx(C9,:)));
VEC.vx9 = (VEC.vx/Vxmax9);
VEC.vy9 = (VEC.vy/Vxmax9);
hold on
Vx9 = VEC.vx9(C9,:);  plot(VEC.y/width9,Vx9,'co-');

%.....................................................
%.............Plotting Newtonian theory...
%.....................................................

YYY = -0.5:0.01:0.5;
T_MAX = 1;
Lam_YYY = T_MAX*(1-(YYY.^2)/(1/2)^2);
   % Theory Profile, using formula, Lam = MAX*(1-
(F.y/(C_W/2)).^2)

hold on;

plot(YYY,Lam_YYY,'r','LineWidth',2); % Plot the average
normalized velocity

axis([-0.6 0.6 0 1]) % setting axis

%............. Parameters of polyacrylamide solution
%.....................................................


rho = 700;      % kg/m^3 density of  polyacrylamide solution

n = 0.27;     % flow index(for 0.2% polyacrylamide it is
0.37 and for 0.4 wt.% polyacrylamide it is 0.37)    % Get
from rheometer measurements

k = 1.2956; % consistency of the solution (for 0.2%
polyacrylamide it is 0.91 and for 0.4 wt.% polyacrylamide it
is 2.34)
```

```
%.....................................................
%Non-Newtonian Theoretical Profile for polyacrylamide
solution
%.....................................................

YYY1 = 0:0.01:0.5;
% Lam_YYY1 = (n/((2*n)+1))*(1-
((YYY1.^((n+1)/n))/((1/2)^((n+1)/n))))*(del_P.*(1/k))^(1/n);
 % Theory Profile, using formula,
 u = [n/(n+1)].[R^(n+1)/n -
r^(n+1)/n].[(dP/dz).(1/(2.k)]^(1/n)

Lam_YYY1 = (1-((YYY1.^((n+1)/n))/((1/2)^((n+1)/n))));

% Lam_YYY2 = real(Lam_YYY1);

YYY3 = -0.5:0.01:0;
% Lam_YYY1 = (n/((2*n)+1))*(1-
((YYY1.^((n+1)/n))/((1/2)^((n+1)/n))))*(del_P.*(1/k))^(1/n);
% Theory Profile, using formula,
u = [n/(n+1)].[R^(n+1)/n -
r^(n+1)/n].[(dP/dz).(1/(2.k)]^(1/n)

Lam_YYY3 = (1-(((-YYY3).^((n+1)/n))/((1/2)^((n+1)/n))));

% Lam_YYY2 = real(Lam_YYY1);

hold on;
   plot(YYY1,Lam_YYY1,'k','LineWidth',2);
 % Plot the non-Newtonian theoretical profile
   plot(YYY3,Lam_YYY3,'k','LineWidth',2);
 % Plot the non-Newtonian theoretical profile

set(gca,'FontSize', 14,'FontName', 'Times New Roman');
xlabel('{\it x/w}','FontSize', 16,'FontName', 'Times New
Roman');
%ylabel('{\it y/w}','FontSize', 14,'FontName', 'Times New
Roman');
ylabel('{\itU / U_{max}} ','FontSize', 16,'FontName', 'Times
New Roman')
%ylabel(c,'{\it\omega} = \Gamma / A','FontSize',
14,'FontName', 'Times New Roman')

legend('{\it x/w} = 0',...
       '{\it x/w} = 2',...
       '{\it x/w} = 4',...
       '{\it x/w} = 6',...
       '{\it x/w} = 8',...
       '{\it x/w} = 10',...
        '{\it x/w} = 12',...
         '{\it x/w} = 14',...
         '{\it x/w} = 16',...
         '{\it x/w} = 18',...
         '{\it x/w} = Newtonian Theory',...
         '{\it x/w} = Non-Newtonian theory');
```

B-2. Code 4

```
%%%%%%%%%%%%%%%%%%%%%%%%%%%%%%%%%%%%%%%%%%%%%%%%%%%%%%%%%%%%%%%%%%%%%%%
%
% Who   : Shadi Ansari
% When  : 2015
% Aim   : Load and plot a vector field using PIVMAT
%       : 1- along the keystone slot with high slot angles.
In %this code the velocity profile of the inlet of channel
was plotted %based on the small window size processing
procedure and the velocity %profile of outlet of channel
were plotted based on the big window size %processing
procedure. %3- velocity vector map
% Data Set: Polyacrylamide in a keystone channel
%%%%%%%%%%%%%%%%%%%%%%%%%%%%%%%%%%%%%%%%%%%%%%%%%%%%%%%%%%%%%%%%%%%%%%%

clear
close all
% Set Parameters

input=120; %pixels of the inlet
output=820;%pixels of the outlet
length=1730;%pixels of the slot length
Originx=180;% set origin in xdir
Originy=917;%set origin in ydir

ratiolength=length/input; %maximum ratio in xdirection for
the inlet
tann = ((output-input)/length)/2;
angle= atand(tann);% angle of the slot
Ratiopixtopic=16;
Ratiopixtopic2=4.16;
% ratio of the pixel to column
AOx = 2000-round(Originx); %Origin in array



% Load data set
v_File= 'keystone_2poly_12degree_min(2).vc7';   % Specify
the file
VEC = loadvec(v_File);  % Load the data into a variable
v_File2= 'keystone_2poly_12degree_min4.vc7';   % Specify the
file
VEC2 = loadvec(v_File2);  % Load the data into a variable

% Size and position figures
figure(1), set(gcf,'color','w');
sz_x = 600; sz_y = 600; % size of the figure
y_pos = 200; x_pos =75;  % position on the screen
set(1,'pos', [x_pos, y_pos, sz_x, sz_y]);
%axes('position',[.1  .1  .85  .85]) % size of the plot in
the figure
VEC=rotatef(VEC,0.005);
VEC2=rotatef(VEC2,0.005);
```

```
%%%%%%%%%%%%%%%%%%%%%%%%%%%%%%%%%%%%%%%%%%%%%%%%
% Set the Origin
%%%%%%%%%%%%%%%%%%%%%%%%%%%%%%%%%%%%%%%%%%%%%%%%
VEC.x = (VEC.x) - Originx;
VEC.y = (VEC.y) - Originy;
% VEC.x = (VEC.x-AOx);
% VEC.y = (VEC.y-AOy);
VEC.vx = abs(VEC.vx);
VEC.vy = abs(VEC.vy);

VEC2.x = (VEC2.x) - Originx;
VEC2.y = (VEC2.y) - Originy;
VEC2.vx = abs(VEC2.vx);
VEC2.vy = abs(VEC2.vy);



step=round((length)/(10*Ratiopixtopic)) % step
step2=floor((length)/(10*Ratiopixtopic2))
C0=round(AOx/Ratiopixtopic2)
 ratio1=0;

C1=round((AOx/Ratiopixtopic2)-step2)
ratio2=round(length/(11*input))

C2=round((AOx/Ratiopixtopic2)-(2*step2));
ratio3=2*round(length/(11*input));

C3=round((AOx/Ratiopixtopic)-(3*step));
ratio4=3*round(length/(11*input));

C4=round((AOx/Ratiopixtopic)-(4*step));
ratio5=4*round(length/(11*input));

C5=round((AOx/Ratiopixtopic)-(5*step));
ratio6=5*round(length/(11*input));

C6=round((AOx/Ratiopixtopic)-(6*step));
ratio7=6*round(length/(11*input));

C7=round((AOx/Ratiopixtopic)-(7*step));
ratio8=7*round(length/(11*input));

C8=round((AOx/Ratiopixtopic)-(8*step));
ratio9=8*round(length/(11*input));

C9=round((AOx/Ratiopixtopic)-(9*step));
ratio10=9*round(length/(11*input));
```

```
 width =input*1.2; %width of the inlet in pixel I dont know
why 2 is needed in this case!!

Vxmax= max((VEC2.vx(C0,:)));
VEC2.vx = (VEC2.vx/Vxmax);
VEC2.v = (VEC2.vy/Vxmax);
hold on
Vx = VEC2.vx(C0,:);  plot(VEC2.y/width,Vx,'r.-');


lp1  = (tann)*(step2)*Ratiopixtopic2
width1 =(width + 2*lp1);
Vxmax1 = max((VEC2.vx(C1,:)));
VEC2.vx1 = (VEC2.vx/Vxmax1);
VEC2.vy1 = (VEC2.vy/Vxmax1);
hold on
Vx1 = VEC2.vx1(C1,:);  plot(VEC2.y/width,Vx1,'ro-');


lp2  = tann*(2*step2)*Ratiopixtopic2;
width2 =(width_2 + 2*lp2);
Vxmax2 = max((VEC2.vx(C2,:)));
VEC2.vx2 = (VEC2.vx/Vxmax2);
VEC2.vy2 = (VEC2.vy/Vxmax2);
hold on
Vx2 = VEC2.vx2(C2,:);  plot(VEC2.y/width2,Vx2,'b.-');


lp3  = tann*(3*step)*Ratiopixtopic;
width3 =(width + 2*lp3);
Vxmax3 = max((VEC.vx(C3,:)));
VEC.vx3 = (VEC.vx/Vxmax3);
VEC.vy3 = (VEC.vy/Vxmax3);
hold on
Vx3 = VEC.vx3(C3,:);  plot(VEC.y/width3,Vx3,'bo-');


lp4= tann*(4*step)*Ratiopixtopic;
width4 =(width + 2*lp4);
Vxmax4 = max((VEC.vx(C4,:)));
VEC.vx4 = (VEC.vx/Vxmax4);
VEC.vy4 = (VEC.vy/Vxmax4);
hold on
Vx4 = VEC.vx4(C4,:);  plot(VEC.y/width4,Vx4,'g.-');


lp5= (tann)*(5*step)*Ratiopixtopic;
width5 =(width + 2*lp5);
Vxmax5 = max((VEC.vx(C5,:)));
VEC.vx5 = (VEC.vx/Vxmax5);
VEC.vy5 = (VEC.vy/Vxmax5);
hold on
Vx5 = VEC.vx5(C5,:);  plot(VEC.y/width5,Vx5,'go-');
```

```
lp6= (tann)*(6*step)*Ratiopixtopic;
width6 =(width + 2*lp6);
Vxmax6 = max((VEC.vx(C6,:)));
VEC.vx6 = (VEC.vx/Vxmax6);
VEC.vy6 = (VEC.vy/Vxmax6);
hold on
Vx6 = VEC.vx6(C6,:);  plot(VEC.y/width6,Vx6,'k.-');


lp7= (tann)*(7*step)*Ratiopixtopic;
width7 =(width + 2*lp7);
Vxmax7 = max((VEC.vx(C7,:)));
VEC.vx7 = (VEC.vx/Vxmax7);
VEC.vy7 = (VEC.vy/Vxmax7);
hold on
Vx7 = VEC.vx7(C7,:);  plot(VEC.y/width7,Vx7,'ko-');


lp8= (tann)*(8*step)*Ratiopixtopic;
width8=(width + 2*lp8);
Vxmax8 = max((VEC.vx(C8,:)));
VEC.vx8 = (VEC.vx/Vxmax8);
VEC.vy8 = (VEC.vy/Vxmax8);
hold on
Vx8 = VEC.vx8(C8,:);  plot(VEC.y/width8,Vx8,'c.-');


lp9= (tann)*(9*step)*Ratiopixtopic;
width9 =(width + 2*lp9);
Vxmax9 = max((VEC.vx(C9,:)));
VEC.vx9 = (VEC.vx/Vxmax9);
VEC.vy9 = (VEC.vy/Vxmax9);
hold on
Vx9 = VEC.vx9(C9,:);  plot(VEC.y/width9,Vx9,'co-');


%.....................Newtonian theory

YYY = -0.5:0.01:0.5;

T_MAX = 1;

Lam_YYY = T_MAX*(1-(YYY.^2)/(1/2)^2);
% Theory Profile, using formula, Lam = MAX*(1-
(F.y/(C_W/2)).^2)


hold on;            % Plot the average normalized velocity

    plot(YYY,Lam_YYY,'r','LineWidth',2);

axis([-0.6 0.6 0 1])
```

```
n = 0.38;      % flow behaviour index      % Get from curve-
fitting parameter

%.....................................................
..Theoretical Profile for 0.2 weight percent polyacrylamide

YYY1 = 0:0.01:0.5;

% Lam_YYY1 = (n/((2*n)+1))*(1-
((YYY1.^((n+1)/n))/((1/2)^((n+1)/n))))*(del_P.*(1/k))^(1/n);
% Theory Profile, using formula, u = [n/(n+1)].[R^(n+1)/n -
r^(n+1)/n].[(dP/dz).(1/(2.k)]^(1/n)

Lam_YYY1 = (1-((YYY1.^((n+1)/n))/((1/2)^((n+1)/n))));

% Lam_YYY2 = real(Lam_YYY1);

YYY3 = -0.5:0.01:0;
% Lam_YYY1 = (n/((2*n)+1))*(1-
((YYY1.^((n+1)/n))/((1/2)^((n+1)/n))))*(del_P.*(1/k))^(1/n);
% Theory Profile, using formula, u = [n/(n+1)].[R^(n+1)/n -
r^(n+1)/n].[(dP/dz).(1/(2.k)]^(1/n)

Lam_YYY3 = (1-(((-YYY3).^((n+1)/n))/((1/2)^((n+1)/n))));

% Lam_YYY2 = real(Lam_YYY1);

hold on;

   plot(YYY1,Lam_YYY1,'k','LineWidth',2);
% Plot the theoretical profile
   plot(YYY3,Lam_YYY3,'k','LineWidth',2);
% Plot the theoretical profile

set(gca,'FontSize', 14,'FontName', 'Times New Roman');
xlabel('{\it x/w}','FontSize', 14,'FontName', 'Times New
Roman');
%ylabel('{\it y/w}','FontSize', 14,'FontName', 'Times New
Roman');
ylabel('{\itU / U_{max}} ','FontSize', 14,'FontName', 'Times
New Roman')
%ylabel(c,'{\it\omega} = \Gamma / A','FontSize',
14,'FontName', 'Times New Roman')

legend('{\it x/w} = ',...
       '{\it x/w} = ',...
       '{\it x/w} = ',...
       '{\it x/w} = ',...
       '{\it x/w} = ',...
       '{\it x/w} = ',...
        '{\it x/w} =',...
         '{\it x/w} =',...
         '{\it x/w} = ',...
         '{\it x/w} = Newtonian Theory',...
         '{\it x/w} = Non-Newtonian theory');
```

B-3. Code 5

```
%%%%%%%%%%%%%%%%%%%%%%%%%%%%%%%%%%%%%%%%%%%%%%%%%%%%%%%%%%%%%%%%%%%%%%%%
%
% Who   : Shadi Ansari
% When  : 2015
% Aim   : Load and plot a vector field using PIVMAT
%       : This code was to plot the color map of keystone
slots. The
% velocity was normalized based on the maximum velocity in
the field %and the position with the width of entrance.

% Data Set: Polyacrylamide and water in a keystone channel
%%%%%%%%%%%%%%%%%%%%%%%%%%%%%%%%%%%%%%%%%%%%%%%%%%%%%%%%%%%%%%%%%%%%%%%%
%%%%%
clear
close all

% Set Parameters
ORIGIN(185,228)
width =100;  % set the channel width in pixels
Ox = 19; % set origin in x dir
Oy = 9.5;  % set origin in y dir
IMoff = -0.1; % offset the scalar file DONT KNOW WHY THIS IS
NEEDED

% Load data set
v_File= 'degree10_water_min2.VC7';   % Specify the file
VEC = loadvec(v_File);  % Load the data into a variable

% Size and position figures
figure(1), set(gcf,'color','w');
sz_x = 1000; sz_y = 400; % size of the figure
y_pos = 500; x_pos =75;  % position on the screen
set(1,'pos', [x_pos, y_pos, sz_x, sz_y]);
axes('position',[.05  .15  .8  .8]) % size of the plot in
the figure


%.....................................................
....%
% Set the Origin
%.....................................................
....%

VEC.x = (VEC.x/width) - Ox;
VEC.y = (VEC.y/width) - Oy;
Vxmax = (max(max(abs(VEC.vx))))
VEC.vx = (VEC.vx/Vxmax);
VEC.vy = (VEC.vy/Vxmax);
VEC=rotatef(VEC,-0.015);
```

```
%.....
....%
% Plot the Scalar and Vector Field
%.....
....%
figure(1) % Set Figure 1 active
hold on
% Get the mean velocity field
Vnorm = vec2scal(VEC,'norm');
vvv = Vnorm.w;
vvv = imrotate(vvv,-91);
vvv = flipdim(vvv ,2);
%Need to rotate to get the scalar field
h = imagesc(VEC.x,VEC.y-IMoff,vvv); % plot this scalar field
colormap('jet(20)'); % Have a contoured color map
c = colorbar;
% PLOT the vector field
showvec(VEC,'off','scalearrow',4,...
        'title','',...
        'spacing',[20,3])

hold off

axis equal
axis([-18.5 0.75 -7 7]); %Define the range of the plot
%axis equal;

%Label the axis
xlabel('{\it x/w}','FontSize', 14,'FontName', 'Times New
Roman');
ylabel('{\it y/w}','FontSize', 14,'FontName', 'Times New
Roman');
ylabel(c,'{\itU / U_{max}} ','FontSize', 10,'FontName',
'Times New Roman')

% Mask out the coutour plot to show the mask in the PIV data
 alphamap = zeros(size(vvv,1),size(vvv,2));
 for i = 0:size(vvv,1)-1
      for j = 0:size(vvv,2)-1
          if(~(vvv(i+1,j+1) == 0))
               alphamap(i+1,j+1) = 0.75;
          end
      end
  end
  set(h, 'AlphaData', alphamap);
```

B-4. Code6

```
F.x  = F.x - Xoff;     % scaling
F.y  = F.y - Yoff;     % scaling

F1.x  = F1.x - Xoff;     % scaling
F1.y  = F1.y - Yoff;     % scaling


F2.x  = F2.x - Xoff;     % scaling
F2.y  = F2.y - Yoff;     % scaling

F3.x  = F3.x - Xoff;     % scaling
F3.y  = F3.y - Yoff;     % scaling
F.vx = abs(F.vx);
F.vy = abs(F.vy);

F1.vx = abs(F1.vx);
F1.vy = abs(F1.vy);

F2.vx = abs(F2.vx);
F2.vy = abs(F2.vy);

F3.vx = abs(F3.vx);
F3.vy = abs(F3.vy);

figure(1); % experimental plot
[first0, last] = size(F.vx);
[first, last] = size(F1.vx);
[first1, last1] = size(F2.vx);
[first2, last2] = size(F3.vx);

MAX0 = max(F.vx(round(first0/2),:)); % Find maximum velocity
of 1st data set
MAX = max(F1.vx(round(first/2),:));  % Find maximum velocity
of 2nd data set
MAX1 = max(F2.vx(round(first1/2),:)); % Find maximum
velocity of 3rd data set
MAX2 = max(F3.vx(round(first2/2),:)); % Find maximum
velocity of 4th  data set

F.vx_scaled = F.vx/MAX0; % Normalize velocity with maximum
velocity of 1st  data set
F1.vx_scaled = F1.vx/MAX; % Normalize velocity with maximum
velocity of 2nd data set
F2.vx_scaled = F2.vx/MAX1; % Normalize velocity with maximum
velocity of 3rd data set
F3.vx_scaled = F3.vx/MAX2; % Normalize velocity with maximum
velocity of 4th data set

hold on;
```

```
% Plot the average normalized velocity of all data in one
figure

grid

    plot(F.y/CW,F.vx_scaled(round(first0/2),:),'-
bo','LineWidth',2);
    plot(F1.y/CW,F1.vx_scaled(round(first/2),:),'-
go','LineWidth',2);
    plot(F2.y/CW,F2.vx_scaled(round(first1/2),:),'-
ro','LineWidth',2);
    plot(F3.y/CW,F3.vx_scaled(round(first2/2),:),'-
ko','LineWidth',2);

hold off;

xlabel('{\it x/w}','FontName','Times New
Roman','FontSize',16);
ylabel('{\itU / U_{max}} ','FontName','Times New
Roman','FontSize',16);

leg1 = legend('Water','0.1 wt.% Polyacrylamide','0.3 wt.%
Polyacrylamide','0.5 wt.% Polyacrylamide','FontName','Times
New Roman','FontSize',18);
set(leg1,'Location','Best');

axis([-0.7,0.7,0,1]);
```

Appendix C. **Graphs of velocity profile for straight mini-channels**

C-1. The velocity profile of water through straight channel at different flow rates

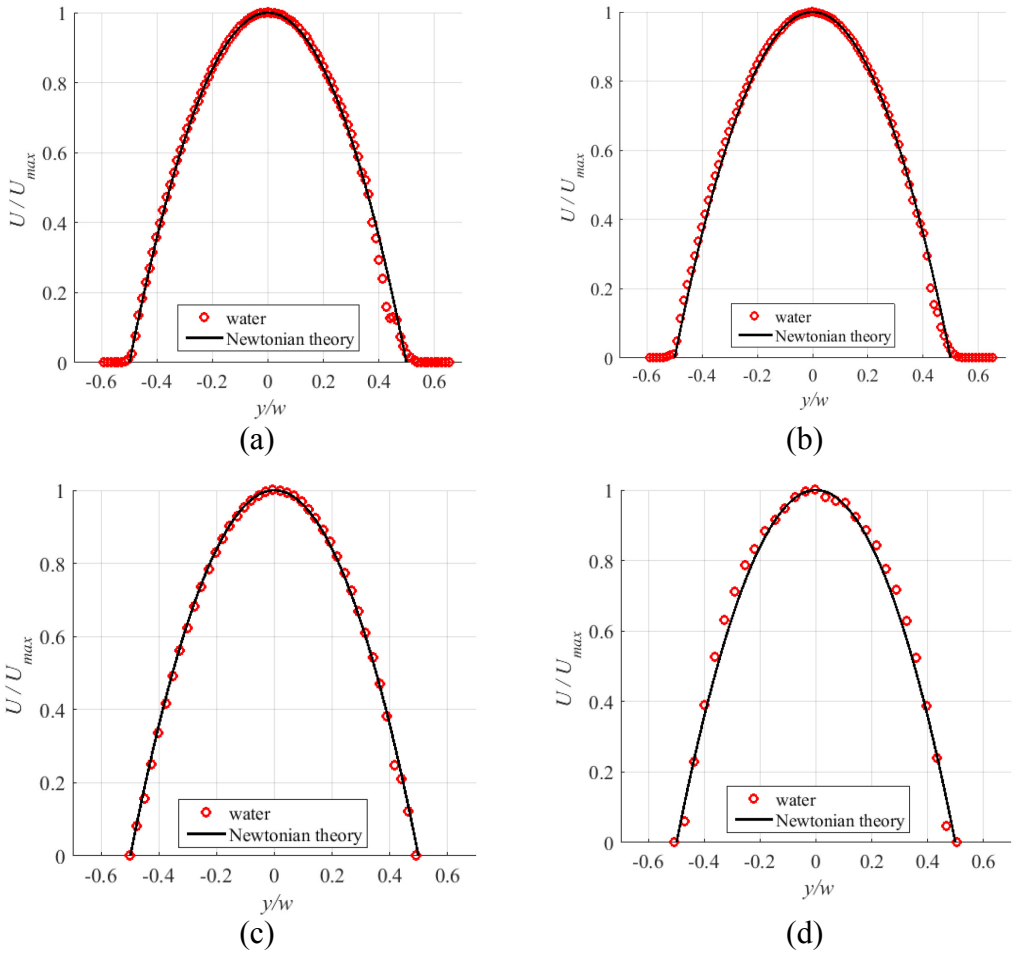

Figure A- 1.Plots for comparison of average velocity profile of water solution at (a) Q = 0.025 ml/min, (b) Q = 0.05 ml/min, (c) Q = 0.075 ml/min and (d) Q = 0.1 ml/min with Newtonian theory

C-2. The velocity profile of 0.1 wt. % polyacrylamide through straight channel at different flow rates

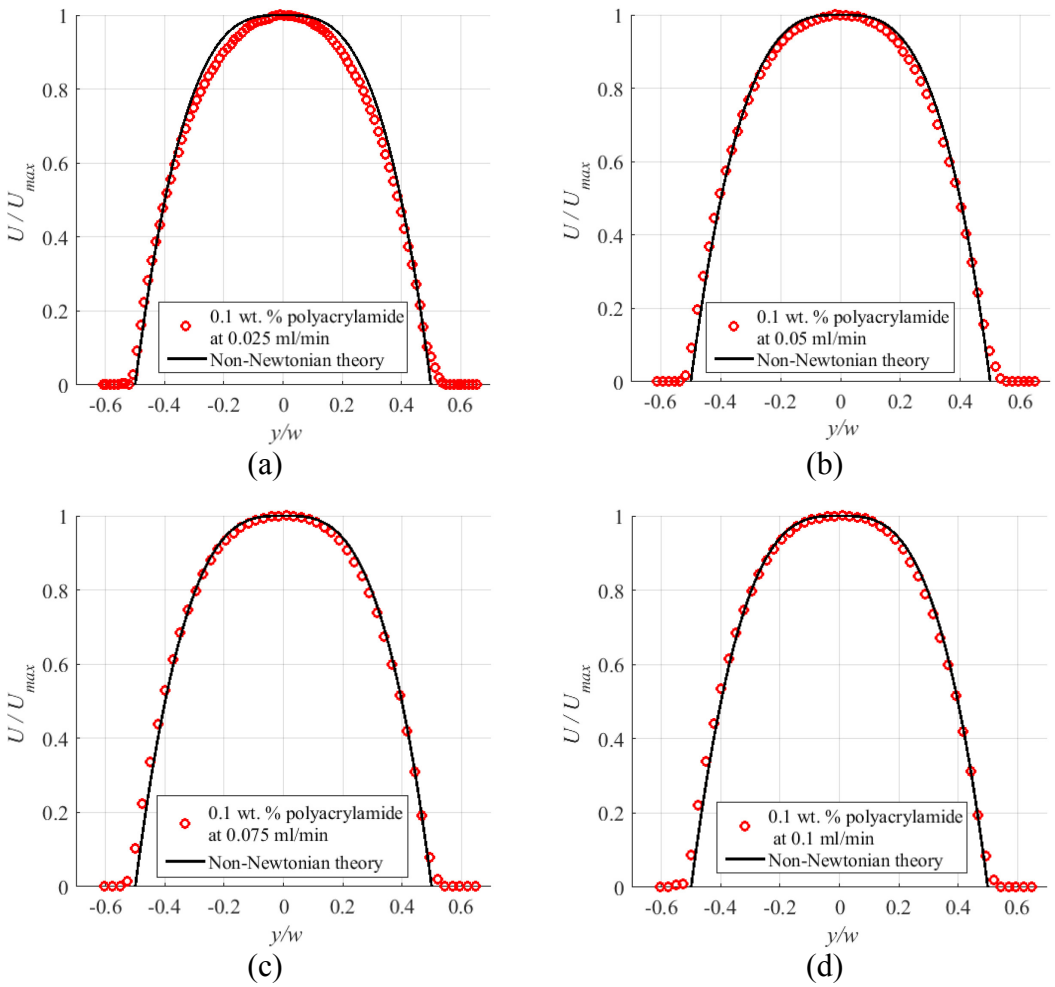

Figure A- 2. Plots for comparison of average velocity profile of 0.1 wt. % polyacrylamide solution at (a) Q = 0.025 ml/min, (b) Q = 0.05 ml/min, (c) Q = 0.075 ml/min and (d) Q = 0.1 ml/min with non-Newtonian theory

C-3. The velocity profile of 0.3 wt. % polyacrylamide through straight channel at different flow rates

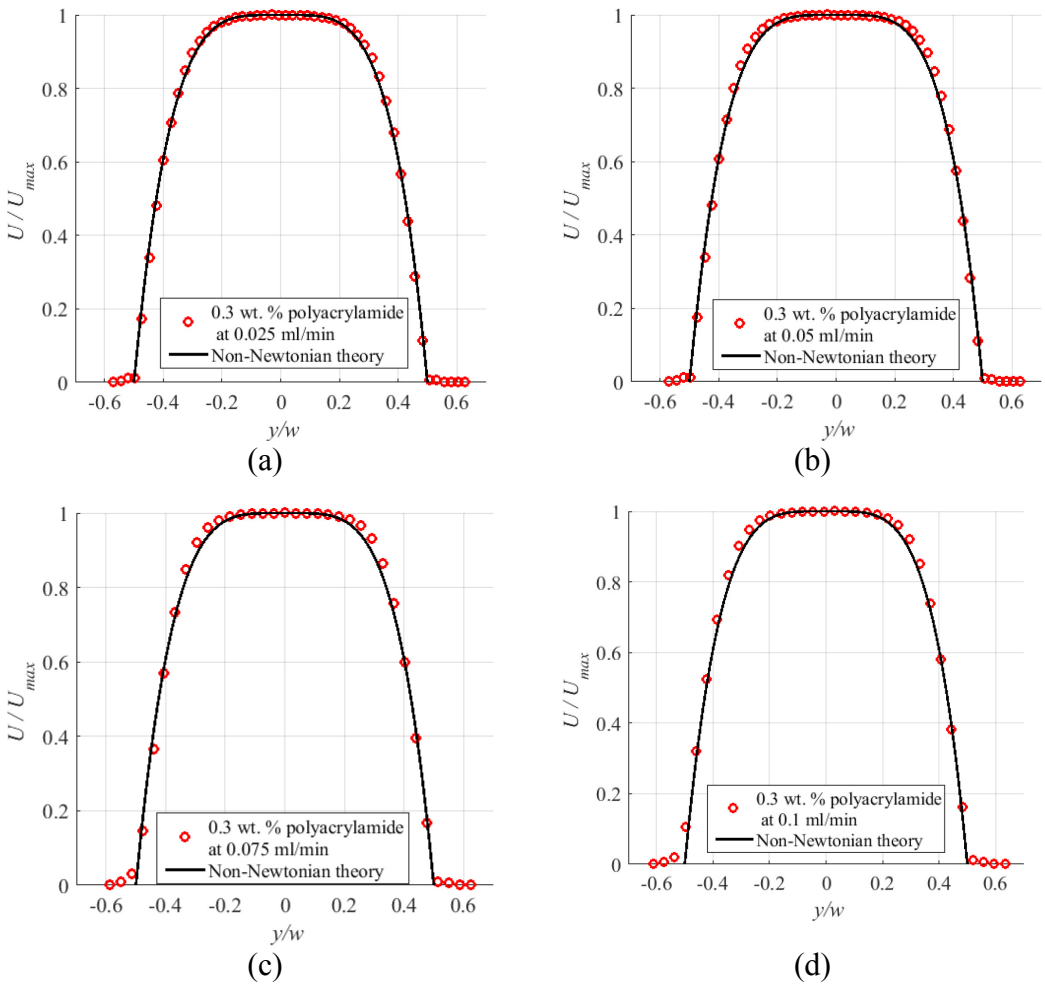

Figure A- 3. Plots for comparison of average velocity profile of 0.3 wt. % polyacrylamide at (a) Q = 0.025 ml/min, (b) Q = 0.05 ml/min, (c) Q = 0.075 ml/min and (d) Q = 0.1 ml/min with non-Newtonian theory

C-4. The velocity profile of 0.5 wt. % polyacrylamide through straight channel at different flow rates

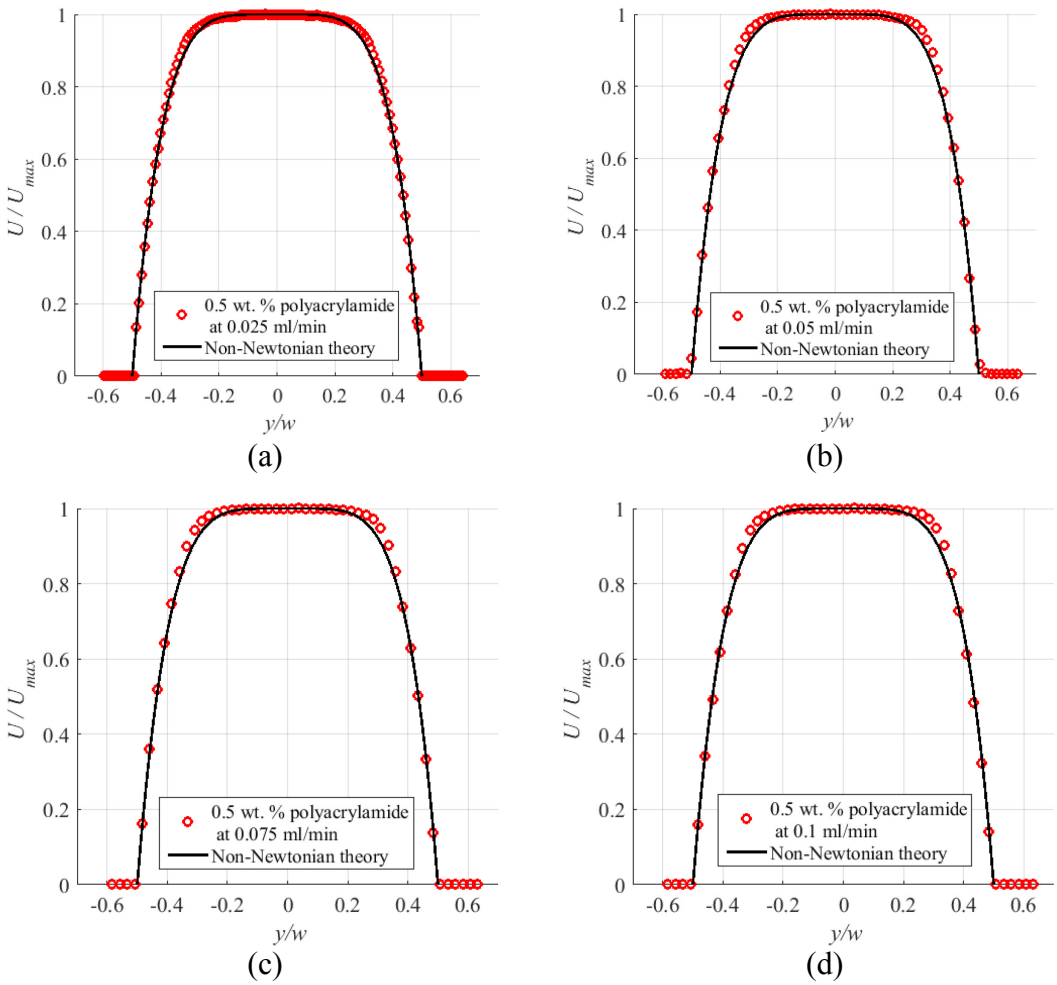

Figure A- 4. Plots for comparison of average velocity profile of 0.5 wt. % polyacrylamide solution at (a) Q = 0.025 ml/min, (b) Q = 0.05 ml/min, (c) Q = 0.075 ml/min and (d) Q = 0.1 ml/min with Newtonian theory non-Newtonian theory

C-5. Plot of velocity profile of 0.1 wt.% polyacrylamide curve fitted with power law

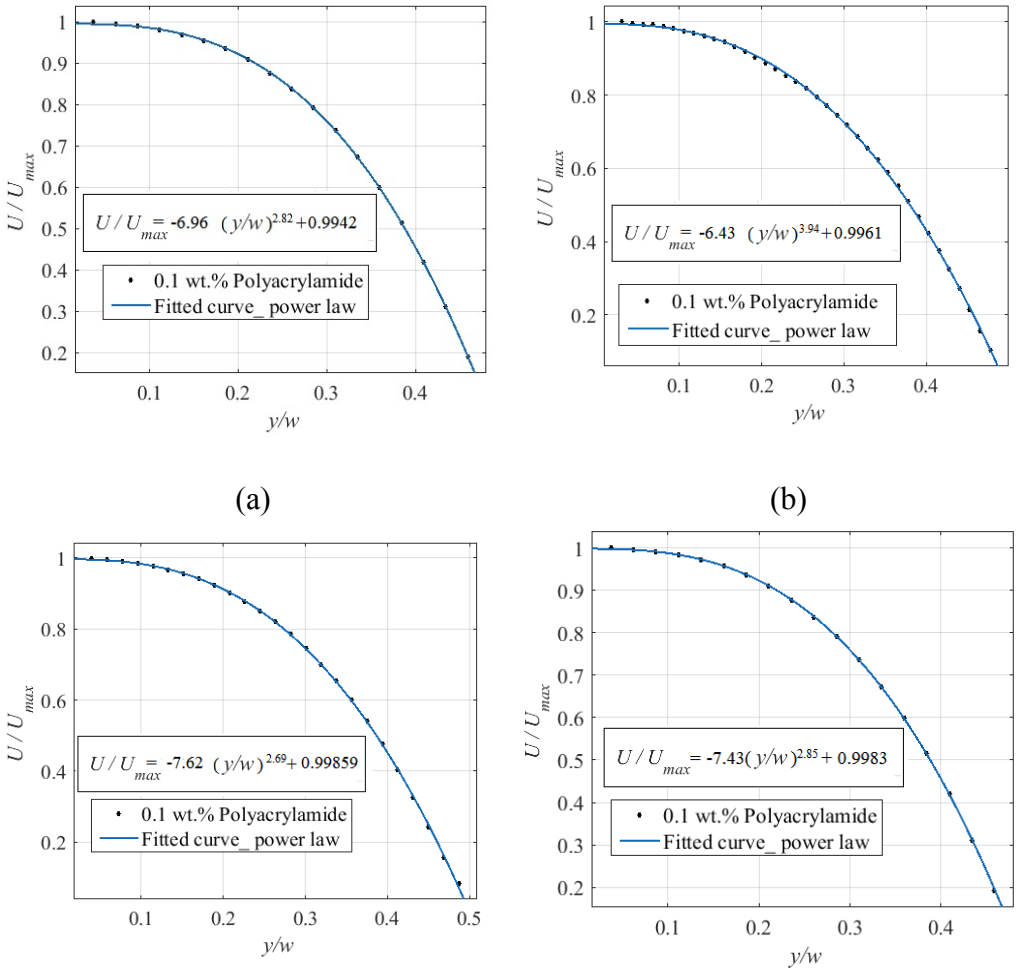

Figure A- 5. Plot of velocity profile of 0.1 wt.% polyacrylamide curve fitted with power law at (a) Q = 0.025 ml/min, (b) Q = 0.05 ml/min, (c) Q = 0.075 ml/min and (d) Q = 0.1 ml/min

C-6. Plot of velocity profile of 0.3 wt. % polyacrylamide curve fitted with power law

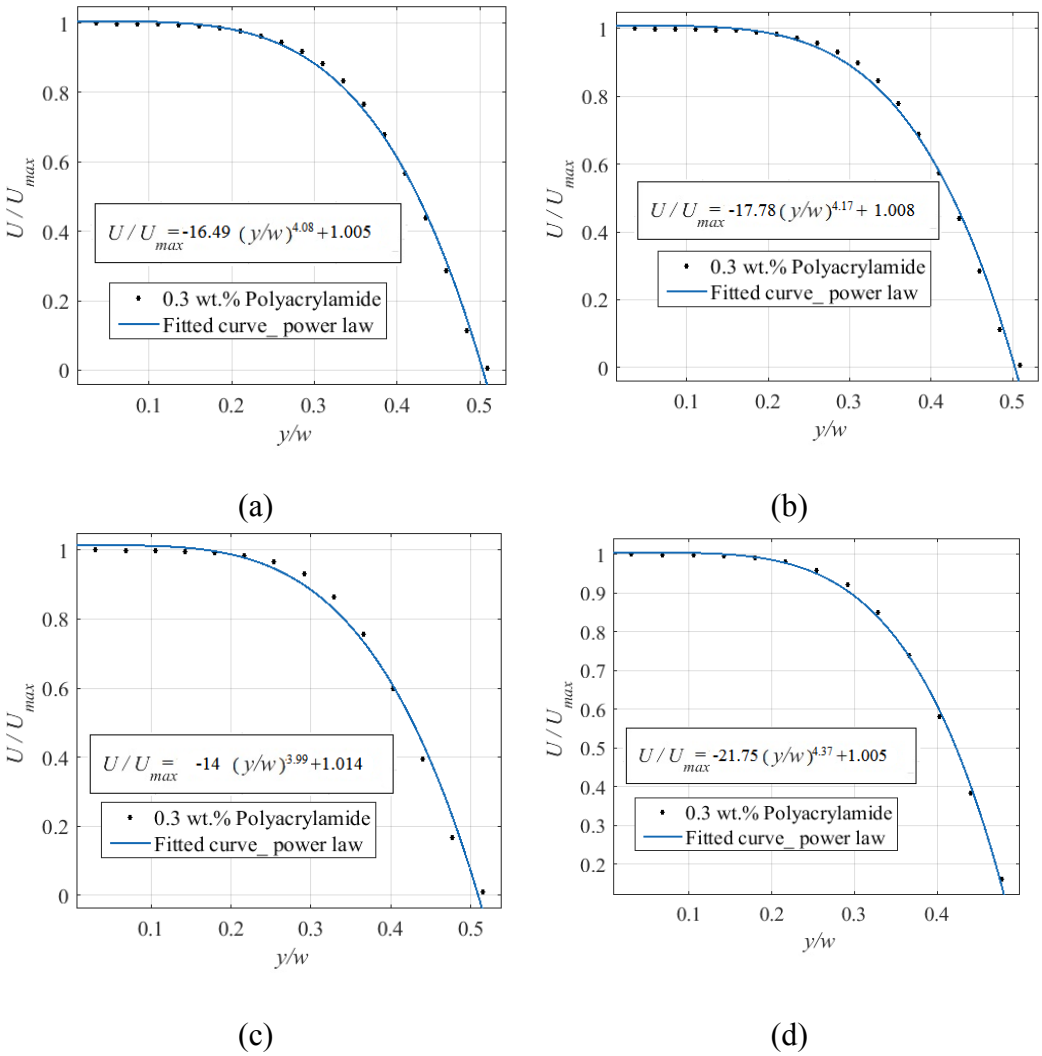

Figure A- 6. Plot of velocity profile of 0.3 slot% polyacrylamide curve fitted with power law at (a) Q = 0.025 ml/min, (b) Q = 0.05 ml/min, (c) Q = 0.075 ml/min and (d) Q = 0.1 ml/min

C-7. Plot of velocity profile of 0.5 wt. % polyacrylamide curve fitted with power law

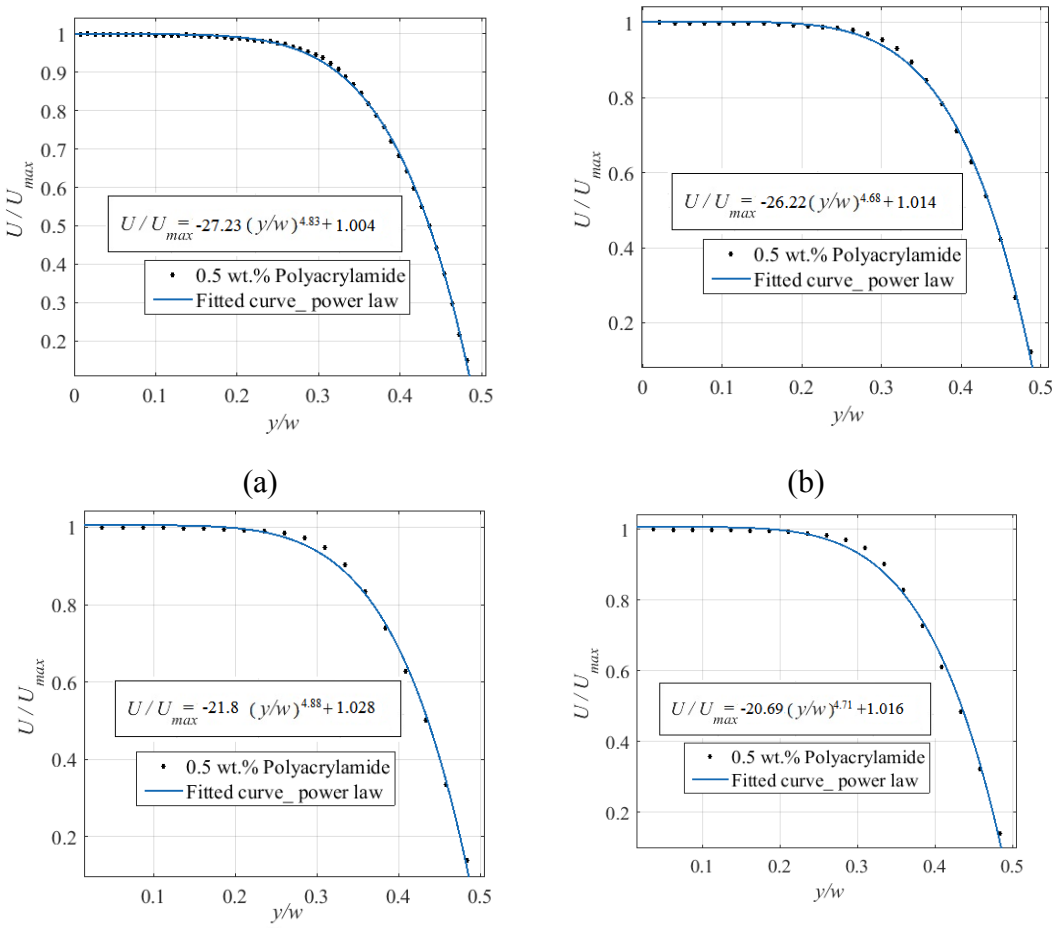

Figure A- 7. Plot of velocity profile of 0.5 wt.% polyacrylamide curve fitted with power law at (a) Q = 0.025 ml/min, (b) Q = 0.05 ml/min, (c) Q = 0.075 ml/min and (d) Q = 0.1 ml/min

Appendix D. **Graphs of Flow of Newtonian and non-Newtonian flow through keystone slots**

D-1. Water flow through different shapes of keystone slot

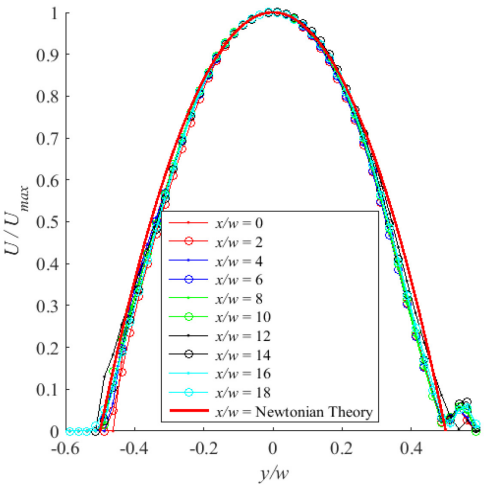

(a) Water flow through keystone slot with θ= 0° (straight) at Q = 5.5 ml/hr

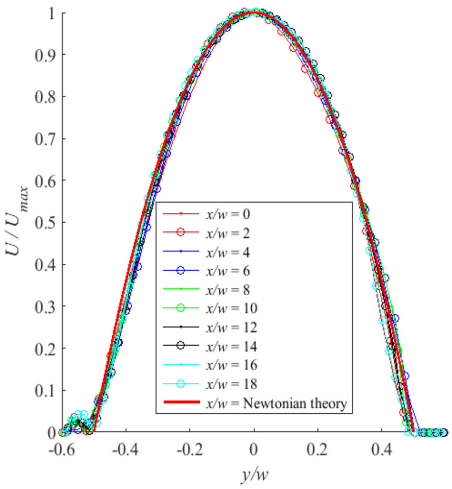

(b) Water flow through keystone slot with θ= 2° at Q = 5.5 ml/hr

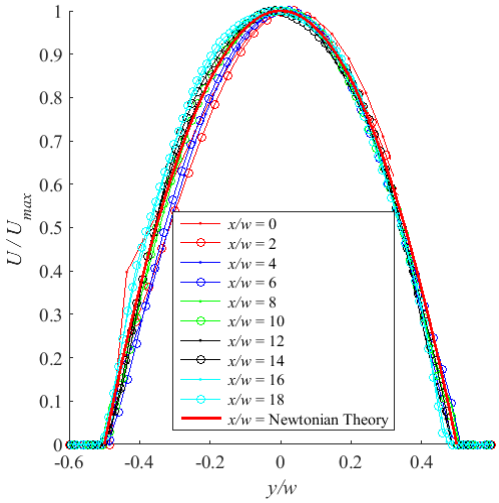

(c)Water flow through keystone slot with θ= 4° at Q = 5.5 ml/hr

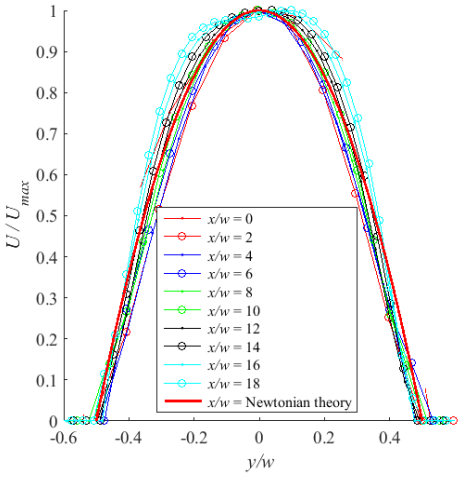

(d)Water flow through keystone slot with θ= 6° at Q = 5.5 ml/hr

Figure A- 8. The velocity profile of water at ten positions starting from the entrance of the channel at Q = 5.5 ml/hr through (a) θ = 0°(straight), (b) θ = 2°, (c) θ = 4°, (d) θ = 6°, (e) θ = 8°, (f) θ = 10°, and (g) θ = 12° keystone slot in compare to Newtonian theoretical profile

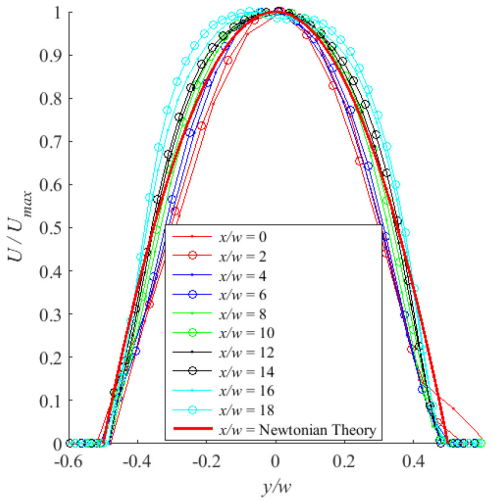

(e) Water flow through keystone slot with θ= 8° at Q = 5.5 ml/hr

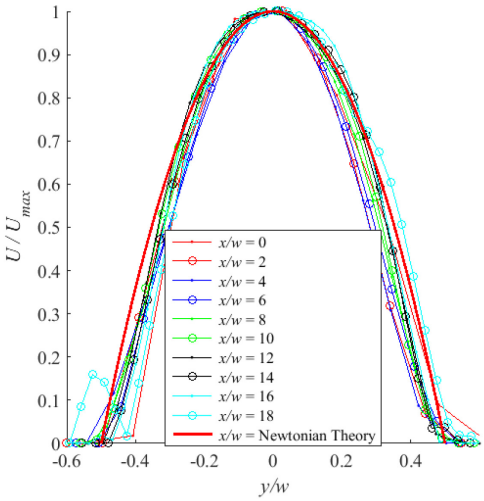

(f) Water flow through keystone slot with θ= 10° at Q = 5.5 ml/hr

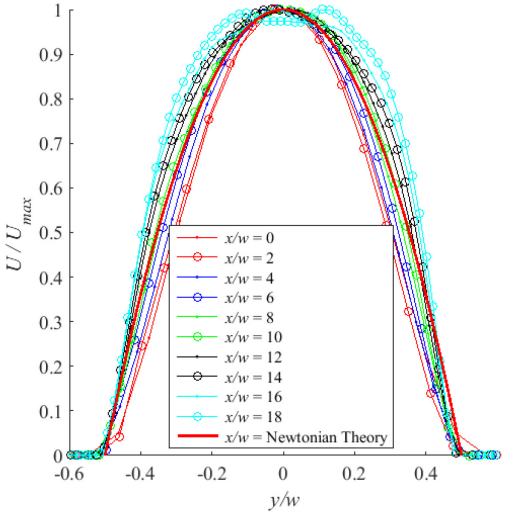

(g) Water flow through keystone slot with θ= 12° at Q = 5.5 ml/hr

Figure A- 8*(continued)*

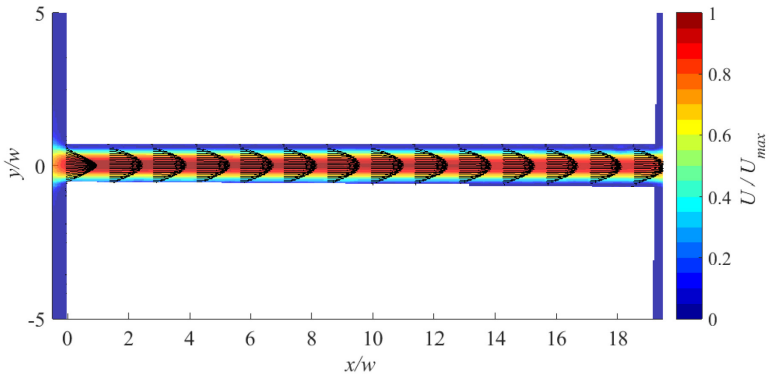

(a) Water flow through keystone slot with $\theta = 0°$(straight) at Q = 5.5ml/hr

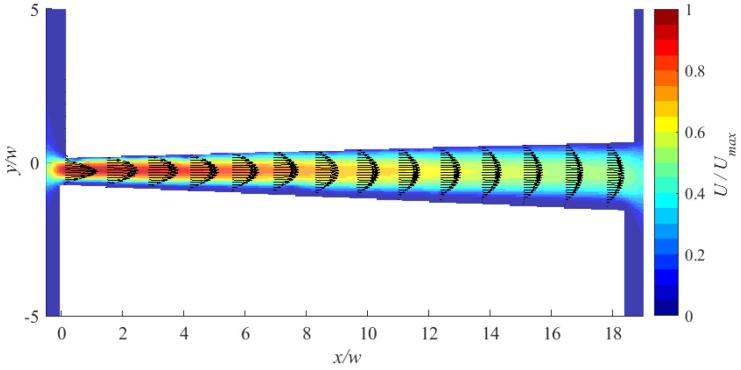

(b) Water flow through keystone slot with $\theta = 2°$ at Q = 5.5ml/hr

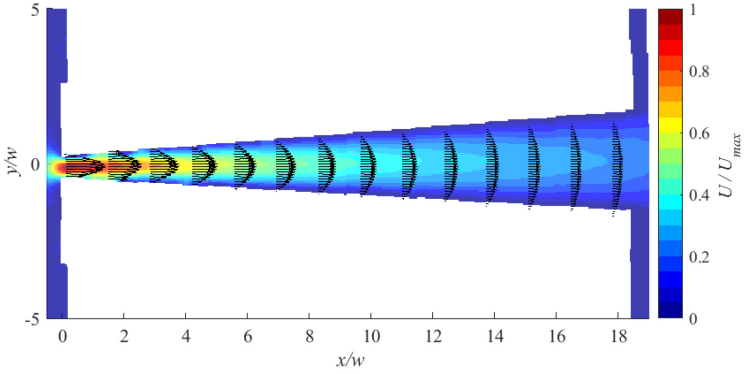

(c) Water flow through keystone slot with $\theta = 4°$ at Q = 5.5ml/hr

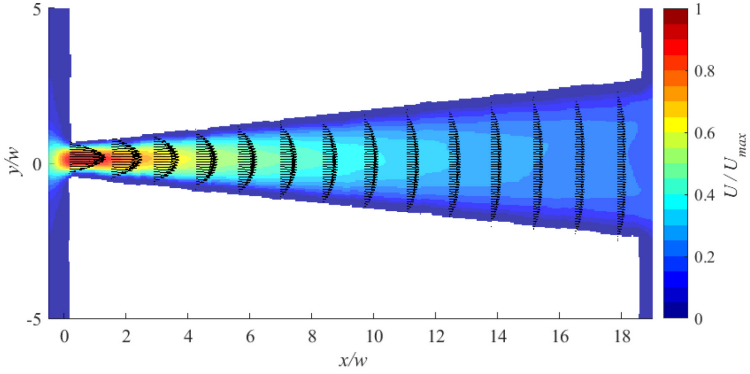

(d) Water flow through keystone slot with $\theta = 6°$ at Q = 5.5ml/hr

Figure A- 9. Vector map of water flow at Q = 5.5 ml/ hr through (a) $\theta = 0°$(straight), (b) $\theta = 2°$, (c) $\theta = 4°$, (d) $\theta = 6°$, (e) $\theta = 8°$, (f) $\theta = 10°$, and (g) $\theta = 12°$ keystone slot

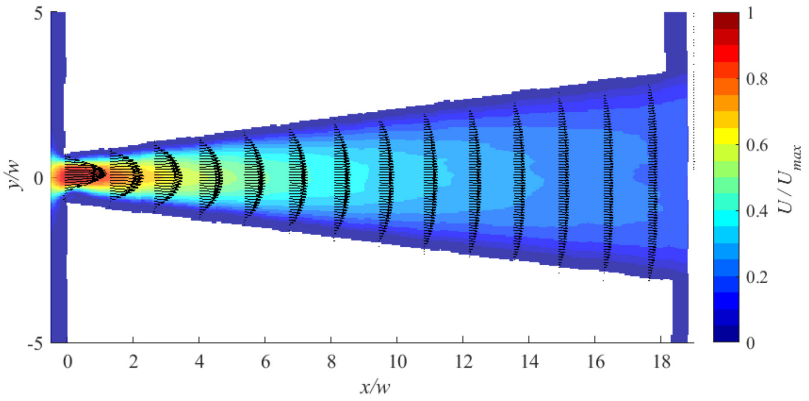

(e) Water flow through keystone slot with $\theta = 8°$ at Q = .55ml/hr

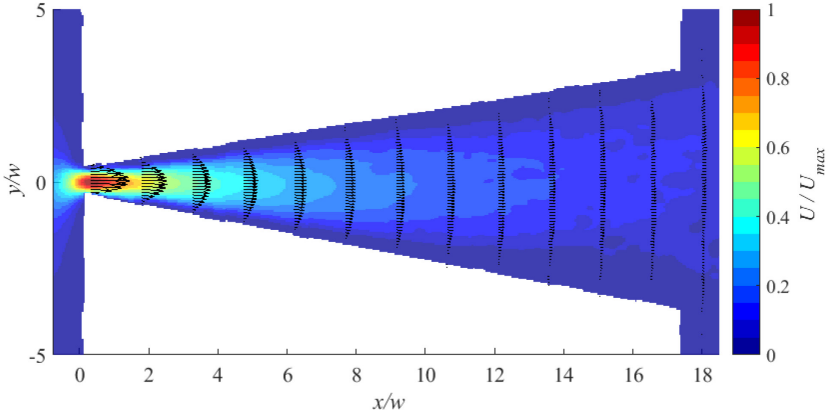

(f) Water flow through keystone slot with $\theta = 10°$ at Q = 5.5ml/hr

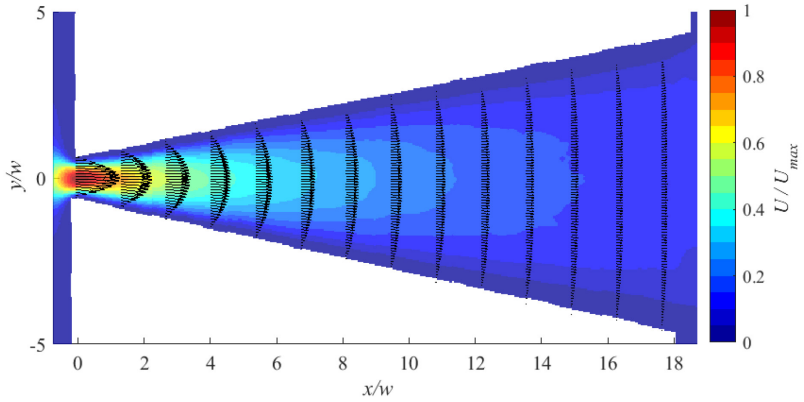

(g) water flow through keystone slot with $\theta = 12°$ at Q = 5.5ml/hr

Figure A- 9*(continued)*

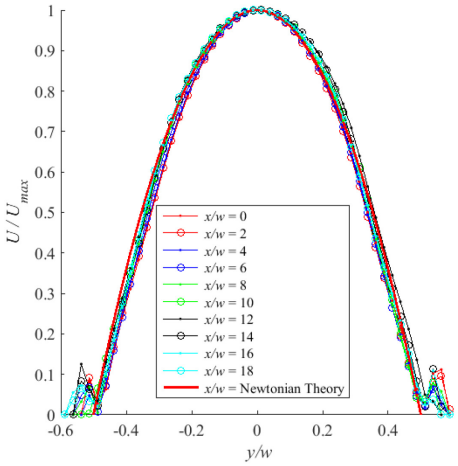

(a) Water flow through keystone slot with θ= 0° (straight) at Q = 10 ml/hr

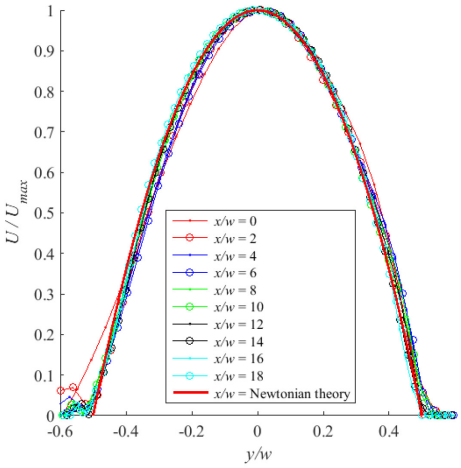

(b) Water flow through keystone slot with θ= 2° at Q = 10 ml/hr

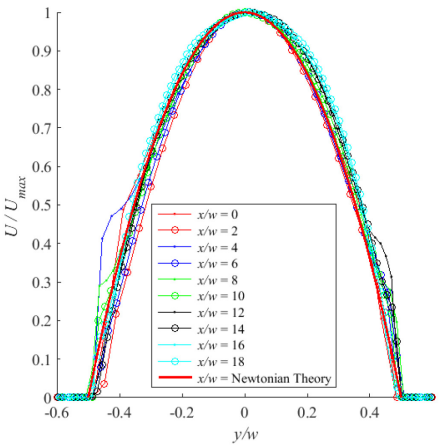

(c)Water flow through keystone slot with θ= 4° at Q = 10 ml/hr

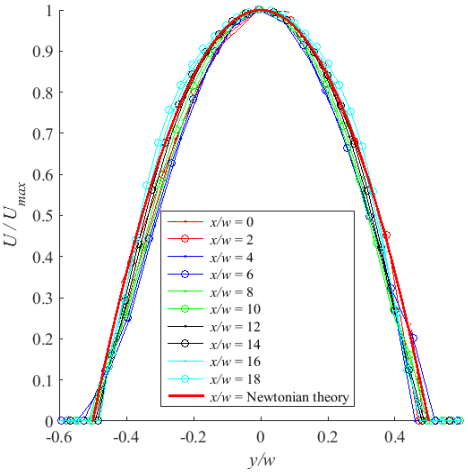

(d)Water flow through keystone slot with θ= 6° at Q =10ml/hr

Figure A- 10. The velocity profile of water at ten positions starting from the entrance of the channel at Q = 10 ml/hr through (a) θ = 0°(straight), (b) θ = 2°, (c) θ = 4°, (d) θ = 6°, (e) θ = 8°, (f) θ = 10°, and (g) θ = 12° keystone slot in compare to Newtonian theoretical profile

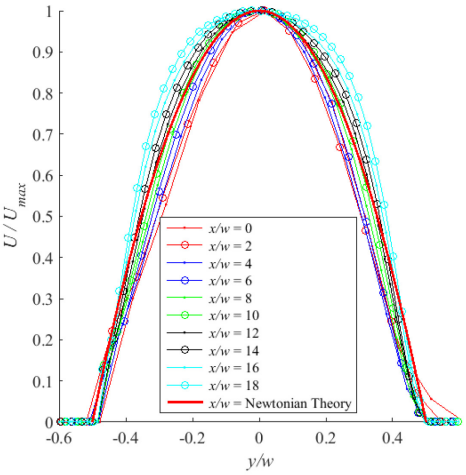

(e) Water flow through keystone slot with θ= 8° at Q = 10 ml/hr

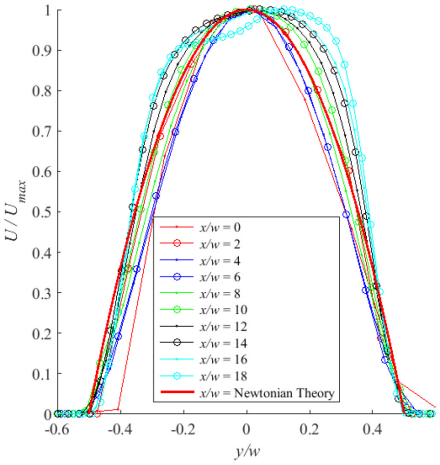

(f) Water flow through keystone slot with θ= 10° at Q = 10 ml/hr

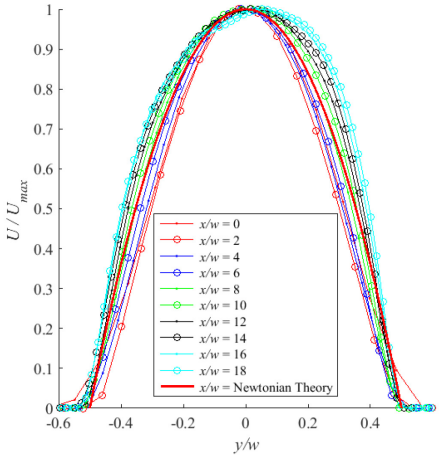

(g) Water flow through keystone slot with θ= 12° at Q = 5.5 ml/hr

Figure A- 10 *(continued)*

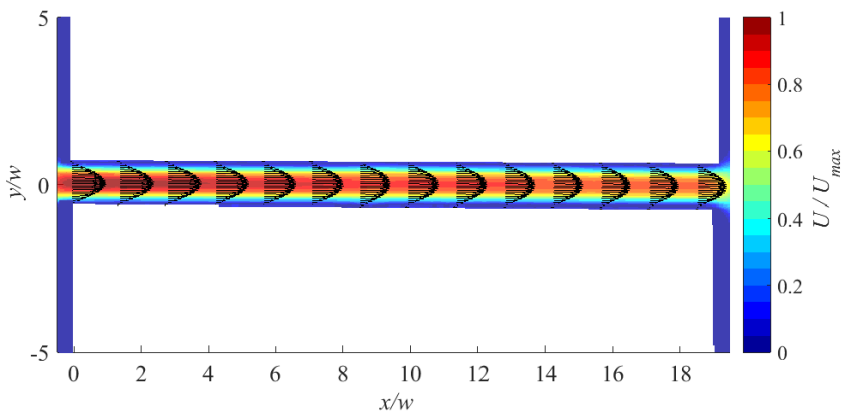

(a) Water flow through keystone slot with $\theta = 0°$(straight) at Q = 10ml/hr

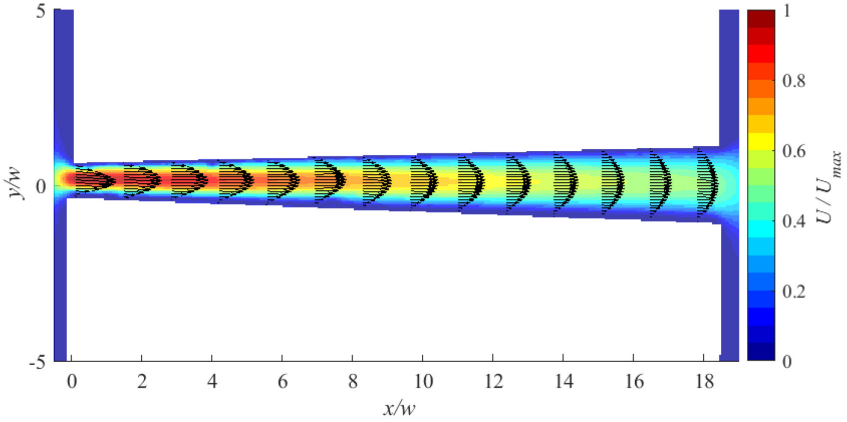

(b) Water flow through keystone slot with $\theta = 2°$ at Q = 10ml/hr

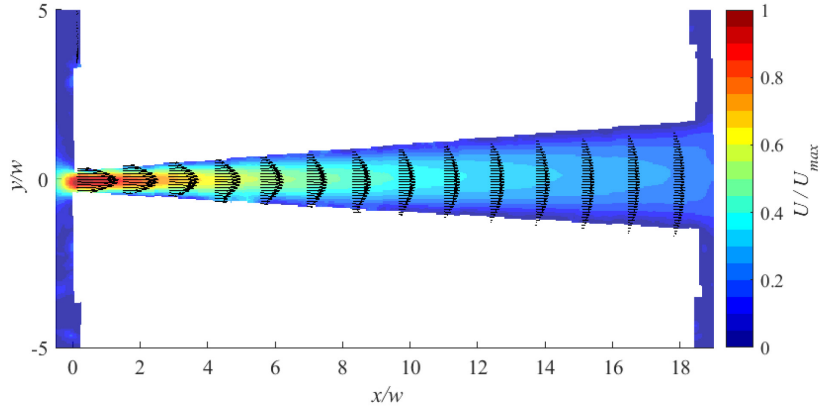

(c) Water flow through keystone slot with $\theta = 4°$ at Q = 10ml/hr

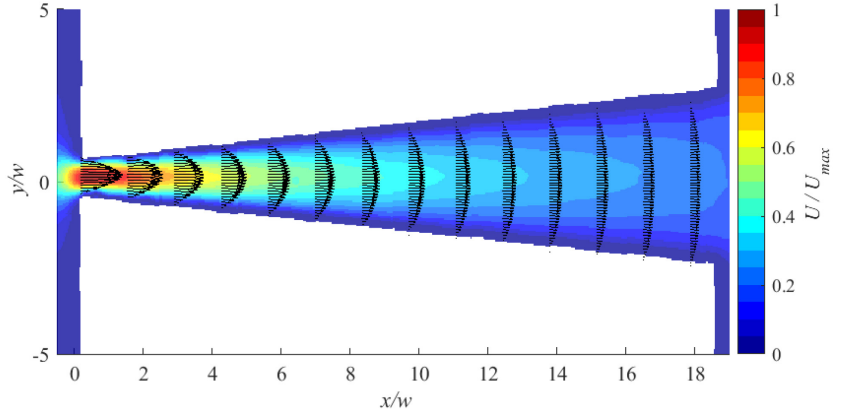

(d) Water flow through keystone slot with $\theta = 6°$ at Q = 10ml/hr

Figure A- 11. Vector map of water flow at Q = 10 ml/ hr through (a) $\theta = 0°$(straight), (b) $\theta = 2°$, (c) $\theta = 4°$, (d) $\theta = 6°$, (e) $\theta = 8°$, (f) $\theta = 10°$, and (g) $\theta = 12°$ keystone slot

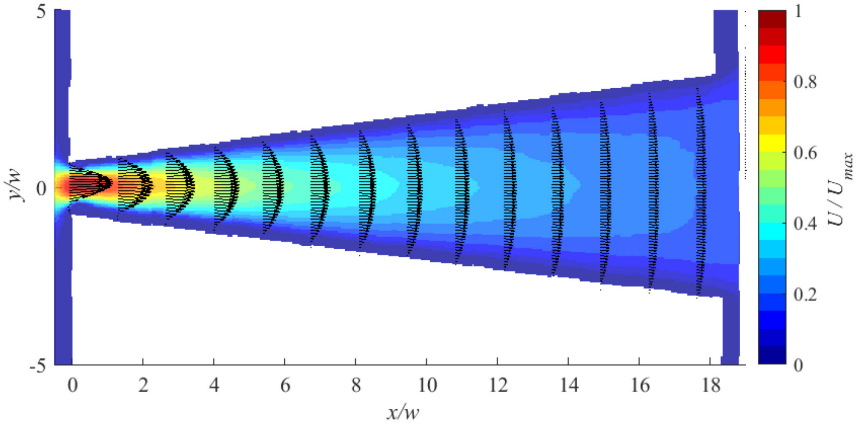

(e) Water flow through keystone slot with $\theta = 8°$ at $Q = 10$ml/hr

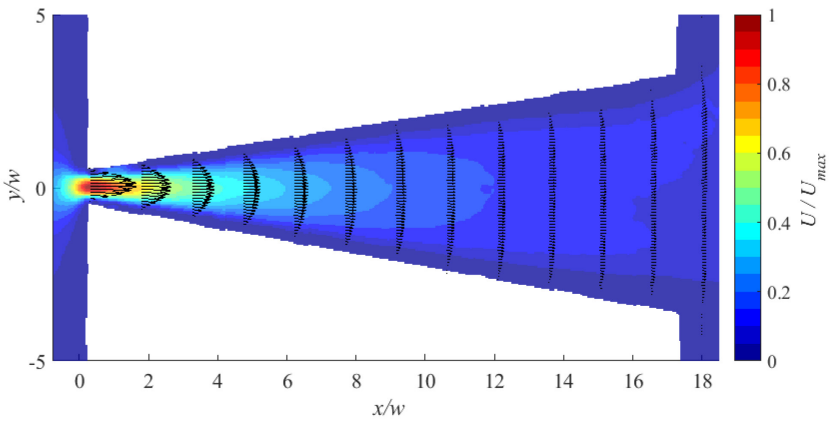

(f) Water flow through keystone slot with $\theta = 10°$ at $Q = 10$ml/hr

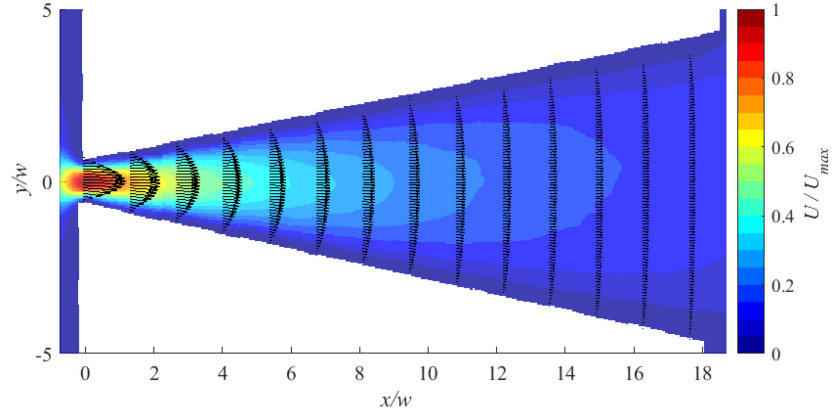

(g) Water flow through keystone slot with $\theta = 12°$ at $Q = 10$ml/hr

Figure A- 11*(continued)*

D-2. 0.2 wt. % Polyacrylamide solution flow through different shapes of keystone slots

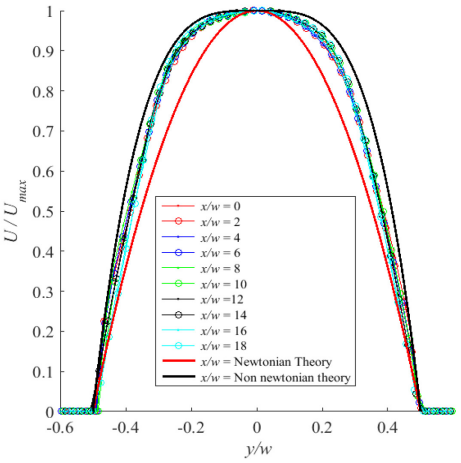

(a) 0.2 wt. % polyacrylamide flow through keystone slot with θ= 0° (straight) at Q = 5.5 ml/hr

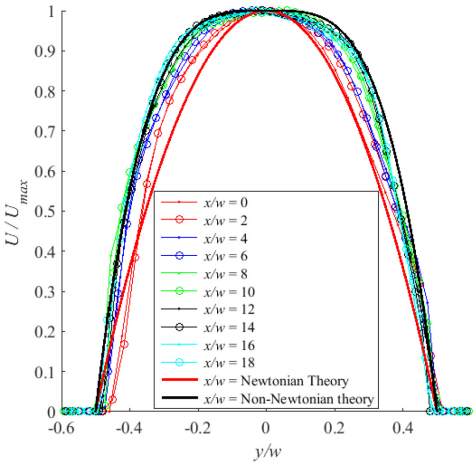

(b) 0.2 wt. % polyacrylamide flow through keystone slot with θ= 2° at Q = 5.5 ml/hr

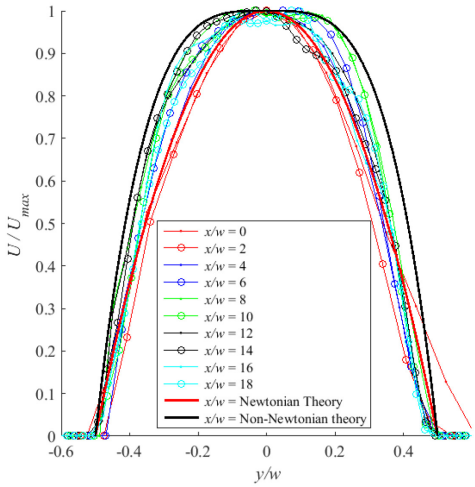

(c) 0.2 wt. % polyacrylamide flow through keystone slot with θ= 4° at Q = 5.5 ml/hr

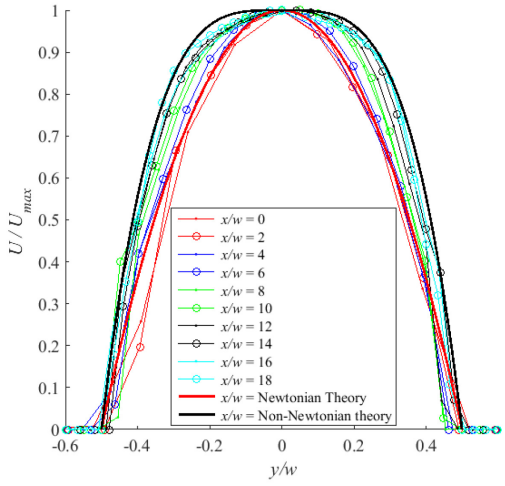

(d) 0.2 wt. % polyacrylamide flow through keystone slot with θ= 6° at Q = 5.5 ml/hr

Figure A- 12.The velocity profile of 0.2 wt. % polyacrylamide at Q = 5.5 ml/hr through (a) θ = 0°(straight), (b) θ = 2°, (c) θ = 4°, (d) θ = 6°, (e) θ = 8°, (f) θ = 10°, and (g) θ = 12° keystone slot in compare to non-Newtonian theoretical profile

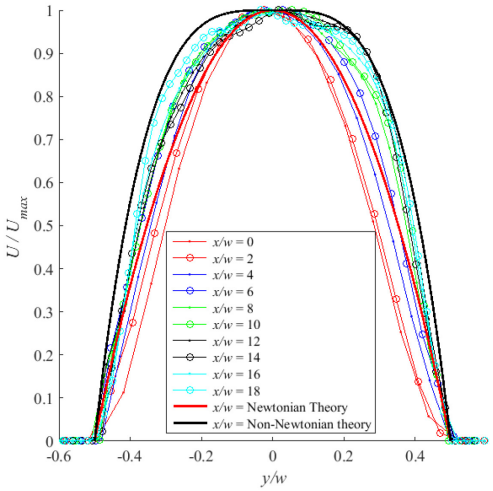

(e0.2 wt. % polyacrylamide flow through keystone slot with θ= 8° at Q = 5.5 ml/hr

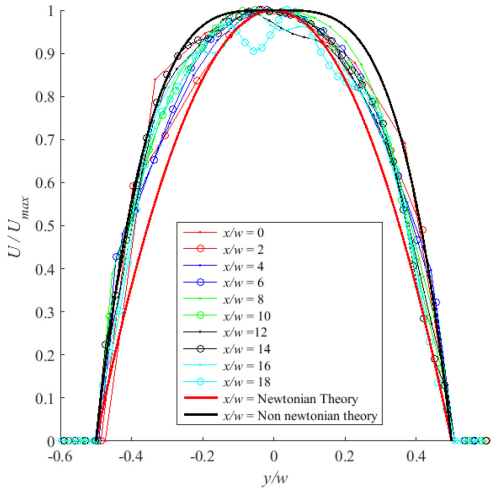

(f) 0.2 wt. % polyacrylamide flow through keystone slot with θ= 10° at Q = 5.5 ml/hr

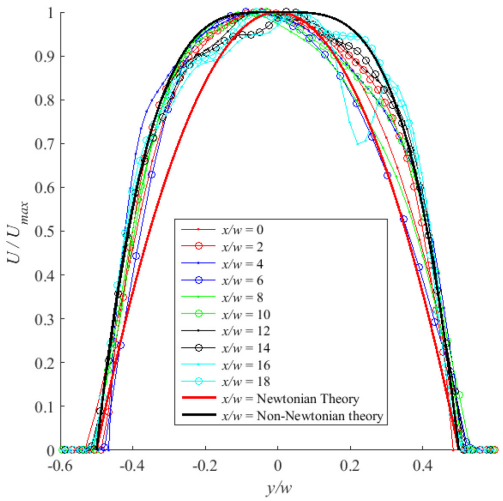

(g) 00.2 wt. % polyacrylamide flow through keystone slot with θ= 12° at Q = 5.5 ml/hr

Figure A- 12 *(continued)*

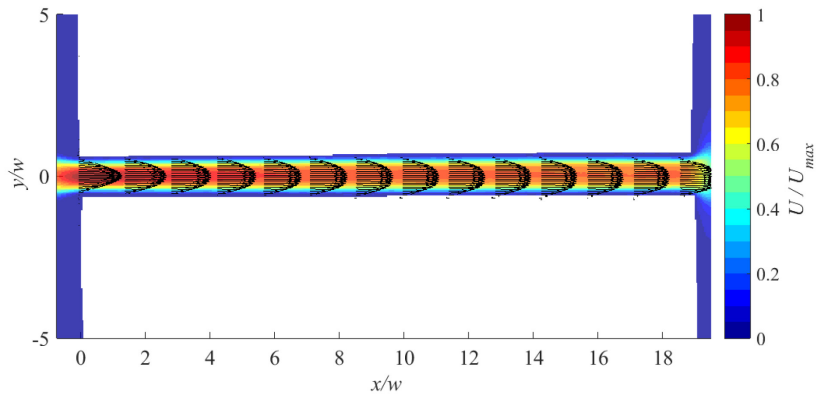

(a) 0.2 wt. % polyacrylamide solution flow through $\theta = 0°$ (straight) slot at 5.5 ml/ hr

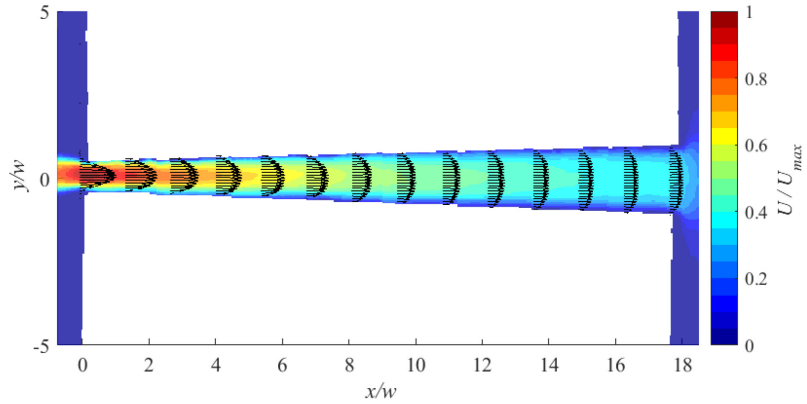

(b) 0.2 wt. % polyacrylamide solution flow through keystone slot with $\theta = 2°$ slot angle at Q = 5.5ml/hr

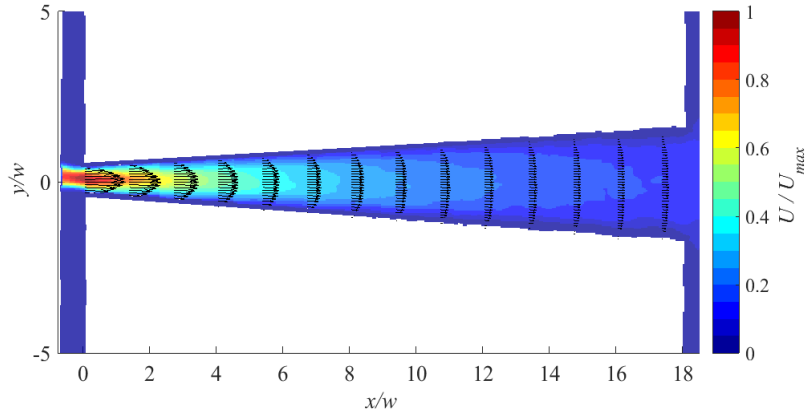

(c) 0.2 wt. % polyacrylamide solution flow through keystone slot with $\theta = 4°$ slot angle at Q = 5.5 ml/ hr

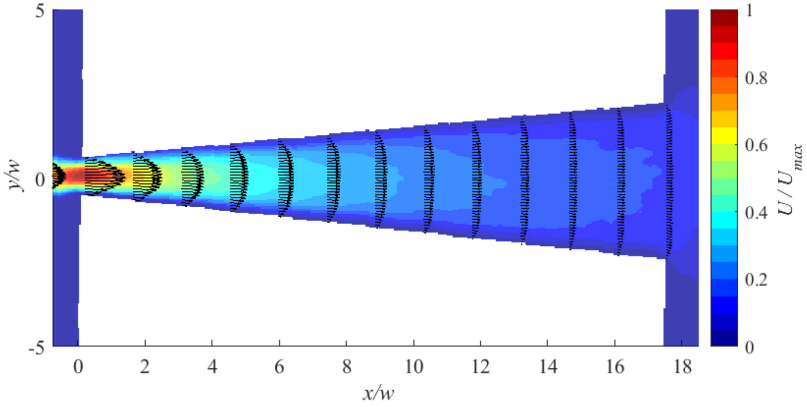

(d) 0.2 wt. % polyacrylamide solution flow through keystone slot with $\theta = 6°$ slot angle at Q = 5.5 ml/ hr

Figure A- 13. Vector map of 0.2 wt. % polyacrylamide solution flow at Q = 5.5 ml/ hr through (a) $\theta = 0°$(straight), (b) $\theta = 2°$, (c) $\theta = 4°$, (d) $\theta = 6°$, (e) $\theta = 8°$, (f) $\theta = 10°$, and (g) $\theta = 12°$ keystone slot

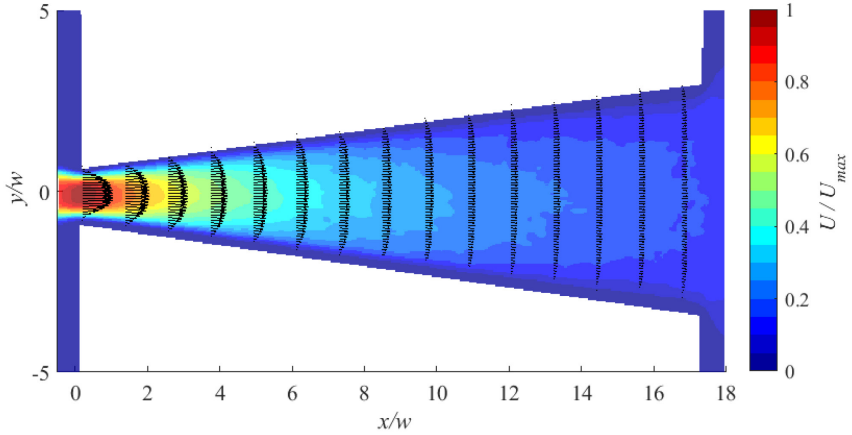

(e) 0.2 wt. % polyacrylamide solution flow through keystone slot with $\theta = 8°$ slot angle at Q = 5.5 ml/ hr

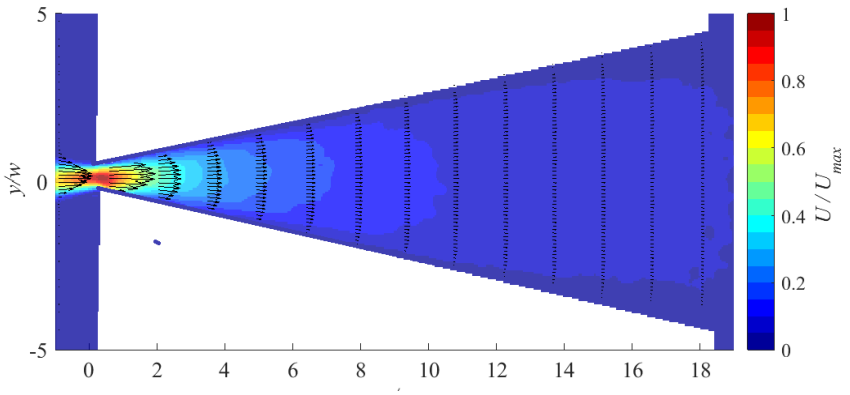

(f) 0.2 wt. % polyacrylamide solution flow through keystone slot with $\theta = 10°$ slot angle at Q = 5.5 ml/ hr

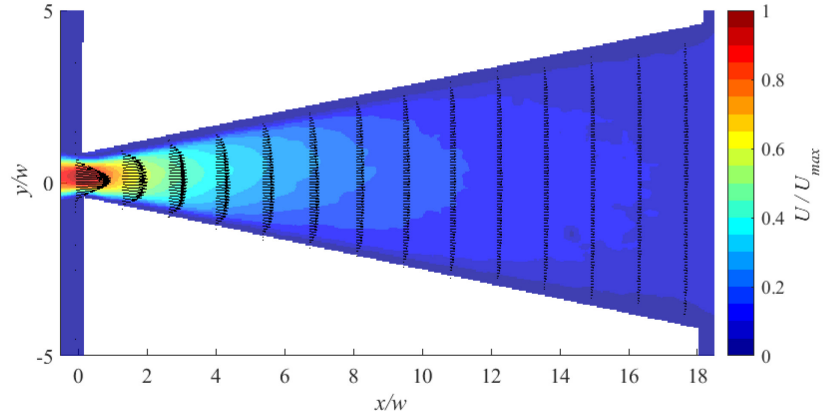

(g) 0.2 wt. % polyacrylamide solution flow through keystone slot with $\theta = 12°$ slot angle at Q = 5.5 ml/ hr

Figure A- 13*(continued)*

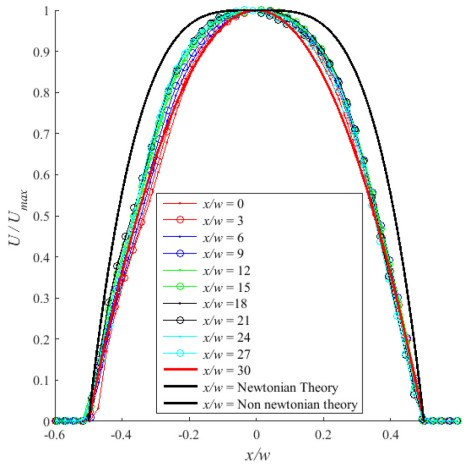

(a) 0.2 wt. % polyacrylamide flow through keystone slot with $\theta = 0°$ (straight) at $Q = 10$ ml/hr

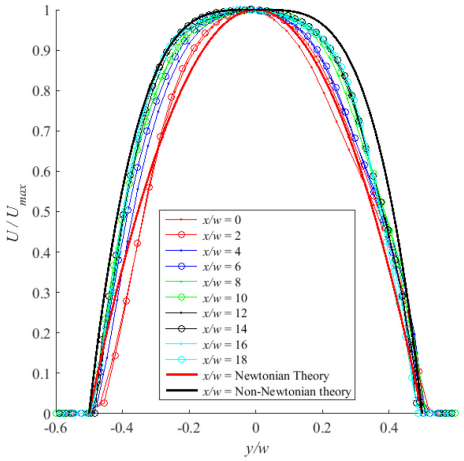

(b) 0.2 wt. % polyacrylamide flow through keystone slot with $\theta = 2°$ at $Q = 10$ ml/hr

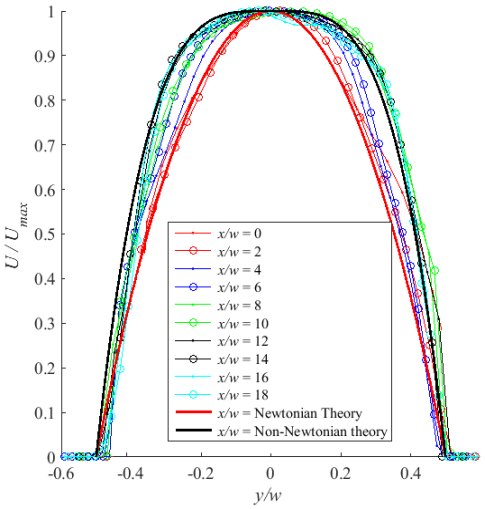

(c) 0.2 wt. % polyacrylamide flow through keystone slot with $\theta = 4°$ at $Q = 10$ ml/hr

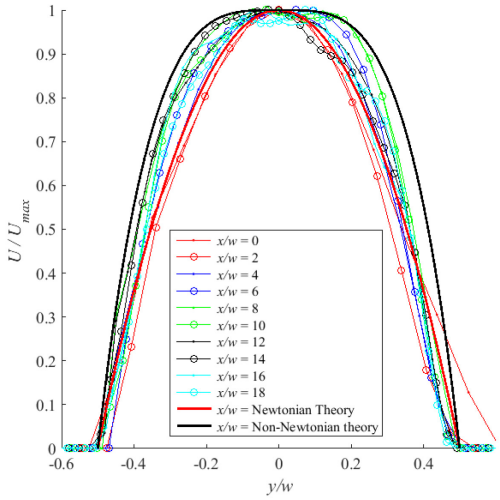

(d) 0.2 wt. % polyacrylamide flow through keystone slot with $\theta = 6°$ at $Q = 10$ ml/hr

Figure A- 14. The velocity profile of 0.2 wt. % polyacrylamide at $Q = 10$ ml/hr through (a) $\theta = 0°$(straight), (b) $\theta = 2°$, (c) $\theta = 4°$, (d) $\theta = 6°$, (e) $\theta = 8°$, (f) $\theta = 10°$, and (g) $\theta = 12°$ keystone slot in compare to non- Newtonian theoretical profile

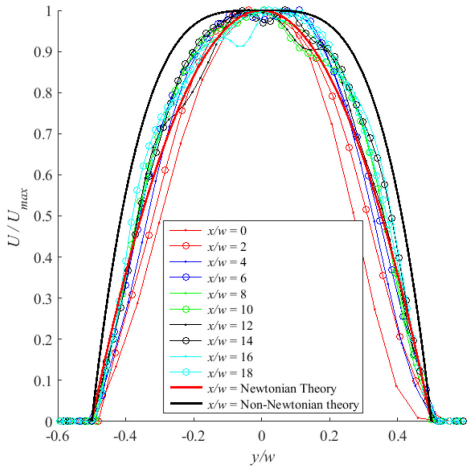

(e) 0.2 wt. % polyacrylamide flow through keystone slot with $\theta = 8°$ at Q = 10 ml/hr

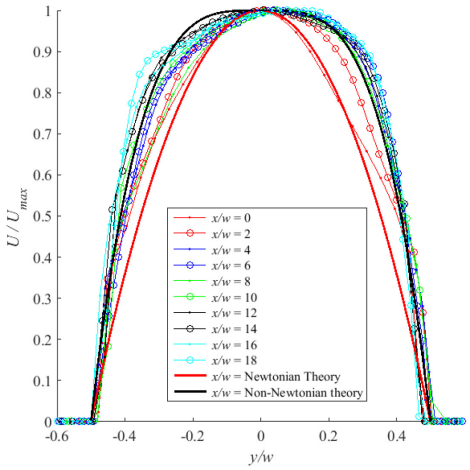

(f) 0.2 wt. % polyacrylamide flow through keystone slot with $\theta = 10°$ at Q = 10 ml/hr

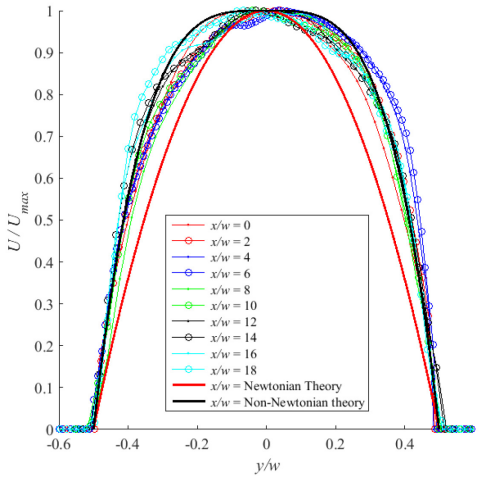

(g) 0.2 wt. % polyacrylamide flow through keystone slot with $\theta = 12°$ at Q = 10 ml/hr

Figure A- 14 *(continued)*

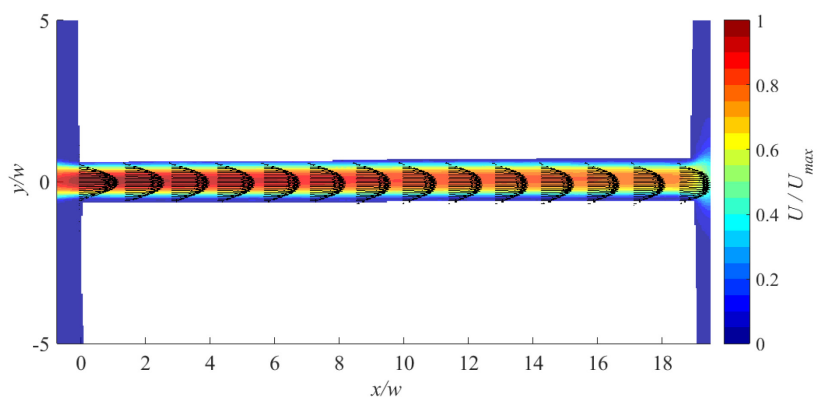

(a) 0.2 wt. % polyacrylamide solution flow through $\theta = 0°$ (straight slot) at 10 ml/ hr

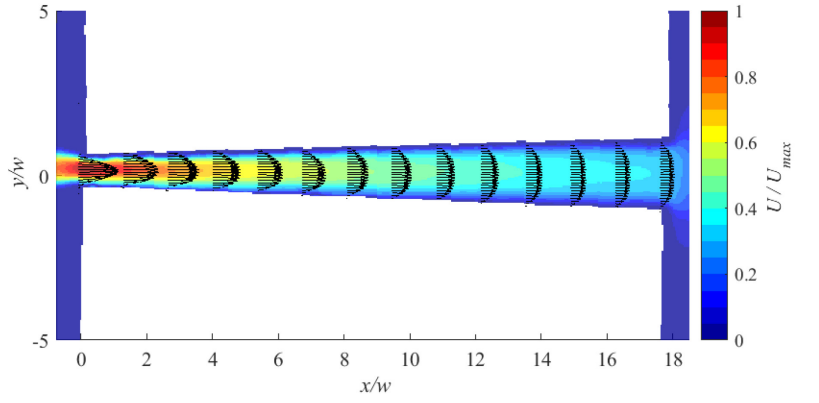

(b) 0.2 wt. % polyacrylamide solution flow through keystone slot with $\theta = 2°$ slot angle at Q = 10ml/hr

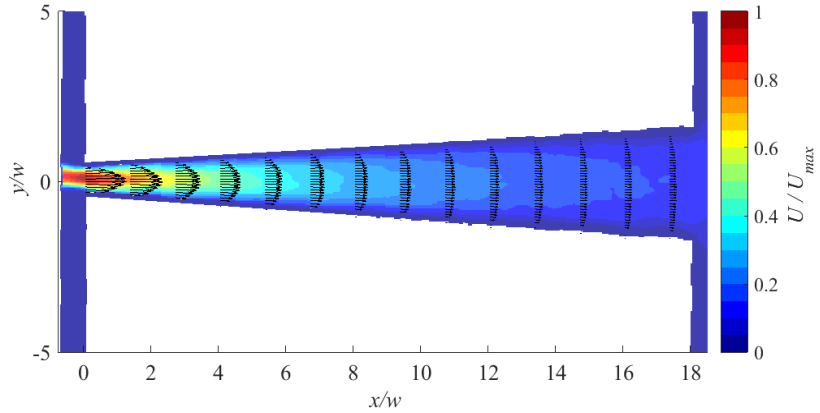

(c) 0.2 wt. % polyacrylamide solution flow through keystone slot with $\theta = 4°$ slot angle at Q = 10ml/hr

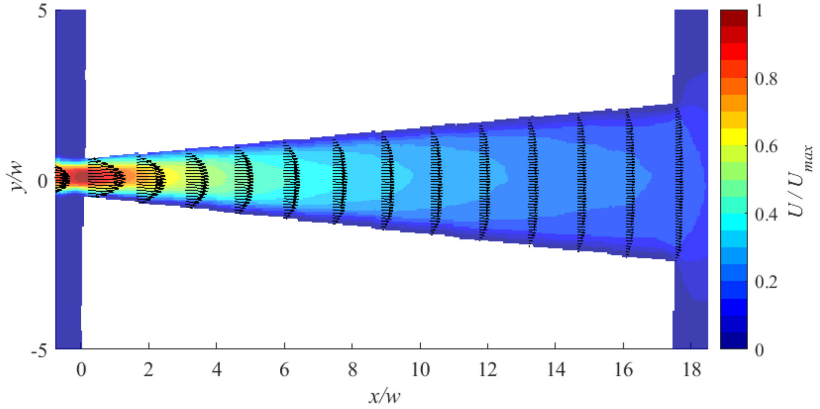

(d) 0.2 wt. % polyacrylamide solution flow through keystone slot with $\theta = 6°$ slot angle at Q = 10ml/hr

Figure A- 15. Vector map of 0.2 wt. % polyacrylamide solution flow at Q = 10 ml/ hr through (a) $\theta = 0°$(straight), (b) $\theta = 2°$, (c) $\theta = 4°$, (d) $\theta = 6°$, (e) $\theta = 8°$, (f) $\theta = 10°$, and (g) $\theta = 12°$ keystone slot

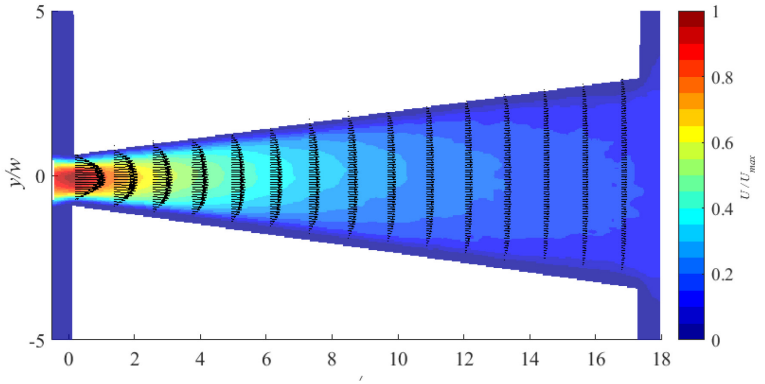

(e)0 .2 wt. % polyacrylamide solution low through keystone slot with θ = 8° slot angle at Q = 10ml/hr

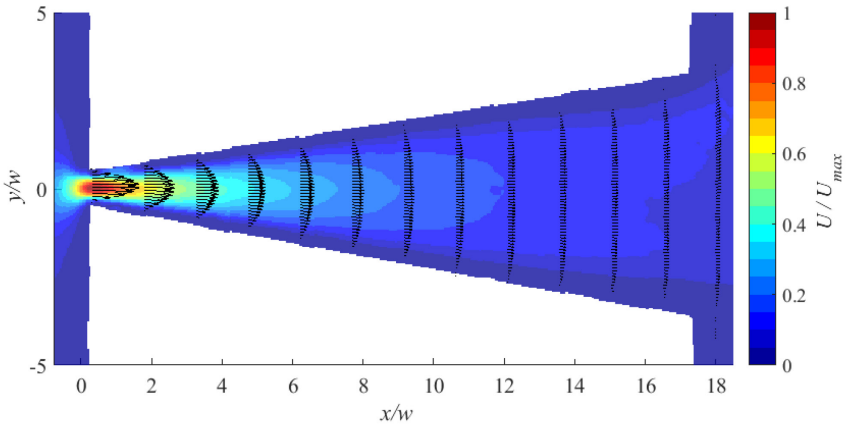

(f) 0.2 wt. % polyacrylamide solution flow through keystone slot with θ = 10° slot angle at Q = 10ml/hr

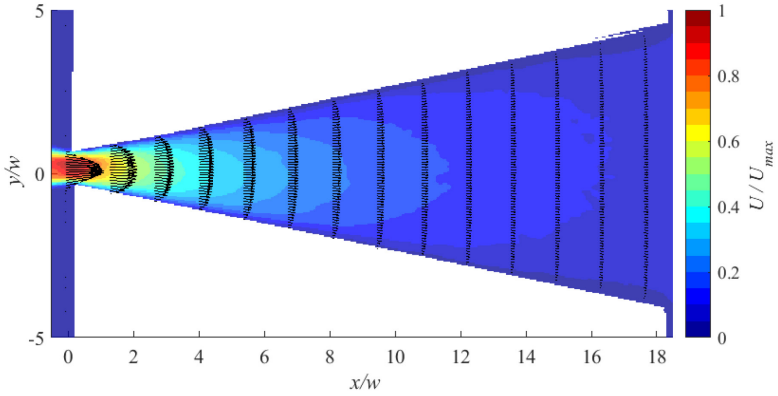

(g) 0.2 wt. % polyacrylamide solution flow through keystone slot with θ = 12° slot angle at Q = 10ml/hr

Figure A- 15 *(continued)*

D-3. 0.4 wt. % Polyacrylamide solution flow through different shapes of keystone slots

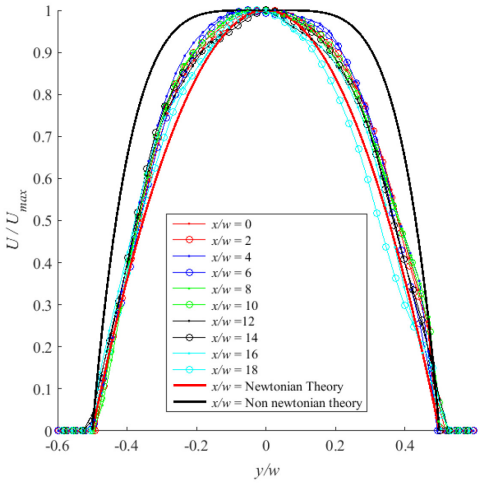

(a) 0.4 wt. % polyacrylamide flow through keystone slot with $\theta = 0°$ (straight) at $Q = 5.5$ ml/hr

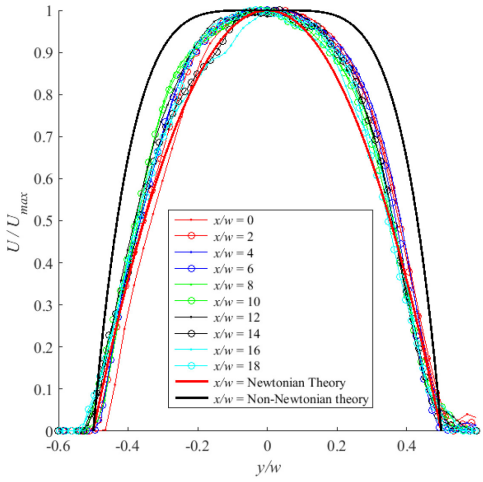

(b) 0.4 wt. % polyacrylamide flow through keystone slot with $\theta = 2°$ at $Q = 5.5$ ml/hr

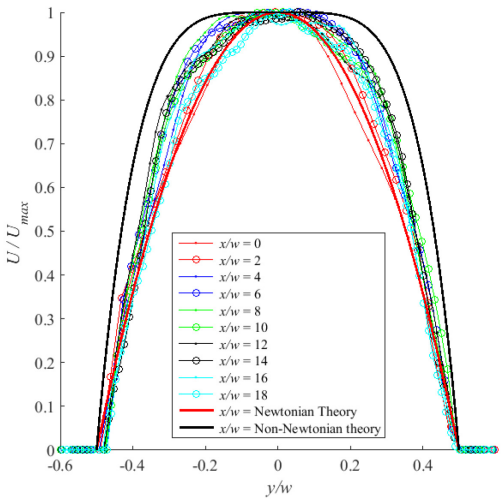

(c) 0.4 wt. % polyacrylamide flow through keystone slot with $\theta = 4°$ at $Q = 5.5$ ml/hr

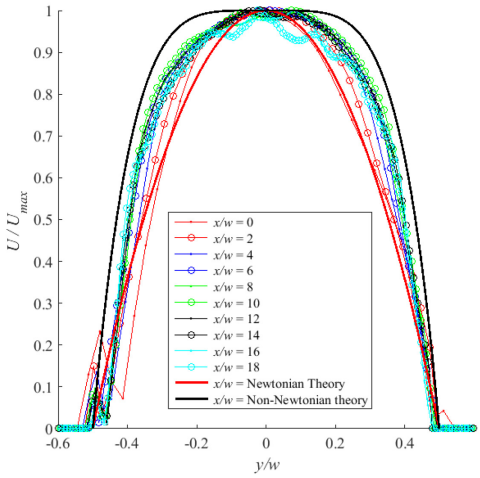

(d) 0.4 wt. % polyacrylamide flow through keystone slot with $\theta = 6°$ at $Q = 5.5$ ml/hr

Figure A- 16. The velocity profile of 0.4 wt. % polyacrylamide at $Q = 5.5$ ml/hr at different (a) $\theta = 0°$ (straight), (b) $\theta = 2°$, (c) $\theta = 4°$, (d) $\theta = 6°$, (e) $\theta = 8°$, (f) $\theta = 10°$, and (g) $\theta = 12°$ keystone slot in compare to non-Newtonian theoretical profile

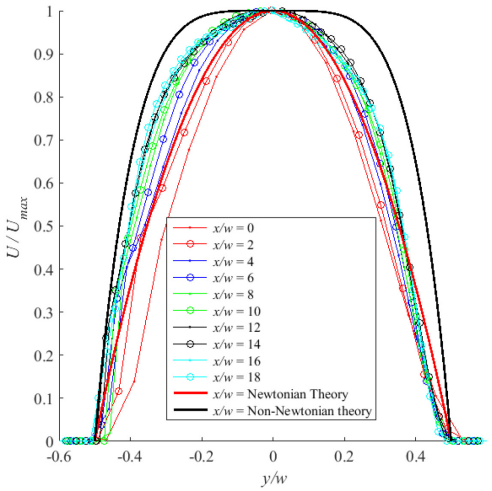

(e) 0.4 wt. % polyacrylamide flow through keystone slot with $\theta = 8°$ at Q = 5.5 ml/hr

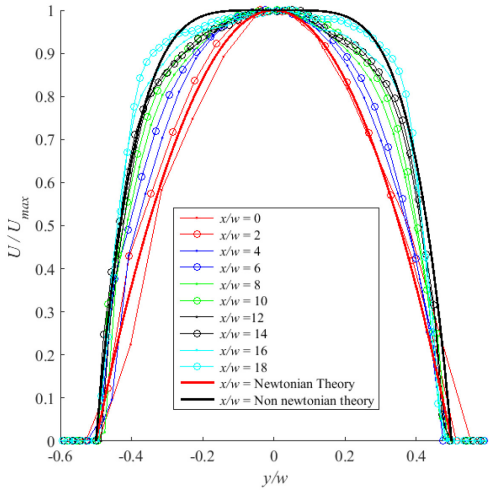

(f) 0.4 wt. % polyacrylamide flow through keystone slot with $\theta = 10°$ at Q = 5.5 ml/hr

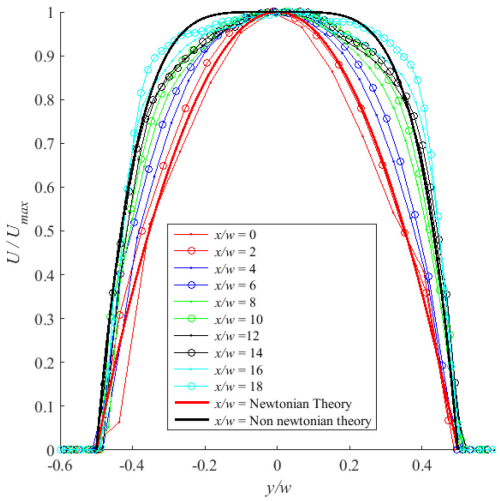

(g) 0.4 wt. % polyacrylamide flow through keystone slot with $\theta = 12°$ at Q = 5.5 ml/hr

Figure A- 16*(continued)*

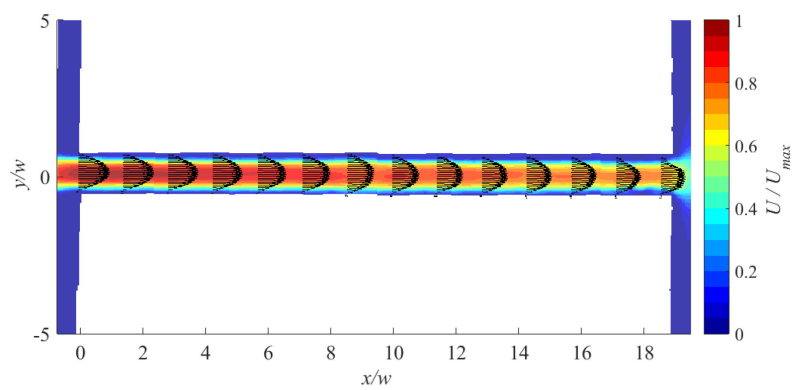

(a) 0.4 wt. % polyacrylamide solution flow through keystone slot with θ =0° (straight) at Q = 5.5ml/hr

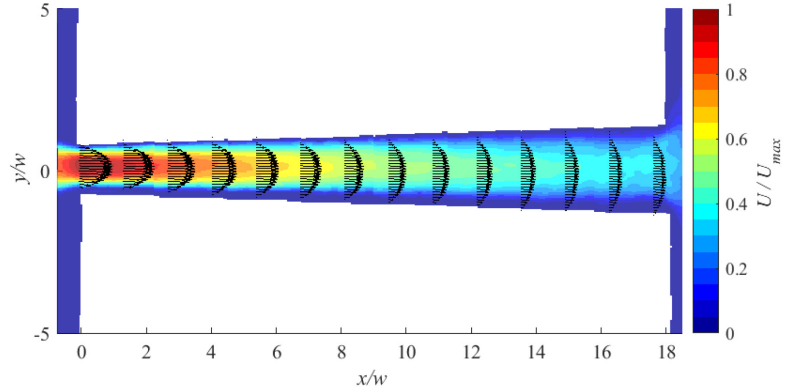

(b) 0.4 wt. % polyacrylamide solution flow through keystone slot with θ = 2° at Q = 5.5ml/hr

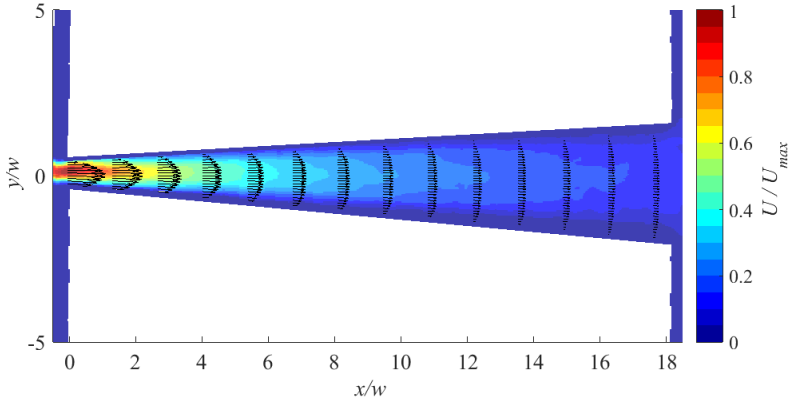

(c) 0.4 wt. % polyacrylamide solution flow through keystone slot with θ = 4° at Q = 5.5ml/hr

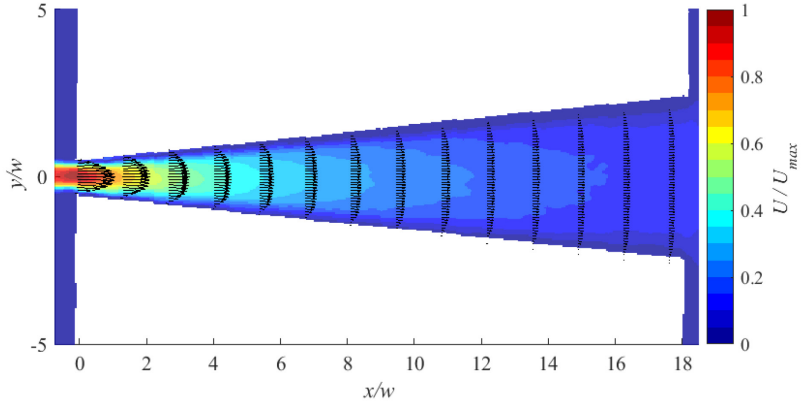

(d) 0.4 wt. % polyacrylamide solution flow through keystone slot with θ = 6° at Q = 5.5ml/hr

Figure A- 17. Vector map of 0.2 wt. % Polyacrylamide solution flow at Q = 5.5 ml/ hr through (a) θ = 0°(straight), (b) θ = 2°, (c) θ = 4°, (d) θ = 6°, (e) θ = 8°, (f) θ = 10°, and (g) θ = 12° keystone slot

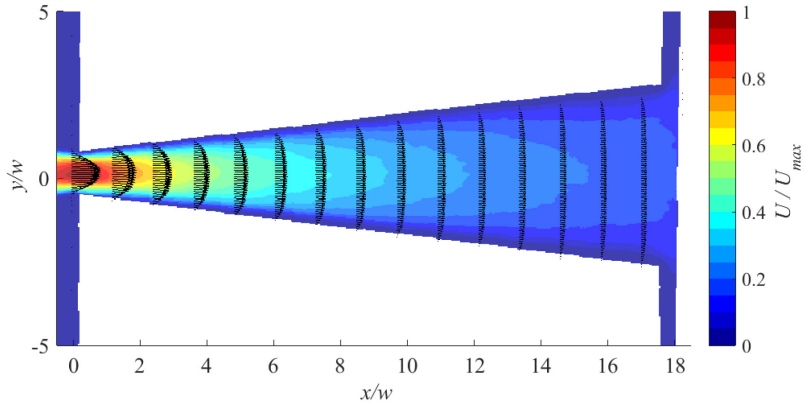

(e) 0.4 wt. % polyacrylamide solution flow through keystone slot with $\theta = 8°$ at $Q = 5.5$ ml/hr

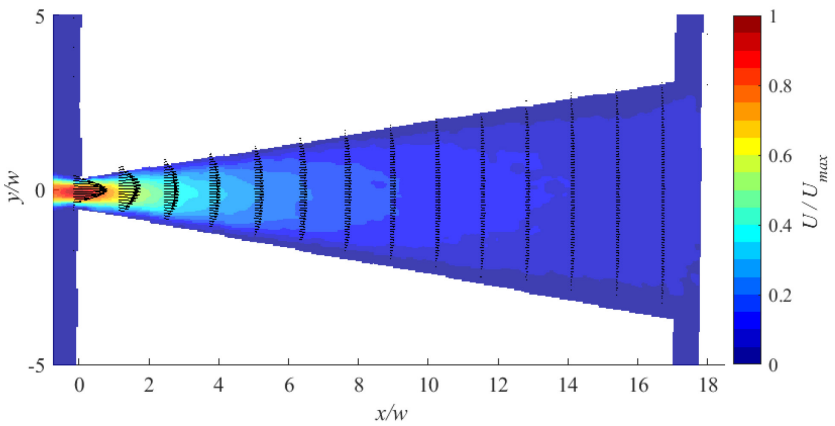

(f) 0.4 wt. % polyacrylamide solution flow through keystone slot with $\theta = 10°$ at $Q = 5.5$ ml/hr

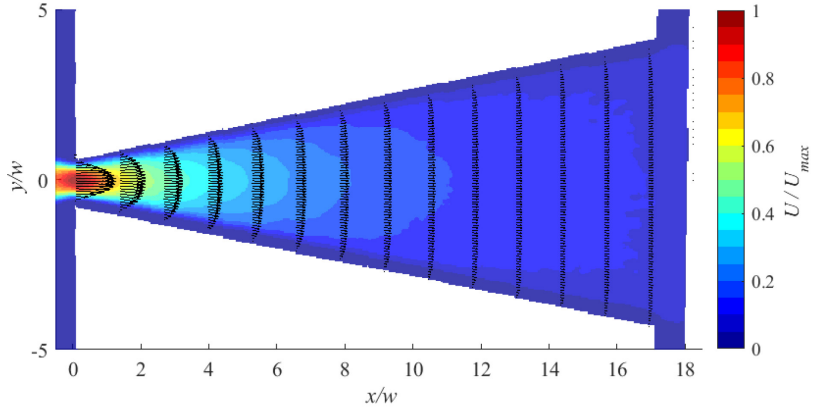

(g) 0.4 wt. % polyacrylamide solution flow through keystone slot with $\theta = 12°$ at $Q = 5.5$ml/hr

Figure A- 17 *(continued)*

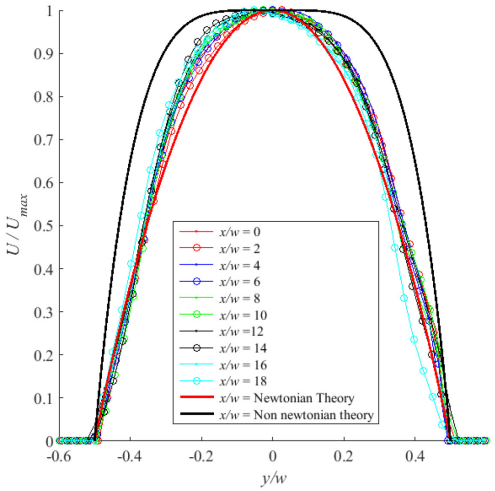

(a) 0.4 wt. % polyacrylamide flow through keystone slot with $\theta = 0°$ (straight) at $Q = 10$ ml/hr

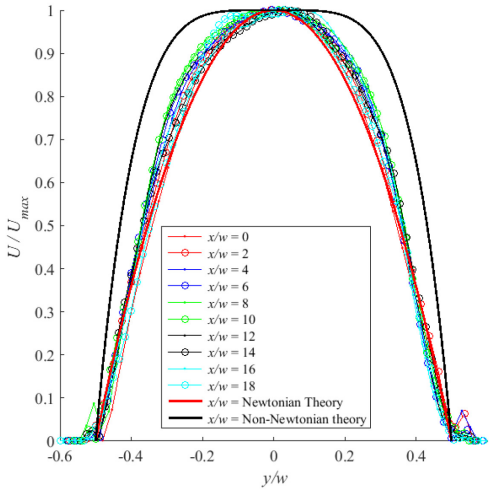

(b) 0.4 wt. % polyacrylamide flow through keystone slot with $\theta = 2°$ at $Q = 10$ ml/hr

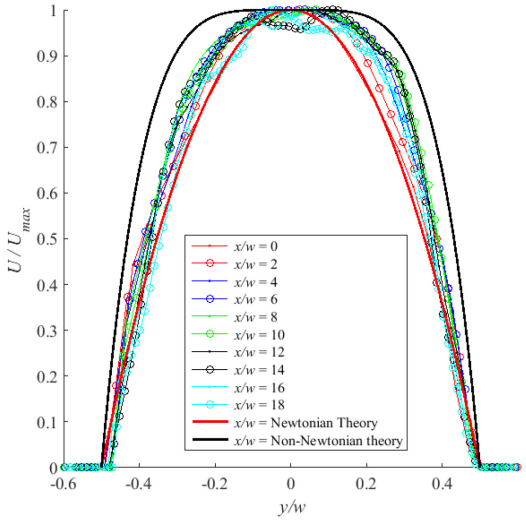

(c) 0.4 wt. % polyacrylamide flow through keystone slot with $\theta = 4°$ at $Q = 10$ ml/hr

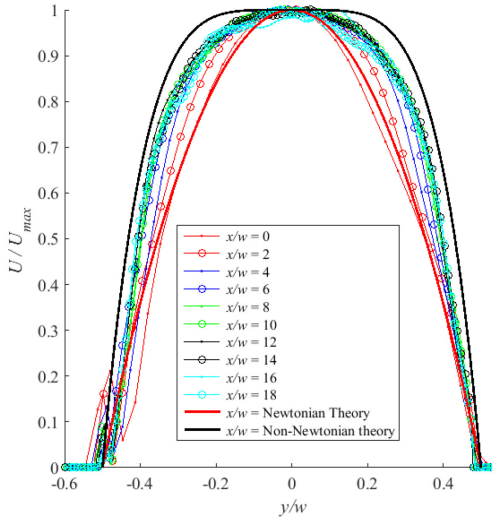

(d) 0.4 wt. % polyacrylamide flow through keystone slot with $\theta = 6°$ at $Q = 10$ ml/hr

Figure A- 18. The velocity profile of 0.4 wt. % polyacrylamide at $Q = 10$ ml/hr at different (a) $\theta = 0°$ (straight), (b) $\theta = 2°$, (c) $\theta = 4°$, (d) $\theta = 6°$, (e) $\theta = 8°$, (f) $\theta = 10°$, and (g) $\theta = 12°$ keystone slots in compare to non-Newtonian theoretical profile

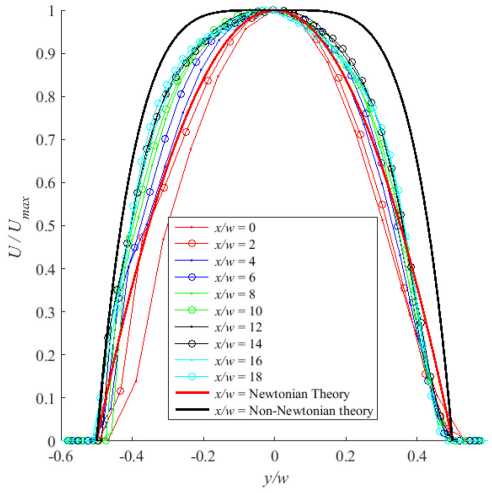

(e) 0.4 wt. % polyacrylamide flow through keystone slot with $\theta = 8°$ at $Q =$ 10 ml/hr

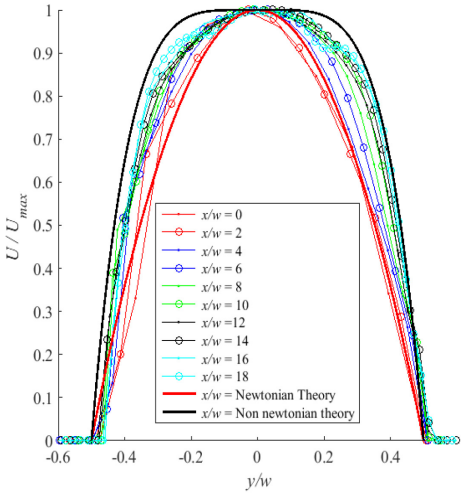

(f) 0.4 wt. % polyacrylamide flow through keystone slot with $\theta = 10°$ at $Q = 10$ ml/hr

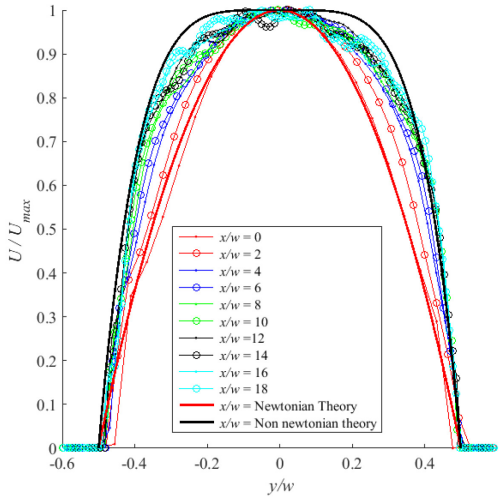

(g) 0.4 wt. % polyacrylamide flow through keystone slot with $\theta = 12°$ at $Q =$ 10 ml/hr

Figure A- 18*(continued)*

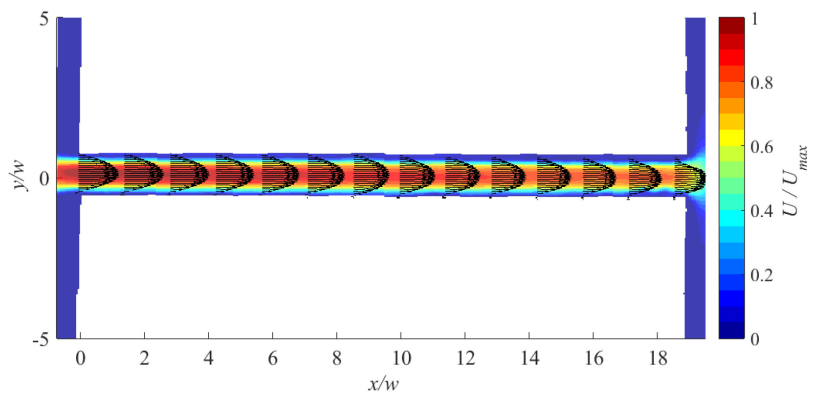

(a) 0.4 wt. % polyacrylamide solution flow through keystone slot with θ =0° (straight) at Q = 10ml/hr

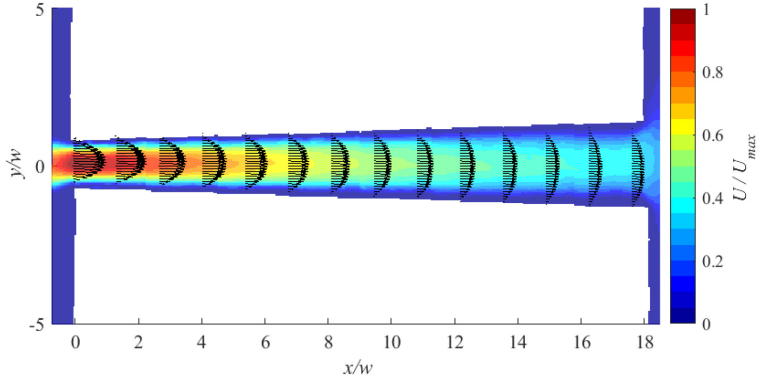

(b) 0.4 wt. % polyacrylamide solution flow through keystone slot with θ = 2° at Q = 10ml/hr

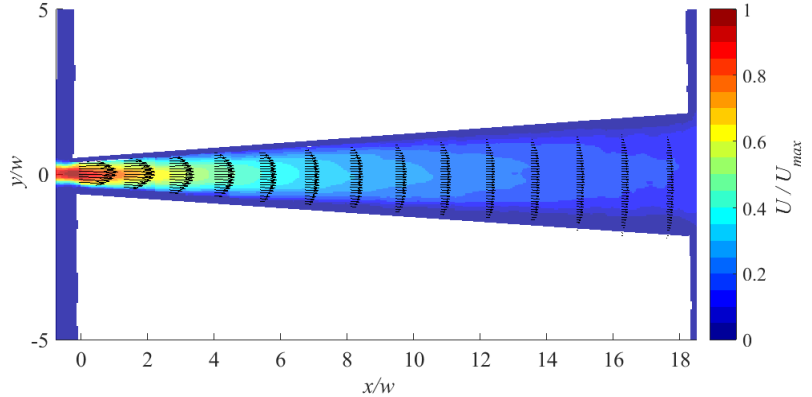

(c) 0.4 wt. % polyacrylamide solution flow through keystone slot with θ = 4° at Q = 10ml/hr

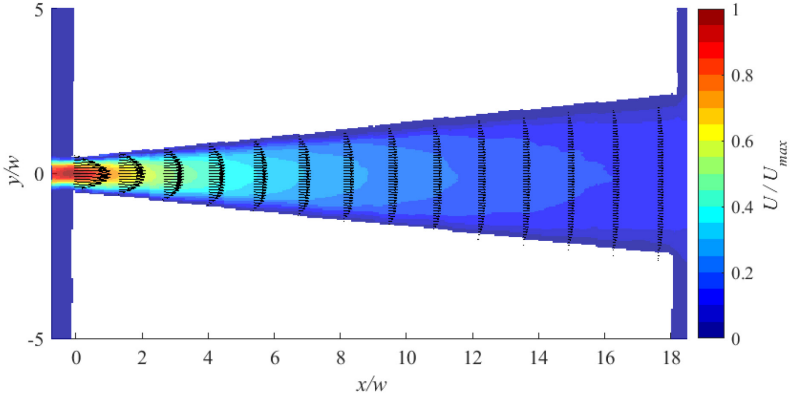

(d) 0.4 wt. % polyacrylamide solution flow through keystone slot with θ = 6° at Q = 1.ml/hr

Figure A- 19. Vector map of 0.4 wt. % Polyacrylamide solution flow at Q = 10 ml/ hr through (a) θ = 0° (straight), (b) θ = 2°, (c) θ = 4°, (d) θ = 6°, (e) θ = 8°, (f) θ = 10°, and (g) θ = 12° keystone slot

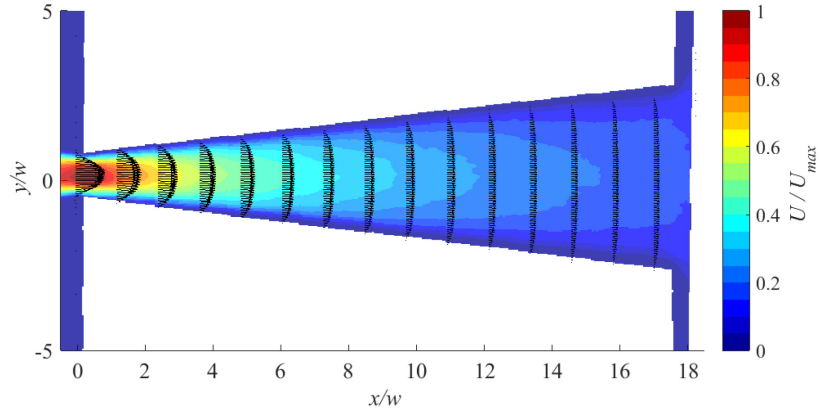

(e) 0.4 wt. % polyacrylamide solution flow through keystone slot with $\theta = 8°$ at Q = 10ml/hr

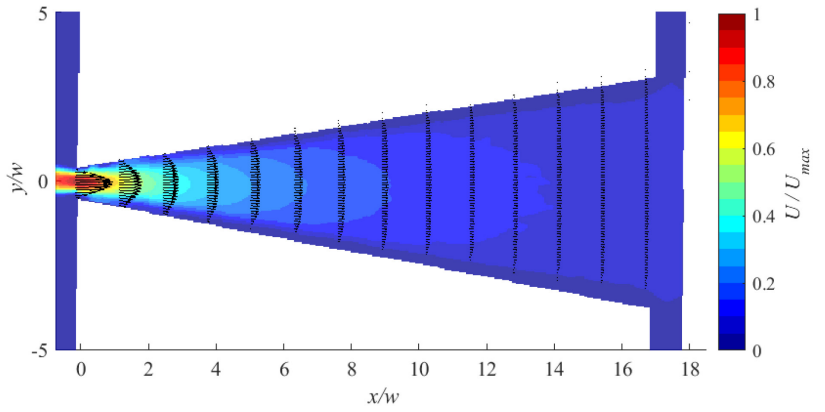

(f) 0.4 wt. % polyacrylamide solution flow through keystone slot with $\theta = 10°$ at Q = 10ml/hr

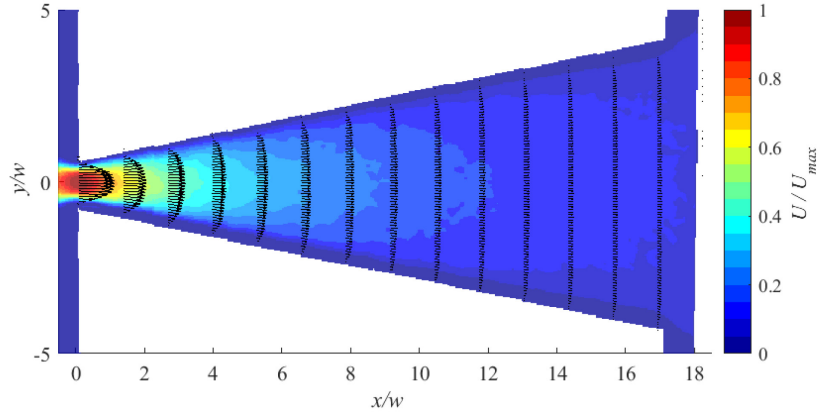

(g) 0.4 wt. % polyacrylamide solution flow through keystone slot with $\theta = 12°$ at Q = 10ml/hr

Figure A- 19*(continued)*

D-4. Centerline velocity decay calculation for different flow through keystone slots

Table A- 1. Parameters of linear regression of reversed normalized velocity vs. normalized position for water flow

Flow rate *(Q)*	Slot angle (θ)	Slope ($1/K$)	y intercept	R^2
1 ml/hr	0°	0.005923	1.008	0.9223
	2°	0.04406	0.929	0.9942
	4°	0.1368	0.9184	0.9986
	6°	0.1931	0.5937	0.961
	8°	0.1561	0.9729	0.9624
	10°	0.2423	0.811	0.9948
	12°	0.254	0.9966	0.9943
5.5 ml/hr	0°	0.004484	0.9953	0.979
	2°	0.04784	0.95	0.999
	4°	0.1499	0.9007	0.9958
	6°	0.1827	0.8101	0.9935
	8°	0.1925	0.8255	0.996
	10°	0.444	0.207	0.974
	12°	0.3507	0.584	0.9942
10 ml/hr	0°	0.01294	1.014	0.972
	2°	0.04986	0.9624	0.995
	4°	0.153	0.9491	0.99
	6°	0.1672	0.8818	0.996
	8°	0.1957	0.828	0.996
	10°	0.449	0.137	0.996
	12°	0.3427	0.68	0.99

Table A- 2. Parameters of linear regression of reversed normalized velocity vs. normalized position for 0.2 wt. % polyacrylamide flow

Flow rate *(Q)*	Slot angle (θ)	Slope ($1/K$)	y intercept	R^2
1 ml/hr	0°	0.02191	0.971	0.966
	2°	0.08151	1.008	0.9941
	4°	0.2602	0.7552	0.996
	6°	0.2826	0.8002	0.9966
	8°	0.2826	0.8002	0.9966
	10°	0.6946	0.3073	0.9872
	12°	0.4587	0.5936	0.9982
5.5 ml/hr	0°	0.008236	1.083	0.808
	2°	0.08207	1.021	0.9978
	4°	0.276	0.6926	0.9941
	6°	0.285	0.594	0.9971
	8°	0.283	0.7812	0.9977
	10°	0.7224	0.02843	0.9981
	12°	0.5249	0.2614	0.9929
10 ml/hr	0°	0.01619	1.021	0.9568
	2°	0.08983	0.9625	0.9969
	4°	0.2204	0.8317	0.9991
	6°	0.2253	0.7649	0.998
	8°	0.2848	0.7437	0.9966
	10°	0.6495	0.07074	0.9978
	12°	0.5271	0.2951	0.9935

Table A- 3. Parameters of linear regression of reversed normalized velocity vs. normalized position for 0.4 wt. % polyacrylamide flow

Flow rate *(Q)*	Slot angle (θ)	Slope ($1/K$)	y intercept	R^2
1 ml/hr	0°	0.01606	1.029	0.9379
	2°	0.1177	0.8287	0.9907
	4°	0.2623	0.639	0.9926
	6°	0.3155	0.6852	0.9966
	8°	0.3045	0.6171	0.9899
	10°	0.5511	0.4533	0.9973
	12°	0.4282	0.7827	0.9991
5.5 ml/hr	0°	0.01575	1	0.9665
	2°	0.102	0.8501	0.9864
	4°	0.2911	0.6396	0.9933
	6°	0.3213	0.7302	0.9962
	8°	0.3513	0.7587	0.9972
	10°	0.4516	0.6699	0.9992
	12°	0.4577	0.6551	0.9993
10 ml/hr	0°	0.01493	1.002	0.9721
	2°	0.09517	0.8992	0.9962
	4°	0.2687	0.7154	0.9968
	6°	0.3085	0.752	0.998
	8°	0.3185	0.8106	0.999
	10°	0.5383	0.4537	0.9976
	12°	0.5524	0.7203	0.9935